Remote Sensing of water leaks from rural aqueducts.

Frances. M. Taylor

(BSc Hons, MSc)

Thesis submitted for the degree of Doctor of Philosphy

School of GeoScience, University of Edinburgh

Declaration

This thesis is the result of my own work. When the work of others has been used it has been duly acknowledged.

Acknowledgements

There are many people to thank for their help, support, advice and generosity with regard to this PhD thesis, but to begin with I would like to express my enormous gratitude to my supervisors Tim Malthus and Iain Woodhouse. I feel very fortunate to have worked with them on this project and greatly appreciate their continued encouragement and advice over the years.

I wish to thank NERC for offering me a studentship and for their financial support. Then there are my NERC Industrial CASE partners at United Utilities to thank for their expertise and technical advice, particular thanks to Peter Morgan, Nick Preston, Richard Duckett, John Tustin, Pete Mahon, and Jeff Sinfield. I must also thank United Utilities for letting me use their Ordnance Survey data sets and also for the financial support they offered me between 1999 and 2002. Next I wish to express my appreciation to those at QinetiQ who were involved in the BNSC link project. Especially Alex Rodriguez, who allowed me to use the corrected HYMAP and E-SAR data and who helped me with some of the trickier post-processing E-SAR problems, and Susan Andrews for her work on the HYMAP data. Finally, thanks to Steven Wilson and Anthony Denniss (of Infoterra) for coordinating the SHAC Campaign and to Peter Bird from DERA (now QinetiQ) for proving the corner reflector during the E-SAR campaign.

I would like to express huge thanks to those who helped me during fieldwork in July 2000. In particular Mrs Dilworth for letting us camp in her garden. Further thanks to Mrs Dilworth, and to the Dakins for letting me make puddles in their fields – not once but twice. And to the dedicated team who braved all weathers to help with the measurements Tim, Vanessa, Chris, Keith, Stephanie, Nick, Sara and Chris Arbuckle. There are also the farmers from around Edinburgh, Lawrence Hodgson Jones, Donald Dunbar and Sandy Allison, who very kindly supported my Edinburgh fieldwork firstly, by allowing me to work on their farms, particularly in the height of the 2001 Foot and Mouth outbreak. Secondly, by allowing me to simulate leaks in their fields, and thirdly by providing bowsers and polythene cubes mounted on palettes – all so I could flood their fields. Last but not least, thanks to Robert Ritchie at CEH for letting me borrow the CEH needle board.

I feel I must thank the NERC Equipment Pool for Field Spectroscopy separately and in particular Ted Milton and Karen Anderson for their continued support throughout my PhD, and for maintaining a great facility.

There are many people in the Geography Department who have helped me and who have made my life much easier by answering my random questions and offering me their expertise. So, big thanks to Chris Place, Keith Morrison, Richard Hedger, Dean Turner, Manuela Grippa, Izza Izzawati and Javier Corripio.

Lastly, there are all the other people outside the Department who will probably never know how much they have helped me throughout my PhD. I must offer thanks to my teacher Laurent and young master Reed not only for training purposes, but also for his repeated explanations of certain aspects of maths and physics! The other important people are my Mum, Jules, Nams, Jess, Herm, Jon, Jo and Charlie. The last words are for Chris Fogwill who is an amazing person and whose timing is impeccable.

Abstract

The development of techniques for the detection of water leaks from underground pipelines is seen as a high profile activity by water companies and regulators. This is due to increasing water demands and problems with current leak detection methods. In this thesis optical reflectance and microwave backscatter were used to identify optimal indices for detecting water leaks amongst a variety of different land cover types at different growth stages. Ground-based surveys and modelling techniques were used to establish optimal wavelengths for detection. Results from these studies suggested that in the optical domain visible/middle infrared ratios show potential for leak detection for a wide range of leak types, under a variety of vegetation canopies at different growth stages. Given the sensitivity of L-band radar to moisture, and the ability to separate contributions from canopy and ground surface, it is possible to detect surface water beneath a range of vegetation canopies. The optimal leak detection indices were then used to idenitfy leaks on airborne image data. The available image data was L - band fully polarimetric E-SAR data, and 126 channel HYMAP hyperspectral airborne data which were acquired over an 8km section of the Vrynwy aqueduct (UK), which included a high concentration of leaks. Four of the five leaks were identifiable on the optical image data and none of the leaks were detectable on the microwave data. However the E-SAR data was obtained under unfavourable conditions. The results of both approaches are used to infer limits of detection in terms of season and meteorological conditions for a range of land covers. Preliminary findings suggest that leaks may be optimally detected when canopy height is low, surrounding soil is dry after a period of no rain, and the leak has been present for at least 2 days. The results from this work suggest that remote sensing is both an effective and feasible tool for leak identification.

Table of contents

PART I

PART IV

List of figures

List of tables

1.1 Introduction

The problem of unaccounted-for distribution water losses is faced by water companies world-wide (Francis, 1994). Such losses become further highlighted during periods of severe drought when continuous supply is threatened. The water industry in England and Wales had unaccounted for losses of 3243 Megalitres per day during 2001. This is 21.6% of the total input of water (OFWAT, 2001). Since 1997 there has been legislation in place to reduce unaccounted for losses with each company having self-imposed annual targets to reduce leakage. This has increased the focus on methods for reducing water leakage and produced the impetus to consider alternative methods. Current methods are typically staff intensive and frequently involve excavation of water mains and diversion of supplies. Consequently, they are both costly and time consuming. Water companies require a quick, cost-justified, large-scale method of identifying areas of actual leakage (WRc 1990, 1994).

Remote sensing of leaks, by definition, would involve no disturbance of the pipeline and therefore supply would not be affected. There is a strong theoretical basis which justifies the use of such a technique for leak detection, with its capacity to provide rapid large-scale and synoptic coverage. The technique is fundamentally physically-based requiring only that reflectance properties of the leak be sufficiently different from surrounding land surface and covers. A pilot study undertaken using optical airborne imagery demonstrated that water leaks could be identified beneath a limited range of land cover types using limited wavebands. However, the findings of this study were that robust indices are required which are capable of accommodating a range of land covers, and that further exploration of potential wavelength ranges for leak identification is required (Pickerill and Malthus, 1998). The aims of this work are to investigate the effectiveness of two complementary techniques for identifying water leaks in a wider range

of different land cover types and at a wide range of wavelengths by process radiative transfer modelling of vegetation canopies, and empirical remote sensing.

For leak detection use of conventional optical space-borne sensors (e.g. Landsat, SPOT) are limited by their coarse spatial resolution, relative to the scale of typical pipeline leaks (1 – 10m^2). Spatial resolution is particularly limiting for thermal waveband imagery (e.g. the finest resolution is Landsat 7 ETM+ imagery at 30m resolution). However, in the optical and microwave domains, the advent of a number of high resolution satellites offering spatial resolutions of 5m or less (e.g. Orbview 3, IKONOS 2, QuickBird, and RADARSAT-2) means that leak detection from space-borne sensors is approaching the level of feasibility. The result will lead to images with high spatial resolution, high geometric precision, short revisit intervals and rapid data supply, possibly simultaneously, and at low-cost (Antenucci 1995). A further limitation of space-borne sensors has been problems of atmospheric interference with optical and thermal wavelengths. However, this can be overcome by the use of sensors operating in the microwave domain. Furthermore, it is highly likely that a combination of different wavelength regions may be most successful in detecting leaks in a range of situations.

Little is known of the reflectance and backscatter characteristics of leaks and their physical expression at the surface. However, several studies have considered remote sensing (predominantly in the microwave domain) of rice paddies, marshes, and flooded and unflooded forests (LeToan *et al.*, 1997; Pope *et al.*, 1997; Wang *et al.*, 1995). While these studies are relevant to this work, aiming to identify water beneath vegetation canopies using remote sensing, leaks often differ markedly from these examples. Leaks tend to occur on a much smaller scale, and are variable in terms of their dimensions and degree of saturation. This work relies on there being a distinct contrast between each leak and the surrounding vegetation. Leaks also vary in their effects on different types of vegetation depending on their duration and the vegetation growth stage. To date, there has been no thorough investigation of water leaks from a remote sensing perspective that considers their expression, duration and possible effects on vegetation over a range of wavelengths.

A systematic approach to the problem is required in order to establish the optical and backscatter characteristics of leaks and their surrounding vegetation. This work adopts a ground-up approach

where field and modelled results were explored, prior to acquisition of a limited range of image results. Modelled and ground-based data were used to establish optimal wavelengths for identifying a range of leaks against a variety of different vegetation types at varying growth stages. Two airborne images were acquired for this project, one in the microwave and one in the optical domain. They were analysed to test whether leak identification was reliable using the optimal wavelengths identified. Field and modelling studies were therefore used to make insightful predictions on leak identification in conjunction with image data. Supporting measurements were provided through field simulations of leaks, and exploring a range of modelled scenarios in both the optical and microwave domains.

1.1.1 Aims and objectives

The challenge here is to assess optical and radar remote sensing techniques for detecting leaks from aqueducts using the new generation of high resolution satellite sensors. Specifically, the research objectives are:

- Through field, image and modelling approaches, to investigate the scale and expression of leaks within different land covers and their spectral reflectance, emittance and backscatter characteristics.
- To investigate candidate optical and microwave returns for leak detection and test their sensitivity in the presence of variations in landcover type, canopy height and soil colour.
- To investigate the individual utility and complementarity of multiwavelength approaches to leak detection.
- To investigate the expression of leaks through the growing season to determine the optimum periods and environmental conditions when leak detection would be most effective.
- To consider optimal characteristics for a suite of spaceborne sensors to facilitate leak identification.

1.1.2 Structure of thesis

The structure of this thesis reflects the radically different theory and application of these two remote sensing approaches used, so to avoid confusion they have been considered separately. As such this work is split into four sections; an introduction and overview, an optical part, a microwave part and finally a discussion and conclusion. The final section attempts to integrate the two approaches and discusses the merits of each from the point of feasibility. The following short paragraphs aim to outline the contents and issues that are dealt within each section.

1.1.2.1 Part I - Introduction and overview

This introduces the topic and considers the context, justification and key points of this work. It considers how water is managed in the UK, the surface expression of leaks including the impacts of excess water on vegetation, and the problems associated with current methods of identifying water leaks. This section also describes the Cheshire and Edinburgh field sites, in terms of local topography, soil and vegetation characteristics. Finally the data chapter describes the acquisition conditions and processing of the optical and microwave data.

1.1.2.2 Part II - Optical part

This section introduces the basic theory of optical remote sensing of soil, water and vegetation and various combinations of them, providing a brief review of vegetation reflectance models. Field methods are discussed including approaches to, and basic theories of, field spectroscopy, followed by a detailed description of the collection of in-situ measurements. Ground-based field results are then presented for both Cheshire and Edinburgh sites, as well as results from the spectroradiometer surveys. Spectral reflectance curves for leak and non-leak surfaces are plotted against each other for each site.

Approaches to modelling are discussed, and followed by model results which provide reflectance curves for a variety of different canopy types at various growth stages and under a range of waterlogging conditions. Optical image data results are then presented in chapter 2.6, before the analysis of all the optical data is presented and discussed in chapter 2.7. The model, spectroradiometer and image results are analysed using spectral comparison maps to highlight

optimal wavelengths for identifying leaks leading towards the formulation of a normalised leak index. The final chapter in part two is a summary of the optical part of this thesis.

1.1.2.3 Part III - Microwave part

Introduces basic theory of microwave remote sensing in relation to soil, liquid water and vegetation, considering effects of changes in dielectric constant, incidence angle and presence of wet soils and standing water against various vegetation backgrounds. It also provides a brief introduction to microwave radiative transfer models.

The field methods and results chapter describes the techniques specific to microwave studies, for example measurements of correlation length and surface roughness. It then presents results tables of in-situ measurements. The approach and design of the modelling strategy used, and parametisation of the model, are considered in chapter 3.3. Results from microwave modelled output are presented for a variety of different crops at different growth stages and under varying wetness conditions. The following chapter presents results taken from the microwave imagery. Microwave modelled data are then analysed and the production of ratio comparisons of wet and dry measurements based on polarisation are used to create a microwave leak index. Part three concludes with a summary of the microwave-based chapters.

1.1.2.4 Part IV - Discussion and conclusions

This section provides a brief review of the work carried out, and reports on the optimal wavelengths for identifying water leaks by considering the leak indices developed. The optimal wavelengths identified from the field and modelling parts of the project (from both the optical and microwave studies) are used to identify leaks on the imagery. The chapter moves on to discuss optimal times of year for data acquisition in terms of weather and crop cover, sensor characteristics and plans for future work. The final chapter offers concluding remarks and summarises the key findings of this work.

References

Antenucci, J. C. 1995. High Resolution Space-Based Imaging: The Potential Nears. International Journal of Geographic Information Systems, October, 52-55.

Francis, C. 1994. Sieving the evidence on leakage. Water and Waste Treatment Journal, **38**, p.18.

Le Toan, T., Ribbes, F., Wang, L., Floury, N., Ding, K., Kong, J. A. Fujita, M. and Kurosu, T. 1997. Rice crop mapping and monitoring using ERS-1 data based on experiment and modeling results. IEEE Transactions on Geoscience and Remote Sensing, **35**, 41-54.

OFWAT. 2001. Leakage and the efficient use of water 2000-2001 report, pp.1-44. http://www.ofwat.gov.uk/pdffiles/leakage.pdf

Pickerill, J. M. and Malthus, T. J. 1998. Leak detection from rural aqueducts using airborne remote sensing techniques, International Journal of Remote Sensing, **19**, 2427-2433.

Pope, K. O., Rejmankova, E., Paris, J. F. and Woodruff, R. 1997. Detecting seasonal flooding cycles in marshes of the Yucatan Peninsula with SIR-C polarimetric radar imagery. Remote Sensing of Environment, **59**, 157 - 166.

Wang, Y. Hess, L. L., Filoso, S. and Melack, J. M. 1995. Understanding the radar backscatter from flooded and nonflooded amazonian forests: results from canopy backscatter modeling. Remote Sensing of Environment, **54**, 324-332.

WRc. 1990. Leakage Control: Ten Years of Progress. *Water Bulletin*, no.398, pp.1-11.

WRc. 1994. UK Water Industry: Managing Leakage: Report J - Leakage Management Techniques, Technology and Training. Engineering and Operations Committee. WRc plc.

1.2 Background

1.2.1 The leakage problem

Drier climatic conditions and higher temperatures from the mid 1980s to the mid 1990s, led to both domestic and industrial water supply shortages and prompted restrictions on usage. At the same time, water demands increased due to greater use of domestic appliances and new technology (for example dishwashers, washing machines and power showers). This is in contrast with certain other European countries and the US, where there has been a drop in demand through the creation of a "greener" culture, tighter water use regulations, active water conservation and demand management programmes. Environmental and social changes have highlighted the need to manage water resources more efficiently, particularly as water losses have reached levels of between 30 and 40% in some regions of the UK. Since privatisation in 1989, the water companies of England and Wales have experienced increasing pressure from the main regulators (OFWAT and the Environment Agency) to reduce water losses. OFWAT introduced a reporting procedure where each company is required to submit an annual report on the volume of water supplied, consumed and lost from each component of the network. The main product of this is a water balance. Each region monitors its own water balance and OFWAT coordinates the information to produce efficiency tables based on inter-regional comparisons. This has put pressure on water companies, leading them to:

- Conduct research into the causes of losses
- Develop more robust mechanisms for measuring/estimating water balance components
- Set economic leakage minimisation targets
- Monitor and reduce leakage
- Improve their customer and media image

As a result of these developments water leakage has been reduced over the last seven years (Figure 1.2.1), however, it remains a serious problem.

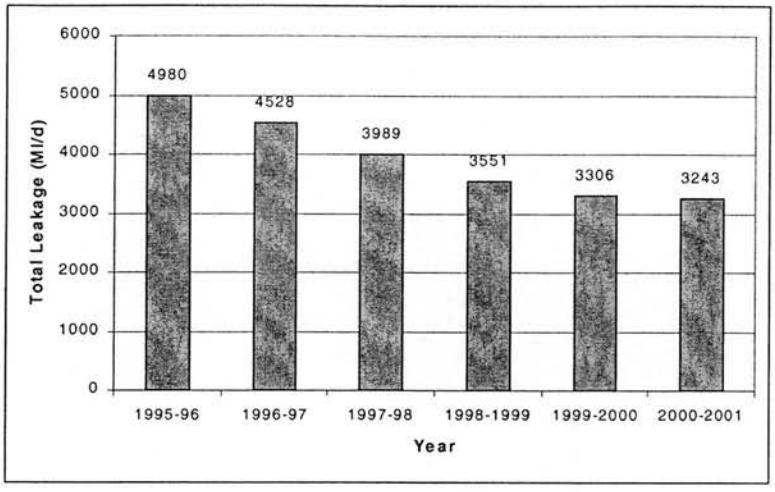

Figure 1.2.1 Graph showing total water industry leakage 1995-96 to 2000-2001.Adapted from OFWAT, 2001.

Control, management and regulation of water in the UK is divided up amongst a wide range of organizations. Therefore, issues relating to leakage management and control are similarly cross-regulatory. Table 1.2.1 shows the main water regulators and their key responsibilities.

Table 1.2.1. List of water regulators and their responsibilities.

Regulator	**Responsibilities**
Department of the Environment, Transport and the Regions (DETR)	• Legislation • General policy • Water bylaws • Mandatory leakage targets • Service pipe leakage • Customer communication
Drinking Water Inspectorate (DWI)	• Water company supply zones • Monitor Government drinking water quality standards • Enforcement • Monitor enforcement and reporting elements • Sampling consistency

Environment Agency (EA)	• Conserve, redistribute and augment water resources to ensure 'proper' use • Control abstraction from surface and underground sources • Promote water saving (demand management) • Pollution monitoring and enforcement penalties
Office of Water Services (OFWAT)	• Balance customer and business interests • Monitor the operation of charging systems • Set price caps by limiting annual price increase • Set and monitor standards of service for customer taps • Require companies to develop water management systems • Monitor performance against leakage targets

1.2.2 Unaccounted for losses

Perhaps the most difficult problem in leakage monitoring and control, is the estimation of losses. Across the UK only 25% of water is sold by volume and can therefore be directly accounted for, the remaining 75% is estimated from water balancing techniques which measure inflow, and outflow (Figure 1.2.2), however, the figures rarely balance. Typically water leakage in the UK is estimated from baseline data for inflow and outflow into a system. The estimates are commonly based on minimum night flow or total integrated flow methods. Night flow measurements are taken between 3.00 and 4.00 am when water usage is considered to be lowest. The metered consumption from industry and households are subtracted from district inflow measurements and the remaining volume is termed 'unaccounted-for losses'. The integrated flow method estimates all the other components of the water balance and the residual is leakage. However both these techniques are best guesses as there are not enough flow meters in the UK to adequately measure the flow of water through the 300,000 km of water mains. For example only 19% of domestic customers in England and Wales have meters to record the volume of water they use (OFWAT, 2001). Water delivered to unmeasured household makes up the largest proportion of the water balance, followed by measured water supply to non-households (i.e. industry and services). The third highest proportion of the water balance is water that is lost.

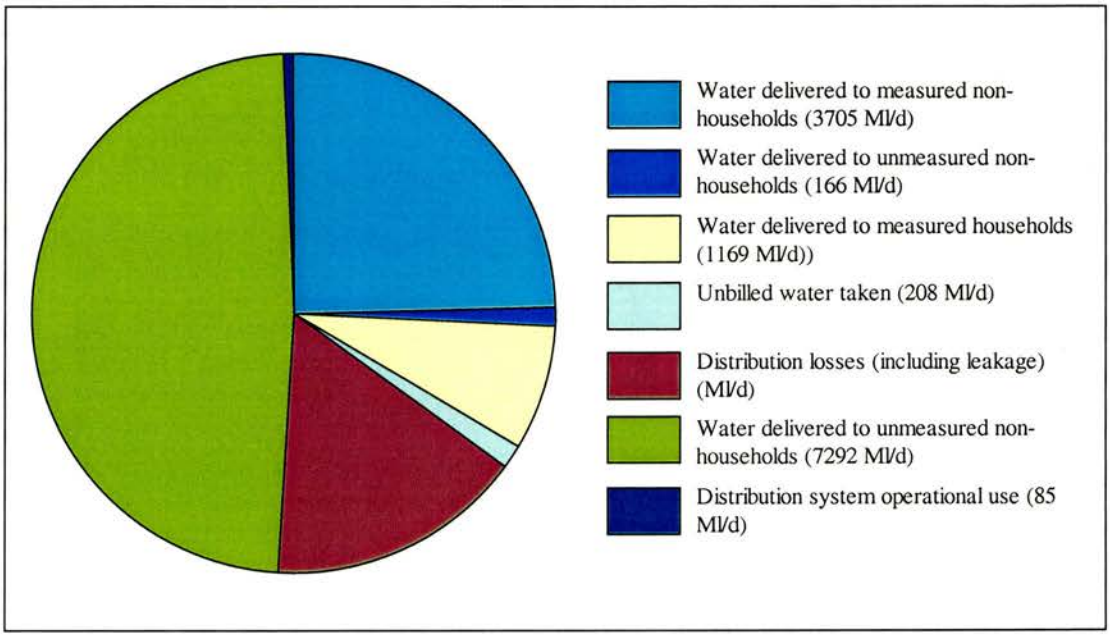

Figure 1.2.2. Components of the water balance.Adapted from OFWAT, 2001.

Leakage reduction is recognised by water companies and the regulators as a high priority activity. There are two measured components of leakage; distribution losses and supply-pipe losses. Distribution losses describe leakage from commercial distribution systems while supply-pipe losses are those from customer supply pipes, the larger percentage of leakage is from distribution losses. For the period 2000-2001, distribution losses were 2365 megalitres and total leakage (distribution losses plus pipe supply losses) was 3243 Ml/d (OFWAT, 2001).

1.2.3 Leak detection methods

Current methods of leakage detection include:

- Customer complaints or visual reports
- Sounding stick – an acoustic or electric stethoscope
- Ground microphones
- Noise correlator surveys – using electronic sounding equipment (correlators)
- Pressure monitoring – pressure gauges

- District metering – flow meters
- Night line measurements - loggers
- Step testing –steptest units
- Acoustic logging
- Network modelling - computers
- Gas detection – hydrogen leak detector

Following detection of losses (for example, through water balancing techniques, telemetry and/or customer reporting), the next stage is to isolate a leak using methods such as acoustic sounding, sub-surface radar, and step testing to locate the leak. While these detection methods meet with some success their usage is limited and they are not always cost effective. For example, the most commonly used sounding stick method is labour intensive and can only be used on a single point basis. Other detection problems include disruption or damage to pipelines and flow interruptions, either in leak identification, or in the fitting of pressure gauges, flow meters, and loggers. Inaccurate baseline data, limits the value of district metering and step testing.

In rural areas detection methods from trunk mains are limited, at present the most popular detection methods are walking the pipeline with a listening stick while looking for wet patches which is both expensive and time consuming, and using noise correlation techniques. A major flaw in the noise correlation method is that it is difficult to detect leaks from plastic pipes because they have poor sound transmission and there is also a problem with background noise. Remote sensing methods with their synoptic coverage would thus seem to offer a solution to the problem of detecting leaks in rural areas, particularly as they offer rapid, continuous coverage without interfering with the pipeline and interrupting flow. This work takes a direct approach by using the presence of water to immediately locate the leak. It is particularly suited to rural areas where the pipelines are buried in soil and covered with vegetation; allowing the leak to be expressed at the surface. Most of the current leak detection methods have been developed for urban areas where leaks are not always expressed at the surface and are more difficult to detect due to greater concentration of pipelines and the complex network distribution systems in urban areas. For economic and logistical reasons, current leak detection methods are not widely or easily applicable to rural pipelines.

1.2.4 Nature of leaks

Due to a sparcity of available information on the nature and frequency of leaks, a questionnaire was designed to get feedback directly from water companies. Questionnaires were sent to 23 of the 25 water companies in England and Wales. There was a 57% response, with 13 replies and 1 refusal. The questionnaire was separated into 3 sections:

- Problems with unaccounted for distribution losses
- Current practise on detection and control
- Potential role of remote sensing for leak detection

A copy of the questionnaire can be found in Appendix 1a and the results of the questionnaire survey are presented in Appendix 1b.

It would appear that more leakage occurs from pipelines in rural areas than in urban centres (results from questionnaire survey carried out by the author in 2001). The main causes are thought to be corrosion or pipeline failure due to old age, corrosion by soil, and constant pressure from through-flow. Pipe age is a significant contributor to the leakage problem, particularly as the majority of water pipelines in England and Wales are at least 50 years old, with some being over 120 years old (questionnaire survey, 2001). Further causes of pipeline failure are ground movement and weather extremes caused by freeze/thaw and wet/dry conditions. The majority of large losses result from pipe bursts, or sudden joint ruptures Small losses tend to be associated with leaking joints, fittings, service pipes and connections (Lambert and Morrison, 1996). The volume of water lost is dependent on the characteristics of the pipe network, methods of leakage detection and company repair policies. These include:

- Network pressure
- Whether the leak can be seen at the surface
- How quickly the leak is detected
- Repair time

The work presented in this thesis is dependent on leaks appearing at the surface. Surface expression of leaks is largely governed by soil type. If a leak from a pipeline occurs in a

particularly sandy soil, then the water will drain away, it may reach a different subsurface layer and reappear at a new location, but it remains difficult to detect. Similarly if there are cracks or fissures in the bedrock then water will effectively 'disappear'. However, when pipelines are buried in soil, leaks tend to appear at the surface due to soil capillary action and soil saturation, resulting in surface ponding. Leaks may vary in scale from centimetres to metres depending on how long they have been in existence and the type of disruption to the pipeline. The questionnaire indicated that there was a seasonal pattern to leakage where leaks tended to occur during winter months which may suggest that extremes of weather contribute significantly to the leakage problem.

1.2.5 Physiological effects of inundation on vegetation

The leaks in this study are in rural areas and against backgrounds of soil and vegetation, one question that arose in the course of the study was 'what are the effects of excess water on vegetation and can they be identified using remote sensing?' Inundation by water has a significant impact on vegetation and it should be possible to monitor many of the changes that occur in vegetation as a result of waterlogging using remote sensing. However, few studies have tackled this subject in relation to remote sensing. In this study information relating to the physiological effects of inundation on vegetation relied on a desk study of biological research into the effects of waterlogging on a variety of plant species at a range of growth stages.

The majority of effects manifesting in plant canopies as a result of flooding are due to root injury and changes in the transportation of minerals, water, hormones and toxins (Jackson and Drew, 1984). When flooding occurs gas exchange between soil and atmosphere is restricted to almost zero due to the water layer. Depending on the soil temperature and respiration rates, dissolved oxygen in the soil is exhausted in a matter of hours or days and the soil becomes anaerobic (Ponnamperuma, 1984). The long-term effects of flooding result in anoxia, which is depletion of O_2 in the plant tissue which subsequently prevents the plant from growing. Despite some elements of growth stimulation, flooding generally results in an overall decrease in shoot growth (Jackson and Drew, 1984). Other effects of waterlogging include accelerated rooting, epinasty (curvature and reorientation of lateral branches towards the ground, i.e. lateral branches appear

to droop), leaf abscission (separation of leaf from stem), premature senescence, increased chlorosis, and wilting (Jackson and Drew, 1984). It is important to note that these effects vary greatly between species and between plant growth stages. Generally speaking, the earlier in the plant growth stage the leak or flooding occurs, the more dramatic and more inhibitory the effect on plant physiology, this is shown in a study on the effects of waterlogging on winter rape (Zhou and Lin, 1995).

1.2.5.1 Factors effecting internal leaf structure and leaf water content

Early effects of flooding restrict root growth and result in a build-up of injurious products in the root which affect metabolism (Jackson and Drew, 1984). Studies have shown that flooding depresses nitrogen, phosphorus and potassium concentrations in the shoots of sunflowers, peas, and wheat (Letey *et al.*, 1962 and 1965; Jackson, 1979; Trought and Drew, 1980b). This suggests that the transportation of ions is adversely affected by flooding. It is likely that changes in the properties of root cell membranes, as a direct result of flooding, affect transportation, although the mechanisms controlling these changes are poorly understood (Trought and Drew, 1980b). It is also possible that xylem and phloem cells are damaged by waterlogging. Despite the lack of understanding of the exact mechanisms controlling responses of vegetation to water inundation, many of the responses have been monitored and observed. Results of flooding include a decrease in photosynthesis (Luxmore and Stolzy, 1969; Jackson and Drew, 1984; Meyer *et al.*, 1987; Ashraf and Habib-ur-Rehman, 1999). There are also changes in osmotic potential of the leaf and thus leaf water content, and the control of the stomata which in turn affect rates of transpiration (Kozlowski and Pallardy, 1984). The most rapid response of herbaceous species to flooding is stomatal closure and reduced leaf growth (Wenkert *et al.*, 1981; Kozlowski and Pallardy, 1984). Stomata control gaseous exchange and water loss mainly from leaves. There is some discrepancy between studies on whether flooding leads to higher or lower leaf water contents as a result of stomatal conductance, and these variations appear to be species dependent (Kozlowski and Pallardy, 1984; Ashraf and Habib-ur-Rehman, 1999). In some species (sunflower, tomato, white oak, maize, and holly), stomata close as a leaf dehydrates. This leaf dehydration has been attributed to decreased water absorption because of root damage from flooding. In contrast other species (*Eucalyptus*, American elm, Eastern cottonwood and Black willow) exhibit higher leaf water potentials despite stomatal closure

(Kozlowski and Pallardy, 1984). It is therefore unlikely that remote sensing of leaf water content alone or indeed of leaf internal structure will tell us whether a plant is suffering from excess water stress. Fortunately there are other more significant differences.

1.2.5.2 Factors effecting leaf area and canopy height

Flooding has been shown to reduce leaf area by inhibiting leaf initiation and expansion. Effects on leaf growth are significant with research showing an 83% decrease in leaf area of wheat after 25 days of root anoxia (Trought and Drew, 1980a). Leaf expansion can slow within 20 to 40 minutes of flooding (Wenkert *et al.*, 1981). While studies on tree seedlings by Tang and Kozlowski (1982) showed that after 40 days the number of leaves on unflooded Sycamore seedlings increased by 115% while flooded seedlings only increased by 21%. Stem extension is also negatively affected by waterlogging. Studies using American elm seedlings showed that the unflooded seedlings were three to five times taller than flooded seedling after 39 days. Similarly, flooded paper birch seedlings were approximately half the height of unflooded seedlings after 60 days (Kozlowski, 1984).

1.2.5.3 Factors effecting leaf angle

Epinasty, leaf abscission and wilting are all significant responses to waterlogging in relation to this study because they affect leaf angle. Epinasty can occur within 48 hours of flooding (Jackson and Campbell, 1976) while wilting can occur within minutes or hours of flooding (Jackson and Drew, 1984); these are relatively rapid responses. Leaf angle influences spectral reflectance (this is discussed in greater detail in section 2.1.4.). The typical epinasty and wilting response is for leaves to droop. This means that more horizontally orientated leaves become closer to the vertical plane and vertically orientated leaves come closer to the horizontal plane. Similarly, with leaf abscission leaf angle becomes more or less acute depending on the original orientation of the leaves. These responses are, however, species dependent and not all species respond in this way.

1.2.5.4 Factors effecting chlorophyll

Premature senescence is yet another response by some species to waterlogging. Studies on barley crops have shown that chlorosis occurs after 2 days, resulting in a breakdown of nitrogen uptake (Drew and Sisworo, 1977). Trought and Drew (1980a) propose that nitrogen uptake in wheat is inhibited by the absence of dissolved oxygen in the soil water 1 day after flooding. This is another factor to consider from a remote sensing perspective as chlorophyll absorption influences reflectance in the blue and red wavelengths.

1.2.6 Summary

In this chapter the management of water in England and Wales has been considered, and the main problems associated with detecting water leakage have been identified. These problems particularly relate to efficiency, cost, accuracy and precision of current methods. How leaks tend to occur has also been discussed along with seasonal leakage patterns. The morphological and physiological effects of inundation on vegetation were established showing that waterlogging has a direct effect on plants. The effects that were considered in most detail were those that could potentially be identified using a remote sensing system i.e. changes in; internal leaf structure, leaf area, canopy height, leaf inclination angle, and chlorophyll content. In the following chapter some examples of real leaks in the field are considered, as well as leaks that were simulated.

References

Ashraf, M. and Habib-ur-Rehman. 1999. Interactive effects of nitrogen and long-term waterlogging on growth, water relations, and gaseous exchange properties of maize (*Zea mays* L.). Plant Science, **144**, 35-43.

Drew, M. C. and Sisworo, E. J. 1977. Early effects of flooding on nitrogen deficiency and leaf chlorosis in barley. New Phytologist, **79**, 567-571.

Jackson, M. B. 1979. Rapid injury to peas by soil waterlogging. Journal of the Science of Food and Agriculture, **30**, 143-152.

Jackson, M. B. and Campbell, D. J. 1976. Waterlogging and petiole epinasty in tomato: the role of ethylene and low oxygen. New Phytologist, **76**, 21-29.

Jackson, M. B. and Drew, M. C. 1984. Effects of flooding on growth and metabolism of herbaceous plants. In Flooding and Plant Growth, 47-128. Edited by T. T. Kozlowski, Academic Press Inc. London.

Lambert, A. and Morrison, J. 1996. Recent developments in application of bursts and background estimates: concept for leakage management. The Chartered Institution of Water and Environmental Management Journal, **10(2),**11-14.

Kozlowski, T. T. 1984. Responses of woody plants to flooding. In Flooding and Plant Growth, 129-163. Edited by T. T. Kozlowski, Academic Press Inc. London.

Kozlowski, T. T. and Pallardy, S. G. 1984. Effects of flooding on water, carbohydrate, and mineral relations. In Flooding and Plant Growth, 165-193. Edited by T. T. Kozlowski, Academic Press Inc. London.

Letey, J., Stolzy, L. H., Valoras, N. and Szuszkiewicz, T. E. 1962. Influence of oxygen diffusion rate on sunflower growth at various soil and air temperature. Agronomy Journal, **54**, 538-540.

Letey, J., Stolzy, L. H. and Valoras, N. 1965. Relationships between oxygen diffusion rate and corn growth. Agronomy Journal, **57**, 91-92.

Luxmore, R. J. and Stolzy, L.H. 1969. Root porosity and growth responses of rice and maize to oxygen supply. Agronomy Journal, **61**, 201-204.

Meyer, W. S., Barrs, H. D., Mosier, A.R. and Schaefer, N. L. 1987. Response of maize to three short-term periods of waterlogging at high and low nitrogen levels on undisturbed and repacked soil. Irrigation Science, **8**, 257-272.

OFWAT. 2001. Leakage and the efficient use of water 2000-2001 report. http://www.ofwat.gov.uk/pdffiles/leakage.pdf

Ponnamperuna, F. N. 1984. Effects of flooding on soils. In Flooding and Plant Growth, 9 – 45. Edited by T. T. Kozlowski, Academic Press Inc. London.

Tang, Z. C. and Kozlowski, T. T. 1982. Physiological, morphological and growth responses of *Platanus occidentalis* seedlings to flooding. Plant Soil, **66**, 243-255.

Trought, M. C. T and Drew, M. C. 1980a. The development of waterlogging damage in wheat seedlings (*Triticum aestivum* L.). Shoot and root growth in relation to changes in the concentrations of dissolved gases and solutes in the soil solution. Plant Soil, **56**, 77-94.

Trought, M. C. T and Drew, M. C. 1980b. The development of waterlogging damage in young wheat plants in anaerobic solution cultures. Journal of Experimental Botany, **31**, 1573-1585.
Wenkert, W. Fausey, N. R. and Watters, H. D. 1981. Flooding responses in *Zea mays* L. Plant Soil, **62**, 351-366.

Zhou, W. and Lin , X. 1995. Effects of waterlogging at different growth stages on physiological characteristics and seed yield of winter rape (*Brassica napus* L.). Field Crops research, **44**, 103 - 110

1.3 Study Areas

1.3.1 Introduction

This chapter introduces the study areas that were used in this project to provide ground-based measurements of a variety of different crops at different growth stages. They include real and simulated leaks situated over the Vrynwy aqueduct (Cheshire) and simulated leaks against a variety of agricultural crops around Edinburgh. The purpose of the Cheshire field area was to obtain measurements of real leaks (and prolonged simulated leaks) in the field. The purpose of the Edinburgh-based field area was to extend the number of leak measurements by simulating leaks over different crops at a variety of growth stages, as the number of real leaks and the range of landcover types in the Cheshire field area were relatively few.

The Cheshire field area was defined by the path of the Vyrnwy aqueduct which runs north from Powys, mid Wales to Merseyside, in England (Figure 1.3.1). The area was chosen as it had a relatively high concentration of leaks. The second field area, located on the outskirts of Edinburgh, was chosen for ease of accessibility throughout the growing season.

1.3.2 Wales and north east England

1.3.2.1 Vyrnwy aqueduct

The Vyrnwy aqueduct is located in Wales and north west England (Figure 1.3.1), it is within the network area of United Utilities (formerly North West Water) and maintained by them. It is 110 kilometres long and runs from Powys in mid Wales to Prescot in Merseyside. It supplies 20% of

the water for Merseyside and Cheshire (Aikman and Boyle, 1990; Critchley and Aikman, 1994). The aqueduct consists of three parallel pipelines (and a fourth that runs between Vyrnwy and Oswestry); this makes a total of 328 kilometres of pipeline. Most of the pipelines work on a partially pressurised gravity flow system with four 'booster' stations at Oswestry, Bickerton, Norton and Cuerdley (Aikman, 1993). The pipelines are made of a variety of materials – the first two built were made from cast-iron and were completed in 1905. The third pipeline was made of bitumen lined and coated steel and was completed in the 1940s, and the fourth was made from welded steel and was completed in 1949 (Kottman, 1988; Aikman and Boyle, 1990; Aikman, 1993; Critchley and Aikman, 1994). Each of these materials, combined with their differences in age, has a different propensity to leakage and bursts.

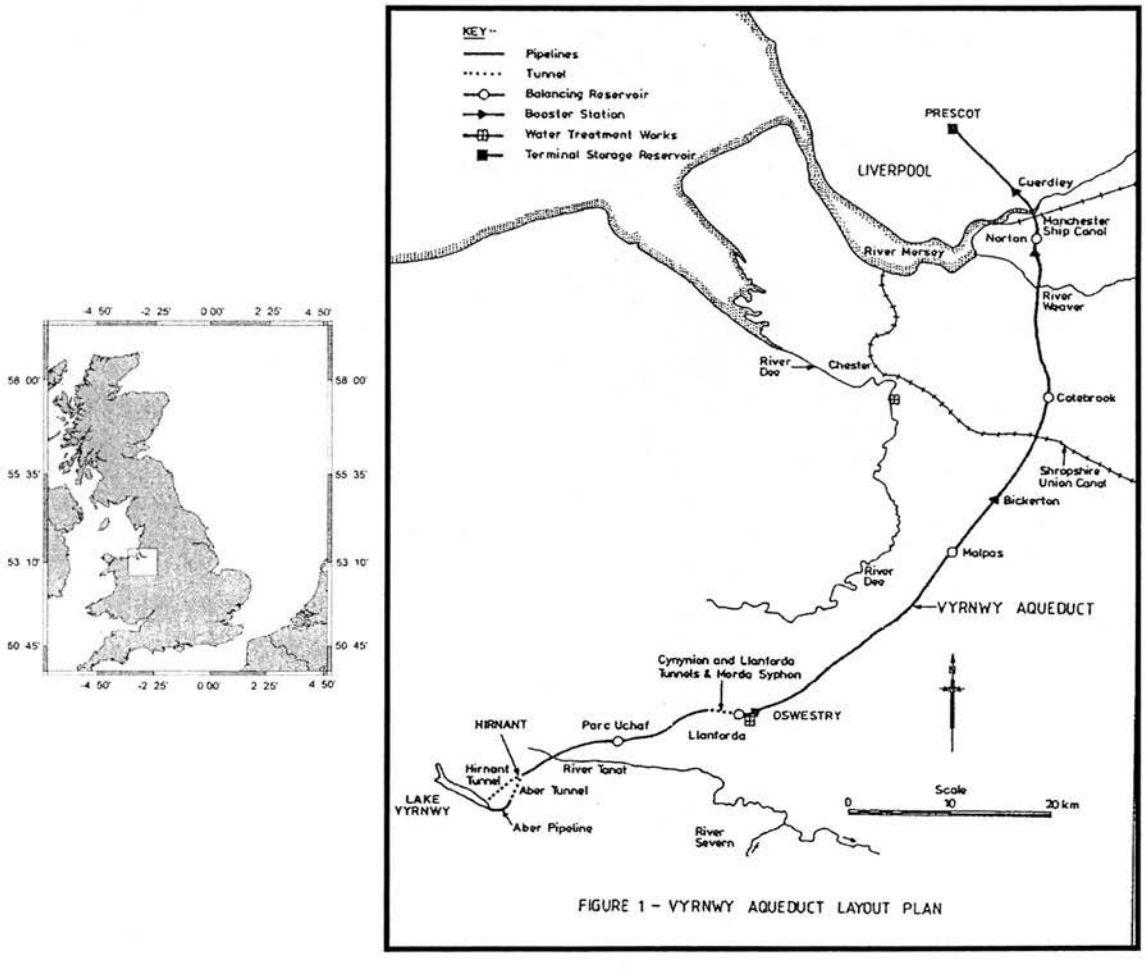

Figure 1.3.1 Cheshire field area location maps. Copied with permission from United Utilities.

Over the 110 kilometres, the path of the aqueduct passes through a variety of land cover types; it crosses several small urban centres and a large section of Liverpool. However, the majority of the aqueduct passes through rural agricultural areas. Topography and landuse vary from the hilly pastures of Wales to relatively flat arable land and livestock grazing in Cheshire. There are small patches of forest and woodland and the aqueduct crosses several rivers and canals. The underlying geology is mainly Lower Silurian in Wales, and Keuper Marl in Cheshire.

1.3.2.2 Choice of field sites

The SAR and Hyperspectral Airborn Campaign (SHAC) in 2000 provided the main source of imagery for this study (the SHAC campaign and image data products are described in more detail in the next chapter). Data provision was limited to a flight line 8 kilometres in maximum length. Therefore, the section of pipeline chosen for detailed study was selected based on a high concentration of leaks in any 8 km stretch along its path. There were seven known leaks along the Vyrnwy aqueduct at the time of data acquisition, all of which were investigated during a reconnaissance trip to the field area in March 2000. The most important factors in deciding what made a 'suitable' leak were determined by several variables:

- Proximity to boundaries. It was considered that if a leak were too near to a field boundary (within a pixel distance – or 3 metres) then the leak may be difficult to locate from an air or spaceborne remote sensing system due to mixed pixels.
- Topography; an optimum site would be one that was relatively flat to maximise leak ponding at the surface and prevent the water draining away due to the gravitational effects of hillslope geometry on water.
- It was important for the leak to be surrounded by a relatively homogeneous cover type, for example a crop, to maximise identification, in keeping with the study aims.
- Ease of access for field investigation.

After these factors had been taken into consideration a section of pipeline with four known leaks was chosen. The location of the leak sites are shown in Figure 1.3.2. In order to increase the number of leaks at the time of acquisition a further two leaks were simulated prior to the flight line being flown.

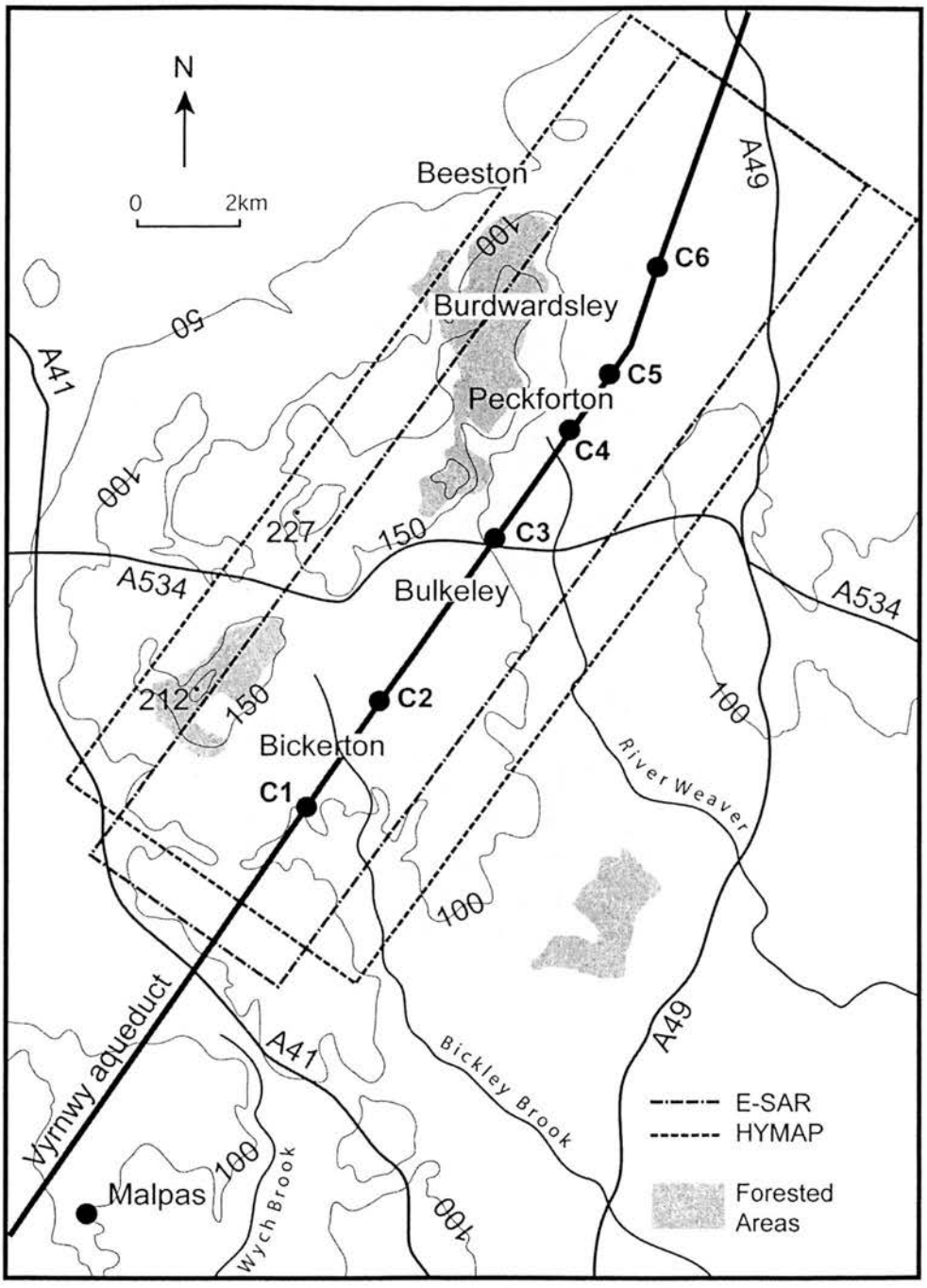

Figure 1.3.2 Cheshire field site location map depicting leak locations (C1 C6) and flight line boundaries for the radar (ESAR) and optical (HYMAP) data acquisition. N.B. C2 and C5 were simulated leaks, the remainder were real leaks.

1.3.2.3 Detailed description of study area

The section of aqueduct selected for this study and for the SHAC campaign lies between the villages of Malpas and Bunbury. This part of Cheshire is relatively flat and the main land use is arable farming with some livestock grazing and small patches of woodland and forest. At the time of data acquisition (growing season of 2000) the vegetation was mainly silage grass, and grazing pasture. There is a short spine of forested hills with an average altitude of 200 metres above msl running from Larkton Hill to Peckforton, parallel to and west of the aqueduct. The local geology is largely Triassic Keuper marl or Triassic Bunter sandstone and the drift maps of this region show a predominance of fluvio-glacial gravel and boulder clays. The soil of the region is characterised by well-drained non-calcareous gleys (King, 1977). A summary of leak site characteristics is given in Table 1.3.1, following a description of the leaks.

1.3.2.4 Detailed description of each leak site

Each of the leaks were characterised in different ways. The leak at C1 had been present for a long time (up to one year). It was located within 3.5 metres of a south western facing field boundary. The leak was in a wheat field and had been present long enough to have a detrimental effect on vegetation. In and around the leak there were no wheat plants present at all, the vegetation had been replaced by grass and low lying weeds. There was a large area around the leak where the wheat crop was also absent (Figure 1.3.3a) the reason for this is unknown, but perhaps the leak had been larger in the past. The conditions of the leak varied dramatically between the ESAR and HYMAP acquisition days, during the wet weather accompanying the ESAR field campaign there was a leak 20.8 x 18 metres. However, 16 days later when we came back for the HYMAP ground campaign – there was no surface water present at all, only bare soil, grass and weeds. This makes C1 a non typical leak site for optical analysis of presence of water.

Leak 2 was surrounded by grass and located in a field of grazing sheep. This was a simulated leak and a hose-pipe and sprinkler were left running for 12 hours before both the ESAR and HYMAP flightlines were flown. It was located in a natural depression that was poorly drained and liable to ponding lying directly over the aqueduct. As such this 'leak' behaved more like a leak than leak 1, for the acquisition of the optical data (Figure 1.3.3b).

Leak 3 was located in a horse field where the grass was well-grazed and included meadow plant species. At this location the pipeline was only 15cm below the surface and it was possible to see the water bubbling out of the pipeline. The leak had been present long enough to have a negative effect on vegetation growth and much of the grass inside the leak had died. The vegetation that was present inside the leak was taller and more spindly than the surrounding grass (Figure 1.3.3c).

The leak at site C4 was subsequently not used in either study as it did not suit the leak criteria. Firstly, it was located in a tree-lined corridor that was 25 metres wide. The height of the trees and the width of the boundary made it difficult to locate the leak on the imagery. Secondly, the surrounding vegetation was not homogeneous, at least 11 different species (predominantly yellow flag, bramble, and wild garlic) were counted around the leak (Figure 1.3.3d).

Leak 5 was the second of the simulated leaks. It was located in a field of silage grass (uncut and cut, during ESAR and HYMAP flightlines respectively). Despite leaving a hose-pipe running prior to image acquisition the soil was so well drained that there was no surface ponding to speak of at the time of acquisition of either dataset. The soil was merely wetter compared with the surrounding area. It would provide a test to see whether it was possible to identify patches of wet soil (rather than ponding) under a vegetation canopy that had not been affected by the presence of water (Figure 1.3.3e).

Leak 6 was in a field that had been grazed but at the time of data acquisition appeared to be lying fallow. The main landcover was grass and thistles. The leak was different from leaks 2, 3 and 5 in that the vegetation in the leak was vigorous. The grass inside the leak was three times as long as the surrounding grass and the earth in the leak was springy and bog-like but it was restricted to an isolated patch (9.9 x 5.5 metres). United Utilities were not able to establish whether there was a leaking pipeline there or not. However, as there was standing water present it was treated as a leak for the purposes of this study (Figure 1.3.3f).

Table 1.3.1 Summary Table of Cheshire field sites

Leak	Location	Altitude (m above MSL)	Land use	Vegetation description	Soil series	Soil texture	Leak dimensions (m)
C1	SJ 510 514	100	Arable land	Barley - vegetation still green but with well developed ears – just prior to ripening	Blackwood	Sandy loam	No water present
C2 *	SJ 517 525	120	Sheep grazing	Grazing grass – green and approx. 7.3 cm high	Clifton	Loamy sand	4.4 x 16.8
C3 †	SJ 533 548	95	Horses field	Grazing grass – yellow/green short cropped grass with buttercups and daisies	Clifton	Loamy sand	6.2 x 6.2
C4	SJ 539 559	80	Woodland	Under-story of wetland vegetation and scrub in a tree-lined corridor	Rufford	Sandy clay	28.2 x 19
C5 *	Sj 542 564	80	Arable land	Cut silage grass – yellowing, one week after second harvest – approx. 18cm	Newport	Loamy sand	5 x 5
C6	SJ 547 575	80	Arable land	Grazing grass – green and approx. 3.5 cm high	Newport	Silty clay loam	9.9 x 5.5

* Indicates sites where leaks were simulated

† Sites that were not included in the study

Figure 1.3.3 Photos of field sites C1-C6.

1.3.3 Edinburgh

1.3.3.1 Choice of field sites

The fieldwork around Edinburgh focussed on reflectance measurements of simulated leaks at ground level over a variety of landcover types at different crop growth stages. The site requirements were thus slightly different from those in Cheshire. The factors controlling site selection were access to water supply, vegetation type, access permission and easy vehicle access. To simulate leaks a nearby water supply was vital. A variety of land covers were necessary for this work to obtain measurements over a number of canopy types, for example continuous canopy, row crops and grass. Permission to perform measurements was required from the landowners and because the equipment used was relatively heavy and it was important to have vehicle access to the sites.

Four sites were selected within three different landcover types. The selected sites provided examples of different continuous canopies and included; spring barley, winter barley and oil seed rape (Figure 1.3.4). Access to farms growing row crops (e.g. potatoes) was sought but denied. It was considered that the field sites in Cheshire provided sufficient examples of grassland canopies.

1.3.3.2 Detailed site description

All the Edinburgh sites, except for site E4, lie in Midlothian between the Pentland Hills to the north west, and the Moor Foot and Lammermuir Hills to the South east (Figure 1.3.4). The area is mainly agricultural, predominantly flat pasture, arable and animal grazing land, interspersed with small patches of woodland and urban areas. Field site E4 was located to the west of the city near Edinburgh Airport. The surrounding area consists of built-up areas and crop farms. The geology around Edinburgh is mixed, however, at most of the field sites the underlying geology comes from the oil-shale group, consisting of; sandstones, mudstones, siltstones, bitumen shales, marine and freshwater limestones. The soil types at the field sites are generally acidic, brown forest soils or non calcareous gleys and vary from being 'freely drained' to 'imperfectly drained' (Bown and Shipley, 1982).

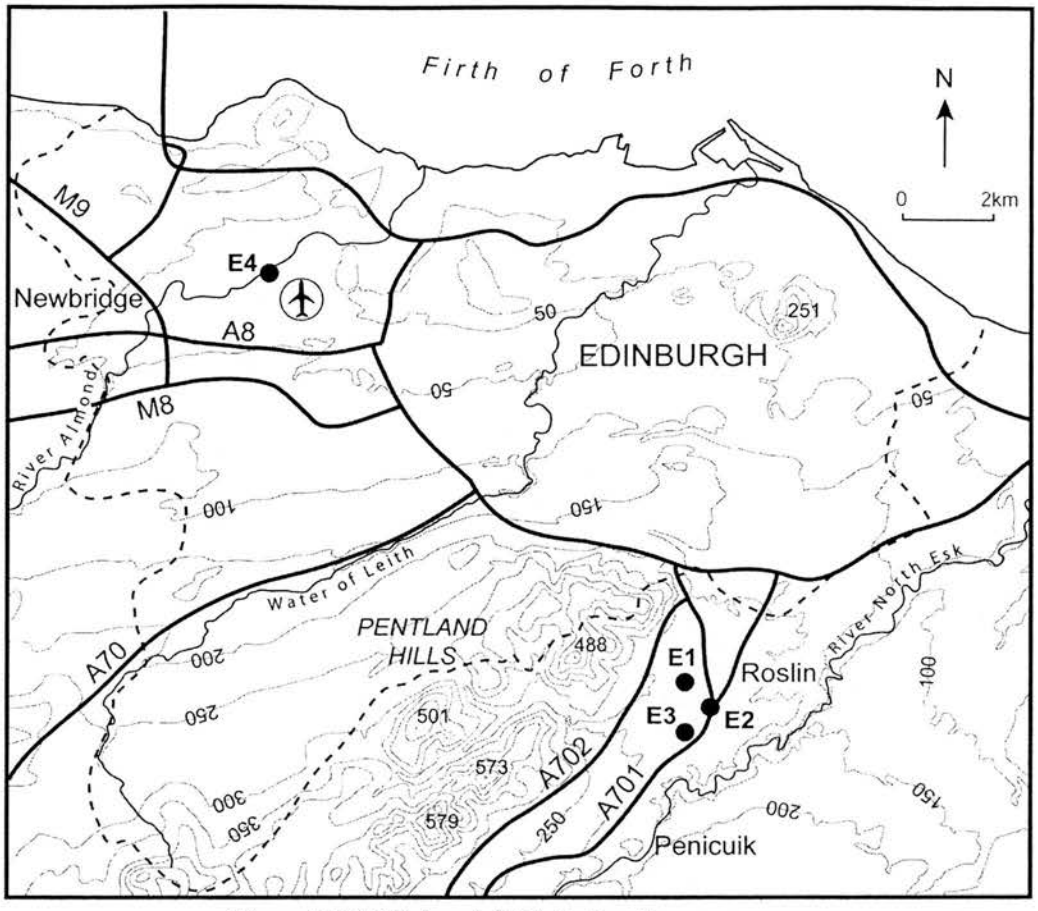

Figure 1.3.4 Edinburgh field site location map.

1.3.3.3 Detailed description of sites

The measurements taken at site E1 - Boghall farm were of winter barley at three separate 'growth' stages. The first measurements were taken when the barley crop was ripening, the crop had begun to develop ears that were green in colour. The second series of measurements were taken when the barley was ripe in early August 2000, two weeks before harvest. The third series of measurements were taken following crop cutting, these measurements were of stubble (not technically a growth stage) and were taken towards the end of August 2000. The topography within the field was flat, and water for leak simulation was taken from a mobile bowser provided by the farmer.

Two sets of oil seed rape measurements were made at site E2 – Gas house. Both sets of measurements were taken in summer 2000 at later growth stages. The first growth stage recorded was post flowering while the oil seed rape canopy was developing seed pods. The last series of measurements were made of the crop once it has desiccated, just prior to harvest. Water supply came from a nearby disused house, and two 50m hose pipes were used to transport water for leak simulation. The topography of the field was gently sloping from west to east.

At site E3 – Glen Corse, one leak was simulated beneath a spring barley crop. Measurements were taken when the spring barley was young and grasslike. Water supply came from a mains pipe attached to a water trough in a neighboring field. The soil at site E3 was well-drained – therefore surface ponding was difficult to achieve. The field has a south facing aspect and slopes from north to south.

Three leaks were simulated at site E4 - the airport farm, underneath an oil seed rape crop at three growth stages (i) when the crop was young (one month after planting), (ii) when the crop was beginning to mature (seven weeks after planting) and (iii) when the crop was in flower (ten weeks after planting). Water was supplied by the farmer in the form of polythene tank mounted on palettes in the field where the measurements were made. The soil was well-drained and surface ponding was again difficult to achieve, particularly as the water supply was more limited at this site than the others. The topography of the field was flat.

Table 1.3.2 provides a summary of the Edinburgh based field sites used for simulating leaks against a variety of vegetation backgrounds and growth stages.

Table 1.3.2 Summary table of Edinburgh field sites.

Site	*Name*	**Altitude (m above MSL)**	**Land use**	**Vegetation description**	**Soil type**	**Soil texture**
E1	Boghall farm	190	Arable land	Winter barley – beginning to ripen - stubble field	Macmerry or Darvel	sandy clay loam
E2	Gas house	190	Arable land	Oil seed rape – later growth stages, post flowering	Undifferentiated alluvial soils	silty clay loam
E3	Glen Corse	190	Arable land	Spring barley – early growth stages - ripening	Macmerry or Winton	clay loam
E4	Airport farm	40	Arable land	Oil seed rape – early growth stages - flowering	Macmerry or Queensferry	sandy clay

References

Aikman, D. I. 1993. Airborne thermal survey: Thirlemere aqueduct. Babtie Shaw and Morton, Preston.

Aikman, D. I. and Boyle, D. A. 1990. An assessment of the integrity of ageing large diameter trunk water mains: Vrynwy aqueduct 1888 - 1988, Pipeline Management. June.

Bown, C. J. and Shipley, B. M. 1982. Soil Survey of Scotland. South-east Scotland, 1:250 000 sheet 7. Published by The Macauley Institute for Soil Research, University Press Aberdeen.

Critchley, R.F. and Aikman, D.I. 1994. Aqueduct management planning: Thirlemere, Haweswater and Vrynwy aqueducts. Institution of Water and Environmental Management Journal, **8**, 502-512.

Kottman, A. 1988. Is the age of cast iron pipe a criterion for its renewal? RRR International 1988, **27(1)**, 55-88.

King, S. J. 1977. Soils in Cheshire III. Soil Survey Record No.43, sheet SJ45E/55W (Burwardsley). Bartholomew Press.

1.4 Remote sensing image data

1.4.1 Introduction

Two flight lines were obtained for this study as part of the SAR and Hyperspectral Airborne Campaign (SHAC). The first image to be acquired was active microwave fully polarimetric E-SAR data, obtained on 3rd June 2000, and the second was HYMAP hyperspectral data obtained on 19th June 2000. This chapter outlines the acquisition strategy that was developed prior to the flight lines being flown and introduces the image data that were acquired for this study. The processing of the data is then considered.

1.4.2 The SHAC campaign

The objective of the campaign was to support academic and industrial Earth Observation research and applications development:

- as a tool for environmental research
- to prepare for planned satellite based SAR and hyperspectral missions (e.g. ENVISAT, TerraSAR.)

32 proposals were submitted of which 14 were selected based on scientific excellence, novelty, applications development potential and collection of common datasets by a joint academic/industrial review committee. It was sponsored by the Natural Environment Research Council (NERC) and Department of Trade & Industry (DTI), both partners of the British National Space Centre (BNSC).

1.4.3 Image acquisition strategy

An image acquisition strategy was devised based on knowledge of existing leaks at the time of acquisition. It was requested that the hyperspectral HYMAP and E-SAR L-band fully polarimetric radar coverage of the selected target sites were acquired concurrently to allow for direct comparison of the two datasets. As the leaks were relatively small in size 3m resolution data were requested for both acquisitions, with a 1.3 km swath for the HYMAP data take, and a 3 km swath for the E-SAR instrument. An acquisition time of near to mid-day and under clear overhead conditions were requested for the optical data, to reduce shadow effects and to minimise atmospheric interference creating a low signal to noise ratio. A further condition imposed on the timing of the acquisition was that the data were collected after a prolonged period of no rain (10 days or greater), to ensure that there was significant contrast between wet leak and dry surrounding vegetation. A summary of the ideal conditions forming the basis of strategy are outlined below:

1.4.3.1 SAR data

Waveband region:	L-band
Spatial resolution:	3m or less
Timing - Time of day:	not important
Timing - Time of year:	mid-summer
Timing - other considerations:	after a period (10 days or more) of no rain
Weather conditions during acquisition:	dry, to maintain contrast between leaks and surrounding areas.

1.4.3.2 Optical data

Spectral resolution:	Preferably hyperspectral for optical data
Spatial resolution:	3 m or less
Timing - Time of day:	mid-day
Timing - Time of year:	mid-summer
Timing - other considerations:	after a period (10 days or more) of no rain
Weather conditions during acquisition:	Clear

Not all the acquisition strategy conditions were met. The DLR plane used for acquiring the imagery was unable to accommodate both the HYMAP and E-SAR sensors. The HYMAP and E-SAR imagery were acquired 15 days apart. With the timing conditions imposed by the SHAC co-ordinators it was not possible to significantly influence timing with respect to the dryness of conditions. Conditions during the E-SAR acquisition were far from ideal with heavy rain falling during the over-flight and with significant periods of rain in the days leading up to the campaign. This meant that soils were saturated during the acquisition. In contrast to the E-SAR campaign, conditions for the HYMAP data takes were near ideal, with very clear overhead conditions and dry soils creating good contrast between leaks and surrounding vegetation. The campaign was pre-planned to be flown in July 2000, therefore, we were unable to influence the timing of acquisition with regard to the choice of month. At the time of acquisition this did not pose a problem as the optimal months for data capture were unknown. However, results presented later in this thesis show that the timing of acquisition is an important factor of leak identification.

Despite the limitations imposed on the ideal acquisition scenario, good data were acquired with the only factors affecting results being the highly inclement weather during the E-SAR acquisition and the temporal separation between the two flight lines.

Figure 1.4.1 summarises precipitation and Soil Moisture Deficit conditions leading up to each campaign, using meteorological data that were obtained from the weather station nearest to the target area. Relatively high precipitation levels before the acquisition of the E-SAR image had caused fully saturated soil conditions (soil moisture deficit of 0 mm). 25 mm of rain also fell on the 3rd of June when the E-SAR data were acquired. Relatively low levels of precipitation in the following weeks had enabled significant drying of the soil by the time of the HYMAP image acquisition on the 18th and 19th of June (soil moisture deficit of greater than 30 mm, Figure 1.4.1).

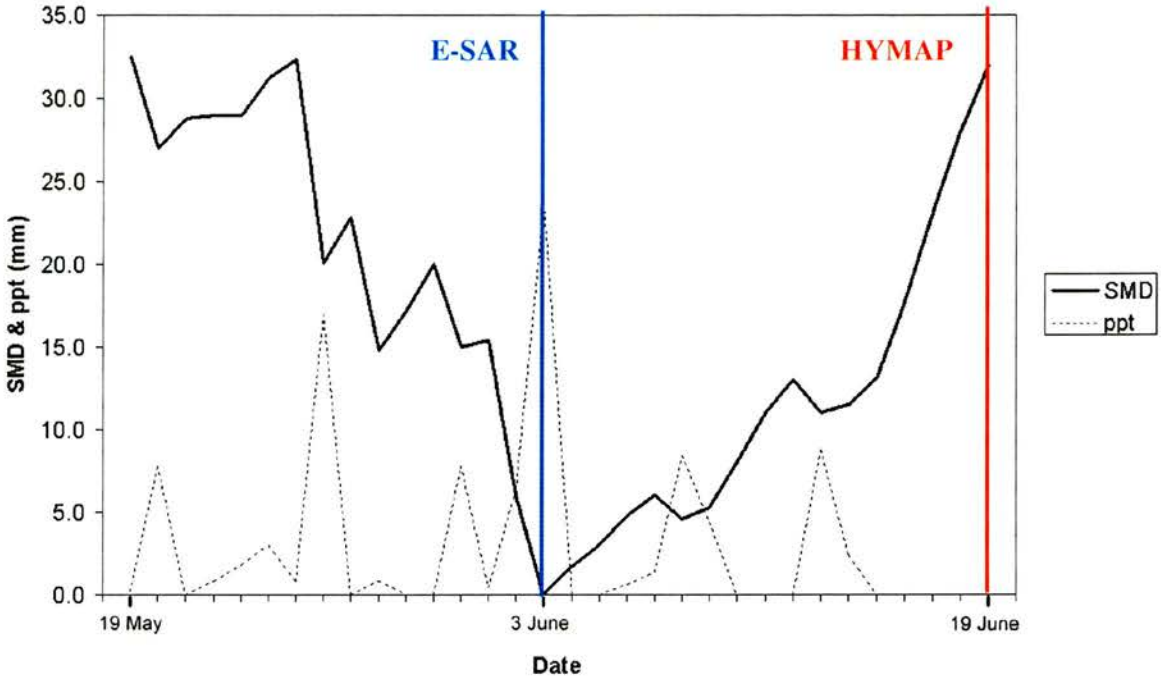

Figure 1.4.1. Measured precipitation (ppt) and estimated soil moisture deficit (SMD) for a grass crop type (Keele weather station, 3819E, 3446N).

1.4.4 The data

Tables 1.4.1 and 1.4.2 provide a summary of the HYMAP and E-SAR image parameters respectively. Both flight lines covered the same section of the Vrynwy aqueduct as indicated in Figure 1.3.2.

Table 1.4.1 HYMAP Image parameters.

Date	18-JUN-2000
Time	09:14:00
Output pixel size	3.0
Average aircraft altitude (masl)	1571
Average scene elevation (from GTOPO30 DEM)	110.3m

Swath width	60-70° (approximately 1.3km)
Signal to noise ratio	> 500:1
No. channels	126
Spectral range	437 – 2486 nm
Spectral bandwidths	10-20 nm
nadir across track spacing	2.97 m

Table 1.4.2 E-SAR Image parameters.

Date	03-JUN-2000
Time	09:59:34
Resolution	2.2 m x 3.0 m (Range and Azimuth)
Aircraft altitude	3012 m
Near range	3325 m
Ground speed	87 m/s
Antenna depression angle	40^0
Centre frequency	1.30 GHz
Pulse Repetition Frequency (PRF)	400 Hz
Number of looks	4
Band	L – band
Polarisation	Fully polarised, HH, VV, HV/VH (calibrated scattering matrix)

Figures 1.4.2 and 1.4.3 are false colour composites of the HYMAP and E-SAR images respectively.

Figure 1.4.2 False colour composite of hyperspectral image in 16 channels.

Figure 1.4.3. Geo-corrected E-SAR image (False colour composite of σ^0, HH, VV and HV/VH polarisations).

1.4.5 HYMAP post processing

1.4.5.1 From radiance to reflectance

The HYMAP data products were geo-corrected radiances which were processed to create reflectances prior to data delivery. A scaling factor was applied to the radiance files; Bands 1-62 (x1000) and Bands 63-126 (x4000). Reflectances were calculated using the HYCORR correction software which combines ATREM (atmospheric model) and EFFORT correction. The atmospheric parameters used in HYCORR were; setting the Aerosol model to continental, and setting the atmospheric model to mid latitude summer.

1.4.5.2 Atmospheric correction

HYMAP data were atmospherically corrected as part of the SHAC acquisition using the ATmospheric REMoval program ATREM, which simulates atmospheric transmittance using the Malkmus narrow band (Perry *et al.*, 2000). Several limitations and error sources with ATREM exist including: (i), limits in its ability to model the effect of haze; (ii), the assumption of no topographic variation; and (iii), the asumption that the surface has Lambertian reflectance (Gao *et al.*, 1993). ATREM's ineffectiveness at modelling haze meant that the leak spectral indices developed were confined to wavelengths greater than 550 nm. To compensate for the assumption of no topographic variation, the retrieved "scaled surface reflectance" data acquired by the HYMAP sensor were converted to 'true reflectance' using topographic normalisation. It was not possible to compensate for the assumption of a lambertian surface as no data existed on the BDRF's of the surfaces imaged by the HYMAP sensor.

1.4.5.3 Geometric correction

Geometric correction of the HYMAP imagery was achieved using a rubber sheeting technique. Rubber sheeting is more accurate than rectification based on a single globally-based polynomial (Devereux *et al.*, 1990) as the local changes in polynomical coefficients provided by a TIN can compensate for the effects of local image distortion caused by topographic variation. This local distortion is relatively large in airborne images because of the relatively low altitude flown by planes. For the purposes of geometrically correcting the HYMAP imagery, 150 ground control

points (GCPs) were established using easily delineated features within the imagery (field boundary intersections, road intersections, building corners) and Ordnance Survey (OS) vector boundary data. The accuracy of the geometric rectification was qualitatively analysed by superimposing OS vector boundary data on the rectified HYMAP image. There was little discrepancy between the vector boundary data and the overlain rectified image (an example is shown in Figure 1.4.4)[1]. Unfortunately there is no available data which quantitatively describes the accuracy of the geometric correction.

Figure 1.4.4. Example of OS vector boundary data superimposed on geometrically rectified HYMAP imagery. Vector boundary data are shown by black lines.

1.4.6 SAR post processing

The initial processing of the E-SAR data was carried out at QinetiQ by Alex Rodriguez and Susan Andrews. It involved image calibration, speckle reduction and geocorrection. A summary of the steps involved is given here.

1.4.6.1 Absolute SAR radiometric calibration

Radiometric calibration was automatically performed by DLR. To independently assess the calibration, a calibration target (trihedral corner reflector) was also deployed in the corner of the field at site C2 during imaging (co-ordinates 53 04 07.568 N and 2 43 12.547 W). This is shown in Figure 1.4.5.

[1] The work described in this section was carried out by Richard Hedger, formerly in the Department of Geography, University of Edinburgh.

The polarimetric response of the calibration target was checked using QinetiQ polarimetric calibration software and the Inter-polarimetric-channel crosstalk was less than -40 dB. HH/VV intensity ratios were offset by no more that 0.1 dB and the HHVV phase imbalance was less than 5 degrees.

Figure 1.4.5. SAR Trihedral calibration target used for absolute calibration of the E-SAR data.

1.4.6.2 Speckle reduction

Speckle is a characteristic feature of SAR data and arises because SAR is a coherent imaging process. Speckle is manifested as a noise-like graininess in the images. This graininess makes quantitative measurements over small areas difficult. There are many techniques for reducing speckle in SAR data. The method chosen for this study was developed at the United States Naval Research Laboratories by Lee *et al.*, (1999). This method is especially beneficial for polarimetric SAR data, as it ensures that each of the polarimetric channels is filtered independently – in this way the polarimetric calibration of the channels is preserved. The filter can be operated on square windows of 3 sizes: 5 by 5 pixels, 7 by 7 pixels and 9 by 9 pixels. A 7 by 7 window was used for this study.

The Lee filter also uses edge detection to perform adaptive filtering. One of 8 possible filtering windows is selected according to the local statistics of the data. The adaptive filtering helps

preserve linear features (for example field boundaries) in the data. Figure 1.4.6 shows an example of the E-SAR data pre- and post- speckle filtering. The speckle reduction process did significantly alter the image spatial resolution, degrading the E-SAR resolution from 3 to approximately 9 metres.

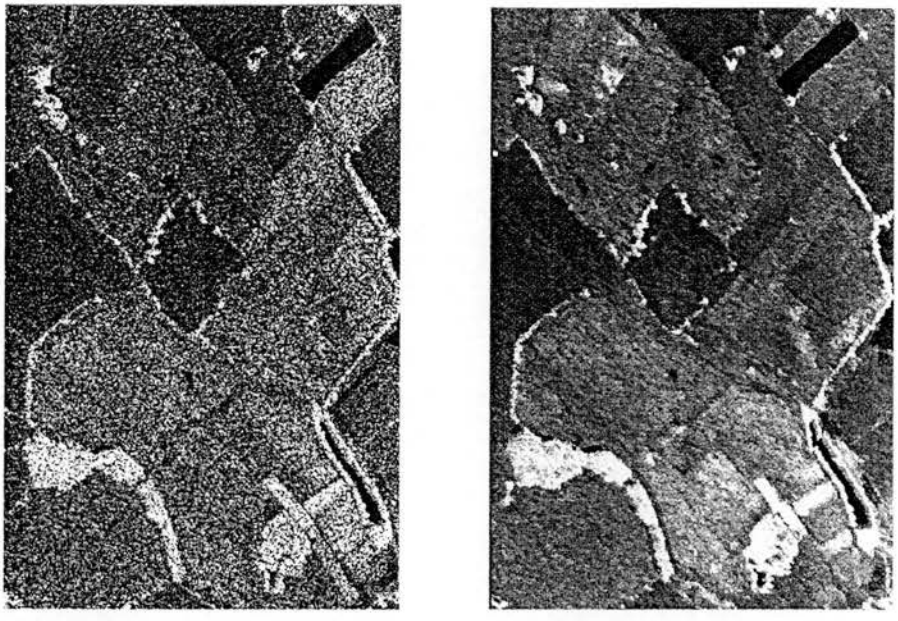

Figure 1.4.6. Adaptive, polarimetric speckle filtering. Pre-filtering (left), post-filtering(right). Courtesy of Rodriguez, QinetiQ.

1.4.6.3 Terrain correction and geolocation

SAR is an oblique-viewing, range-finding system by design. If the local terrain height varies, this method of imaging can introduce local distortions in the image. If the SAR data is to be coregistered to other image data, it is essential that these distortions are removed. By using ancillary local height information, the terrain correction process removes these image distortions. This ancillary height information is provided by a Digital Elevation Model (DEM). In order to correct for the terrain variations in the Vyrnwy scene, a 50 m resolution DEM of the scene was used. The SAR data were then geo-referenced manually using the already geo-located HYMAP data as a reference.

1.4.7 Data summary

The image data that we use from this point onwards in the study is fully polarimetric, L-band geocoded and speckle reduced E-SAR data, with a spatial resolution of approximately 9 m. The optical data is 126 channel, geocorrected, hyperspectral image data with 3 m resolution.

References

Devereux, B.J., Fuller, R.M, Carter, L. and Parsell, R.J. 1990. Geometric correction of airborne scanner imagery by matching delaunay triangles. International Journal of Remote Sensing, **11,** 2237-2251.

Gao, B. –C., Heidebrecht, K. B. and Goetz, A. F. H. 1993. Derivation of scaled surface reflectances from AVIRIS data. Remote Sensing of Environment, **44**, 165-178.

Lee, J.S., Grunes, M.R., Ainsworth, T.L. Papathanassiou, K.B. and Reigber, A.1999. Speckle filtering of SAR data for polarimetric interferometry applications. IEEE Geoscience and Remote Sensing Symposium. IGARSS'99 Proceedings, **4** , 2203 -2205.

Perry, E.M., Warner, T. and Foote, P. 2000. Comparison of atmospheric modelling versus empirical line fitting for mosaicking HYDICE imagery. International Journal of Remote Sensing, **21,** 799-803.

2.1 Optical Background Theory

2.1.1 Introduction

Spectral reflectance is controlled by 3 electromagnetic energy interactions for any given surface – reflection, absorption and transmission. The proportions of reflection, absorption and transmission vary according to the feature being observed – this makes it possible to distinguish between features on the earth's surface, they also vary with wavelength allowing different features to be identified at different wavelengths. Figure 2.1.1 shows typical spectral reflectance curves for healthy vegetation, soil and water. Interpretation of spectral reflectance curves typically involves considering the general shape of the curve, the relative position of peaks and troughs, the gradient of the curve and the ratio of one part of the spectrum with another.

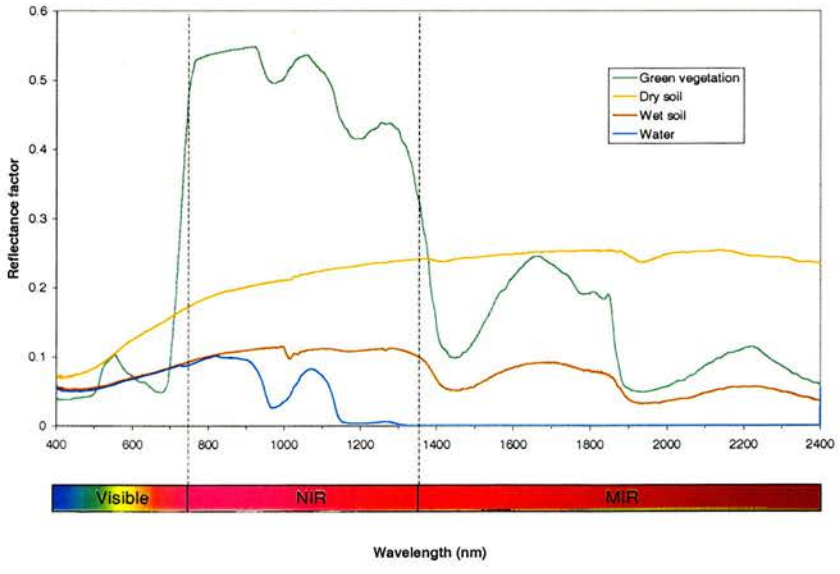

Figure 2.1.1 Graph showing typical spectral reflectance curves for green vegetation, soil and water.

In the specific case of identifying water leaks on a bare soil the problem of identification is relatively simple as water is the dominant influence on reflectance and significant differences between a rough bare soil surface and the specular water surface are apparent. As a result it is easy to distinguish between water, wet soil and dry soil (Figure 2.1.1). However, distinguishing between vegetation, soil and water is more complex due to the energy interactions between these variables and the large range of possible spectral responses.

This chapter considers the optical properties of soil, water, and vegetation separately, before looking at a combined spectral response. Important spectral trends that can be identified through changes to soil moisture content, vegetation height and density, and presence of standing water are highlighted. Vegetation indices are briefly discussed, followed by a short review of vegetation models.

2.1.2 Optical properties of soil

Soil spectral reflectance is strongly affected by colour, texture and moisture content. Surface roughness and presence of specific minerals and organic matter can also affect reflectance (Jackson *et al.,* 1978). Figure 2.1.1 presents 2 examples of wet and dry soil spectra in the 400 – 2400 nm region. Typically, the reflected radiant energy decreases with increasing water content (Jackson *et al.*, 1978). The important features to be seen are the water absorption bands around 1400 and 1900 nm, and the soil reflectance peaks around 1600 and 2200 nm.

2.1.3 Optical properties of water

A typical spectral reflectance curve for water shows a reduction in reflectance with increasing wavelength. Clear water reflects between 300 and 600 nm in the blue and green regions of the spectrum. Absorption occurs most strongly after 600 nm and particularly in absorption bands in the near infrared and in the middle infrared where reflectance is close to zero (Baret, 1991). Water absorption regions in the near-infrared bands have been used for detecting water whether

it is water bodies, or water contained in vegetation and soil. However, the spectral reflectance of water is also affected by concentration of dissolved and suspended organic and inorganic material. Specular reflectance also depends on the surface roughness of the water and the relationship between sensor and illumination source. Under calm flat conditions water may act as a specular reflector, whereas if there are waves on the water surface more scattering is likely to occur and thus reflectance will be strongly influenced. Depending on the surface state, electromagnetic radiation may either be absorbed, selectively absorbed by suspended and dissolved material or scattered by suspended particles. Strong bottom reflections have been shown to contribute significantly to the spectral signature of water (Spitzer and Dirks, 1987; Estep and Holloway, 1992). For studies on suspended matter the bottom contribution must be removed. However in this study, the water surfaces being considered are assumed to be flat (i.e. specular), shallow (never more than 15cm deep and thus are likely to have strong bottom reflectance contributions) and relatively small in area (maximum 20 x 20 m). However, as the remote sensing of leaks is concerned with gross differences relative to vegetation and soil, the need for detailed studies of water optics and water chemistry is negated. The possible influence from bottom reflectance has not been considered, particularly as the presence of water is not measured directly. The presence of water is most typically measured as the combined spectral response from water beneath a vegetation canopy.

2.1.4 Optical properties of vegetation

There can be large variations between different vegetation canopy spectra, due to the large number of variables contributing to the overall reflectance of vegetation. Most significantly these include:

- Soil colour and texture
- Soil moisture content
- Canopy geometry
- Canopy height
- Leaf pigment content
- Leaf angle
- Leaf size and shape
- Internal leaf structure

- Vegetation moisture content
- Vegetation biomass
- View angle
- Illumination angle

Despite the large number of variables affecting vegetation reflectance spectra, optical remote sensing lends itself to the identification of vegetation characteristics as it is sensitive to a large number of vegetation features. Some of the distinguishing features of vegetation in relation to optical remote sensing are considered further.

2.1.4.1 Leaves

Absorption, reflectance and transmittance of radiant energy by dense vegetation canopies is predominantly a function of its leaves, and more specifically of leaf physiology, pigment concentration, tissue water content and leaf surface characteristics at the scale of an individual leaf (Vogelman, 1993; Gausman, 1985; Curran, 1980; Gates, *et al.*, 1965). Leaf optical characteristics can be split into three main wavelength domains; the visible (400 – 750 nm), near infrared (750 – 1350 nm) and middle infrared (1350 - 2700 nm) (Figure 2.1.1).

Absorption in the visible wavelengths is predominantly controlled by pigment concentrations, particularly chlorophylls (Knipling, 1970; Woolley, 1971). This is perhaps most easily demonstrated by comparing the spectral reflectance of a green leaf, with a section from the white part of a variegated leaf which contains no chlorophyll (Figure 2.1.2). This example also reveals the lack of influence chlorophyll has on reflectance in the near infrared wavelengths beyond the NIR shoulder (around 740 nm), as the green and white parts of a variegated leaf show very similar reflectance beyond this point (Knipling, 1970; Woolley, 1971). In a separate study, isolated chloroplasts have been shown to absorb no infrared radiation (Woolley, 1971).

The main pigments found in higher plants are chlorophylls a and b, and carotenoids. Chlorophyll generally contributes the largest proportion of pigments in a green leaf (65%) with carotenoids making up the remaining 35%. Carotenoids absorb strongly in the blue region (around 445 nm), while chlorophylls absorb in both the red (centering around 670 nm), and blue regions. Leaf pigments do not absorb as much radiant energy in the green wavelengths. Hence the peak of

reflected light in the green (centering around 550 nm), giving leaves their characteristic green colour. In senescing leaves it is usual for chlorophylls to break down before the yellow, brown, orange or red carotenoid pigments, giving autumn leaves their characteristic colours. Therefore, in the absence of chlorophylls to absorb in the red region, absorption decreases with increasing wavelength leading to higher reflectance values in senescing leaves.

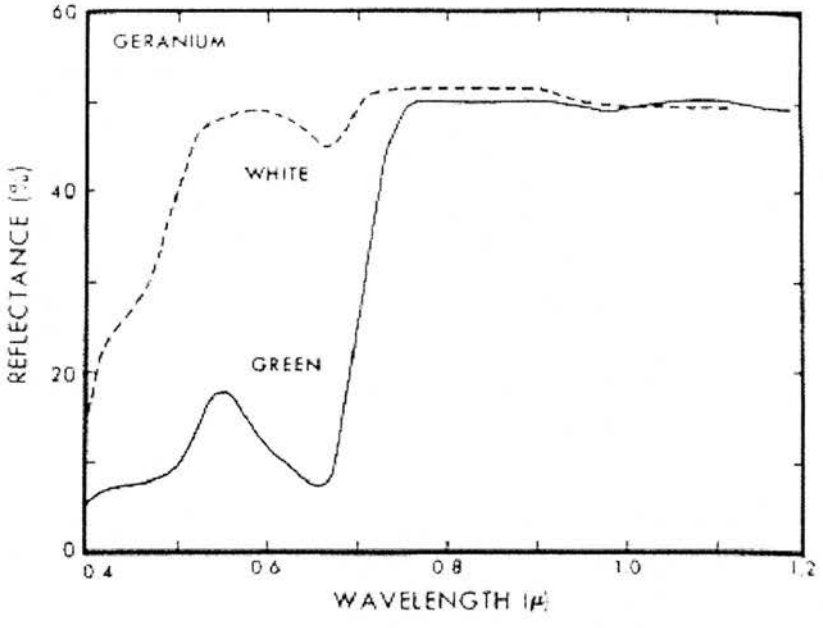

Figure 2.1.2 Spectral reflectance from the green (solid line) and white (dotted line) parts of a geranium leaf. Modified from Knipling 1970.

The maximum gradient of leaf reflectance occurs between approximately 690 and 740 nm, termed the 'red edge', and relates to the boundary between red and near infrared parts of the spectrum (Miller *et al.,* 1990). The position of the red edge or inflection point (IP) has been correlated with leaf and canopy chlorophyll content (Collins, 1978; Horler *et al.,* 1983; Lichtenthaler, 1995; Pinar and Curran, 1996). An increase in chlorophyll concentration causes a broadening of the chlorophyll absorption band at 670 nm therefore moving the position of the red edge inflection point towards longer wavelengths (Collins, 1978; Horler *et al.,* 1983;

Salisbury *et al.*, 1987; Boochs *et al.*, 1990). Canopy red edge characteristics have been correlated with estimations of canopy biomass, leaf area index, vegetation stress and maturity.

Reflectance in the near infrared (750-1350 nm) is largely controlled by internal leaf structure and little or no light is absorbed internally in this wavelength range; between 40 and 60% of the light is scattered upwards and the remainder is scattered downwards and transmitted (Knipling, 1970). Incident light is diffused and scattered through the epidermal and pallisade mesophyll layers of the leaf into the spongy mesophyll. Light is then further scattered by the hydrated mesophyll cell walls into the air spaces between cells, increasing leaf reflectance in the absence of pigments and in the near infrared (Vogelman, 1993; Gausman and Allen, 1973, Knipling, 1970). An increase in the number of intercellular air spaces leads to an increase in light reflectance due to the presence of large refractive index discontinuities between the air spaces and hydrated cell walls (Gausman, *et al.*, 1969). However, if the air spaces are filled with water or oil, thus reducing the refractive indices of internal air and cell surfaces, reflectance is significantly reduced revealing the importance of internal cell structure (Knipling, 1970; Woolley, 1971; Gausman and Allen, 1973). Changes in leaf structure and specifically the number of air spaces, change with species. Leaves of monocotyledonous plants are generally thin and compact with fewer air spaces while leaves of dicotyledonous plants have thicker leaves with spongy mesophyll and more air spaces (Baret, 1991; Danson, *et al.*, 1992; Gausman, 1985). Internal leaf structure also changes over time, with very young leaves tending to have larger numbers of air spaces. As a leaf matures internal tissue space can become more compact. This reverts during senscence where internal leaf structure breaks down and the number of air spaces increases. However these responses are somewhat species dependent (Gausman *et al.*, 1969; Gates, 1965).

Reflectance in the middle infrared region (1300 – 2500 nm) is influenced predominantly by leaf water content (Gates *et al.*, 1965; Knipling, 1970; Woolley, 1971; Carter, 1991). In the middle infrared strong absorption of radiation by leaf water content results in lower reflectance values with increasing leaf water content (Carter, 1991). Thomas *et al.*, (1966, cited in Tucker, 1980) showed that leaf water content accounted for 78 – 83% of the variability in reflectance between 1300 and 2500 nm. Tucker (1980) identified the wavelengths 1550 – 1750 nm as those most appropriate for monitoring plant water status from spaceborne sensors given solar spectral

irradiance and atmospheric transmission characteristics, whereas the 1480 – 1750 nm spectral interval was the best suited for ground-based monitoring. However, Ripple (1986), using other methods, showed that the best interval for identifying leaf water content was between 2080 – 2350 nm. It would appear that both these middle infra-red regions are effective although the wavelengths identified by Tucker - are more commonly cited in the literature. Many space-borne sensors do not operate in the longer middle infrared wavelengths due to sensor design constraints and the large contribution in this region from atmospheric noise. These factors have perhaps limited the value of the longer middle infra-red wavelengths identified by Ripple - for space-borne remote sensing studies.

2.1.4.2 Canopies

Canopy reflectance is typically less than that of an individual leaf because of attenuation by variations in illumination angle, leaf orientation, shadow effects, and non vegetated surfaces, e.g. soil (Knipling, 1970). However, canopy reflectance is still dominated by leaf reflectance. In order to understand canopy reflectance the other factors influencing canopy reflectance are considered further.

2.1.4.3 Surface characteristics, illumination angle and viewing geometry

In the absense of background influences vegetation canopy reflectance is affected by leaf angle distribution, view angle, incident light angle and wavelength (Goel, 1988; Norman *et al.*, 1985; Kimes, 1984). Specifically, the radiation scattered from a leaf depends on angle of incident radiation and scattering direction (Goel, 1988). Specular reflectance occurs when smooth surfaces (relative to the wavelength of incident energy) reflect energy at the same angle as the incident energy. Diffuse (or Lambertian) reflectance occurs when the reflecting surface is rough relative to wavelength, and the incident energy is scattered equally in all directions (Figure 2.1.3). Surface objects rarely behave as one or the other, but lie somewhere in between. There are variations in the specular properties of leaves due to the cuticle layer – with waxy leaves producing a more specular reflecting surface than leaves with non waxy cuticles.

Specular reflectance Diffuse reflectance

Figure 2.1.3. Diagramatic representation of specular and diffuse Lambertian reflectance.

Vegetation rarely behaves as a Lambertian reflector (i.e. it does not reflect incident light equally in all directions) because measurements of reflectance are dependent on the angle of incident radiation (usually the solar zenith) and the angle at which reflectance is measured (sensor view angle) (Figure 2.1.4). The position of the sun and the sensor are governed by the solar and view zenith (θ_i and θ_r) angles in relation to the upward normal, and the solar and view azimuth angles (Φ_i and Φ_r), thus such reflectance measurements are referred to as bidirectional.

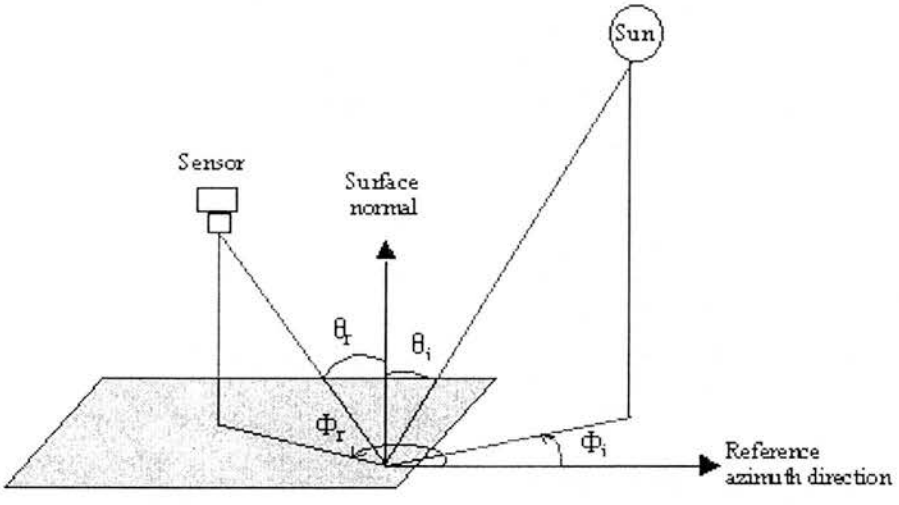

Figure 2.1.4 Geometry relating to sun and sensor positions.

A sensor operating in the optical wavelengths does not observe and detect all the reflected energy from a surface object over an entire hemisphere, it records the reflected energy that is returned at a particular angle. This angle is dependent on the angle of incident flux, surface characteristics (roughness and orientation angle) and azimuth angle. Therefore, to measure reflected energy from a target it is necessary to measure reflectance over an entire hemisphere.

This is termed the 'bi-directional reflectance distribution function', or BRDF, and is the ratio of reflectance in one direction over the incident radiation

$$BRDF = \frac{dL(\theta_r, \phi_r)}{dE(\theta_i, \phi_i)} \qquad 2.1.1$$

where dL is the reflected radiance per solid angle and dE is the irradiance per unit solid angle. (Milton, 1987).

Reflectance properties of vegetation are strongly affected by view and solar zenith and azimuth angles such that as solar zenith angle decreases relative to the upward normal, the closer the surface behaves to a diffuse reflector. This results in relatively lower spectral reflectance both in visible and near infrared wavelengths (Goel, 1988). In general, increases in solar zenith angle mean that a surface becomes less diffuse which results in increased vegetation reflectance in the forward scattering direction as a result of specular reflectance and a decreased soil contribution (Baret, 1991; Goel, 1988).

In many cases, and to standardise measurements, the reference azimuth angle used is 180° to the solar azimuth which means that the sensor faces into the sun. Shadow effects increase when the angle of incident radiation is either side of the surface normal, thus spectral reflectance measurements are often taken around midday or when the sun is relatively high in the sky. Sensor view angle largely determines the amount of soil contribution to vegetation reflectance; the greater the view angle relative to the surface normal, the lower the direct reflectance from soil background.

2.1.4.4 Leaf angle distribution

A sensor may measure radiant energy from single vegetation components, energy from multiple scattering within the vegetation canopy, as well as soil reflectance either reaching the sensor unintercepted or intercepted by the canopy and further scattered. Reflectance from a vegetation canopy could then be seen to be a product of leaf orientation and density, assuming that view angle is constant. Leaf angle distribution (LAD) can be described by a density distribution

function dependent on leaf inclination and leaf azimuth (Goel, 1988). LAD varies between different vegetation canopies but broad canopy classifications may be described by the following angular distributions; planophile, erectophile, plagiophile, extremophile, uniform and spherical (Goel and Strebel, 1984). These distributions affect BDRF in different ways. Horizontal leaf angle distribution canopies show the least variability in reflectance as a function of solar and view zenith angles and overall have high reflectance (Kimes, 1984). More erect canopies have reduced reflectance with increasing solar zenith angle in visible wavelengths, but increased reflectance in near infrared wavelengths, and, as view zenith angle increases, so does canopy reflectance.

2.1.4.5 Hotspot effect

If the sun is directly behind the sensor a greater proportion of directly illuminated vegetation components will be viewed. Shadows within the canopy or on the soil surface will be hidden by the foliage that is illuminated by the sun. This creates a peak in reflectance that is referred to as the 'hotspot' effect (Suits, 1972). The magnitude of the hotspot effect is dependent on LAD and leaf size.

2.1.4.6 Leaf area Index

Leaf area index (LAI) is used as an indicator of vegetation biomass and/or vegetation density. It is a representation of leaf area per unit area, and is a dimensionless measure. Goel (1988) considers the influence of LAI on BDRF and suggests that in the visible region as LAI increases, reflectance decreases exponentially due to strong absorption by chlorophyll in the leaves in this wavelength domain. The ceiling LAI is given as being 2-3 where visible reflectance becomes close to zero. In the near infrared the opposite occurs with increasing LAI leading to an increase in reflectance up to a LAI ceiling value of 6-8. Leaf area index is commonly used as an input into canopy reflectance models as discussed later.

2.1.5 Vegetation indices

Vegetation indices are commonly used to quanitatively evaluate vegetation covers using discreet spectral measurements (Bannari *et al.,* 1995). They are used to minimise the effects of external factors on canopy reflectance, for example soil, rock and leaf litter by identifying specific wavelength bands that lend themselves towards identification of specific vegetation features. Vegetation indices are usually created by calculating the ratio of one wavelength band with another. The most commonly used vegetation index is the normalised difference vegetation index (NDVI) which uses a combination of visible red and near infrared wavelengths, utilising the differential between red and near infra red. It was developed by Rouse (1973) and has been used to identify the presence of green vegetation (Sellers, 1985), vegetation amount (Tucker, 1979), light absorption capacity (Wiegand and Richardson, 1984) and photosynthetic potential (Choudhury, 1987). However, it has been shown to be susceptible to soil background effects (Huete *et al.*, 1985) and changes in canopy colour caused by vegetation stress (Demetriades-Shah and Steven, 1988). There have been many developments in vegetation indices over the last 25 years and there are now over 40 different vegetation indices (Bannari, 1995). For this work the challenge was to investigate whether there were specific wavelengths combinations that could be used to create a leak or water index. Gao (1996) developed a normalized difference water index from two near infrared wavebands but his focus was on vegetation water content. Similar work has been done on the estimation of leaf and canopy water content (Hunt and Rock, 1989; Rollin and Milton, 1989; Ceccato *et al.,* 2001) with identification of near infrared and middle infrared wavelength combinations.

2.1.6 Vegetation models

2.1.6.1 Bidirectional canopy reflectance models

A vegetation canopy is a complex structure with vegetation elements including stalks, stems, branches, flowers and seed heads, each orientated in different directions with different absorption and scattering properties. There have been various attempts to simplify interactions in the vegetation radiation environment, using canopy reflectance models. These can be split into

four main categories: (i) geometrical models, (ii) turbid medium models, (iii) hybrid models and (iv) computer simulation models. Goel (1988) provided a thorough account of these models so only turbid medium models are considered here, as they are used in this study.

Turbid medium models can either be based on radiative transfer theory, canopy transmittance theory, or both. In turbid medium models the vegetation elements are treated as scattering objects randomly distributed in uniform and parallel layers with constant optical and structural properties. They are best used for dense, homogenous and horizontally orientated canopies where the vegetation elements are small in relation to canopy height (Goel, 1988). Turbid medium models can be split into 3 further categories: Kubelka-Munk theory based models, discreet models, radiative transfer equation models.

Kubelka-munk theory models provide one means of solving the radiative transfer equation, by using a four-flux approximation of upward (diffuse) and downward (specular) flux for a parallel plane. It is used to model light scattering and extinction for diffuse surfaces (Verhoef, 1984). This theory has been applied in many bi-directional canopy reflectance models, perhaps one of the most widely used being the SAIL model (Verhoef, 1984). The SAIL model was developed from Suits (1972) model which was the first to account for solar viewing angles and to relate different scattering elements within a canopy structure to canopy reflectance.

Discrete models are based on average canopy transmission theory where the interception of incident light is a function of leaf angle distribution, leaf area index and a canopy density parameter. The Id-so Wit model is an example of a discrete model and it divides radiation into downward and upward fluxes irrespective of diffuse or specular components (Goel, 1988). The canopy is divided into many discrete layers and equations are derived for scattered light entering each layer from the layers above and below. Incident and view direction hemispheres are also split into discrete zenith angle zones which are subsequently treated as direct beams then added together to give the penetration from the entire hemisphere.

Radiative transfer equation models use numerical methods for solving the radiative transfer equation (rather than the flux methods used by Kubelka-Munk models). An important radiative transfer equation model is the Ross-Nilson model developed in 1966 (cited in Goel, 1988). The

model is for a plane parallel canopy which is described by many thin, horizontal layers. Each layer is composed of one type of vegetation element (for example stems or leaves) and it is assumed that a ray of light propagating in the vertical direction will intercept a single vegetation element. It also assumes that each layer is composed of many scattering elements.

2.1.6.2 Leaf reflectance models

Leaf reflectance models have been developed based on the well-documented spectral properties of leaves. They serve to provide more accurate and exhaustive descriptions of leaf optical properties (Jacquemoud *et al.*, 1996). There are several types of leaf reflectance models, these include; ray tracing, stochastic and radiative transfer models. Ray tracing and stochastic models are computationally intensive and require detailed information on internal leaf structure. Examples of ray tracing models include a model developed by Allen *et al.* (1973) and RAYTRANS developed by Govaerts *et al.*, 1996. Stochastic methods include those developed by Tucker and Garret (1977) and the Stochastic model for Leaf Optical Properties (Maier *et al.*, 1999). Radiative transfer models require few input parameters and are quick to compute. Perhaps the most commonly used leaf reflectance model is PROSPECT, developed by Jacquemoud and Baret (1990) and upgraded to include leaf biomchemical content in 1996. It is based on Allen *et al.*'s (1970) multiple layer plate model and was first designed to illustrate the effects of chlorophyll and water content on leaf spectral reflectance. It was later modified to predict leaf optical properties using specific absorption coefficients for nitrogen, carbon, cellulose, lignin and protein. LIBERTY, another radiative transfer leaf reflectance model, works using a similar construct to PROSPECT, although it was specifically designed to reproduce reflectance measurements from conifer needles (Dawson *et al.*, 1998).

References

Allen, W. A., Gausman, H. W. and Richardson, A. J. 1970. Mean effective optical constants of cotton leaves. Journal of the Optical Society of America, **60**, 542-547.

Allen, W. A., Gausman, H. W. and Richardson, A. J. 1973. Willstätter-Stoll theory of leaf reflectance evaluated by ray tracing. Applied optics, **12**, 2448-2543.

Bannari, A., Morin, D., Bonn, F., and Huete, A. R. 1995. A review of vegetation indices. Remote Sensing Reviews, **13**, 95 - 120.

Baret, F. 1991. Vegetation canopy reflectance factors of variation and application for agriculture. In Remote Sensing and Geographical Information Systems for Resource Management in Developing Countries. Edited by A.S. Belward and C.R. Valenzuela. Published by Dordrecht ; London : Kluwer.

Boochs, F., Kupfer, G., Dockter, K. and Kubauch, W. 1990. Shape of the red edge as vitality indicator for plants. International Journal of Remote Sensing, **11**, 1741 - 1753.

Carter, G. A. 1991. Primary and secondary effects of water content on the spectral reflectance of leaves. American Journal of Botany, **78** (7), 916-924.

Ceccato, P., Flasse, S., Tarantola, S., Jacquemoud, S. and Gregoire, J. 2001. Detecting vegetation leaf water content using reflectance in the optical domain. Remote Sensing of Environment, **77**, 22-33

Choudhury, B. J. 1987. Relationships between vegetation indices, radiation absorption and net photosynthesis evaluated by a sensitivity analysis. Remote Sensing of Environment, **22**, 209-233.

Collins, W. 1978. Remote sensing of crop type and maturity. Photogrammetric Engineering and Remote Sensing, **44**, 43 - 55.

Curran, P. J. 1980. Multispectral remote sensing of vegetation amount. Progress in Physical Geography, **4**, 315-341.

Danson, F. M., Steven, M. D., Malthus, T. M. and Clark, A. 1992. High-spectral resolution data for determining leaf water content. International Journal of Remote Sensing, **13**, 461 - 470.

Dawson, T. P., Curran, P. J. and Plummer, S. E. 1998. LIBERTY – modeling the effects of leaf biochemical concentration on reflectance spectra. Remote Sensing of Environment, **65**, 50-60.

Demetriades-Shah, T. H. and Steven, M. D. 1988. High spectral resolution indices for monitoring crop growth and chlorosis. In Proceedings of the Fourth International Colloq on Spectral Signatures of Objects in Remote Sensing, Aussios, France, ESA SP-287, 299-302.

Estep, L. and Holloway, J. 1992. Estimators of bottom reflectance spectra. International Journal of Remote Sensing, **13**, 393-397.

Gao, B.-C. 1996. NDWI – a normalised difference water index for remote sensing of vegetation from space. Remote Sensing of Environment, **58**, 257-266.

Gates, D. M., Keegan, H. J., Schleter, J. C and Weidner, V. R., 1965. Spectral properties of plants. Applied Optics, **4** (1), 11-20

Gausman, H. W. 1985. Plant leaf optical properties in visible and near infrared light. Graduate Studies, Texas Tech University (No. 29). Texas Tech Press.

Gausman, H. W. and Allen, W. A. 1973. Optical parameters of 30 plant species. Plant Physiology, **52**, 57-62.

Gausman, H. W., Allen, W. A. and Cardenas, R. 1969. Reflectance of cotton leaves and their structures. Remote Sensing of Environment, **1**, 19-22.

Goel, N. S. 1988. Models of vegetation canopy reflectance and their use in estimation of biophysical parameters from reflectance data. Remote Sensing Reviews, **4**, 1 - 221.

Goel, N. S and Strebel, D. E. 1984. Simple beta distribution representation of leaf orientation in vegetation canopies. Agronomy Journal, **76**, 800-802.

Govaerts, Y. M., Jacquemoud, S., Verstraete, M. M and Ustin, S. L. 1996. Three-dimensional radiation transfer modeling in a dictyledon leaf. Applied Optics, **35**, 6585-6598.

Horler, D. M., Dockray, M. and Barber, J. 1983. The red edge of plant leaf reflectance. International Journal of Remote Sensing, **4**, 273-288

Huete, A. R., Jackson, R. D. and Post, D. F. 1985. Spectral response of a plant canopy with different soil backgrounds. Remote Sensing of Environment, **17,** 37 - 53.

Hunt, E. R. and Rock, B. N. 1989. Detection of changes in leaf water content using near and middle infrared reflectances. Remote Sensing of Environment, **30,** 43 - 54.

Jackson, R. P., Ahler, J., Estes, J. E., Heilman, J. L., Kahle, A., Kanemasu, E. T., Millard, J., Price, J. C. and Wiegand. C. L. 1978. Soil moisture estimation using reflected solar and emitted thermal infrared radiation, Soil Moisture Workshop, NASA, 4-1 - 4-47.

Jacquemoud, S. Ustin, S. L., Verdebout, J., Schmuck, G., Andreoli, G. and Hosgood, B. 1996. Estimating leaf biochemistry using the PROSPECT leaf optical properties model. Remote Sensing of Environment, **56**, 194-202.

Jaquemoud, S. and Baret, F. 1990. PROSPECT: A model of leaf optical properties spectra. Remote Sensing of Environment, **34,** 75 - 91.

Kimes, D. S. 1984. Modeling the directional reflectance from complete homogenous vegetation canopies with various leaf-orientation distributions. Journal of the Optical Society of America, **A1**, 725-737.

Knipling, E. B. 1970. Physical and physiological basis for the reflectance of visible and near-infrared radiation from vegetation. Remote Sensing of Environment. **1,** 155 - 159.

Lichtenhaler, H. K, Gitelson, A. and Lang, M. 1996. Non-destructive determination of chlorophyll content of leaves of a green and an aurea mutant of tobacco by reflectance measurements. Journal of Plant Physiology, **148**, 483-493.

Maier, S. W., Lüdeker, W. and Günther, K. P. 1999. SLOP: a revised version of the stochastic model for leaf optical properties. Remote Sensing of Environment, **68**, 273-280.

Miller, J. R., Hare, E. W. and Wu, J. 1990. Quantitative characterization of the vegetation red edge reflectance I. An inverted gaussian reflectance model. International Journal of Remote Sensing, **11**, 1755-1773.

Milton, E. J. 1987. Principles of field spectroscopy. International Journal of Remote Sensing, **8**, 1807 - 1827.

Norman, J. M., Welles, J. M. and Walter, E. A. 1985. Contrasts among bidirectional reflectances of leaves, canopies and soils. IEEE Transactions of Geoscience and Remote Sensing, **GE-23**, 659-668.

Pinar, A. and Curran, P. J. 1996. Grass chlorophyll and the reflectance red edge. International Journal of Remote Sensing, **17**, 351 - 357.

Ripple, W. J. 1986. Spectral reflectance relationships to leaf water stress. Photogrammetric Engineering and Remote Sensing, **52**, 1669-1675.

Rollin, E. M. and Milton, E. J. 1998. Processing of high spectral resolution reflectance data for the retrieval of canopy water content information. Remote Sensing of Environment, **65,** 86 - 92.

Rouse, J. W., Haas, R. H., Schell, J. A. and Deering, D. W. 1973. Monitoring vegetation systems in the great plains with ERTS. Third Earth Resources Technology Satellite Symposium 1, NASA, 309-317.

Salisbury, J.W., Milton, N. M. and Walsh, P.A. 1987. Significance of non-isotropic scattering from vegetation for geobotanical remote sensing. International Journal of Remote Sensing, **8**, 997-1009

Sellers, P. J. 1985. Canopy reflectance, photosynthesis, and transpiration. International Journal of Remote Sensing, **6**,1335-1372.

Spitzer, D. and Dirks, R.W.J. 1987. Bottom influence on the reflectance of the sea. International Journal of Remote Sensing, **8,** 279-290.

Suits, G. H. 1972. The calculation of the directional reflectance of vegetative canopy. Remote Sensing of Environment, **2**, 117-125.

Tucker, C. J. 1980. Remote sensing of leaf water content in the near infrared. Remote Sensing of Environment, **10**, 23-32.

Tucker, C. J. 1979. Red and photographic infrared linear combinations for monitoring vegetation. Remote Sensing of Environment, **8**, 127 - 150.

Tucker. C. J. and Garret, M. W. 1977. Leaf optical system modelled as stochastic process. Applied Optics, **16**, 635-642.

Verhoef, W. 1984. Light scattering by leaf layers with application to canopy reflectance modeling: the SAIL model. Remote Sensing of Environment, **16**, 125 - 141.

Vogelman, T. C., 1993. Plant tissue optics. Annual Review of Plant Physiology and Plant Molecular Biology, **44**, 231-251.

Wiegand, C. L. and Richardson, A. J. 1984. Leaf area, light interception and yield estimates from spectral components analysis. Agronomy Journal, **76**,543-548.

Woolley J. T. 1971. Reflectance and transmittance of light by leaves. Plant Physiology, **46**, 656 - 662.

.

2.2 Field methods

2.2.1 Introduction

The aim of the fieldwork in this study was twofold; to produce a series of ground-based reflectance measurements using a spectroradiometer, and to take a series of in-situ ground truth measurements in support of the acquired ground- and airborne-based reflectance data. However, before the measurements obtained with the spectroradiometer are considered, approaches to field spectroscopy are discussed.

2.2.2 Field spectroscopy

A spectroradiometer works by comparing the radiance of a surface object (target) with a standard of known spectral characteristics (Robinson and Biehl, 1979; Milton, 1987). The standard used is typically a panel that acts as a perfectly diffuse (lambertian) reflector. These two measurements can be compared, as long as the same irradiation and geometry conditions are used for the target and reference measurements. The spectral characteristics measured by the spectroradiometer are dependent on the physical properties of the target, scattered light from surrounding objects, and illumination conditions.

With regard to illumination conditions the important factors are sun zenith and azimuth angles, sensor view angle, and incoming solar radiation which is affected by cloud cover. To standardise measurements in relation to solar angles, the spectroradiometer was always positioned into the sun and measurements were only carried out between the times 10am and 3pm when the sun was sufficiently high in the sky. The sensor was also always positioned in the nadir to avoid angle dependent variations in the detected radiance (Egbert and Ulaby, 1972; Duggin, 1980). This was the same view angle as the centre line of the airborne sensor data. It is also the view angle adopted by most optical space-borne sensors.

In order that a comparison can be made between the surface of interest and a referenced panel it is important that as many variables as possible are the same. Perhaps one of the most difficult factors to stabilise is the illumination conditions. Bright, clear days with no cloud cover are favoured for field spectroscopy where there are few changes in irradiance over time. Variations in irradiance due to clouds passing in front of the sun, can account for changes in reflectance of up to 32% where scattered cumulus clouds are present (Milton *et al.*, 1995). This is not a problem if two sensors are used to measure the radiance of the target and reference panel simultaneously (Duggin, 1980). However, Milton (1987) highlights that variations between sensors introduce unaccounted for errors, as well as errors from target specific differences arising from the physical separation of the sensors. There are also effects on solar and viewing geometry with regard to surrounding objects. In this study only one spectroradiometer was used, and as the sensor was not moved between the reference and target measurements, it was ensured that the geometry remained the same.

In some instances it was not possible to carry out measurements under perfect conditions. In such situations reference measurements were taken with minimal temporal separation. One technique to improve measurements such as these is to average over a larger number of scans. During times when there was an increased chance of changing irradiance conditions i.e. when it was cloudy, every target measurement was preceded by a reference measurement and the spectroradiometer averaging rate was increased from 6 scans (the default setting) to 12. Percentage cloud cover and a description of the atmospheric conditions were also recorded on the fieldwork sheets.

A further atmospheric factor to consider is wind speed and direction. It has been shown that the effect of wind on the movement of a vegetation canopy can significantly change canopy reflectance by up to 60% in the case of strong gusts, and 12% where leaves were caused to flutter (Lord et al., 1985). Therefore in designing a field spectroscopy protocol, it was important not to take measurements on windy days.

Other important factors affecting radiance measurements include (i) shadows falling on the panel or target while measurements are being taken, (ii) the sensor field of view not being fully occupied by the panel during reference measurements, (iii) bright clothing worn by the spectroradiometer operators, and (iv) scattered light from surrounding objects such as the sensor tripod (Duggin, 1980; Milton, 1987). To mitigate these factors the reference panel

was mounted on a tripod at a known height and calculated to ensure that the entire field of view (FOV) was occupied by the panel only. The radiometer was pointed into the sun and the operators stood behind the sensor while measurements were being made so shadows fell behind the instrument. The operators wore dark clothing and the sensor legs were painted with matt black paint (Duggin, 1980).

The instrument used was a GER 3700^{TM} spectroradiometer obtained on loan from the NERC Equipment Pool for Field Spectroscopy (EPFS) based at the University of Southampton (figure 2.2.1). The instrument records in 704 wavebands over the range 350 – 2500 nm, with a spectral resolution of 3-8nm (Geophysical Research Corporation, 1994). It has 3 detectors; one Si based (350-1050 nm, with a spectral resolution of 1.5nm) and two PbS based detectors (1050-1900 and 1900-2500 nm, with sampling intervals of 6.5 and 9.5 nm, respectively). The instrument thus acquires data at a greater spectral resolution than the HyMAP sensor and therefore, provides data directly comparable to it.

Spectroradiometer field settings

Entrance optic: Unity function

Averaging: 6-12 scans depending on light conditions

Si Integration: default

Pbs Integration: default

Matching: reflectance

Figure 2.2.1 GER3700 spectroradiometer and panel.

All measurements were taken in nadir view, with a lens aperture of 10 degrees. The height of the instrument lens above the canopy varied with plant species and growth stage but the majority of measurements were taken 165 cm above the ground at 2/3 tripod extension

which gave a ground surface field of view diameter of 28.8cm. For multiple measurements of the same crop, the sensor height was not altered and only in the case of the advanced oil seed rape crop, where the canopy height was over 1m was the full tripod extension used. All spectral measurements were referenced to an erbium oxide (Spectralon^{TM}) panel, whose absolute reflectance had been determined over the range 200-2000 nm at a resolution of 0.8 nm. All radiance measurements were post-processed to calculate absolute reflectance and a correction factor was applied to account for the fact that the panel is not a perfectly diffuse reflector.

Further fieldwork discussion is split between the two study areas. The first is the series of ground-based vegetation and soil radiance measurements taken at the Cheshire sites, concurrent with the overflights of the hyperspectral airborne data. The field measurements not only provided data to calibrate the airborne imagery, but also provided data for use as input into the modelling study. These data helped to parameterise the canopy and leaf reflectance models used later in this work by providing us with representative vegetation and soil measurements.

The second ground-based campaign involved the collection of in-situ field measurements around Edinburgh. These were taken over 2 growing seasons and included measurements of a variety of crops and different growth stages. The spectroradiometer was used to increase the range of optical measurements over a variety of vegetation types at different growth stages. The aim was to use these data to provide empirical information on when leaks are most easily detected in relation to canopy cover, and thus point to an optimal time of year for detecting leaks. The spectroradiometer also provided us with further optical measurements over a wide spectral range comparable to the image data, and it increased the number of optical measurements that we had for leaks, albeit simulated ones.

2.2.3 Leak simulation

Leaks were simulated by leaving a hose-pipe running at selected sites for a given length of time. For the two Cheshire-based simulated leaks a sprinkler was set-up 12 hours prior to the flight line being flown, with the aim of achieving surface ponding over a 12 m^2 area at each site. For the Edinburgh-based simulated leaks the purpose was to wet the soil to field

saturation capacity beneath the vegetation canopy. This was achieved by leaving a hose-pipe running for 20-30 minutes which was considered sufficient time to ensure soil saturation over a relatively wide area.

2.2.4 Vegetation spectra measurements

2.2.4.1 Cheshire

Vegetation spectral measurements were recorded on the day of image acquisition with the spectroradiometer. At each leak site three to five target and reference measurements were taken at 3 separate and random locations within the field to obtain a sample of typical non-leak vegetation reflectance. Three target and reference measurements were also taken within the leak at three different points.

2.2.4.2 Edinburgh

The spectral reflectance of three different crops (oil seed rape, spring and winter barley), at a series of different growth stages were measured over the growing seasons of 2000 and 2001. Ideally, two full sets of measurements would have been obtained over both growing seasons. However, wet weather inhibited the number of sampling days available, and the 2001 Foot and Mouth outbreak severely restricted access to the farm sites. This meant that only one full set of measurements representing four different growth stages for barley (a combination of spring and winter), and five different growth stages for oil seed rape were obtained.

At all of the Edinburgh sites, leaks were simulated beneath the selected vegetation canopy. To do this, the spectroradiometer was placed at a random location (within the range of water supply) in the relevant field and three 'dry' target measurements were taken consecutively without moving the instrument. Following this, a hose-pipe was positioned directly beneath the instrument lens and under the vegetation canopy, and left running. Target and reference measurements were then repeated with the wet background soil.

2.2.5 Other field measurements

The measurements taken in support of the spectroradiometric scans can be separated into 4 main categories; topographic, atmospheric, vegetation and soil. The series of measurements were similar for all phases of fieldwork but not exactly the same (fieldwork sheets can be found in Appendix 2). With regard to the 'real' leaks found at the Cheshire sites, fieldwork involved taking vegetation and soil measurements, both inside the leak and from the vegetation in the field surrounding the leak. Where the leaks were simulated only dry measurements were made as the vegetation and soil parameters remained the same, with the exception of soil moisture content.

2.2.5.1 Topographic measurements:

- Slope description
- Slope direction
- Proximity to boundaries e.g. hedges or roads – metres

Slope angle was observed in the field using an Abney level. At each of the field sites the slope angle was assigned a category of inclination from the following relief angles: flat, (0-1°), gentle (2-3°), moderate (4-7°), strongly sloping (8-11°) and steep (> 12°) (Soil Survey of Scotland, 1984). All the slope descriptions for all the sites were flat or gently sloping. The direction of slope was measured using a compass and drawn on to the paper map. This information, coupled with contour data, was used to predict gravitational flow of water away from the pipeline. This could potentially explain why a leak might not sit directly over the pipeline. However, while this is an important measurement to make for a study such as this, the measurements were deemed largely irrelevant due to the flat nature of the terrain at all the sites studied. The proximity of each leak to 2 field boundaries was also measured up to 15m.

2.2.5.2 Atmospheric measurements:

- Horizontal line of sight
- Solar irradiance
- Air temperature
- Cloud cover

- Cloud type
- Wind speed
- Wind direction

It has been shown (Robinson and Biehl, 1979) that on a hazy day (where visibility <= 8km) reflectance can be affected by up to 3 percent compared with clear days, due to sky light variations. On clear days horizontal line of sight was estimated and was used as an indication of atmospheric haze and thus gave basic information regarding irradiance conditions. During the image acquisition ground campaign, the horizontal line of sight remained greater than 8km throughout the day.

Air temperature was measured using a field thermometer. At each site the maximum temperature was recorded in degrees centigrade.

Cloud cover was measured qualitatively by estimating percentage cover. This method was useful for the Edinburgh field measurements when we did not have use of a sun photometer. Cloud type was recorded using cloud classification descriptions (i.e. nimbus, cumulus etc.). Wind speed and direction were recorded using an anemometer and compass. Wind speed provided an insight into potential vegetation movement while image or spectroradiometer measurements were being acquired. The effect of wind on stem and leaf angle distributions was also a consideration. Field measurements were therefore made on days where there were light or moderate breezes which had little impact on vegetation movement or alignment. Fortunately, during the imaging campaigns, the winds were light, with average wind speed of 1.5 m s^{-1}.

2.2.5.3 Vegetation measurements:

- Vegetation type
- Canopy height
- Percentage cover
- Vegetation biomass
- Vegetation and leak spectra
- Leaf area
- Leaf density

Vegetation type was recorded along with canopy height in centimetres. For an indication of canopy height, 20 randomly chosen plants from within a selected field were measured using a tape measure and then averaged. Percentage cover was estimated qualitatively using quadrats and digital photographs were taken of each quadrat for further quantitative analysis using a computer, if required.

Quadrats were also used for sampling vegetation biomass. Six quadrats were taken at each site from separate locations, three inside the leak and three outside the leak. Biomass was calculated by harvesting $625cm^2$ of vegetation from each quadrat. Fresh weights were determined in the laboratory the vegetation was then dried at 60 degrees centigrade for 48 hours, or until a stable weight had been achieved. Dry weights and percentage moisture were then calculated and averaged. Leaf area was also estimated by taking sampling 30 leaves from each site, measuring the length and width and applying the equation for an ellipse to the measurements.

$$\text{Area of an ellipse} = \pi\, ab \qquad 2.2.1$$

where a is leaf half length and b is leaf radius.

Leaf density refers to the numbers of leaves per square metre. Grass leaf density was calculated by counting the number of leaves touching 2 perpendicular sides of a $625cm^2$ quadrat. These two numbers were multiplied together and then scaled to create leaf density for a square metre. For less dense crops, the number of leaves per $625cm^2$ were simply counted and similarly multiplied up to one square metre.

Leaf Area Indices (LAI) for each crop were then calculated from leaf density and area estimates, where:

$$\text{LAI} = \text{leaf density} \times \text{leaf area in } m^2 \qquad 2.2.2$$

Leaf density and leaf area index estimates are likely to contain the most error of all the field measurements, particularly for grass where leaf density is high. Estimates are difficult to make unless every blade is counted and measured, however, they give an indication of

conditions. As such they serve as a useful basis for comparing overall vegetation characteristics both inside and outside the leak.

2.2.5.4 Soil measurements:

- Soil texture
- Soil type
- Soil colour
- Soil moisture
- Soil reflectance

Soil samples were taken from all Cheshire leak sites and were classified in terms of texture and plasticity using the United States Soil Survey Staff (1951) methodology. Soil series was determined from 1:25000 soil maps of the study areas and soil colour was determined with the aid of Munsell colour charts. Soil moisture measurements were taken in the field using a Theta probe, in addition to direct estimates where soil samples were taken back to the laboratory and soil moisture content was determined from wet and dry weights. The soil was dried in an oven at 90 degrees centigrade for 24-48 hours, or until the dry weight was constant. Soil dry weight and moisture content were calculated for each sample. A description of soil parameters can be found in Part II, Chapter 3 (Study areas). Table 2.2.1 gives the differences in soil moisture content between leak and non leak areas.

Table 2.2.1 Leak and non leak soil measurements.

Site	Leak % soil moisture	Non leak % soil moisture
C1	22.2	31.1
C2	31.9	44.8
C3	22.0	34.7
C5	13.4	27.7
C6	56.8	70.0

The GER 3700^{TM} spectroradiometer was used to take wet and dry soils reflectance measurements under laboratory conditions at the University of Edinburgh. A room was prepared by covering the walls and work benches with matt back paper to reduce reflective surfaces from interfering with the measurements. Two 500 watt halogen lamps were

positioned to provide an illumination angle of 45 degrees. A small round dish, 19cm in diameter, was filled with dry soil and positioned under the spectroradiometer. The sensor was positioned on a frame, 90cm above the target. The lens aperture was 3 degrees giving an FOV of 4.7cm diameter. A reference measurement of the Spectralon™ was taken, followed by three consecutive target measurements. The soil was then wetted to saturation capacity (but without ponding) and reflectance measurements were again determined.

References

Duggin, M. J. 1980. The field reflectance measurement of reflectance factors. Photogrammetric Engineering and Remote Sensing, **46**, 5, 643-647

Egbert, D. D., and Ulaby, F. T. 1972. Effect of angles on reflectivity. Photogrammetric Engineering and Remote Sensing, **38**, 556-564.

Geophysical Research Corporation. 1994. GER3700 spectroradiometer user manual. Geophysical Research Corporation, Millbrook, New York.

Lord, D., Desjardins, R. L. and Dube, P. A. 1985. Influence of wind on crop canopy reflectance measurements. Remote Sensing of Environment, **18**, 113-123.

Milton, E. J. 1987. Principles of field spectroscopy. International Journal of Remote Sensing, **8**, 12, 1807-1827.

Milton, E. J., Rollin, E. M. and Emery, D. R. 1995. Advances in field spectroscopy. Advances in Environmental Remote Sensing. Edited by F. M Danson and S. E. Plummer. John Wiley and Sons Ltd.

Robinson, B. F. and Biehl, L. L. 1979. Calibration procedures for measurement of reflectance factor in remote sensing field research. SPIE volume 196, Measurements of Optical radiations, pp.16-26.

Soil Survey of Scotland. 1984. Soil and land capability for agriculture, 1:250 000 survey: organization and methods. Published by The Macauley Institute for Soil Research, University Press Aberdeen.

Soil Survey Staff. 1951. Survey manual. U. S. Department of Agriculture, hand-book **18**. Washington: United States Department of Agriculture.

2.3 Fieldwork results

The results presented here are divided into two sections; those taken at the Cheshire study sites and those taken around Edinburgh, these sections are further sub-divided into field and spectroradiometer results. The first results introduced are the Cheshire-based ground truth measurements, followed by spectral reflectance curves for leak and surrounding vegetation made with a spectroradiometer at each of the leak sites. The second set of measurements cover a wider range of vegetation types and growth stages and were taken over two growing seasons on farms around Edinburgh. They were made over simulated leaks only and were used to extend the range of spectral measurements as examples of real leaks were few and the vegetation types were limited. All graphs in this chapter show reflectance curves representing interpolated 1 nm interval data. Error bars show standard deviation from the mean and were sampled at twelve intervals, selected to represent the shape of the reflectance curve and the locations of main peaks and troughs in reflectance.

2.3.1 Cheshire measurements

At the time of the optical data acquisition, the landcover types found at the Cheshire leak sites were limited to grass at different growth stages, and a wheat crop at the ripening development stage. Tables 2.3.1 and 2.3.2 summarise ground-based vegetation and soil measurements taken on the day the flight line was flown, inside and outside the leak, respectively. Reflectance measurements were made over three real leaks and two simulated ones situated over the Vyrnwy aqueduct. Table 2.3.3 provides a summary of atmospheric conditions at the time of data acquisition and spectroradimeter field of view (FOV) calculations.

Table 2.3.1. Vegetation description outside leak.

Site	Crop	Canopy height (cm)	Percentage cover	Dry weight (g/625 cm^2)	% moisture content	Leaf area (cm^2)	Leaf density/m^2
C1	Wheat	80	80	14	81.63	106.81	396
C2	Grass	7.25	95	13.9	66.01	1.77	12449
C3	Grass	6	80	2.7	66.25	1.12	16977
C5	Grass	19.3	100	9.3	82.25	4.71	10616
C6	Grass	3.6	100	11.4	70.16	0.85	24705

Table 2.3.2. Inside Leak, vegetation description.

Site	Crop	Canopy height (cm)	Percentage cover	Dry weight (g/625 cm^2)	% moisture content	Leaf area (cm^2)	Leaf density/m^2	Leak area (m^2)
C1	Low vegetation	7.3	65	8.9	83.14	3.38	8876	No leak present
C2	Grass	3.3	30	2.6	87.74	0.78	12820	73.92
C3	Grass	10	70	4.5	75.14	1.96	4082	38.44
C5	Grass	19.3	95	9.6	81.95	4.71	10616	62.69
C6	Grass	34.6	55	4.6	79.91	13.84	7328	54.45

Table 2.3.3. Summary of Cheshire-based field spectroscopy measurements (FOV measurements are based on canopy heights of non leak vegetation).

Site	Date of measurement	Growth stage	Height of lens above ground (cm)	FOV diameter	Cloud Cover (%)	Cloud type
C1	19-Jun-00	Ripening wheat	165	14.9	5	Cirrus
C2	19-Jun-00	Grazing grass	165	28.3	5	Cirrus
C3	19-Jun-00	Grazing grass	165	27.3	5	Cirrus
C5	19-Jun-00	Silage grass	165	27.1	5	Cirrus
C6	19-Jun-00	Grazing grass	165	25.5	5	Cirrus

2.3.1.1 Field results

The field results demonstrate that in all cases with the exception of simulated leak C5, vegetation percentage cover was less dense inside the leak than the surrounding area. It is suggested that this is due to the negative effect of water inundation on vegetation. In the case of simulated leak C5 a hose pipe was left running for 12 hours prior to measurements being made – this was not long enough for the presence of water to negatively affect vegetation growth. Simulated leak C2 had characteristics more typical of a real leak. A description of leak C2 is provided in section 1.3.2.4. Vegetation moisture content was greater for vegetation samples taken from inside the leaks than from the surrounding vegetation at all sites, except C5 where the leak was simulated. Leaf area is less than surrounding vegetation for samples inside leaks C1 and C2. For site C3 the average vegetation height inside the leak was taller than the surrounding vegetation with an increased leaf area and dry weight, but leaf density was dramatically lower. For site C5 there is no change in leaf area, and for C6 the presence of water appeared to have a positive effect on vegetation growth resulting in an increased leaf area, although leaf density was lower than for the surrounding vegetation. For leaks C1 and C2 vegetation density inside the leak was greater than for the 'dry' samples, however leaf area was significantly reduced.

It should be noted that the field results show variations between sites in terms of vegetation physiology and morphology. However, these measurements do not fully characterise individual variations between different sites and different leaks.

2.3.1.2 Spectroradiometer results

Figure 2.3.1 shows spectral reflectances made with a spectroradiometer of the Cheshire sites both inside and outside the leaks during the HYMAP ground campaign on 19th June 2000.

The graphs represent fairly typical spectral reflectance curves for green vegetation (Figure 2.3.1): a small peak in green reflectance, a large peak in the NIR region (700 – 1350 nm) and two further peaks in the MIR region (1500 – 1750 nm and 2000 – 2400 nm). Also present were the water absorption features (characterised by low reflectance regions) at approximately 990, 1170, 1450, and 1900 nm (Gao, 1996).

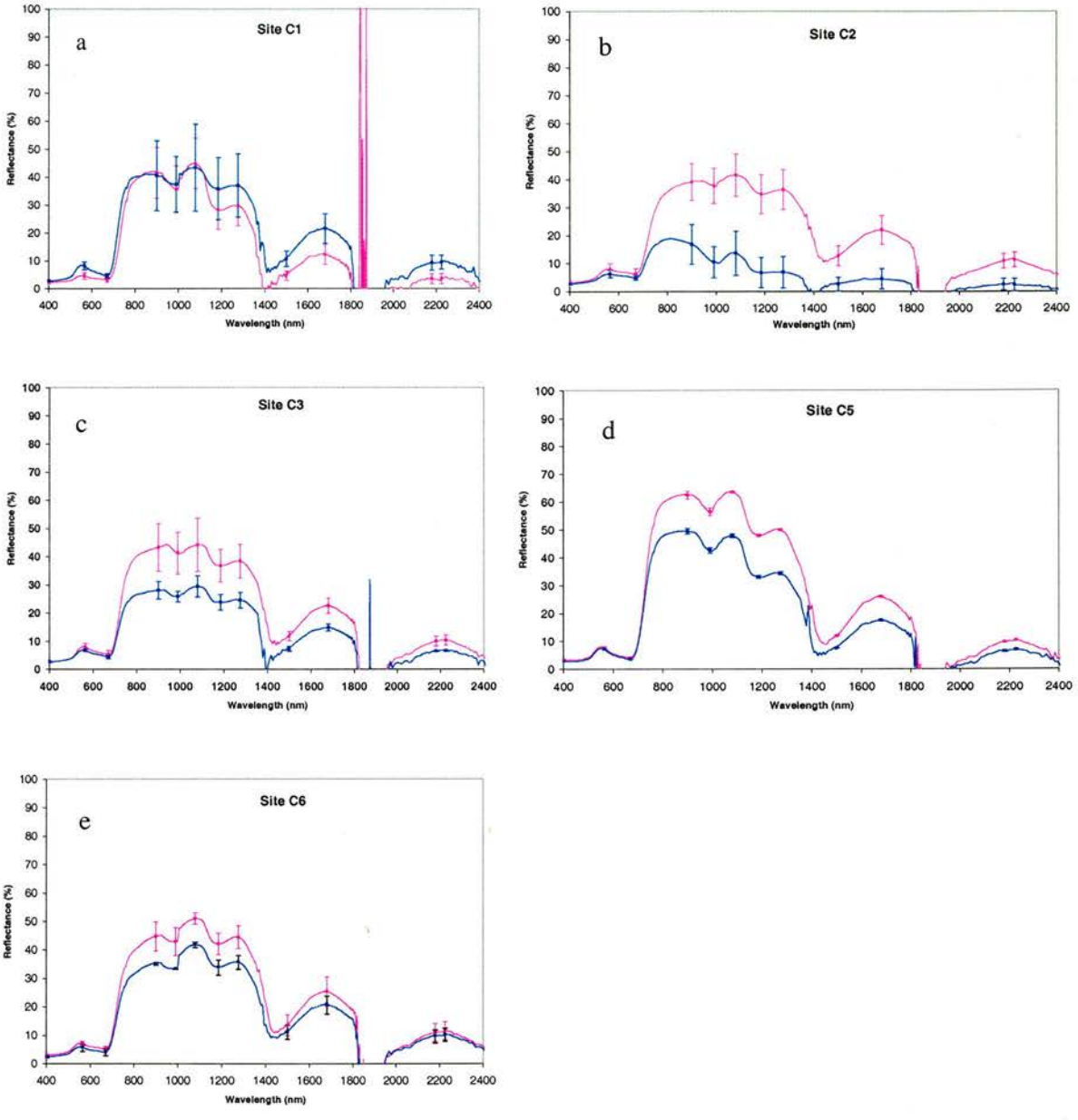

Figure 2.3.1. Graphs a-e showing average wet and dry reflectances made inside (blue) and outside (pink) the leaks using the GER3700 spectroradiometer. The error bars show standard deviation.

For sites C2-C6 clear differences exist between the leak and surrounding vegetation reflectances, with leak reflectance being lower than non-leak reflectance. It is suggested that this was due to

the strong influence of water on reducing spectral reflectance, particularly in the near and middle infrared wavelengths (Woolley, 1971; Knipling, 1970). The exception to this trend is the graph for site C1 (graph a) where the 'leak' reflectances are greater than the non leak reflectances across most of the spectrum, except around 860 and 1080 nm. However, at this site there was no 'leak' evident at the time of acquisition. The large puddle that was observed during the E-SAR image campaign and reconnaissance trips made previously had dried up (or been fixed - although this could not be confirmed), leaving bare soil and a variety of low story plant species growing on the exposed soil.

Site C1 demonstrates the largest standard deviation from the mean of all the sites for in-leak measurements. The combination of bare soil influences, several different vegetation types and low percentage cover led to great surface heterogeneity which influenced the leak measurements, and helps to explain the large error bars. However, there were also large standard deviations in the measurements of the wheat crop that surrounded the leak. This is more unexpected as cereal crop measurements typically produce fairly homogenous reflectance measurements, but this may be related to the small footprint size of the spectroradiometer being sensitive to subtle variations between the different sets of wheat measurements. At the other sites, the non-leak landcover was grass, which, whilst also fairly heterogeneous, produced a denser canopy which means that less soil is visible, and it has fewer vegetation components (e.g. obvious stems and ears). These factors combine to produce less variation in the spectral reflectance measurements over grass.

The standard deviations for both leak and non-leak measurements at site C1 are such that leak identification would not be possible as each lies within the error of the other. While the other site measurements also display some heterogeneity (described by standard deviation), particularly in the surrounding vegetation measurements, it is possible to clearly distinguish between leak and non-leak reflectances.

2.3.2 Edinburgh measurements

2.3.2.1 Field Results

Table 2.3.1 summarises the vegetation (and spectroradiometer) measurements taken around Edinburgh. Due to the problems previously mentioned (section 2.2.4.2) affecting the feasibility of obtaining a full set of measurements in any one growing season, the crop growth measurements were not taken chronologically and the range of crop types measured were also limited. There were no 'inside' and 'outside' leak measurements obtained as the leaks were simulated. The physiology and morphology of the vegetation was not affected negatively by the leak simulations over the time periods involved, there are thus only one set of vegetation measurements for each crop growth stage measured.

Table 2.3.4. Field measurements of vegetation parameters recorded at the Edinburgh sites with spectroradiometer parameters.

Site	Crop	Date	Growth stage	%age cover	Canopy height (cm)	Dry weight (g/625 cm^2)	Height of lens above ground (cm)	FOV diameter	Cloud Cover (%)	Cloud type
E4	Oil seed rape	11-Apr-01	Young	62	28.4	15.2	165	23.9	65	Cumulo nimbus
E4		03-May-01	Pre-flowering, beginning to bud	68	68.1	24.4	178	19.2	70	Cumulus
E4		31-May-01	In flower	100	134.7	37.3	190	9.7	56	Cumulus
E2		04-Jul-00	Green seed pods	100	125	34.4	190	11.4	70	Cumulus
E2		11-Aug-00	Desiccating canopy	99	128	22.1	190	10.8	35	Cumulo nimbus and cumulus stratus
E3	Barley	4-Jul-00	Young spring barley -	85	22	34.4	155	23.3	100	Cumulus
E3		22-Aug-00	Ripening winter barley	92	73.5	20	165	16.0	35	Alto cumulus
E1		11-Aug-00	Ripe winter barley - 2 weeks before cutting	92	67	90.4	165	17.1	95	Cumulus
E1		25-Aug-00	Winter barley - stubble field, day after cutting	82	9	-	165	27.3	35	Alto Cumulus

2.3.2.2 Oil seed rape spectroradiometer results

Figure 2.3.2 presents a series of five separate spectroradiometer measurements taken of oil seed rape over the growing seasons of 2000 and 2001.

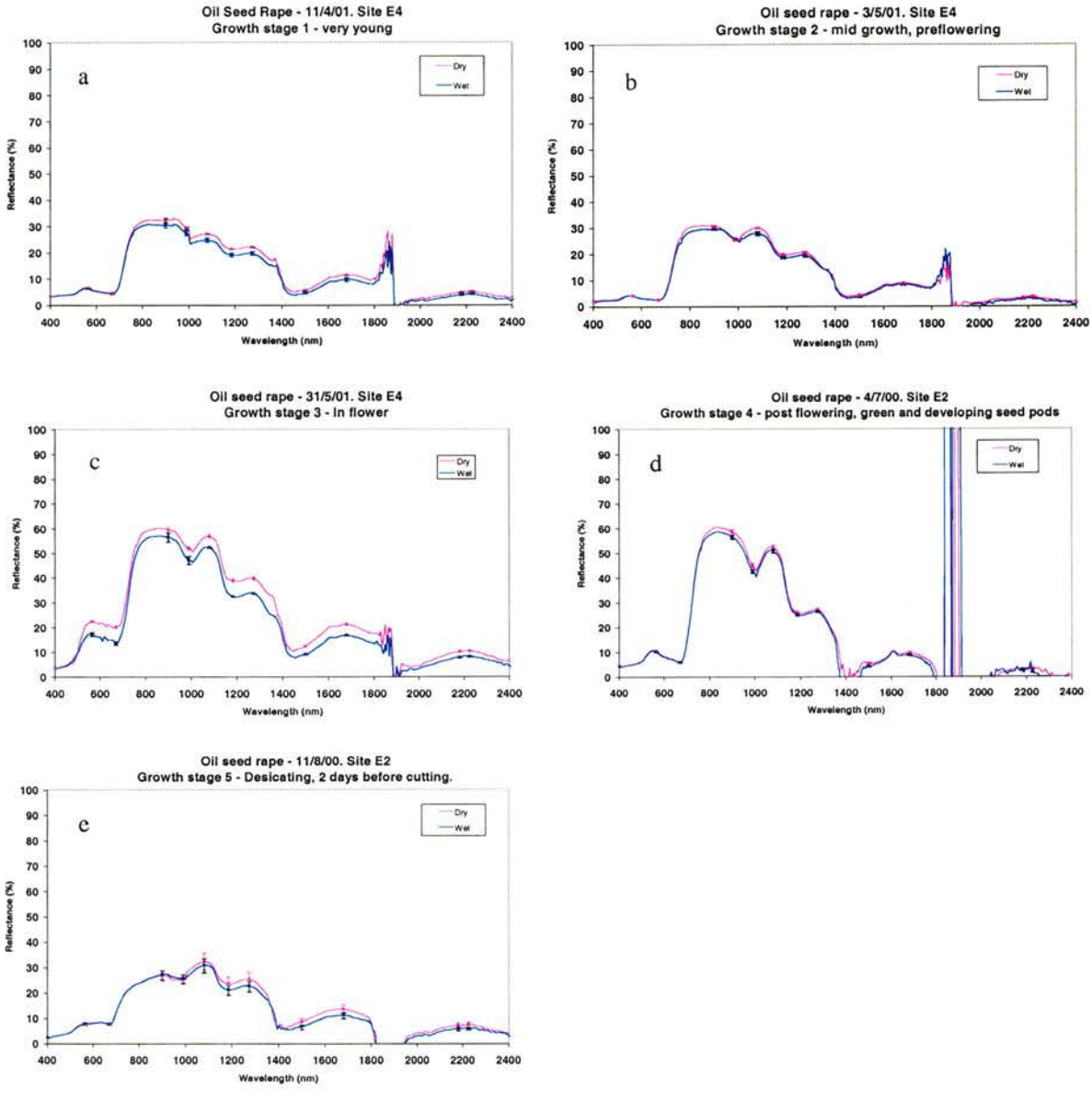

Figure 2.3.2 a-e. Spectroradiometer spectral reflectances, showing oil seed rape crops at 5 different growth stages. The measurements were taken over 2 growing seasons, at 2 different sites.

Figure 2.3.2 shows typical green vegetation spectra but, importantly, also shows the influence of growth stage on spectral reflectance. For example, at the early growth stages (graphs a and b) the near infrared peaks around 1080 nm and 1300 nm are flatter than those at later growth stages, suggesting that canopy water absorption is low. At the later growth stages the second near infrared peak is indicative of a dense green vegetation canopy. For vegetation curves the internal leaf structure and moisture content strongly affect spectral reflectance creating the characteristic near infrared peaks (Woolley, 1971). The flatness of the peaks at the early growth stages also represents soil contributions to the overall spectral reflectance.

At growth stage 3 the rape canopy was in flower which lead to an increase in reflectance in the visible region and a peak in reflectance around 560 nm. It was also possible to observe changes in spectral reflectance as the crop desiccated. As the crop turned brown there was an increase in reflectance in the red region as the photosynthetic pigments broke down. There were also observable changes in the near infrared as the internal leaf structure broke down resulting in lower reflectance. As the crop dried out, the near infrared water absorption features were also less distinguishable due to water loss.

Over the rape canopies it is only just possible to distinguish between wet and dry measurements. In all cases except growth stage 5 (graph e), the differences between wet and dry reflectances are within the standard deviation. The error bars for growth stage 5 are such that it would not be possible to separate the wet from dry conditions.

At the later growth stages (graphs c - e), difficulty might be expected in distinguishing between wet and dry measurements as the canopies were tall (1.25-1.35 m) and dense, therefore greatly reducing the opportunity for reflectance to come from soil or surface water contributions. However, there was also a lack of variation between wet and dry measurements at early growth stages when the bare soil background was clearly visible and the canopy height was low. This may have been the result of the hose pipe not being left running for long enough beneath the canopy. This is particularly important where the soils are well-drained. It is also possible that the soil was already quite wet and the contrast between wet and dry soil backgrounds was greatly reduced.

2.3.2.3 Barley spectroradiometer results

Figure 2.3.3 shows measurements of barley crops at four different growth stages around Edinburgh.

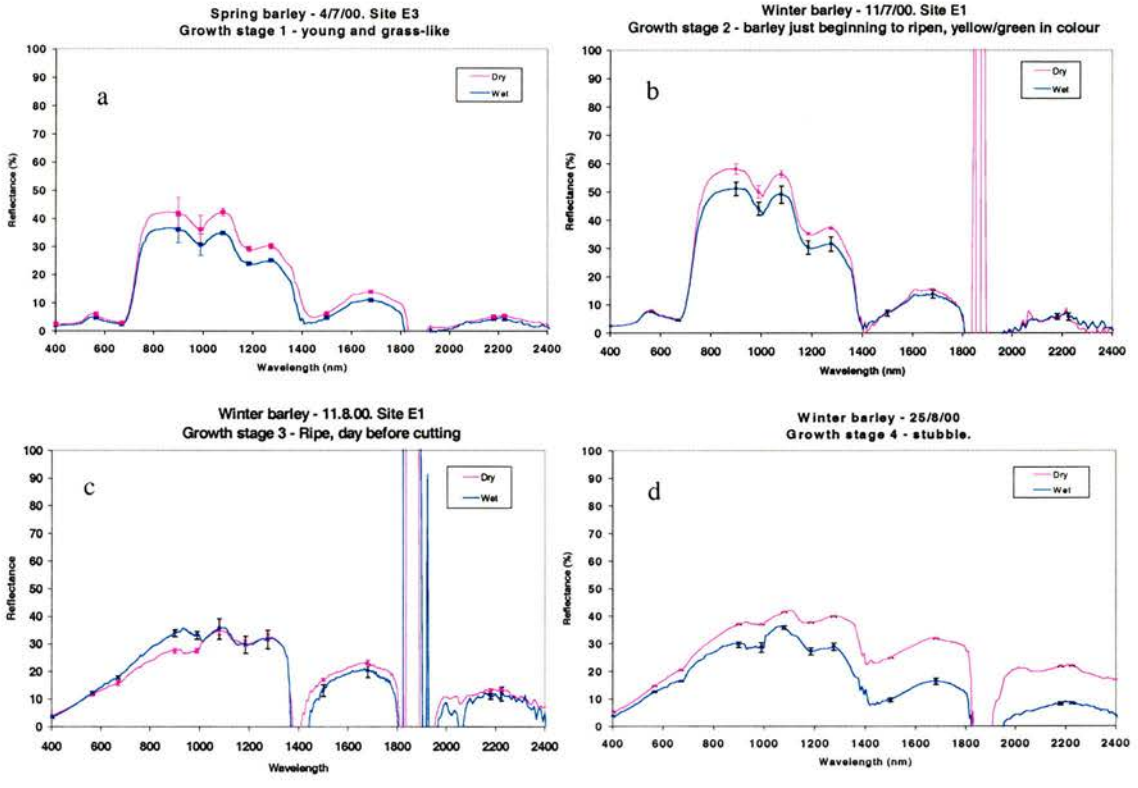

Figure 2.3.3. Graphs a-d show GER3700 spectroradiometer measurements for spring and winter barley at 4 different growth stages over 1 growing season.

The barley measurements were made under changeable atmospheric conditions (Figure 2.3.3). This is most evident in graphs b and c where atmospheric noise in the middle infrared is apparent and the reflectances are generally noisier. The error bars for these two sets of measurements are relatively large compared with similar spectroradiometer measurements, particularly considering the spectroradiometer was not moved and no physical changes to the vegetation were made. An explanation, apart from the influence of wind, is changing irradiance arising from significant cloud cover on both these days. For both graphs b and c, the levels of noise between 1800 and 2000 nm are indicative of low light levels. For growth stage 2 (graph b),

measurements were taken during bright spells on an otherwise cloudy day but high levels of atmospheric noise suggest that there may have been changing light conditions during acquisition. During growth stage 3 data collection (graph c), the sky was overcast. It can be seen that in the near infra red wavelengths the dry measurements have lower reflectance than the wet measurements which is atypical, the reasons for this are not fully understood.

Despite problems with atmospheric conditions, the first two growth stages show that the presence of water is most marked in near infrared wavelengths, and that its presence reduces reflectance across the spectrum. Graph c shows reflectance curves representative of ripening barley. The break down of carotenoid and chlorophyll pigments affect reflectance in the blue and red visible region – there is very little absorption by pigments in the visible wavelengths. For graph d there is a clear distinction between wet and dry conditions because the crop has been cut with only short stems left leaving the presence of water clearly visible.

2.3.3 Summary

- All real leak sites display lower wet reflectances than surrounding dry area reflectance. The contrast between wet and dry is particularly marked between 700 and 1900 nm.
- For simulated leaks under oil seed rape canopies it was possible to identify an overall decrease in reflectance in the near and middle infrared for a wet background, in relation to a dry background, at all growth stages. However, differences between wet and dry measurements were small. This may be due to problems with leak simulation or the soil being wet to start with.
- Measurements made over simulated leaks beneath barley crops were affected by changing light conditions particularly at growth stages 1 – 3. The growth stages demonstrate a typical pattern where wet reflectances are characteristically lower than the dry reflectances across the spectrum, but particularly in the near infrared wavelengths.

References

Gao, B.-C. 1996. NDWI – a normalised difference water index for remote sensing of vegetation from space. Remote Sensing of Environment, **58**, 257-266.

Knipling, E. B. 1970. Physical and physiological basis for the reflectance of visible and near-infrared radiation from vegetation. Remote Sensing of Environment. **1,** 155 - 159.

Woolley J. T. 1971. Reflectance and transmittance of light by leaves. Plant Physiology, **46**, 656 - 662.

2.4 Optical modelling methods

2.4.1 Introduction

For the optical modelling phase of this project two coupled models have been used. These were the PROSPECT model, a leaf reflectance model adapted from Allen's generalised plate model (Allen *et al.*, 1969), and developed by Jacquemoud and Baret (1990), and the SAIL model (Scattering by Arbitarily Inclined Leaves) a canopy reflectance model based on Suits' model (Suits, 1972) and developed by Verhoef (1984). Both of these models are based on Kubelka-Munk Theory (Kubelka and Munk, 1931, cited in Goel, 1988).

The PROSPECT model is a leaf radiative transfer model which allows relatively accurate computation of the 400 - 2400 nm reflectance and transmittance spectra of leaves with few input variables (these are shown on next page). The input parameters are categorized by (i) leaf area and internal structure, (ii) leaf pigment content, (iii) leaf water content, and (iv) atmospheric variables. There are other models available that are suitable for this application, for example LIBERTY (Dawson et al., 1998). However, the combined PROSPECT and SAIL model (developed by Baret, 1991) was selected for two principle reasons; it is perhaps one of the most frequently used leaf and canopy reflectance models and therefore, allows inter-comparison with other studies, and a copy of the combined model was made available to the author.

The SAIL model is a turbid medium model for homogenous canopies. It is theory based, rather than being a discreet or radiative transfer equation model. A one layer version was used in this study and simulated canopy reflectance as a function of the following canopy and illumination variables:

- leaf reflectance and transmittance - obtained from the PROSPECT model;
- leaf area index;
- soil reflectance;
- ratio of diffuse light to direct irradiation;
- solar zenith angle,
- zenith view angle and sun view azimuth angle;
- leaf inclination angle;
- hot spot parameter (ratio of horizontal correlation length to canopy height).

N.B. The model assumes the view angle is nadir.

2.4.2 Modelling strategy

The aim of the modelling was to consider different types of leaks, from a wet soil through to surface ponding, against a variety of different vegetation types, at a variety of growth stages. In this way the range of measurements beyond the limited examples of real leaks that were measured in the field could be extended.

For the purposes of modelling a leak was defined as a supply of water resulting in surface ponding from centimetres to metres squared, that is in excess of the vegetation's normal requirements. Typically, the presence of excess water can have five possible impacts on vegetation (section 1.2.5):

1. No impact, but the leak is manifested as wet soil beneath the vegetation canopy.
2. No impact but a pond develops beneath the canopy. In this case, and the case above, there is no change to the vegetation which may occur when a leak has been present for a short time only (hours). The duration of this period may be longer (weeks) where leaks occur below mature vegetation and the vegetation is more resiliant to the effects of inundation.

3. A positive effect on vegetation growth. It relates to a situation where initially the leak has an irrigating effect on the plant, but after a short time the presence of excess water causes plant injury. This scenario may have a short temporal window of a few days only and a positive growth response to inundation may be limited to a very few plant species. This makes it unlikely to be encountered in the field.
4. A negative effect on vegetation growth; this has a long temporal window which makes it good for measurement by remote sensing.
5. Lastly, a case where the leak has been present for long enough such that the original species has died and been replaced by a water tolerant species. This final scenario was not modelled because of the wide range of possible outcomes due to site specific variations.

The first four scenarios, as well as a dry scenario for comparative purposes, were used in this study. The modelling was achieved by varying the input parameters for a given vegetation canopy and changing the soil moisture content between dry and wet. Leaf area index and the internal leaf structure parameter were varied to represent vegetation at different growth stages. By varying leaf inclination angle it was possible to model the responses for different canopy types.

2.4.2.1 Leak scenarios

Different wetness scenarios were modelled to represent a variety of different types of leak. These included:

- *Dry soil* – used as a comparison for the following four wet scenarios
- *Wet soil* - a leak in its immediate expression, which has had no time to have any influence on the overlying canopy. Changes in the colour of the underlying soil is the only variation between the dry and wet scenarios. As all other values are constant, this is a similar scenario to the leaks simulated in the field.
- *Ponding* - a recent leak where there has been no time for the presence of excess water to have an influence on the overlying canopy. The only difference between W*et soil* and *Ponding* is the volume of water. For W*et soil* scenarios the soil background changes

colour, whereas for *Ponding* scenarios there is a 'pond' effect (i.e. a smooth water surface) underneath the vegetation canopy.

- *Puddling* - a leak of more prolonged duration but which has led to a positive response from the vegetation in the form of increased growth (LAI). This scenario is similar to that encountered at site C6 in Cheshire.
- *Waterlogging* - a very prolonged leak which has had a negative effect on the vegetation leading to a reduction in LAI and discolouring of the canopy. This scenario is similar to those encountered at sites C1 and C3 in Cheshire.

Figure 2.4.1 provides a schematic diagram of the modelling approach.

2.4.2.2 Growth stages

In order to characterise the seasonal variations in canopy cover, four growth stages were modelled for each crop, with the exception of sugar beet where only three growth stages were modelled. The aim of the modelling was to represent the main developmental stages for each crop. An early growth stage, a developing stage, a maximum growth stage and a senescent stage. In the case of sugar beet only an early growth stage, a maximum development stage and a senescent stage were modelled, as these three stages seems to best reflect the development of sugar beet. Growth stages are also described in Figure 2.4.1.

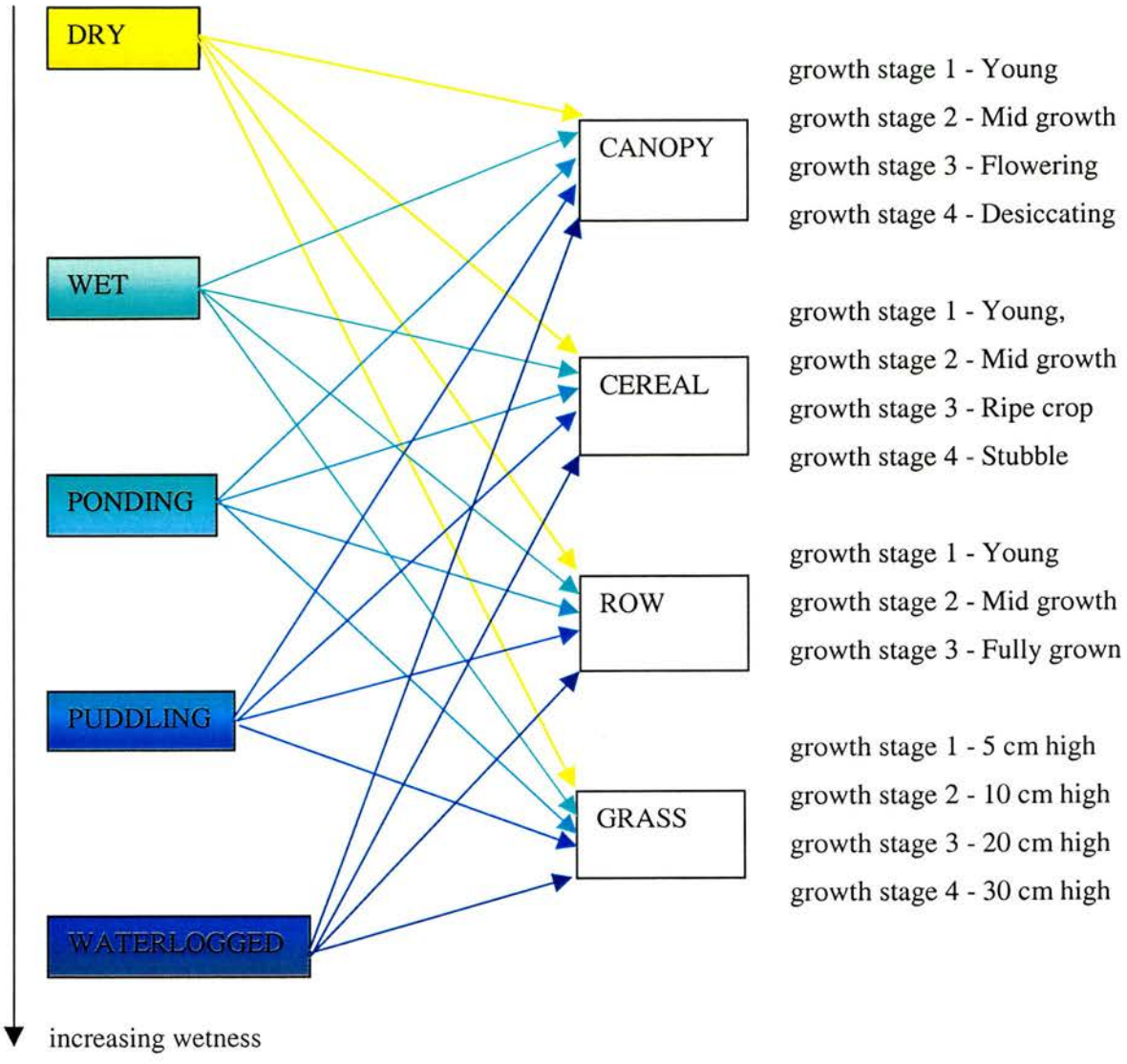

Figure 2.4.1. Diagram of the approach taken for the optical modelling using the PROSPECT+SAIL models.

2.4.3 Parameterising the model

The combined PROSPECT and SAIL model calls for 8 input parameters relating to leaf and canopy structure:

- Leaf area index (L)
- Leaf internal structure parameter (N)
- Leaf chlorophyll content (mg cm^2)
- Leaf water content (g cm^2)
- Leaf dry matter content (g cm^2)
- Average leaf angle (degrees)
- Hotspot parameter
- Soil reflectance spectra (same number of spectra as leaf reflectance output)

Leak area index values varied depending on the crop being modelled (Table 2.3.1). Leaf area index (L) values obtained from field measurements of grass, oil seed rape (growth stage 1) and barley (growth stage 3) canopies during the field campaign, were used. The remaining leaf area indices required for the modeling strategy outlined above, were derived from the literature; winter wheat (Wilhelm, 1998); sugar beet (Malthus *et al.*, 1993); oil seed rape and cereals (Hay and Walker, 1989). Grass LAIs were compared with those described by Parsons *et al.* (1983).

The leaf internal structure parameter (N) is dependent on leaf thickness and whether the plant is monocotyledonous or dicotyledonous (Jacquemoud and Baret, 1990). Monocotyledons have a compact mesophyll layer giving them N values in the range 1.0 - 1.5. Dicotyledons are characterised by a spongy mesophyll layer with many air spaces and they typically have N values of between 1.5 and 2.5. Senescent plants have disorganised internal structure due to the breakdown of cell material which leads to N values of greater than 2.5. Assigning values to the N parameter in this study was thus largely controlled by species.

Leaf chlorophyll contents for a variety of crops at different growth stages were taken from the literature where similar studies had been carried out (Malthus, 1991; Zhou and Lin, 1995; Pinar and Curran, 1996). Leaf water contents were calculated from wet and dry leaf measurements sampled during fieldwork and dried later in the laboratory. Leaf angles were also taken for a variety of crops in the field. The hotspot parameter was not altered and remained at the model default of 1.0 as there was not sufficient data from the field sites to accurately estimate hotspot effects. Soil reflectance properties were those obtained over a range of different coloured soils,

both wet and dry, using the spectroradiometer (section 2.2.4.4). For leak scenarios where surface water was present beneath the vegetation canopy (ponding, puddling and waterlogged), a spectrum for water was used in place of the soil spectra (Malthus, 1991). Diffuse light was set at 0.2 based on measurements taken in the field on 12th May 2000 using a sun photometer. This value gives a realistic indication of the proportion of diffuse light that might be expected on a clear day. The total list of parameters used for modelling and their values for the various scenarios are given in Table 2.4.1.

Table 2.4.1 Specific parameters used in the optical modeling of leak scenarios.

Crop / scenario	Growth stage	LAI	N	Chlorophyll	Leaf H_20 (g cm^{-2})	Dry leaf weight (g cm^{-2})	Leaf angle	Hot spot	Diffuse light
CANOPY									
Dry	1	0.8	2	35	0.041	0.006	25	1	0.2
	2	3	2.2	40	0.037	0.007	30	1	0.2
	3	4.3	2.5	40	0.029	0.008	30	1	0.2
	4	3.7	3	25	0.018	0.006	40	1	0.2
Wet soil	1	0.8	2	35	0.041	0.006	25	1	0.2
	2	3	2.2	40	0.037	0.007	30	1	0.2
	3	4.3	2.5	40	0.029	0.008	30	1	0.2
	4	3.7	3	25	0.018	0.006	40	1	0.2
Ponding	1	0.8	2	35	0.041	0.006	25	1	0.2
	2	3	2.2	40	0.037	0.007	30	1	0.2
	3	4.3	2.5	40	0.029	0.008	30	1	0.2
	4	3.7	3	25	0.018	0.006	40	1	0.2
Puddle	1	1.2	2	35	0.166	0.006	35	1	0.2
	2	3.4	2.2	40	0.263	0.007	30	1	0.2
	3	4.5	2.5	40	0.361	0.008	30	1	0.2
	4	3.9	3	20	0.223	0.006	40	1	0.2
Water	1	0.4	2	25	0.166	0.006	35	1	0.2
logging	2	1.5	2.2	25	0.263	0.007	30	1	0.2
	3	1.5	2.5	25	0.361	0.008	30	1	0.2
	4	1.5	3	15	0.223	0.006	40	1	0.2

Crop / scenario	Growth stage	LAI	N	Chlorophyll	Leaf H_20 (g cm^{-2})	Dry leaf weight (g cm^{-2})	Leaf angle	Hot spot	Diffuse light
CEREAL									
Dry	1	1.8	1.5	70	0.01	0.002	50	1	0.2
	2	4.0	2.0	70	0.019	0.006	61	1	0.2
	3	3.8	2.7	20	0.008	0.006	65	1	0.2
	4	0.8	4.0	05	0.005	0.004	75	1	0.2
Wet soil	1	1.8	1.5	70	0.01	0.002	50	1	0.2
	2	4.0	2.0	70	0.019	0.006	61	1	0.2
	3	3.8	2.7	20	0.008	0.006	65	1	0.2
	4	0.8	4.0	05	0.005	0.004	75	1	0.2
Ponding	1	1.8	1.5	70	0.01	0.002	50	1	0.2
	2	4.0	2.0	70	0.019	0.006	61	1	0.2
	3	3.8	2.7	20	0.008	0.006	65	1	0.2
	4	0.8	4.0	05	0.005	0.004	75	1	0.2
Puddle	1	2.2	1.5	70	0.24	0.002	50	1	0.2
	2	4.4	2.0	70	0.03	0.006	61	1	0.2
	3	4.0	2.7	20	0.014	0.006	65	1	0.2
	4	0.8	4.0	05	0.012	0.004	75	1	0.2
Water	1	0.3	1.5	70	0.024	0.008	50	1	0.2
logging	2	1.5	2.0	70	0.03	0.01	61	1	0.2
	3	1.5	2.7	20	0.014	0.007	65	1	0.2
	4	0.3	4.0	05	0.012	0.008	75	1	0.2
ROW	1	1.4	2.2	30	0.1	0.009	45	1	0.2
Dry	2	3.38	2.2	40	0.2	0.24	45	1	0.2
	3	3.14	2.2	37.5	0.2	0.21	45	1	0.2
Wet soil	1	1.4	2.2	30	0.1	0.009	45	1	0.2
	2	3.38	2.2	40	0.2	0.24	45	1	0.2
	3	3.14	2.2	37.5	0.2	0.21	45	1	0.2
Ponding	1	1.4	2.2	30	0.1	0.009	45	1	0.2
	2	3.38	2.2	40	0.2	0.24	45	1	0.2
	3	3.14	2.2	37.5	0.2	0.21	45	1	0.2

Crop / scenario	Growth stage	LAI	N	Chlorophyll	Leaf H_20 (g cm^{-2})	Dry leaf weight (g cm^{-2})	Leaf angle	Hot spot	Diffuse light
Puddle	1	3.4	2.2	40	0.18	0.024	40	1	0.2
	2	3.5	2.2	50	0.19	0.03	40	1	0.2
	3	1.8	2.2	40	0.1	0.012	40	1	0.2
Water	1	1	2.2	20	0.1	0.008	30	1	0.2
logging	2	2	2.2	20	0.2	0.01	30	1	0.2
	3	2	2.2	20	0.2	0.007	30	1	0.2
GRASS									
Dry	1	3	1.2	40	0.0026	0.0013	75	1	0.2
	2	4	1.2	40	0.007	0.0023	60	1	0.2
	3	5	1.2	40	0.017	0.0037	50	1	0.2
	4	5	1.2	40	0.027	0.0053	45	1	0.2
Wet soil	1	3	1.2	40	0.0026	0.0013	75	1	0.2
	2	4	1.2	40	0.007	0.0023	60	1	0.2
	3	5	1.2	40	0.017	0.0037	50	1	0.2
	4	5	1.2	40	0.027	0.0053	45	1	0.2
Ponding	1	3	1.2	40	0.0026	0.0013	75	1	0.2
	2	4	1.2	40	0.007	0.0023	60	1	0.2
	3	5	1.2	40	0.017	0.0037	50	1	0.2
	4	5	1.2	40	0.027	0.0053	45	1	0.2
Puddle	1	3.5	1.2	42	0.003	0.0046	50	1	0.2
	2	4.5	1.2	42	0.01	0.01	50	1	0.2
	3	5.5	1.2	42	0.02	0.014	45	1	0.2
	4	5.5	1.2	42	0.02	0.017	45	1	0.2
Water	1	0.8	1.2	30	0.0012	0.0005	30	1	0.2
logging	2	1	1.2	35	0.003	0.001	40	1	0.2
	3	1.5	1.2	35	0.008	0.002	40	1	0.2
	4	1.5	1.2	35	0.014	0.004	40	1	0.2

Some sensitivity analysis was performed on the model and this revealed that the factor with the greatest influence on reflectance was LAI.

2.4.4 Model validation

Preliminary results from the combined PROSPECT and SAIL model are outlined in Figure 2.4.2, and are compared with spectroradiometer measurements made in the field.

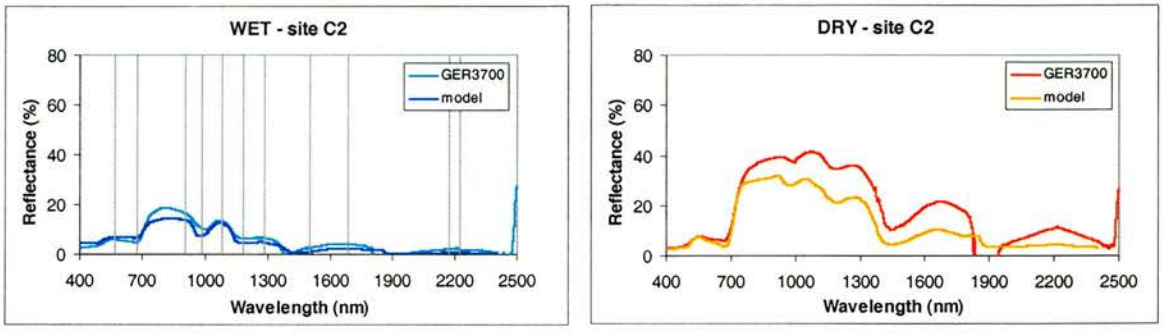

Figure 2.4.2. Comparison of the combined PROSPECT+SAIL model's ability to reproduce spectral reflectances with spectroradiometer observations for site C2 (where the graph on left shows a comparison between modeled, and measured spectroradiometer reflectances for leaks. The graph on the right shows a comparison between modelled, and measured spectroradiometer reflectances for surrounding vegetation). The lines on the left hand graph (wet) show selected wavelengths used for a more detailed comparison of modelled and spectroradiometer data, shown in Table 2.4.2.

Table 2.4.2. Reflectance comparison between modelled and spectroradiometer data for wet and dry measurements respectively, over a range of 11 wavelengths from 569 nm to 2224 nm. Columns 4 and 7 show the percentage difference between the GER3700 and the model. The relative positions of these selected wavelengths are shown in Figure 2.4.2.

Wavelength	WET 3700	WET MODEL	% difference	DRY 3700	DRY MODEL	% difference
569	6.08	6.96	-12.63	7.72	6.99	9.43
676	4.90	6.84	-28.34	6.34	3.80	40.08
905	16.51	13.90	15.81	39.12	31.60	19.21
984	10.48	7.43	29.10	37.76	28.30	25.06
1078	13.55	12.50	7.73	41.42	29.20	29.50
1181	6.58	4.62	29.81	34.57	21.40	38.10
1281	6.72	4.82	28.29	36.12	23.40	35.21
1503	2.62	1.05	59.92	12.69	5.47	56.89
1685	4.24	2.48	41.52	21.68	10.30	52.49
2172	2.31	0.80	65.21	10.48	4.40	58.01
2224	2.27	0.90	60.14	11.16	4.55	59.22

These data demonstrate the model's ability to predict actual vegetation canopy reflectance with reasonable accuracy across the optical spectrum (Table 2.4.2). This gives confidence in the use of the model to further investigate leak properties. It is questionable whether a more detailed statistical analysis (for example, the student T-test or regression analysis) would significantly improve on the validation presented in Figure 2.4.2, and in Table 2.4.2. The example above is a model/spectroradiometer, comparison for site C2. Comparison graphs and tables for modelled and spectroradiometer data for the remaining sites can be found in Appendix 3.

References

Allen, W. A., Gausman, H. W., Richardson, A. J. and Thomas, J.R. 1969. Interaction of isotropic light with a compact leaf. Journal of the Optical Society of America, **59**, 1376-1379.

Baret, F. 1991. Vegetation canopy reflectance factors of variation and application for agriculture. In Remote Sensing and Geographical Information Systems for Resource Management in Developing Countries. Edited by A.S. Belward and C.R. Valenzuela. Published by Dordrecht ; London : Kluwer.

Dawson, T. P., Curran, P. J. and Plummer, S. E. 1998. LIBERTY – modeling the effects of leaf biochemical concentration on reflectance spectra. Remote Sensing of Environment, **65**, 50-60.

Goel, N. S. 1988. Models of vegetation canopy reflectance and their use in estimation of biophysical parameters from reflectance data. Remote Sensing Reviews, **4**, 1 - 221.

Hay, R. K. M. and Walker, A. J. 1989. An introduction to the physiology of crop yield. Published by John Wiley and Sons, New York.

Jaquemoud, S. and Baret, F. 1990. PROSPECT: A model of leaf optical properties spectra. Remote Sensing of Environment, **34**, 75 - 91.

Kubelka, P. and Munk, F. 1931. Ein beitrag zur optik der farbanstriche. Z. Tech. Physik, **12,** 593.

Malthus, T.J. 1991. Anglo-French collaborative reflectance experiment. Experiment I, Brooms Barn Experimental Station, July 1989. Report and Data. Department of Physiology and Environmental Science, University of Nottingham.

Malthus, T. J., Andrieu, B., Danson, F. M., Jaggard, K. W. and Steven, M. D. 1993. Candidate high spectral resolution infrared indices for crop cover. Remote Sensing of Environment, **46,** 204 - 212.

Parsons, A. J., Leafe, E. L., Collett, B., Penning, P.D. and Lewis, J. 1983. The physiology of grass production under grazing. Journal of Applied Ecology, **20**, 127-139.

Pinar, A. and Curran, P. J. 1996. Grass chlorophyll and the reflectance red edge. International Journal of Remote Sensing, **17**, 351 - 357.

Suits, G. H. 1972. The calculation of the directional reflectance of vegetative canopy. Remote Sensing of Environment, **2**, 117-125.

Verhoef, W. 1984. Light scattering by leaf layers with application to canopy reflectance modeling: the SAIL model. Remote Sensing of Environment, **16**, 125 - 141.

Wilhelm, W. W. 1998. Dry matter partitioning and leaf area of winter wheat grown in a long-term fallow tillage comparisons in the US Central Great Plains. Soil and Tillage research, **49**, 49 - 56.

Zhou, W. and Lin , X. 1995. Effects of waterlogging at different growth stages on physiological characteristics and seed yield of winter rape (*Brassica napus* L.). Field Crops research, **44**, 103 - 110

2.5 Optical reflectance modelling results

The results presented here are from the optical modelling study which used the combined PROSPECT and SAIL reflectance model. The modelling survey was used to further extend the range of measurements that were obtained in the field. An outline of the modelling strategy was given in chapter 2.4.

2.5.1 Canopy crop

The reflectance measurements obtained for a theoretical canopy crop based on oil seed rape (Figure 2.5.1) are considered first. Of the modelled canopy types, this crop has the highest canopy density and height at its maximum growth stages. It might therefore, be considered to provide the greatest challenge to identifying differences between leak and surrounding vegetation.

From the graphs it is possible to distinguish the waterlogged scenario from all other scenarios at all growth stages. The waterlogged scenario represents a situation where a leak has been present for long enough to have a negative effect on vegetation growth to the extent that the vegetation is reduced to at least one third of its normal height and density. It is possible to identify variations between leak and non-leak against the surrounding vegetation at any growth stage. The wet scenario represents a very recent leak, or a slow forming leak where the soil is saturated, but where there is no surface water (refer to 2.4.2.1). In this case it was only possible to observe this condition at the earliest growth stage when vegetation density and canopy height were low – thus, a larger proportion of the observed reflectance was contributed from the soil, which when wet significantly reduced reflectance. The ponding scenario, which represents surface water beneath a vegetation canopy with no effect on the vegetation, is more observable at the later growth stages two and four, than the wet scenario making it slightly easier to identify the leak against the vegetation canopy.

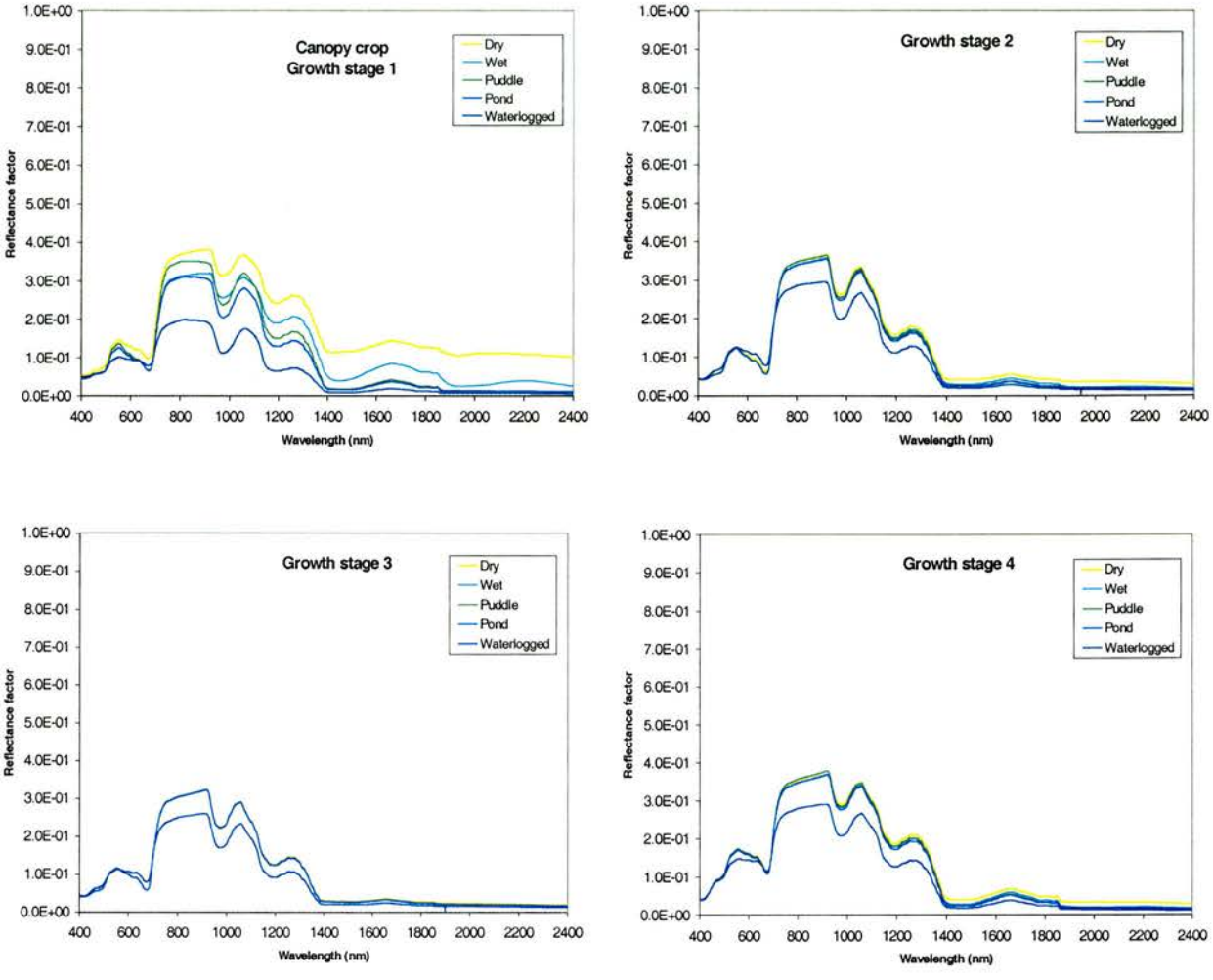

Figure 2.5.1. SAIL and PROSPECT modelled spectral reflectance over a theoretical canopy crop (based on oil seed rape) under five different wetness conditions and at growth stages 1-4. Where leak scenario reflectances are the same or similar (for example growth stages 3 and 4), the only line clearly visible is the ponding scenario, which overlies, the puddle, wet and dry scenarios (the reflectance curves are drawn in the order that they appear in the legend).

Thus, generally, at the earliest growth stage every leak scenario was distinguishable from the dry scenario. It should therefore be possible to identify any kind of leak in this situation. However, as the canopy becomes denser over time (up to growth stage three), there is less difference in reflectance between the dry, wet, ponding and puddling scenarios. At the maximum growth stage three, the thickness of the canopy appears to be sufficient to fully mask influences from the underlying water, making leak identification difficult except in the waterlogged scenario. As the canopy desiccates (growth stage four) the canopy becomes a little more transparent, increasing the contrast between the dry vegetation and the wet soil or pond below the canopy. However, the differences are subtle.

2.5.2 Cereal crop

The four stages of the cereal crop growth modelled were growth stage 1 is young and grass-like, growth stage 2 is developing ears (green), growth stage 3 is a ripe and golden crop, and growth stage 4 is stubble. While the stubble stage is not exactly a growth stage, it is included because it is commonly found in the British countryside later in the growing season and is usually present for several weeks (or even months) at the end of the summer.

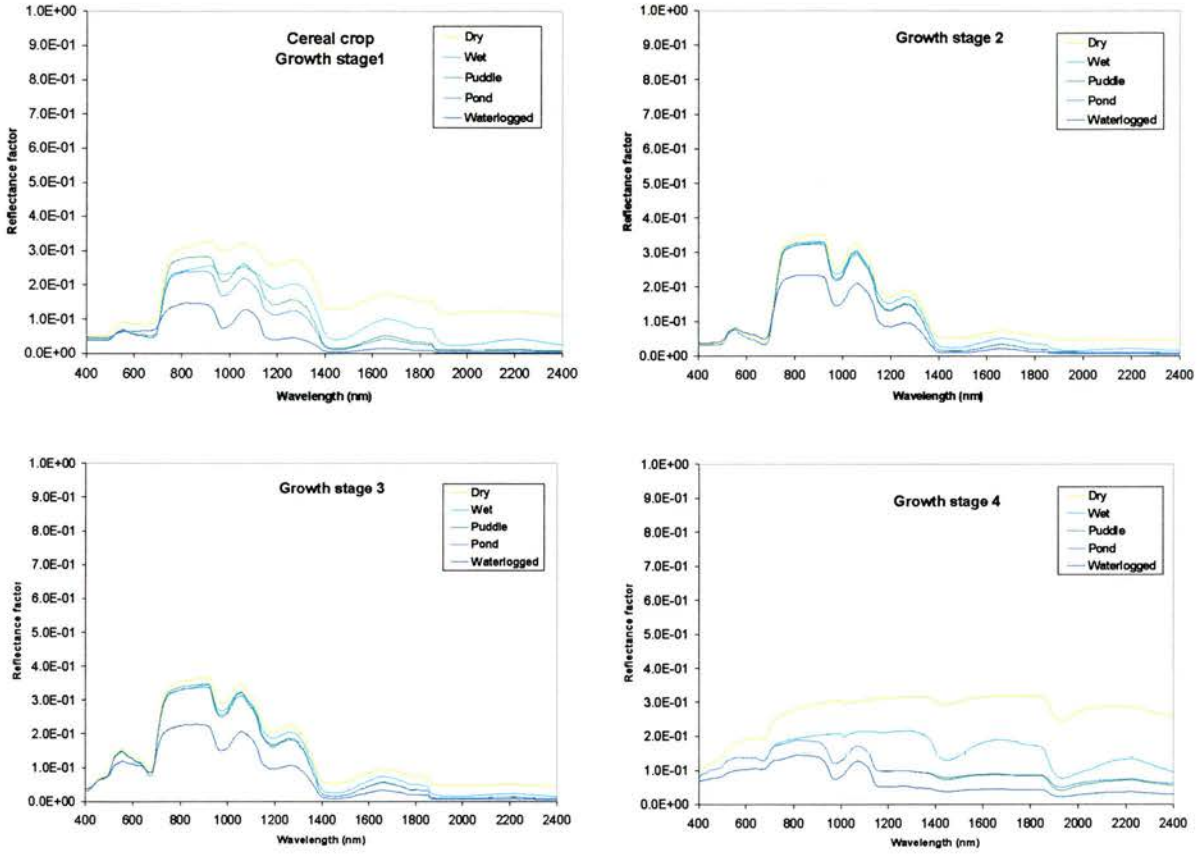

Figure 2.5.2. SAIL and PROSPECT modelled spectral reflectance over a theoretical cereal crop under five different wetness conditions and at growth stages 1-4.

Similar to the continuous canopy crop simulations, the waterlogged scenario was again clearly apparent at all cereal canopy growth stages (Figure 2.5.2). Generally, all the wetness scenarios at all growth stages for the cereal crop were more apparent than for the canopy crop. It was also possible to distinguish between wet and dry scenarios at all the growth stages. This suggests that differences between leak and surrounding vegetation may be more easily identified behind a cereal crop than against a canopy crop. The ponding and puddling scenarios produced similar

spectral reflectance values, particularly at longer wavelengths. This is probably because beyond a certain leaf area index value of 3.5 (Baret, 1991) the effect on reflectance of increasing leaf area index in the near and middle infrared does little to increase reflectance (Chance and Le Master, 1977).

The difference between dry and ponding scenarios was much less at growth stage 3 than at earlier growth stages perhaps due to the increased leaf area index and biomass masking leak effects. However, in comparison to the canopy crop, there was a more marked difference between dry and ponding scenarios for the cereal crop. This is most likely due to a greater contribution from ground reflectance as a result of the more open structure and vertical orientation of a cereal canopy, when viewing in the nadir. It was possible to distinguish all types of leak from the dry scenario at all growth stages due to decreases in overall reflectance for the wet results. However, the ponding and waterlogged scenarios stood out as those most easily distinguishable against a cereal crop.

2.5.3 Grass crop

For the grass crop a similar pattern was observed across all growth stages to that of the canopy crop, with the earliest growth stages revealing all types of leak. With the later growth stages, only the waterlogged scenario was easily distinguishable from the other scenarios (Figure 2.5.3). The grass crop shows a significant soil contribution to reflectance when canopy densities are low, producing a flatter vegetation reflectance curve (except for the water absorption regions). The effects on reflectance of these four wetness scenarios is minimal at the later growth stages particularly stages 3 and 4. The dry, wet, ponding, and puddling input parameter for leaf area index at the later grass growth stages assumed a very dense canopy and it is possible that canopy density has been over-estimated. Marked differences between the leak and surrounding vegetation are identifiable for all wetness scenarios at growth stages 1 and 2, however only the waterlogged scenario is distinguishable from the dry crop at the later growth stages.

The input values for leaf area index at growth stages three and four are greater than for any other canopy type at any of the growth stages, even the canopy crop, and yet the estimates for grass leaf area index are based on field measurements. A possible source of error is in the estimation of leaf number density for grass, as it runs into thousands per square metre and therefore, errors easily propagate. However it may also highlight a problem with the model in that it uses leaf

area index to represent canopy characteristics. For example, a situation may be encountered where a relatively sparse canopy with large leaves has the same leaf area index as a denser canopy with smaller leaves; then the model assumes that these canopies would have the same spectral reflectance. Yet this is clearly an oversimplification and a source of possible error in the model. The main variable influencing reflectance in the combined SAIL and PROSPECT model is leaf area index, and even changing the biomass input parameter does not significantly alter reflectance.

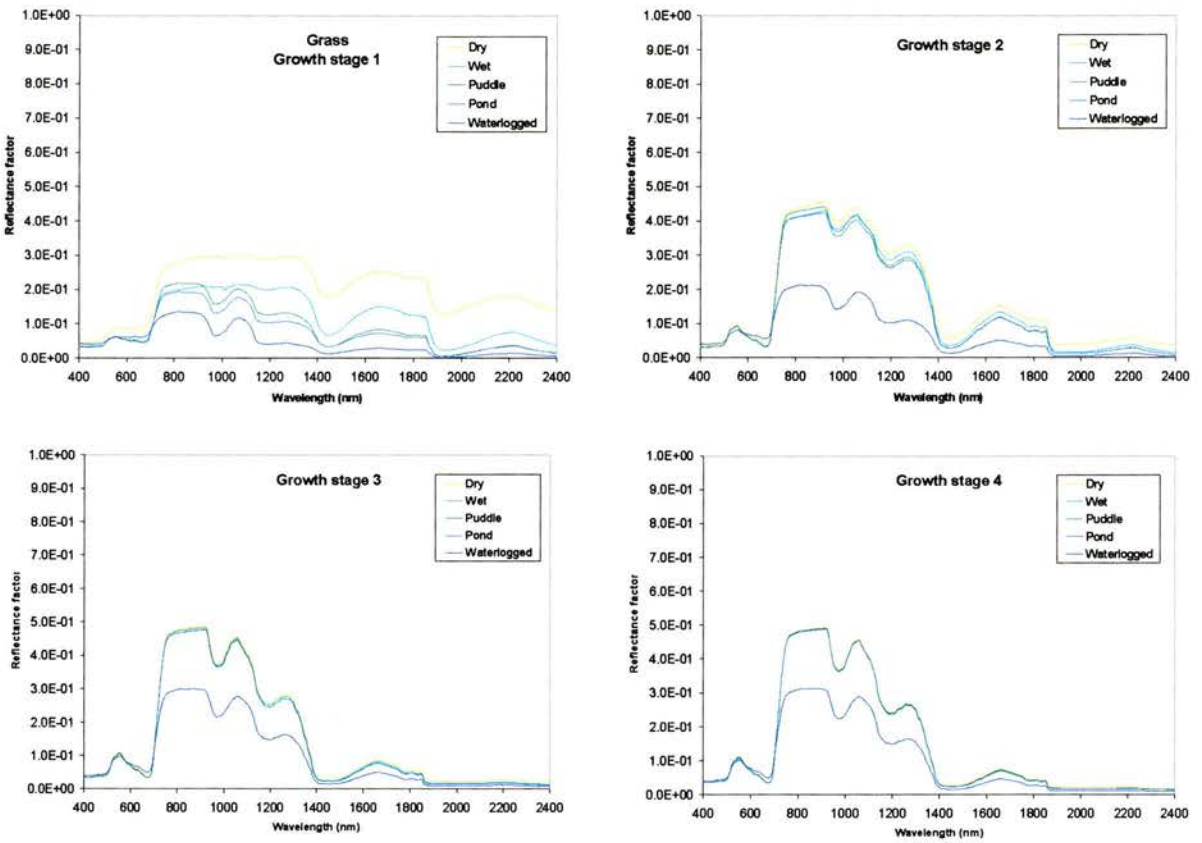

Figure 2.5.3. SAIL and PROSPECT modelled spectral reflectance over a theoretical grass crop under five different wetness conditions and at growth stages 1-4. Where leak scenario reflectances are the same or similar (for example growth stages 3 and 4), the only line clearly visible is the ponding scenario, which overlies, the puddle, wet and dry scenarios. The reflectance curves are drawn in the order that they appear in the legend.

2.5.4 Row crop

The row crop modelling scenarios were based on a sugar beet canopy and only three growth stages were modelled: growth stage one represents a young canopy, growth stage two canopy at maximum growth stage, and growth stage three is a senescing canopy (Figure 2.5.4).

As with all the other modelled canopies the waterlogged scenario showed the greatest impact on reflectance at all growth stages. Perhaps the most interesting point about row crop reflectances is that the more horizontal leaf angular distribution defined for this crop has had a significant influence on reflectance. The row crop leaves provided a greater surface for reflection which explains the higher reflectance observed for this canopy compared to the grass canopy, despite the row crop having a lower leaf area index. All types of leak influenced reflectance at the earliest growth stage, while only the ponding and waterlogged scenarios were clearly distinguishable from the dry scenario at the later growth stages.

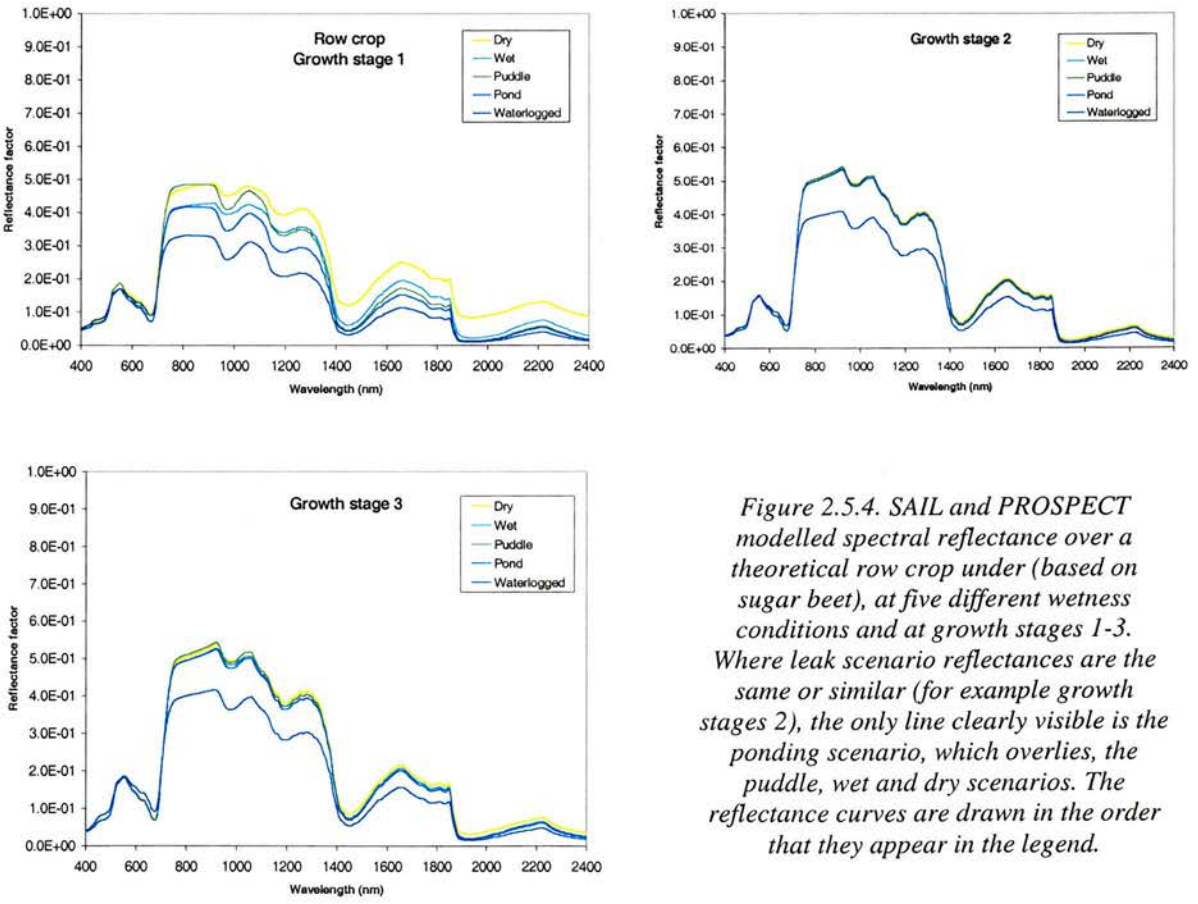

Figure 2.5.4. SAIL and PROSPECT modelled spectral reflectance over a theoretical row crop under (based on sugar beet), at five different wetness conditions and at growth stages 1-3. Where leak scenario reflectances are the same or similar (for example growth stages 2), the only line clearly visible is the ponding scenario, which overlies, the puddle, wet and dry scenarios. The reflectance curves are drawn in the order that they appear in the legend.

2.5.5 Summary

- The dry scenario produced the highest reflectance values across the spectrum.
- For all the cases of optical modelling, at all the growth stages and for all the vegetation types, the waterlogged scenario produced the lowest reflectance values across the whole spectrum (400 - 2400 nm). This is due to the presence of surface water absorbing light, and depleted vegetation reducing canopy reflectance.
- The ponding scenario resulted in mid range values.
- The effects of the 'extra' vegetation added to the puddling scenario meant that there was a trade-off between increasing LAI and background effects such that as LAI increased, the background effects decreased making the puddling scenario very difficult to identify except at the earliest growth stages, and for the modelled cereal crop.
- It was only possible to identify the wet scenario at the first growth stage of all crops, except for the cereal modelling, where the wet scenaio was apparent at all growth stages.
- It is suggested that the identification of all wetness scenarios at all growth stages for the cereal crop modelling is due to the open canopy structure and vertical orientation of the canopy in relation to view angle.

References

Baret, F. 1991. Vegetation canopy reflectance factors of variation and application for agriculture. In Remote Sensing and Geographical Information Systems for Resource Management in Developing Countries. Edited by A.S. Belward and C.R. Valenzuela. Published by Dordrecht ; London : Kluwer.

Chance, J. E and LeMaster, E. W. 1977. Suits reflectance models for wheat and cotton: thoeretical and experimental tests. Applied Optics, **16**, 407-412.

2.6 HYMAP image results

The results presented here are taken from the HYMAP image data. After the image data had been geocorrected and further processed, 5-8 pixel reflectance values were sampled from the vegetation surrounding the 5 sites. 3-6 pixels were sampled from inside each leak (as the leaks were generally smaller in area it was difficult to get more than 6 pixels over the leak per site). The locations of the leaks were identified on the image using GPS points obtained in the field at the time of acquisition. The graphs included show reflectance in the wavelength range sampled by the three HYMAP sensors over 126 channels between 437 and 2486 nm. The spectral sampling interval varies between 13 and 17 nm.

Figure 2.6.1 shows the spectral reflectance curves for leaks and surrounding vegetation at each of the Cheshire sites for both the image data and spectroradiometer data. With the exception of site C1 reflectance of the surrounding vegetation is greater than in-leak reflectances for all sites. Site C1, in which there was no leak present on the day of acquisition, showed greater leak reflectance than those of the surrounding vegetation. All sites showed fairly typical reflectance measurements of green vegetation. The leak that produced the greater overall reflectance was simulated leak C5 as there was no surface water present (refer to section 1.3.2.4) and no negative effects on vegetation associated with the presence of excess water as observed at sites C1, C2 and C3. The in-leak measurements at site C6 were also high because the vegetation was more vigorous inside the leak than the surrounding vegetation. However, there was sufficient surface ponding beneath the denser vegetation to reduce spectral reflectance overall. The non-leak reflectance measurements at sites C2 and C3 were grass with similar canopy heights and densities and as a result they have comparable values.

Much of the difference between leak and surrounding cover is greatest in the near and middle infrared regions due to strong absorption of water. There is little to distinguish between leak and non-leak areas in the visible wavelengths.

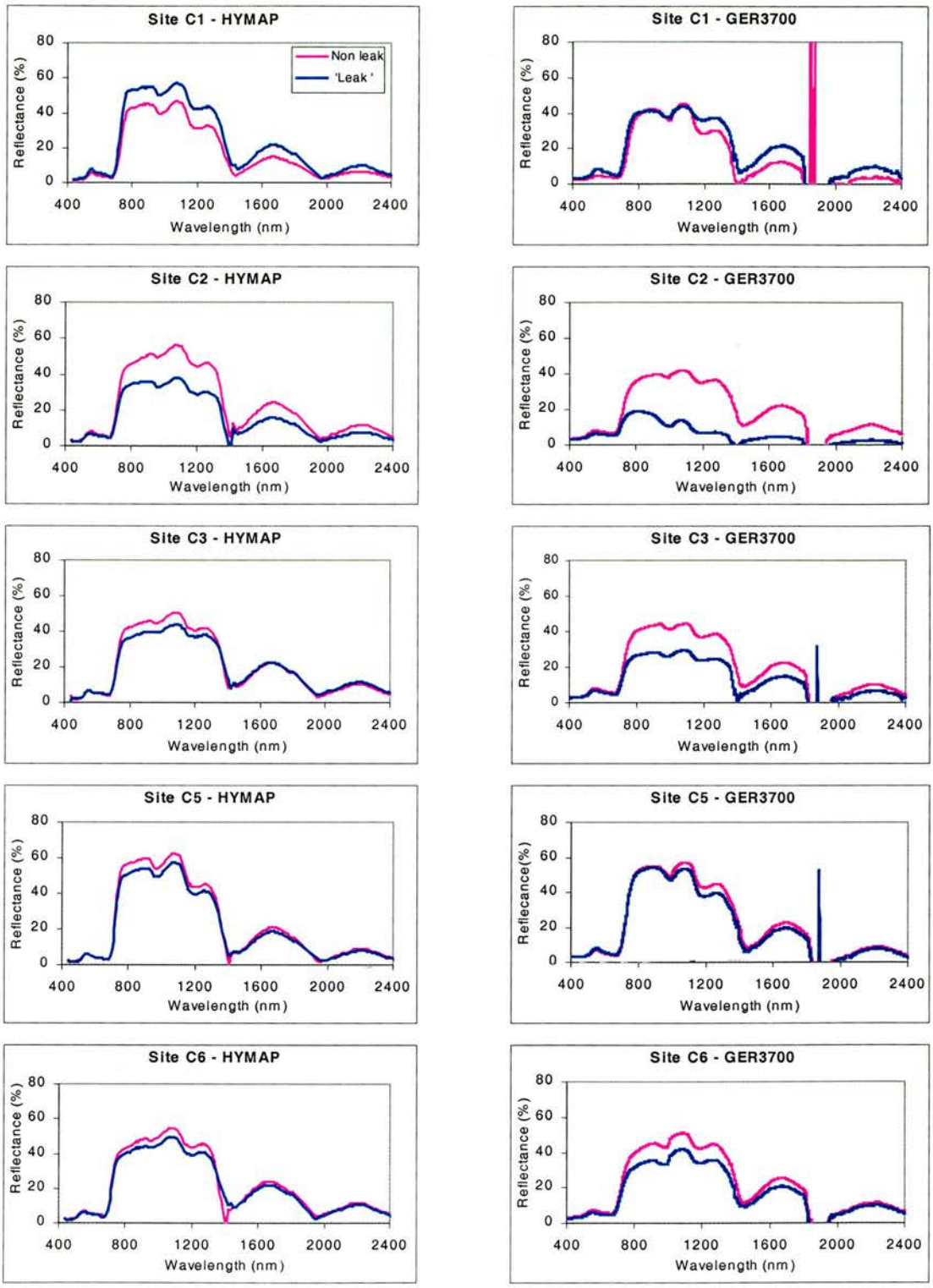

Figure 2.6.1. Comparison between the HYMAP and GER3700 spectroradiometer reflectance measurements for the Cheshire sites taken on 19th June 2000 (pink line is non-leak reflectance, blue line is leak reflectance).

The spectral reflectances obtained from the imagery generally support those made using the spectroradiometer taken on the same day. For sites C1, C2 and C3, NIR reflectances from the spectroradiometer were less than those measured using the HYMAP sensor. In contrast, spectroradiometer and HYMAP reflectances of the surrounding area were relatively similar. These sensor-specific differences in leak reflectance may be attributed to a difference in footprint size. The footprint of the spectroradiometer (less than 0.5 m^2) was approximately an order of magnitude less than that of HYMAP imagery. GER 3700 reflectances were also measured in the leak centre (which showed greatest leak characteristics); HYMAP pixel reflectances were the integral of an area of 9 m^2 which may have included leak edges and effects from the transition from a leak to surrounding cover. This would explain why NIR reflectance is less in the spectroradiometer measurements over leaks in some instances.

2.6.1 Summary

- Using HYMAP hyperspectral data at 3m resolution it is possible to detect reflectance differences in all leaks, at all sites. Differences between leaks and non leak areas are most apparent between 700 and 1900 nm.
- Specroradiometer and image reflectance data show good agreement for the Cheshire sites and the reflectance curves are of similar shape and magnitude.
- In-leak spectroradiometer measurements are typically lower than HYMAP image leak measurements – this is likely due to differences in footprint size with HYMAP leak measurements being influenced by mixed pixels.

2.7 Optical analysis

2.7.1 Creation of an optical leak index

To establish the most appropriate wavelengths for identifying water leaks an analysis of candidate spectral ratios was undertaken using the optical data. The intention was to reveal where in the reflectance spectrum there is most variation in reflectance between leak and non-leak areas. As there are no existing water leak indices, comparisons across the entire spectrum were considered. This was possible because of the high spectral resolution multi-wavelength data available. A normalised difference leak index was created by calculating the ratio of each wavelength to every other wavelength for each vegetation curve. The wavelength ranges for the three available data sets were:

- 400 and 2400 nm (modelled),
- 400 to 1753 nm (spectroradiometer)
- 437 to 2486 nm (image).

This created a matrix for each series both modelled and imaged. The normalised difference leak index was calculated using the following equation (2.7.1).

$$NDLI = \left(\sum_{i=1}^{n} \left(\sum_{j=1}^{n} \left(\frac{\left(\frac{L_i}{L_j} \right) - \left(\frac{NL_i}{NL_j} \right)}{\left(\frac{L_i}{L_j} \right) + \left(\frac{NL_i}{NL_j} \right)} \right) \right) \right) \qquad 2.7.1$$

where L and NL are the leak and non-leak (or wet and dry) reflectances. This equation effectively calculates the normalized difference between two matrices, one containing leak

values the other containing non-leak values. The first matrix is calculated by ratioing each leak reflectance value at every wavelength with every other leak reflectance value for every wavelength, the second matrix is calculated the same way, but for non-leak reflectances. From the resulting normalised difference calculations two dimensional leak and non-leak spectral comparison maps were produced. These are described later in the chapter. Wavelengths from 1300 to 1500 nm, from 1753 to 2010 nm, and longer than 2391 nm were omitted from the image data because of the high level of atmospheric absorption of radiation at these wavelengths, largely by water vapour, which causes a very low signal to noise ratio. For similar reasons, wavelengths shorter than 493 nm were not used because the ATREM atmospheric correction software used to process the HYMAP imagery was unable to fully compensate for the effects of Rayleigh scattering (Perry, 2000). The spectra of leaks and their surrounding vegetation covers were found to be noisy at these wavelengths (Figure 2.7.1).

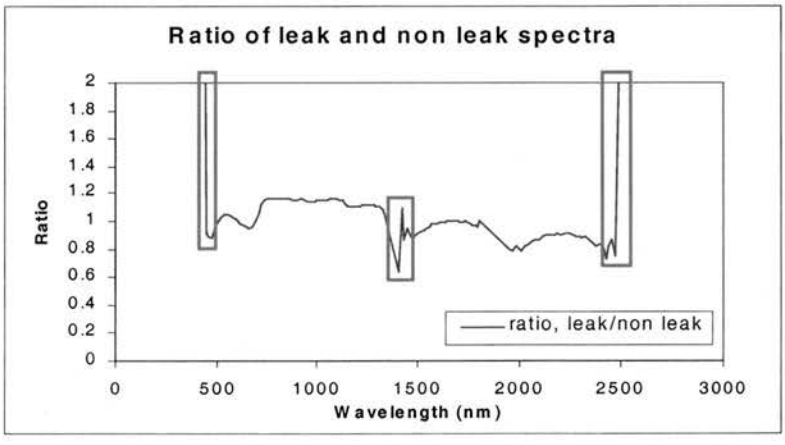

Figure 2.7.1. Regions of reflectance where noisy values were identified using ratio analysis. The red boxes outline the wavelengths that were cut from the data.

Longer wavelengths (greater than 1753 nm) in the spectroradiometer datasets were found to be prohibitively noisy (Figure 2.7.2), to the extent that the variance measurements displayed noise rather than leak/non-leak variances. For this reason wavelengths beyond 1753 nm were removed in addition to those between 1280 and 1500 nm (as for the HYMAP image spectral comparison surfaces) and those shorter than 400 nm.

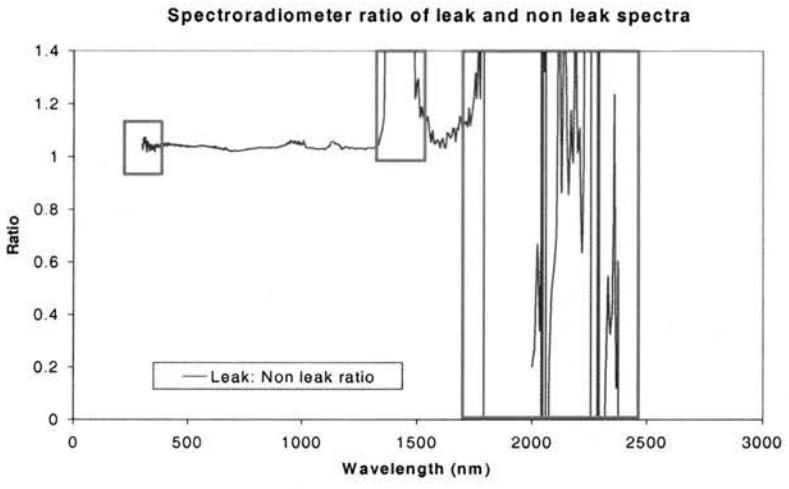

Figure 2.7.2. The ratio of wet to dry spectroradiometer measurements showing regions of considerable data noise. The red boxes outline the wavelengths that were eliminated from the data.

2.7.2 Analysis of the spectral comparison maps

The spectral comparison maps highlight the most appropriate wavelength regions for identifying leaks by showing where the variation between each leak and non-leak area is at a maximum. Areas of largest difference are shown by the yellow colours. For each spectral comparison map there is an accompanying table showing the band ratios that produce the maximum variances, data for which are taken directly from the spectral comparison maps. The 'max 1' column defines the spectral region showing the greatest variation between leak and surrounding vegetation and therefore, the waveband ratios best suited to leak identification for each particular site. 'Max 2' gives the next optimal waveband ratio and 'max 3' gives the third optimal waveband ratio. There is not always a third variance cluster. The broad waveband ranges are: VIS 300-700 nm, NIR 701-1300 nm, MIR 1301-2500. Ranges in the visible and middle infrared may vary depending on the data being used (refer to section 2.7.1). The scale bar is example specific, and shows the range of variation from minimum to maximum. Figure 2.7.3 is a demonstration spectral comparison map. It includes the optical waveband regions, and the omitted wavelength regions (these vary with each data set as described in the previous section). The scales on the x and y axes are the same for all spectral comparison maps in this chapter. The following example comes from spectroradiometer-based measurements.

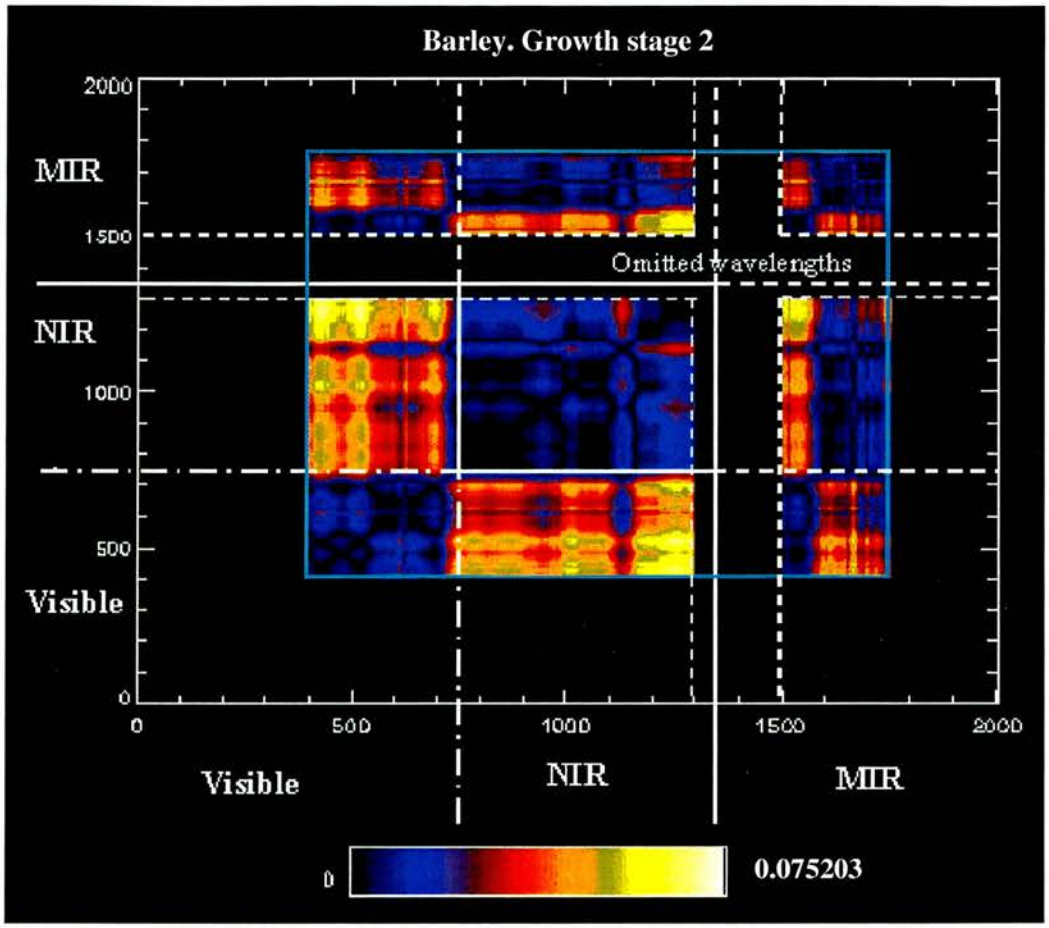

2.7.3. Example spectral comparison map showing waveband regions (visible; 400 – 750 nm, NIR; 750 – 1350 nm and MIR; 1350 – 1753 nm) and omitted wavelengths (<400 nm; 1280 – 1500 nm; > 1753 nm).

In the example, maximum variations between leak and non-leak occur in the visible and near infrared, and near infrared and middle infrared regions of the spectral comparison map. They are identified as yellow clusters. In the visible and near infrared region there are several different wavelength combinations within the matrix, i.e. (420,1240), (520,1240), (700,1240), (420,1010), and (510,1010). Where multiple clusters are identified the largest, and those demonstrating maximum variations, are described in the supporting table. In this case the optimal waveband combinations in order of scale and magnitude are VIS – NIR, VIS - NIR and NIR – MIR. The maximum variation value is 0.075 (to the right of the scale bar) and is unitless because it is a ratio based product of the normalised difference index. The closer to 1 the variation value is, the greater the spectral difference between leak and non-leak, thus making the leak more easily identifiable.

2.7.3 Spectroradiometer analysis

2.7.3.1 Cheshire sites

Figure 2.7.4 shows spectral comparison maps for the five Cheshire leak sites where there were three real and two simulated leaks, and included one wheat canopy and four grass canopies. Table 2.7.1 details the three optimal waveband ratios identified as showing the greatest variations between leak and surrounding vegetation, for each of the sites.

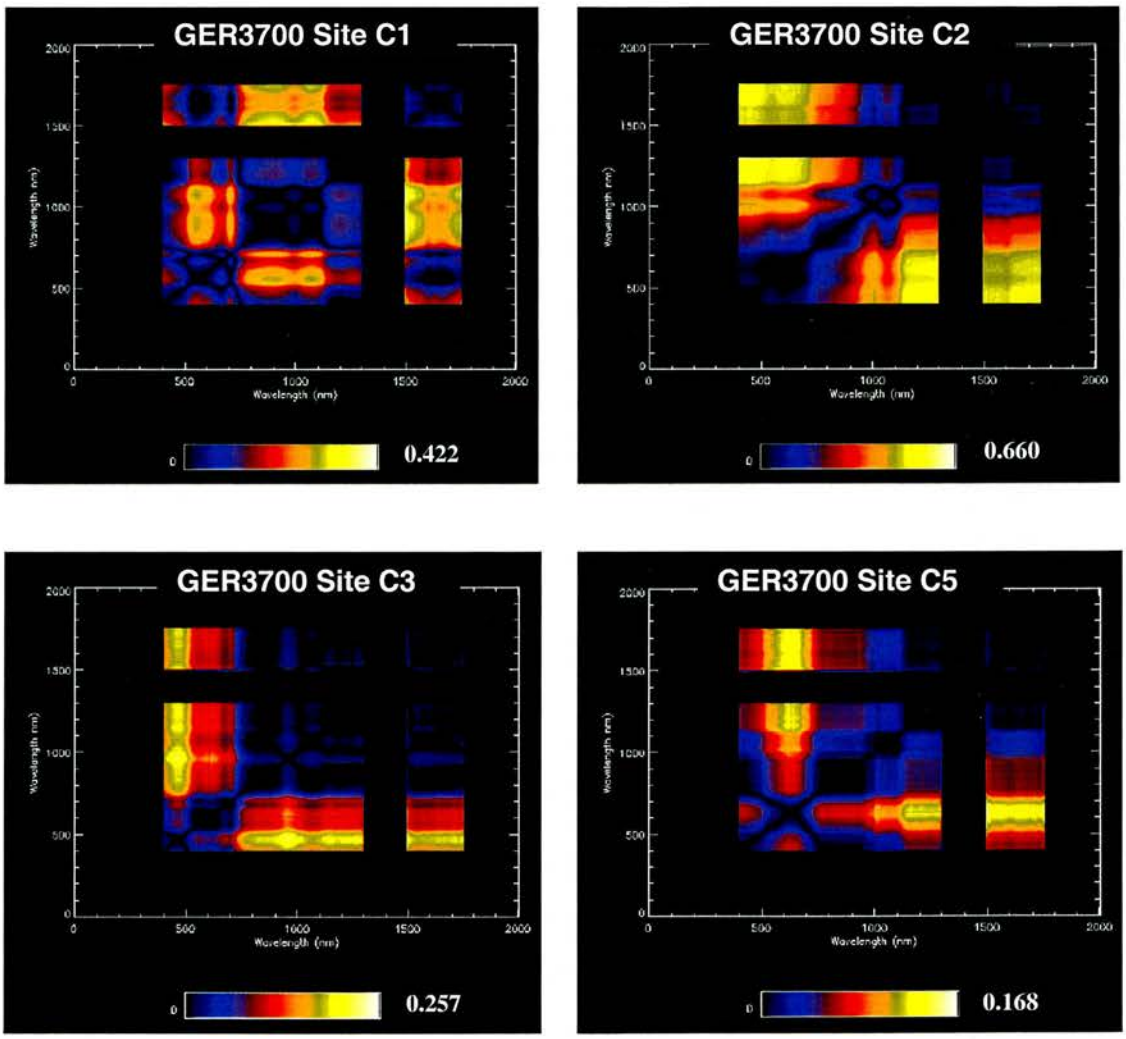

Figure 2.7.4 is continued on the next page.

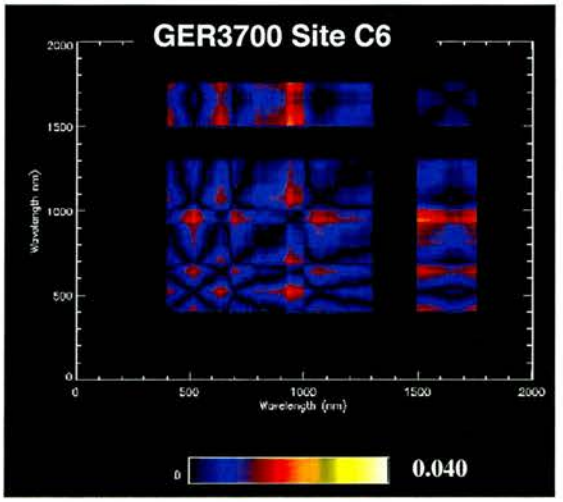

Figure 2.7.4. Spectral comparison maps showing variations between leak and non-leak for wavelengths between 400 and 1753 nm, for Cheshire spectroradiometer measurements.

Table 2.7.1. Summary of optimal wavebands for identifying maximum variations between leak and non-leak from spectral comparison surfaces, based on Cheshire spectroradiometer measurements.

	MAX 1	MAX 2	MAX 3
Site C1	NIR - MIR	NIR – MIR	
Site C2	VIS - MIR	VIS - MIR	VIS - MIR
Site C3	VIS - NIR	VIS – MIR	VIS - MIR
Site C5	VIS (red) – MIR	VIS (red) - MIR	
Site C6	NIR - MIR	NIR - MIR	VIS - NIR

The spectral comparison maps in Figure 2.7.4 show that the leak site demonstrating maximum variation between leak and surrounding vegetation is C2, where the variation is 0.660. Sites C1 and C3 have values demonstrating variations of 0.422 and 0.257 respectively, and site C5 shows a variation value of 0.168. The leak site showing the lowest variation is C6, with a value of 0.040. These results show relatively small variations for simulated leak C5 where surface ponding was not achieved, and C6 where the vegetation inside the leak was vigorous, and therefore masked the underlying leak. At leak sites C1 – C3 the leaks had been present long enough to have a negative effect on vegetation, thus creating a significant difference between leak and surrounding vegetation, despite there being no water present at site C1, and C2 being a simulated leak.

Optimal wavebands for leak identification vary between the three highlighted waveband regions (Table 2.7.1) such that it would be difficult to establish a single optimal leak index for all Cheshire leaks based on the spectroradiometer data.

2.7.3.2 Oil seed rape

Figure 2.7.4 shows the spectral comparison maps for the Edinburgh-based spectroradiometer measurements for simulated leaks under oil seed rape at five growth stages.

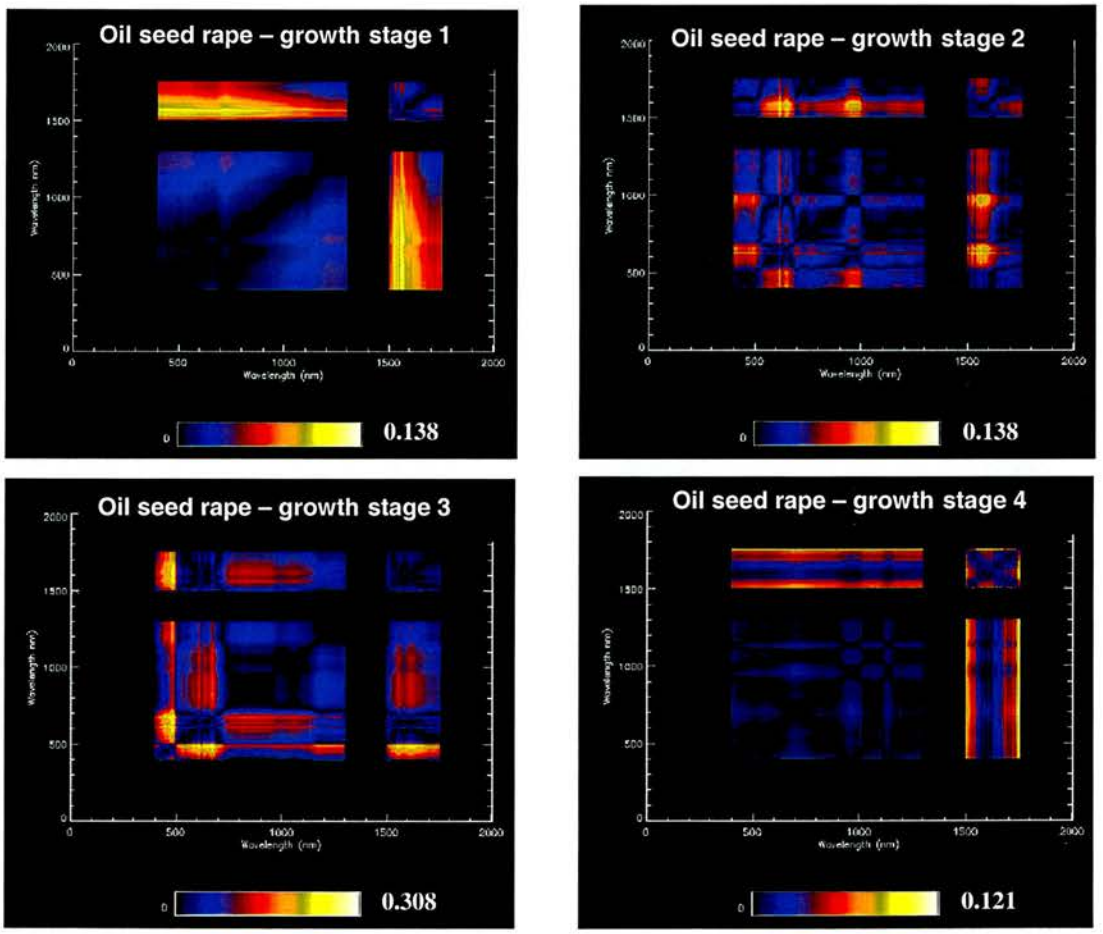

Figure 2.7.5 is continued on the next page.

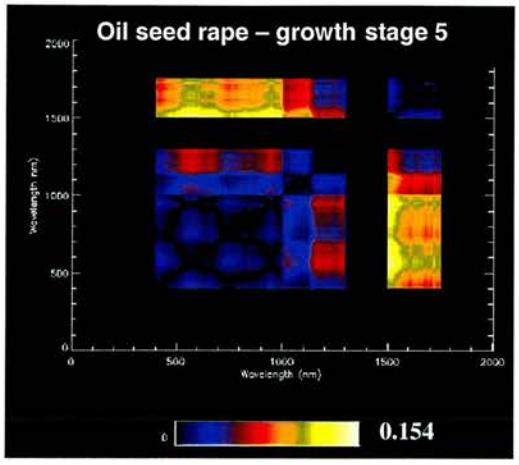

Figure 2.7.5. Spectral comparison maps showing variations between leak and non-leak for wavelengths between 400 and 1753 nm, for oil seed rape spectroradiometer measurements at 5 growth stages.

Table 2.7.2. Summary of optimal wavebands for identifying maximum variations between leak and non-leak from spectral comparison surfaces, based on oil seed rape spectroradiometer measurements.

SPECTRO	MAX 1	MAX 2	MAX3
Oil seed rape 1	VIS – MIR	VIS – MIR	
Oil seed rape 2	VIS – MIR	VIS – MIR	VIS – NIR
Oil seed rape 3	VIS – NIR	VIS – MIR	
Oil seed rape 4	VIS – MIR	NIR - MIR	
Oil seed rape 5	VIS - MIR	NIR - MIR	

Despite wavelengths being cut from the data it still appears to be noisy, particularly for oil seed rape, growth stage 4. The results for the spectral comparison surfaces show that the greatest variation between wet and dry occurs at growth stage three with a value of 0.308. Minimum variation between leak and non-leak is found at growth stage 4 with a value of 0.121. This is expected due to the dense canopy cover at the later growth stage. However, the difference between growth stage 1 and 2 variations is small compared to those for growth stage 4 with both 1 and 2 demonstrating variations between leak and surrounding vegetation of 0.138. Growth stage 5 has a variation value of 0.154. The results suggest that there is little variation between leak and surrounding vegetation at early and later growth stages, with growth stage 3 appearing to be the optimal growth stage for leak identification. For growth stages 1, 4 and 5 the variation clusters cover wide spectral regions, while for growth stages 2 and 3 the clusters are small. This makes leak identification for growth stages 1, 4 and 5 less wavelength specific and potentially

suited to sensors with lower spectral resolution than the GER3700. The optimal waveband combination for oil seed rape at a variety of growth stages is identified as visible and middle infrared (although this does not apply to growth stage 3 which shows the maximum variation). At later growth stages a near and middle infrared index may also be successful at identifying leaks (Table 2.7.2).

2.7.3.3 Barley

Figure 2.7.6 shows four spectral comparison maps representing simulated leaks under four different growth stages of a barley crop. Table 2.7.3 provides a summary of the optimal waveband regions identified for each growth stage where maximum variation between leak and non-leak occurs.

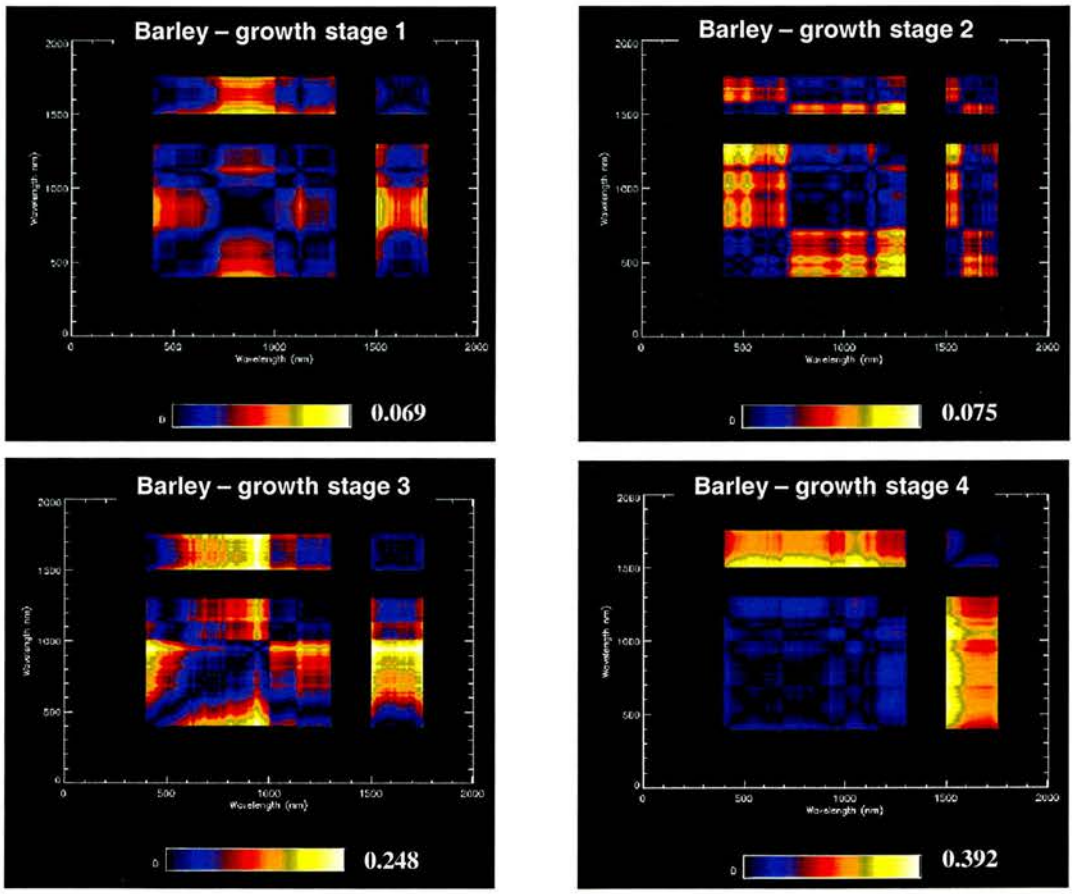

Figure 2.7.6. Spectral comparison maps showing variations between leak and non-leak for wavelengths between 400 and 1753 nm, for barley spectroradiometer measurements at 4 growth stages.

Table 2.7.3. Summary of optimal wavebands for identifying maximum variations between leak and non-leak from spectral comparison surfaces, based on oil seed rape spectroradiometer measurements.

SPECTRORADIOMETER	MAX 1	MAX 2	MAX 3
Barley 1	NIR - MIR	NIR - MIR	VIS - NIR
Barley 2	VIS - MIR	VIS (red) - MIR	VIS - NIR
Barley 3	NIR - MIR	VIS - NIR	
Barley 4	VIS – MIR	NIR – MIR	MIR - MIR

The results for the barley measurements show that the optimal growth stage for identifying leaks is 4 (stubble, after the crop has been harvested) with a variation value of 0.391. The second highest variation is the maximum growth stage (3) with a value of 0.248. The early growth stages had low variance values (less than 0.1). The reasons for these results are not fully understood but may be due to noisy data resulting from changing light conditions during acquisition of the original data, particularly for growth stages 3 measurements. Overall the optimal wavelengths are divided between waveband combinations of near and middle infrared, and visible and middle infrared (Table 2.7.3).

2.7.4 Modelled data

The results presented here are for predicted leak indices based on the modelled data. The maximum and minimum growth stages are presented for canopy, cereal, grass and row crops under 2 different wetness scenarios. The selected wetness scenarios are waterlogged and ponding as these were the most frequently encountered leak conditions observed in the field, and they showed the most interesting results. Furthermore, they represent the most extreme leak scenario (waterlogged) and also an example of a recent leak (ponding scenario). While the ponding scenario was not the least extreme leak scenario (i.e. the wet soil scenario), it was believed that in practical terms a leak index to identify wet soil would not be feasible and would result in the misidentification of leaks.

2.7.4.1 Canopy crop growth stages 1 – 4 (ponding and waterlogged scenarios)

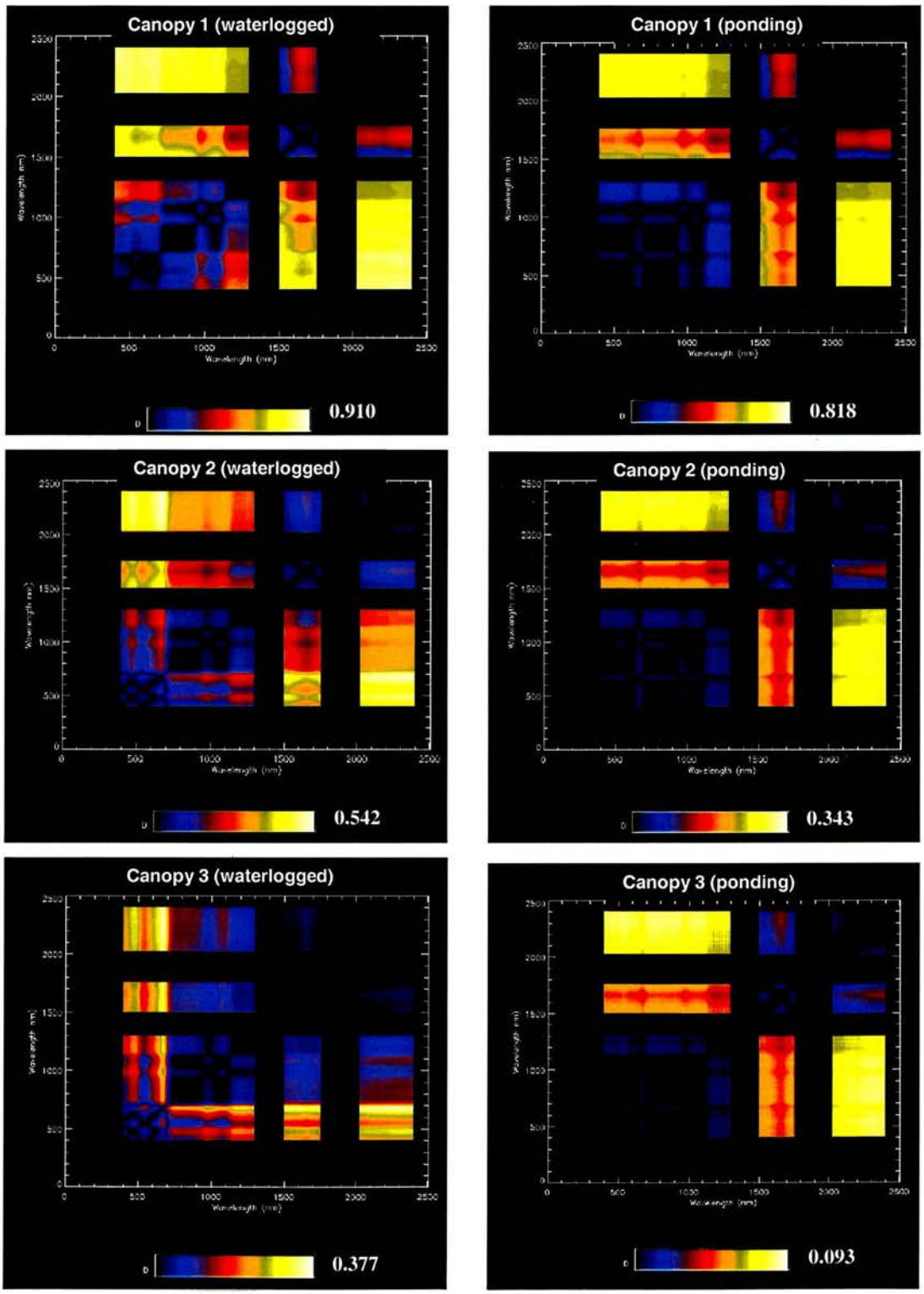

Figure 2.7.7 is continued on the next page.

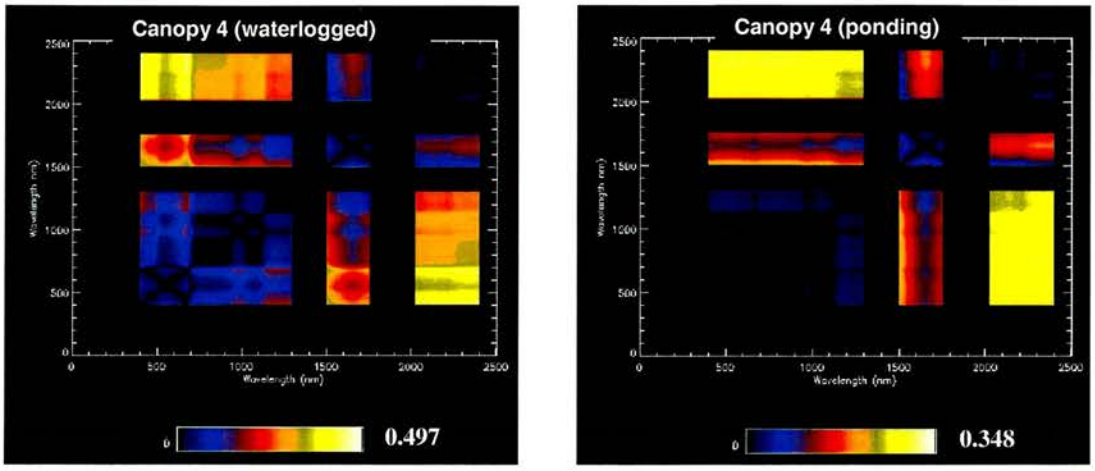

Figure 2.7.7. Spectral comparison maps showing variations between leak and surrounding vegetation based on modelled results for a canopy crop at growth stages 1 - 4, under waterlogged (left) and ponding (right) leak scenarios. The spectral range is 400-2400 nm.

Table 2.7.4. Summary of optimal leak identification wavebands for a modelled canopy crop.

MODEL	MAX 1	MAX 2	MAX 3
Canopy 1 waterlogged	VIS – MIR	VIS - NIR	
Canopy 1 ponding	VIS – MIR	VIS - NIR	
Canopy 2 waterlogged	VIS – MIR	VIS – MIR	
Canopy 2 ponding	VIS – MIR	NIR - MIR	
Canopy 3 waterlogged	VIS – MIR	VIS – MIR	VIS - MIR
Canopy 3 ponding	VIS – MIR	VIS - NIR	
Canopy 4 waterlogged	VIS – MIR	VIS – MIR	
Canopy 4 ponding	VIS – MIR	NIR - MIR	

Analysis on the modelled canopy spectral reflectance maps shows that overall the greatest variation values relate to growth stage 1, and the least variation between leak and non-leak is at the maximum growth stage 3. Typically differences between leak and surrounding vegetation are greater in terms of scale and magnitude for the waterlogged scenarios compared with ponding scenarios in Figure 2.7.7, particularly at growth stage 3 where the waterlogged scenario has a maximum variation value of 0.376 compared with 0.093 for the ponding scenario. This is due to the negative effects of waterlogging on vegetation growth where contrasts are greatest when surrounding vegetation is vigorous in relation to the depleted vegetation inside the leak. The spectral comparison maps derived from the modelled canopy crop waterlogged scenarios produce broad spectral regions where variations between leak and non-leak are high, indicating that a wide range of spectral indices may be suitable for identifying leaks (Table 2.7.4).

At growth stage 1 while both the waterlogged and ponding scenario variance values are high, there is very little difference between them (0.818 and 0.865), suggesting that below a certain vegetation density threshold the most important factor controlling reflectance is the presence of water rather than vegetation. At this early growth stage there is also little to separate optimal leak indices between the visible, near and middle infrared wavelengths for both scenarios. The predicted optimal wavelengths for identifying leaks against a canopy crop at the above-mentioned growth stages are visible and middle infrared wavelength combinations.

2.7.4.2 Cereal crop growth stages 1 – 4 (ponding and waterlogged scenarios)

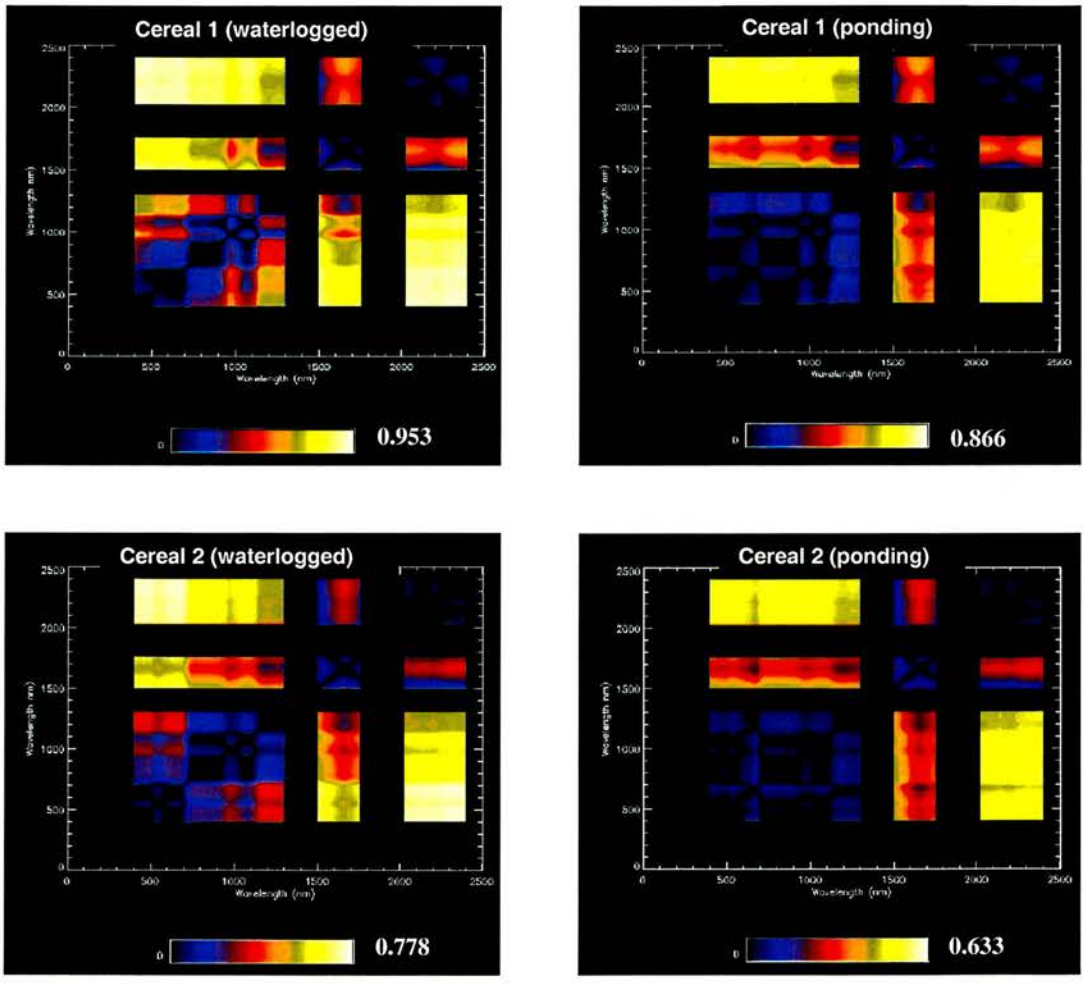

Figure 2.7.8 is continued on the next page.

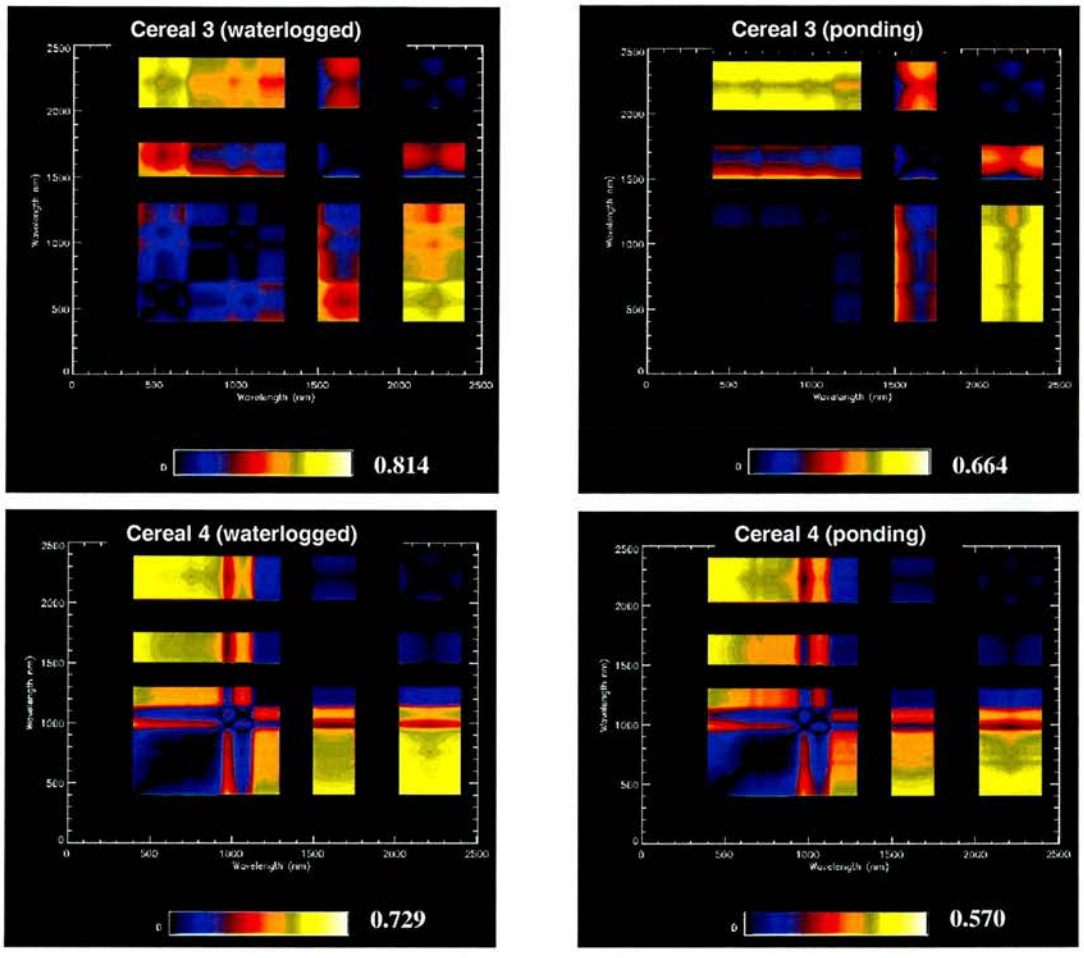

Figure 2.7.8. Spectral comparison maps showing variations between leak and surrounding vegetation based on modelled results for a cereal crop at growth stages 1 - 4, under waterlogged (left) and ponding (right) leak scenarios. The spectral range is 400 – 2400 nm.

Table 2.7.5. Summary of predicted optimal leak identification wavelengths for a modelled cereal crop.

MODEL	MAX 1	MAX 2	MAX 3
Cereal 1 waterlogged	VIS – MIR	VIS (red) - MIR	NIR - MIR
Cereal 1 ponding	VIS – MIR	NIR - MIR	
Cereal 2 waterlogged	VIS - MIR	VIS - MIR	
Cereal 2 ponding	VIS - MIR	VIS - MIR	
Cereal 3 waterlogged	VIS – MIR	NIR - MIR	
Cereal 3 ponding	VIS – MIR	NIR - MIR	
Cereal 4 waterlogged	VIS - MIR	VIS - MIR	
Cereal 4 ponding	VIS - MIR	VIS - MIR	

For the spectral comparison maps for modelled cereals in Figure 2.7.8 the variation values are high compared with other modelled crops. Maximum variation values relate to growth stage 1 for both waterlogged and ponding scenarios with values of 0.953 and 0.865 respectively. The growth stage showing the least variation between leak and surrounding vegetation is growth stage 4 (stubble). This is due to differences in absolute reflectance with the 'dry' stubble have relatively low reflectances relative to the waterlogged and ponding stubble reflectances, compared to the dense and vigorous vegetation reflectances for wet and dry scenarios at growth stages 2 and 3. This results from the normalising process.

At all growth stages the variation values for the waterlogged scenarios are greater than the ponding scenarios, the differences are greatest between the two leak scenarios at growth stage 3. As with the canopy crop analysis, this is due to contrasts between the unaffected vegetation in the ponding scenario, and the depleted vegetation in the waterlogged scenario. At growth stage 1 the differences between the waterlogged and ponding scenario are small due to significant contributions from water rather than vegetation. The wavelength regions are broader (i.e. high value clusters show little variation across wide spectral regions) when vegetation density is low and for the waterlogged leak/non-leak spectral comparisons. This shows that significant variations between leak and surrounding vegetation occur over several wavebands, increasing the range of potential waveband combinations for leak identification. Visible and middle infrared are the dominant wavelengths for identifying leaks against a cereal background, although due to the latter point other possible wavelength combinations include near and middle infrared (Table 2.7.5). It is suggested that at early growth stages soil reflectance greatly contributes to the observed differences between wet and dry in the visible part of the spectrum. Similar wet and dry values in the visible region occur when vegetation density is greater. Therefore, more vegetated surfaces provide a good basis for ratio analysis creating a contrast between where values are similar (i.e. in the visible part of the spectrum) and where values are different (i.e. in the near and middle infrared parts of the spectrum).

2.7.4.3 Grass crop growth stages 1 – 4 (ponding and waterlogged scenarios)

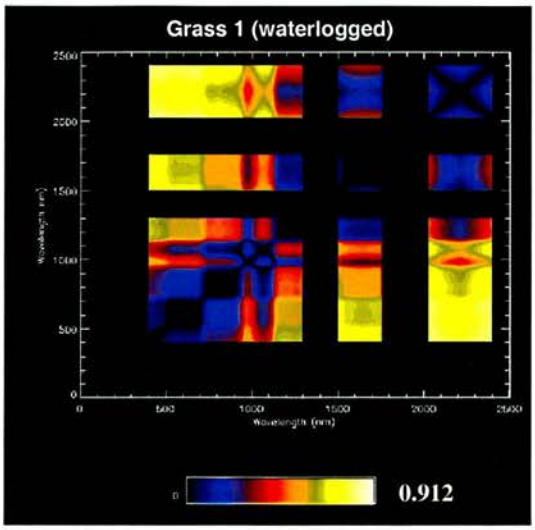

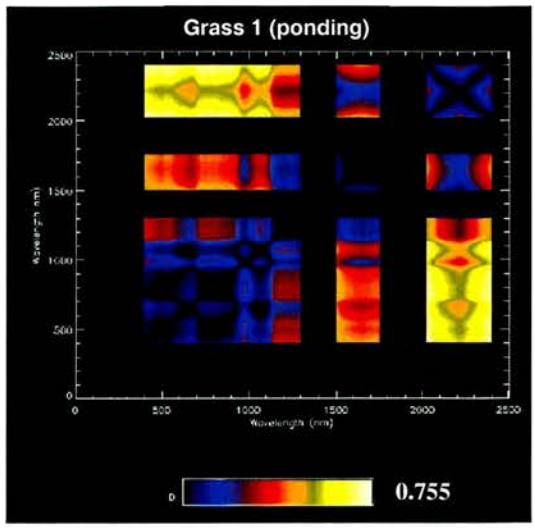

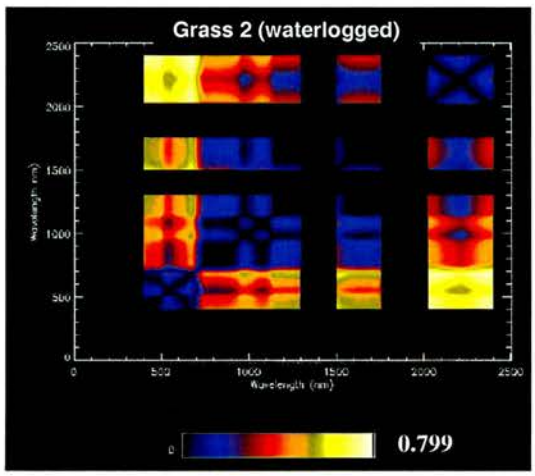

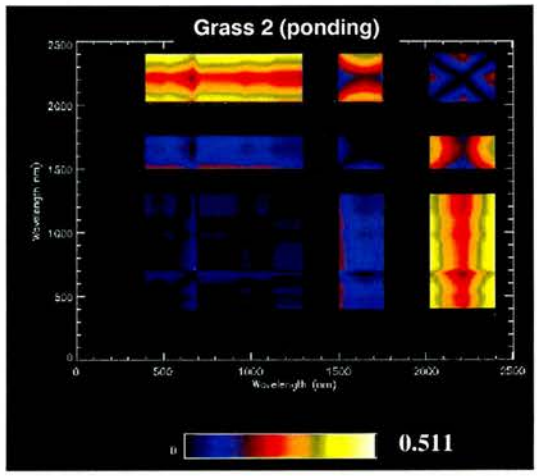

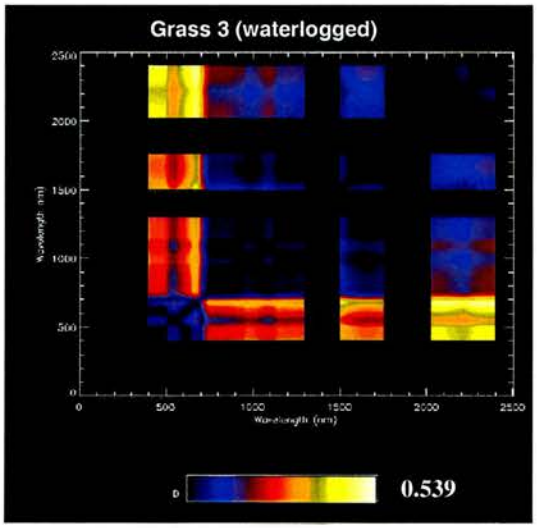

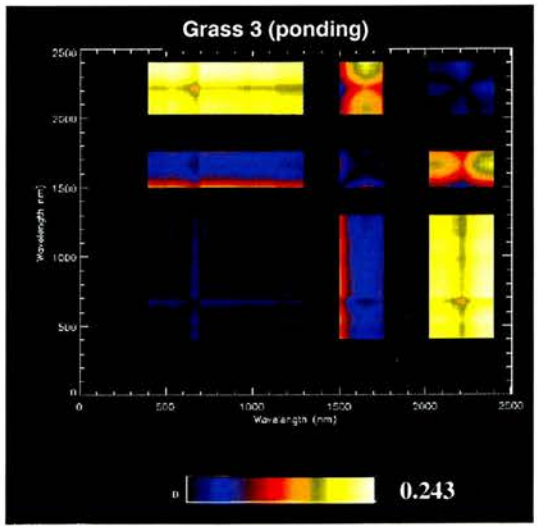

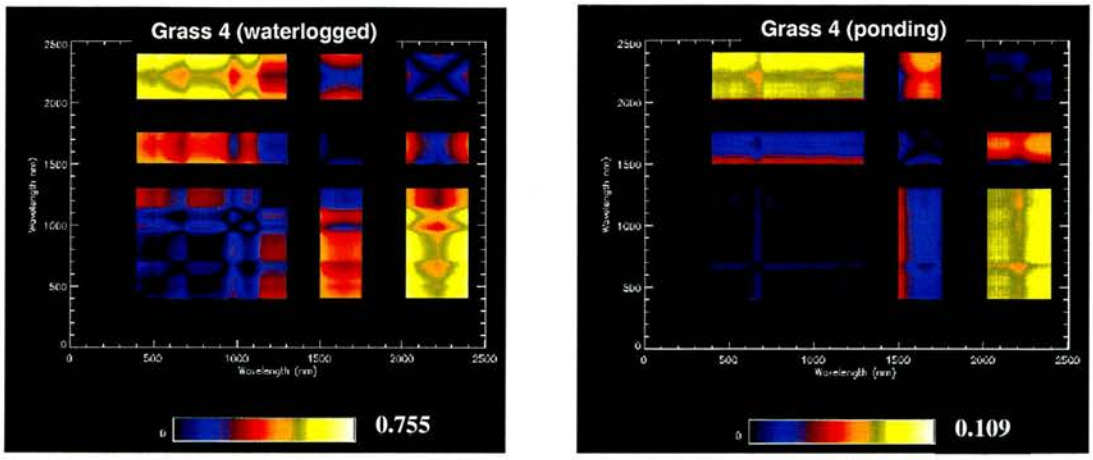

Figure 2.7.9. Spectral comparison maps showing variations between leak and surrounding vegetation based on modelled results for a grass canopy at growth stages 1 - 4, under waterlogged (left) and ponding (right) leak scenarios. The spectral range is 400 – 2400 nm.

Table 2.7.6. Summary of predicted optimal leak identification wavelengths for a modelled grass canopy.

MODEL	MAX 1	MAX 2	MAX 3
Grass 1 waterlogged	VIS – MIR	VIS - MIR	VIS - MIR
Grass 1 ponding	VIS – MIR	NIR - MIR	VIS - MIR
Grass 2 waterlogged	VIS – MIR	VIS – MIR	
Grass 2 ponding	VIS - MIR	NIR - MIR	
Grass 3 waterlogged	VIS - MIR	VIS - MIR	
Grass 3 pond	VIS - MIR	NIR – MIR	MIR - MIR
Grass 4 waterlogged	VIS - MIR	NIR – MIR	
Grass 4 ponding	VIS - MIR	NIR – MIR	

The ponding variations between leak and non-leak modelled grass canopies exhibit lower values than the waterlogged variation values for all growth stages. The grass canopy spectral comparison maps (as already demonstrated for canopy and cereal crop calculations), show that there is relatively little difference between the waterlogged and ponding scenarios at growth stage 1, and a more marked difference at growth stage 3. The distinction between leak and surrounding vegetation variation values for the two scenarios increases with vegetation density. The differences between leak and non-leak, at later grass growth stages and for ponding type leaks are such that the potential for identifying leaks is reduced compared with waterlogged scenarios. The predicted optimal wavelengths for identifying water leaks behind a grass crop at different growth stages are visible and middle infrared for both wetness scenarios. Other possible wavelength combinations identified are near and middle infrared wavelengths (Table 2.7.6).

2.7.4.4 Row crop growth stages 1 – 3 (ponding and waterlogged scenarios)

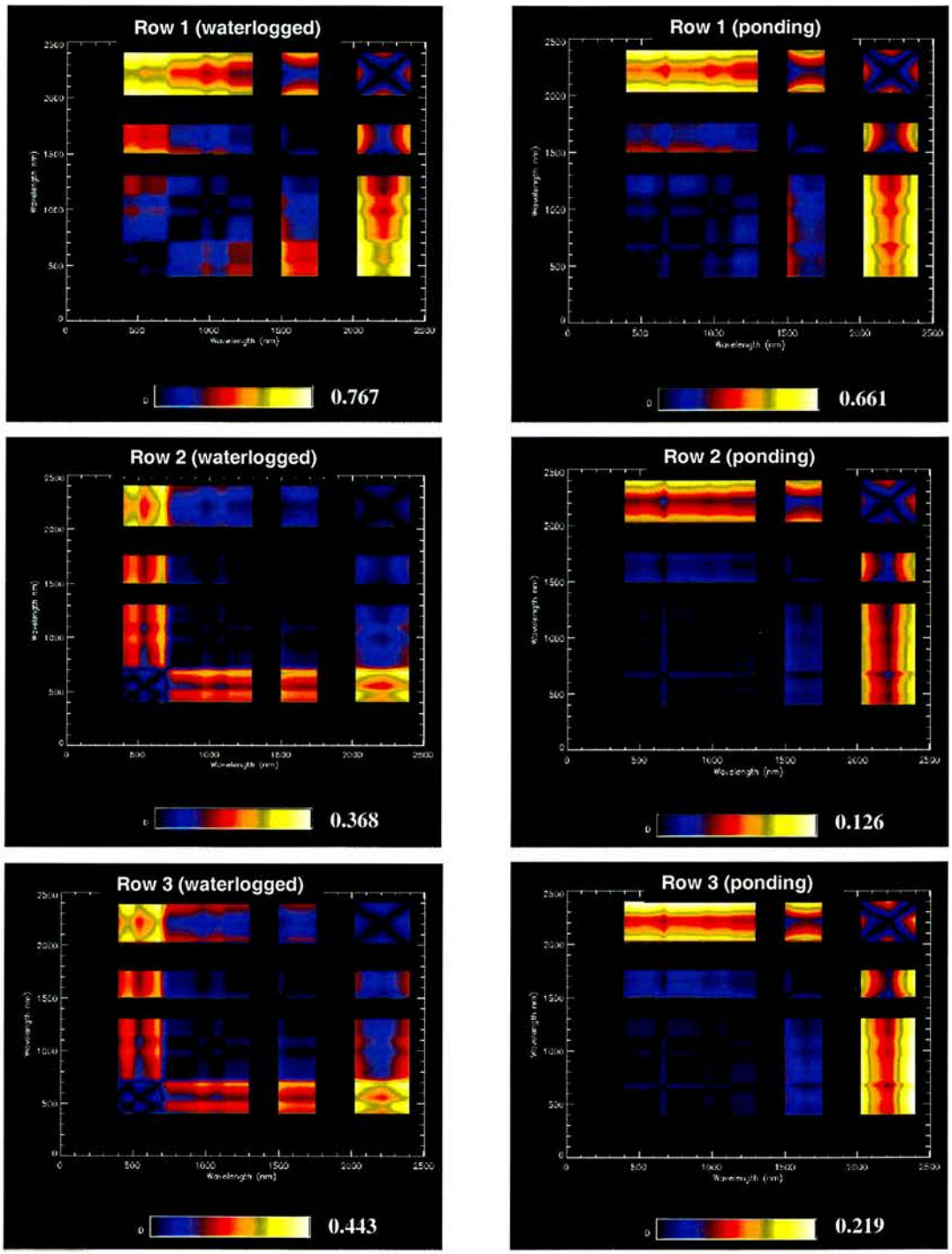

Figure 2.7.10. Spectral comparison maps showing variations between leak and surrounding vegetation based on modelled results for a cereal crop at growth stages 1 - 4, under waterlogged (left) and ponding (right) leak scenarios. The spectral range is 400 – 2400 nm.

Table 2.7.7. Summary of predicted optimal leak identification wavelengths for a modelled row crop.

MODEL	MAX 1	MAX 2	MAX 3
Row 1 waterlogged	VIS – MIR	VIS - MIR	
Row 1 ponding	VIS - MIR	NIR – MIR	
Row 2 waterlogged	VIS – MIR	VIS - MIR	
Row 2 ponding	VIS - MIR	NIR – MIR	
Row 3 waterlogged	VIS – MIR	VIS - MIR	
Row 3 ponding	VIS - MIR	NIR – MIR	

The maximum variation between leak and surrounding modelled row crop vegetation of all growth stages is identified at growth stage one, for both leak scenarios. The variance values for both the ponding and waterlogged scenario are lower at the later growth stages this is due to increased contribution from vegetation reflectance masking ground contribution. At growth stage 1 the leaves have not reached their full leaf area therefore, the ground (and thus standing water behind the vegetation canopy for the leak scenarios) remains visible. As the leaves increase in area they mask the ground completely so that even the depleted vegetation in the waterlogged scenario covers a large proportion of the ground area. These effects are more apparent for the modelled row crop than for other crops due to the horizontal orientation and relatively large area of the leaves. Overall, the waterlogged scenarios (as with other crop analyses), show greater maximum variation values than the ponding scenarios making leak identification easier under waterlogged conditions at all growth stages. The optimal waveband combinations identified as highlighting the greatest variations between leak and non-leak for a modelled row crop are visible and middle infrared. However, the variation clusters in the waterlogged spectral comparison maps and the early growth stages tend to show similar variation values over broad spectral regions, thus increasing the range of potential waveband combinations for leak identification to include near and middle infrared wavelengths.

2.7.5 Image analysis

Figure 2.7.11 shows spectral comparison for the five Cheshire leak sites using values extracted from the HYMAP image data. Table 2.7.1 gives a summary of the optimal broad wavelength categories for identifying water leaks at each of the Cheshire sites.

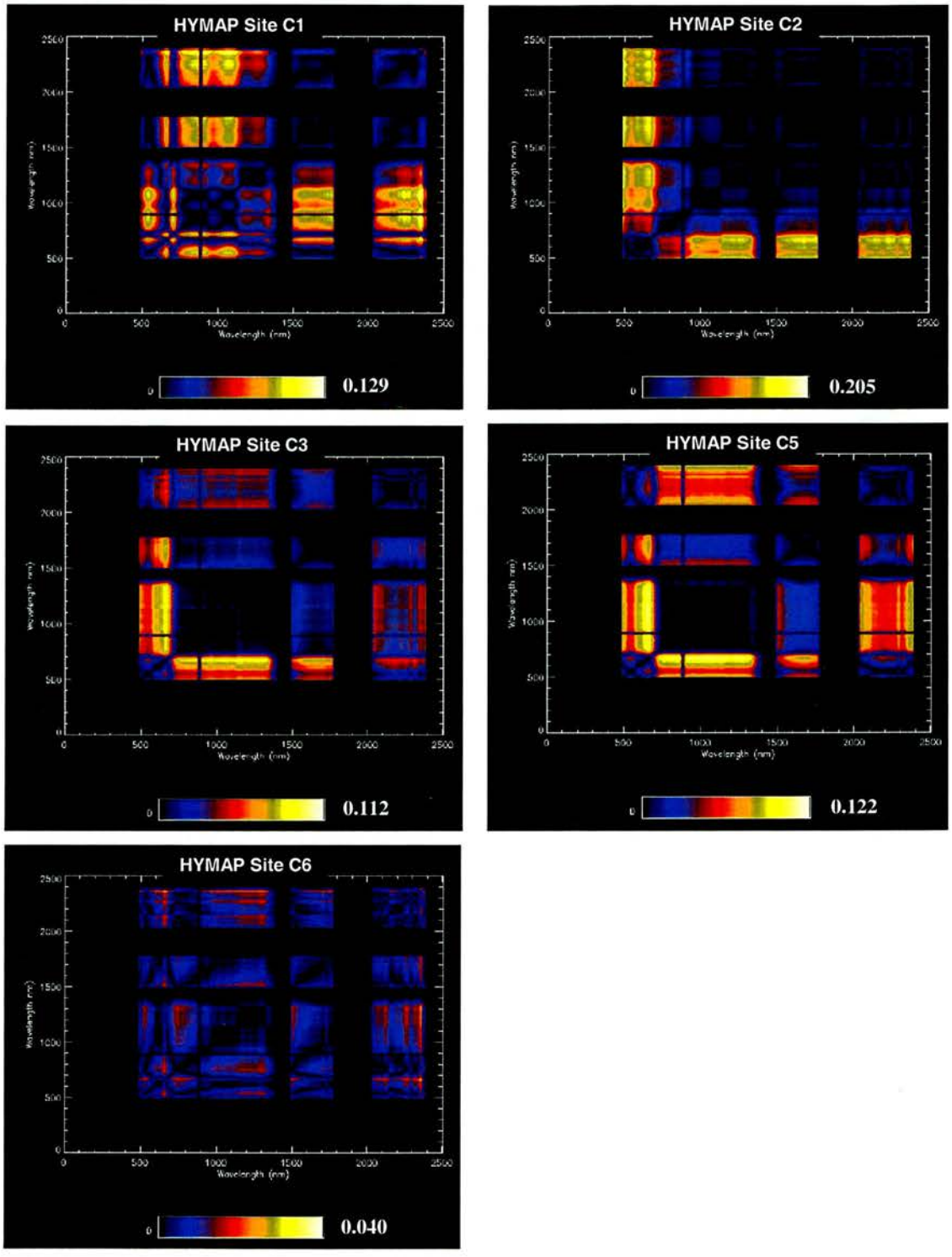

Figure 2.7.11. Spectral comparison maps showing variations between leak and non-leak for wavelengths between 437 and 2486 nm, for Cheshire leak sites, based on HYMAP image data.

Table 2.7.8. Summary of optimal wavebands for identifying maximum variations between leak and non-leak from spectral comparison surfaces, for each of the Cheshire leak sites, based on HYMAP image data.

	MAX 1	MAX 2	MAX3
Site C1	NIR – MIR	NIR – MIR	VIS - NIR
Site C2	VIS (red) - MIR	VIS (red) – MIR	VIS (red) - MIR
Site C3	VIS (red) – MIR	VIS (red)- NIR	VIS (red) - MIR
Site C5	VIS (red) – MIR	VIS (red) - NIR	
Site C6	VIS (red) – MIR	VIS(red) – NIR	VIS (red) - MIR

Results show that as for the spectroradiometer spectral comparison maps, the site demonstrating the greatest difference between leak and surrounding vegetation is C2, with a maximum variation value of 0.205 for the reasons explained previously. Again, as with the spectroradiometer analysis results, the leak that is least easy to identify site is C6 with a variance of 0.0402.

The clusters of variation values for the grass sites (C2 – C6) tend to cover a range of spectral regions. The optimal wavebands for maximizing differences between leaks and surrounding vegetation (and hence for best detecting them) are identified as visible and middle infrared, and visible and near infrared combinations (except site C1). Site C1 is the only site where a combination of NIR and MIR wavelengths are identified as the optimal wavelengths for leak identification. However, it is important to remember that there was no water present at this site at the time of acquisition. This example can be considered atypical as shown by the results.

The waveband regions identified from the image data spectral comparison maps differ from those identified in the analysis of the Cheshire-based spectroradiometer comparison maps. For the spectroradiometer analysis there was no single optimal waveband combination identified for optimal leak identification across all sites. For the image analysis clear wavebands can be identified for the grass covered sites. An explanation is that the spectroradiometer highlighted more of the variations between sites in terms of leak conditions and vegetation characteristics due to it having a greater spectral resolution and higher spatial resolution (but smaller footprint size) than the HYMAP sensor.

2.7.6 Summary

- Maximum differences between leak and surrounding vegetation occur at the earliest growth stages and for waterlogged scenarios.
- For the spectral comparison maps of Cheshire spectroradiometer data there were no clear waveband combinations suitable for leak identification across all sites.
- Spectroradiometer spectral comparison maps for simulated leaks under oil seed rape produced an optimal waveband combination of visible and middle infrared for all growth stages except growth stage 3 (the reasons for this are unknown).
- Spectroradiometer spectral comparison maps for simulated leaks under barley produced no clear wavelength combinations suitable for leak identification across all growth stages. The reason may be due to noise in the original data.
- For the modelled output, the predicted optimal wavebands are broad regions in the visible and middle infrared parts of the spectrum.
- For the HYMAP image data the optimal index for most leaks encountered was a combination of visible and middle infrared, and visible (red) and near infrared wavebands.
- The reasons for differences between the HYMAP and spectroradiometer spectral comparison maps for the Cheshire leak sites are due to differences in spectral and spatial resolution.
- The second optimal normalised leak index for all the data types is a visible and near infra red wavelength combination.
- For modelled scenarios there is a greater difference in variance values between waterlogged and ponding scenarios at growth stage 3, than growth stage 1. At early growth stages much of the variation is due to the presence of water, rather than vegetation. Therefore, waterlogged and ponding values are high, but similar. At later growth stages the contrasts are due to the vigorous vegetation associated with the ponding scenario and the depleted vegetation associated with the waterlogged scenario.
- The modelled spectral comparison maps for waterlogged scenarios and for early growth stages tend to produce broad variation clusters with similar variation values across several waveband regions – increasing the range of potential waveband combinations for leak identification.

Reference

Perry, E.M., Warner, T. and Foote, P. 2000. Comparison of atmospheric modelling versus empirical line fitting for mosaicking HYDICE imagery. International Journal of Remote Sensing, **21,** 799-803.

2.8 Part two summary

This chapter provides an outline of the approaches and methods used to identify differences between leak and surrounding vegetation in the optical domain, drawing out the key findings from the results and analysis chapters. These key findings point towards optimal wavelengths for identification of leaks from optical image data, as well as optimal times of year and sensor characteristics that lend themselves to leak analysis. These are considered in the discussion chapter (4.1) of this thesis, along with the key findings from the microwave part of this thesis.

It has been demonstrated how differences in spectral reflectance are used to identify different spectral signatures for different earth surfaces with particular reference to soil, water and vegetation and the interaction between them. The concept of vegetation indices has been introduced and current vegetation reflectance models reviewed. The field methods outlined in chapter two discussed the theory and practical application of field spectroscopy to record reflectances under different leak and non-leak conditions in the field.

The collection of a suite of ground based measurements was described. Details of the models used and the approach to modelling were outlined and applied to a wide range of vegetation types at different growth stages and under a variety of leak conditions. Model input parameters were based on measurements made in the field.

Fieldwork results showed that under 'typical' conditions vegetation in long standing leaks was different to vegetation in recent or simulated leaks. Vegetation in long standing leaks was typically less dense than the surrounding vegetation, but effects on leaf area varied between leaks. Spectroradiometer results showed that all types of leak had lower reflectance than the surrounding vegetation and further that real leaks showed greater differences in reflectance than

simulated leaks. Spectroradiometer results also showed that differences between simulated leaks and 'dry' vegetation could be identified at different growth stages of oil seed rape and barley.

The results of the modelling study depended on canopy architecture, growth stage and leak type. However, the waterlogged scenario stood out against most vegetation types and growth stages in having lower overall reflectance than the other leak scenarios. The early growth stages for all vegetation types were found to be optimal for identifying differences between leak and non-leak for a range of leak types. The identification of leak types at later growth stages was more limited.

Hymap image results showed that there were appreciable differences between leak and surrounding vegetation for all sites identified on the image. This chapter also compared the optical and spectroradiometer results for the Cheshire sites. The results showed good agreement but spectroradiometer reflectances were typically lower than the image reflectances. It was suggested that this was due to differences in footprint size. While it was possible to compare the spectroradiometer measurements made at the Cheshire sites with the obtained imagery, there were no supporting image data for the Edinburgh-based spectroradiometer measurements.

To analyse the results a leak index was calculated using normalised difference ratios. It provided the optimal wavelengths for identifying maximum normalised differences between leak and surrounding vegetation for a variety of real, simulated and modelled leaks over different vegetation types and at varying growth stages. The overall result was an optimal waveband combination of visible and middle infrared, but the spectroradiometer analysis results were marginally different than the modelled and image results. The purpose of these analyses was to enable identification of leaks on optical imagery. This is further discussed in chapter 4.1.

3.1 Microwave Background

3.1.1. Introduction

In this chapter the properties of soil, vegetation and liquid water are considered from a microwave perspective. It is important to understand the unique response from each of these elements, to try to understand how microwave interactions produce specific responses under certain conditions that may be encountered in the field, and also consider how they may combine to produce collective return signals.

First, an explanation of how backscatter is measured is provided. The specific physiological properties of soils, vegetation and water that lend themselves to monitoring by microwave remote sensing are then considered, these include, dielectric properties, and scattering characteristics. The effects of frequency and incidence angle are then explored in relation to radar remote sensing of vegetation to understand the role of the sensor and how these variables also affect backscatter.

Interactions between soil, vegetation and water and the combined responses of these elements to radar backscatter are investigated, with particular attention to the influence of soil moisture on microwave backscatter from vegetation, and the influence of standing water beneath vegetation canopies on signal responses. Comparisons are made with 'dry' soil backgrounds. By considering the influence of soil moisture and standing water on vegetation signals compared with dry scenarios, a closer understanding of microwave interactions with water leaks and surrounding 'dry' soil and vegetation is made.

Later in this study radiative transfer modelling is used to explore microwave interactions between vegetation, soil, soil moisture and liquid water. Section 3.1.8 provides a short discussion on the background and use of radiative transfer models in microwave remote sensing.

3.1.2. Backscatter

The radar cross-section (RCS) equation is one way of measuring backscatter (Woodhouse, 2003). It describes the proportion of the incoming radiation that is scattered back (returned) in relation to an idealised scatterer. The RCS is defined by:

$$I_{received} = \frac{I_{incident}}{4\pi R^2}\sigma \quad \text{Watts/m}^2 \qquad 1.3.1$$

where R is the range (distance between target and sensor), σ is the target cross sectional area (the RCS) based on the measured intensity of received incoming radiation ($I_{received}$) and $I_{incident}$ is the intensity of incident radiation. It assumes that scattering is isotropic, i.e. equal in all directions and is most appropriate for discreet (rather than distributed) targets. The above equation is not normalised to unit area, in practical terms this means that if the spatial resolution of the sensor was increased then the amount of backscatter from a distributed target would also increase making inter-sensor comparison difficult. Therefore it is common to normalise the radar cross-section, to define σ^0 (Woodhouse, 2003). This relates the target area σ to a geometrical target area *dA* and can be used to describe the backscatter from distributed targets, e.g. vegetated surfaces rather than individual objects, such as leaves. σ^0 is defined by:

$$\sigma^0 = \frac{\sigma}{dA} \qquad 1.3.2$$

It is important to note that it is only appropriate to use σ^0 when surfaces are flat, or where there is a detailed knowledge of the surface topography for example where image data is supported by a digital elevation model of the same (or smaller) spatial resolution as the image. As a surface

becomes uneven, its surface area per unit projected area increases, which affects the backscatter response. For uneven surfaces where detailed surface characteristics are unknown β^0 should be used. Where β^0 is the radar brightness per pixel area rather than ground surface area (Henderson 1985). In this study the E-SAR image data were converted to σ^0 in relation to a 50 metre resolution digital elevation model.

In terms of the relationship between backscatter and surface objects, σ^0 will be close to zero when little or none of the returned signal reaches the sensor. This may be due to:

- specular surface scattering characteristics (e.g. flat water surfaces)
- the size of an object being small in relation to wavelength (e.g. from small vegetation components)
- attenuation (e.g. dry sand) by objects.

High σ^0 values result when a large proportion of the incident radiation is returned to the sensor. This occurs when there is a strong directional component of the return signal towards the sensor. The most common example of this is the so-called "double bounce" which occurs when two targets meet at right angles (Figure 3.1.1). This may result from interactions with man-made objects such as corner reflectors, sides of buildings, or naturally occurring objects, for example, vertical tree trunks.

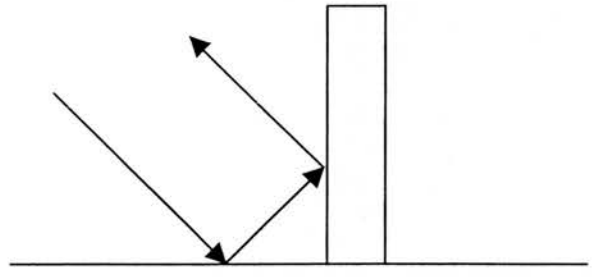

Figure 3.1.1. Double bounce, dihedral scattering.

3.1.3. Interactions with soil

Soil liquid water content and soil roughness are important factors governing soil backscatter measurements in the microwave region of the spectrum (Ulaby *et al.*, 1982a). Liquid water content determines reflectivity, and roughness determines the manner in which the microwaves are scattered. Both these variables are pertinent to this project. By considering the effects of liquid soil moisture content on backscatter it may be possible to identify leaks that are manifested as patches of wet soil, compared with surrounding dry soil. Similarly there is a distinct contrast in roughness between soil and water surfaces, which may aid in the identification of leaks.

3.1.3.1. Dielectric theory and properties of soil

An object's electrical character is measured using the complex dielectric constant. The dielectric properties of an object or surface relate to how well that object or surface can sustain an electric field. The dielectric constant describes the relative permittivity of surfaces or objects and is given as the measure of the propagation characteristics of an electromagnetic wave through a medium.

$$\varepsilon = \varepsilon' - j\varepsilon'' \qquad 1.3.3$$

where, ε' is the permittivity of the material, the real part of the dielectric constant defining the velocity and wavelength of the refracted wave in the medium, and ε'' is the dielectric loss factor and imaginary component, expressing energy lost through absorption of the wave in the medium (Ulaby *et al.*, 1986). A reasonable approximation for the dielectric properties of surface objects is that good electrical conductors are good reflectors, and good insulators are poor reflectors. Factors affecting changes in dielectric constant for soil include; liquid moisture content, wavelength and soil texture.

When incident radiation interacts with the interface between surfaces with different dielectric properties eg air and soil, the waveform changes. Since radar systems have control over the incident wave, they are able to detect changes in dielectric constant that are associated with surface interactions. A dry soil has a dielectric constant of 3-5 and a very wet soil can have a

dielectric constant of around 20. An increase in soil moisture content and thus soil dielectric constant, results in higher reflectivity or backscatter values in the microwave domain (Figure 3.1.1) (Ulaby *et al.*, 1982a). When the water within soil freezes, however, the dielectric constant will drop to extremely low values. Water and dielectric constant are inextricably linked. This makes microwave sensors appropriate for identifying water content of surface objects (when ambient temperatures are greater than 0° C) and many studies have focused on this relationship, particularly in relation to soil moisture content (Wang, 1980; Dobson, *et al.*, 1985; Hallikainen *et al.*, 1985; Ulaby *et al.*, 1986; van Oevelen, 2000).

Dielectric responses are wavelength dependent and as microwave frequency increases, sensitivity to soil moisture decreases for the real component of the dielectric constant and increases for the imaginary component (Figure 3.1.2) (Ulaby *et al.*, 1986). This means that at longer wavelengths more energy is absorbed, and less is reflected. This suggests that shorter wavelengths are more appropriate for estimations of soil moisture (Hallikainen *et al.*, 1985). Soil texture has also been shown to affect the dielectric constant with sandy soils displaying lower dielectric constants than clay soils. This is likely to be due to the water holding capacity and chemical composition of these different soil types (Hallikainen *et al.*, 1985; Dobson *et al.*, 1985). In sandy soils there is more free water than in clay based soils (where tight bonds form between clay particles and water). It is the presence of free water that increases the dielectric constant.

3.1.3.2. Soil scattering

Scattering from soil can be described in one of two ways, either by surface scattering or volume scattering. For surface scattering, the assumption is that there is no contribution from radiation that has penetrated the soil surface and is reflected from a subsurface layer; thus, all the scattering occurs from the surface, surface scattering generally relates to homogeneous surfaces. Volume scattering occurs due to inhomogeneities within a medium and can be used to describe scattering from vegetation or soils. It represents situations where radiation penetrates a surface or layer and interacts with sub layers.

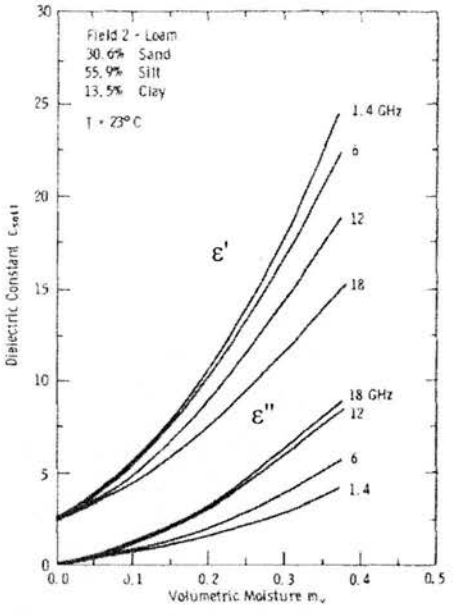

Figure 3.1.2. Graph showing relationship between soil moisture content and dielectric constant (both real and imaginary parts) at a range of frequencies (Ulaby et al., 1982a).

The depth of volume scattering, referred to as penetration depth, is dependent on the dielectric properties of the layers, wavelength and incidence angle. Soil penetration depth increases with decreasing dielectric constant and increasing wavelength, such that a wet soil appears more opaque to a microwave sensor, even at the longer microwave wavelengths considered in this work (i.e. P-band). A wet soil surface can thus be considered to demonstrate surface scattering despite inhomogeneities within the soil. The inhomogeneities within the soil layer are therefore, not sufficient to cause volume scattering (Ulaby *et al.,* 1982a). For dry, homogenous surface layers such as hyper-arid sand, L-band microwaves may penetrate up to several metres (Schaber and Breed, 1999).

3.1.3.3. Effects of soil roughness

Soil roughness has a direct influence on microwave backscatter. If the soil surface is smooth, specular (coherent) reflection occurs. This means that the scattered waves reflect in an ordered way combing constructively in the forward direction. Smooth soil surfaces do not often occur in

nature. However, a dry mudflat provides an example of a specular soil surface. Whether a surface is rough or smooth is a factor pertaining to scale and is therefore dependent on frequency. At longer wavelengths surfaces appear to be smoother. If the soil surface is slightly rough in relation to wavelength, scattering can be divided into two component parts; coherent (specular) and incoherent (diffuse). The coherent part has a smaller magnitude than for a smooth surface, but it is larger than the incoherent part. For a very rough surface the reverse is the case so that the magnitude of the incoherent part is larger than the coherent part, but both are smaller than the wave magnitude scattered from a specular surface (van Oevelen, 2000) (Figure 3.1.3).

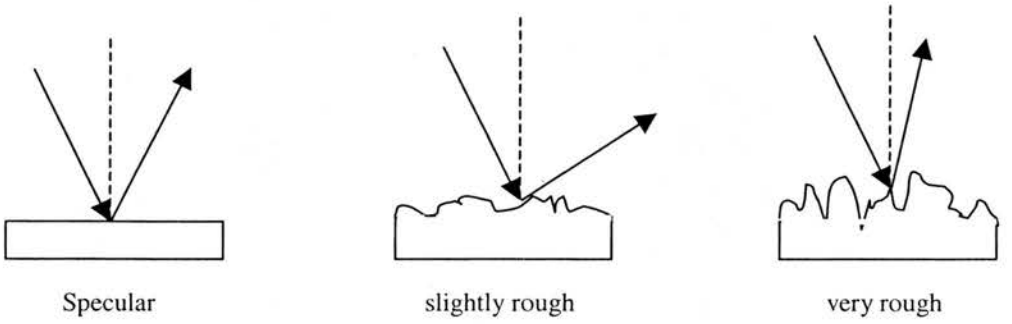

Figure 3.1.3. Effects of surface roughness on radiation scattering

Thus, for active microwave systems at off-nadir incidence angles, scattering from smooth surfaces produce low backscatter responses because the direction of scattering is forward and away from the sensor, assuming that the incidence angle is sufficient to avoid interception of the return signal by the sensor. Scattering from rough surfaces occurs in all directions, including scattering towards the sensor, resulting in a greater direct backscatter response. However, it is important to note that the backscatter response varies significantly with incidence angle so that air-borne and space-borne side looking radar images will also vary across the swath. The effects of incidence angle are greater from air-borne than space-borne systems (Figure 3.1.4).

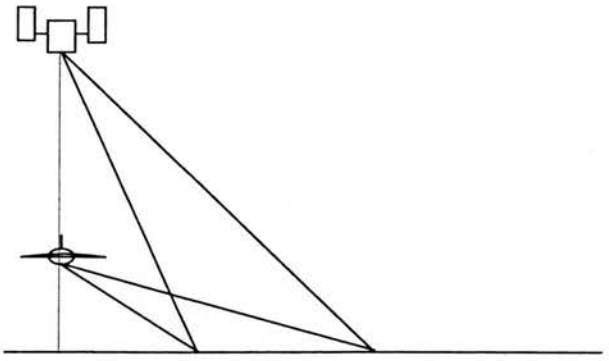

Figure 3.1.4. Variation of incidence angle across the swath with sensor height for aircraft and satellite radar systems.

Surface roughness is most commonly classified by the *Rayleigh criterion*. This states that when the phase difference between two rays reflected from a given surface is less than $\pi/2$, then the surface may be considered to be smooth:

$$h < \frac{\lambda}{8\cos\theta_{inc}} \qquad 1.3.4$$

where h is the difference in height between 2 points on the surface, λ is wavelength and θ_{inc} is incidence angle. However, Ulaby *et al.*, (1982a) found that a more accurate description of smoothness for natural surfaces is the *Fraunhofer criterion*

$$\sigma < \frac{\lambda}{32\cos\theta_{inc}} \qquad 1.3.5$$

where σ is the standard deviation in surface height. This equation provides a more rigorous description of smoothness with regard to wavelength. These equations provide a quantitative description of whether a surface is "smooth" or not and it may be used as a required condition or assumption in soil scattering models.

Other measurements of soil roughness are often described by reference to a flat plane, for example, root mean square of height differences from a local mean, surface correlation length and height probability density function. These estimates are commonly derived from field measurements, for example, needle boards, contact spray, gridded panes or laser profilers (van Oevelen, 2000; Borgeaud *et al.*, 1995; Davidson *et al.*, 2000). Such measurements provide averaged or interval measures of a rough surface assuming a random spatial distribution. Because adequate descriptions of complex geometrical soil surfaces are difficult to attain, simple approximate models are used. Perhaps the most well-known of these are the Kirchoff models which include the widely used small perturbation and physical optics models. These models require an input parameter describing soil roughness by means of the surface correlation function. They are used to characterise surface roughness in the calculation of direct backscatter in the microwave radiative transfer canopy modelling used later this study.

3.1.4. Interactions with water

3.1.4.1. Dielectric properties of water

As described in section 3.1.3.1, water has strong dielectric properties, with pure water having a dielectric constant of approximately 80. The distinctive dielectric nature of water and the influence it has on backscatter lends itself to microwave remote sensing, and in particular the application under study in this project. The focus is gross differences between wet and dry surfaces, and in the most extreme case, differences between surface water and dry soil with overlying vegetation.

3.1.4.2. Scattering

With microwaves there is little or no penetration of water surfaces, unlike optical wavelengths. This is mainly due to differences in the dielectric properties at the interface between air and water. This results in high levels of scattering. As with soil, for a specular surface this means coherent forward scattering and little of the return signal reaching the sensor (assuming off-nadir incident angles). The reflection of a flat or smooth surface-air interface can be described by the

Fresnel equations (Ulaby *et al.*, 1982a). For horizontally polarised waves the power Fresnel reflection coefficient (R_h) is:

$$R_h = \frac{\cos\theta_{inc} - \sqrt{\varepsilon_r - \sin^2\theta}_{inc}}{\cos\theta_{inc} + \sqrt{\varepsilon_r - \sin^2\theta}_{inc}} \qquad 1.3.6$$

and for vertically polarised waves

$$R_v = \frac{\varepsilon_r \cos\theta_{inc} - \sqrt{\varepsilon_r - \sin^2\theta}_{inc}}{\varepsilon_r \cos\theta_{inc} + \sqrt{\varepsilon_r - \sin^2\theta}_{inc}} \qquad 1.3.7$$

where ε_r is the relative complex permittivity, and θ_{inc} is the incidence angle. These equations describe the interaction between flat surfaces and reflected waves as a function of incidence angle and the direction of the electric field relative to the surface or in other words, polarisation. Rough water surfaces are not considered here, for example, ripple or small wave effects from wind or rain. It is inappropriate to collect data on windy days due to the effects of wind on the orientation of vegetation elements (section 2.2.2). With regard to rain affecting water surfaces, due to the nature of the project it is also inappropriate to acquire data in the rain as it is likely to inhibit the potential for identifying leaks (section 1.4.2.2). Bragg scattering describes the scattering that occurs from surfaces with regular, periodic patterns and it can lead to waves combining constructively or destructively to give very strong or weak reflectance. To consider Bragg scattering is therefore likely to confuse the already complex series of interactions discussed in this project.

3.1.5. Interactions with vegetation

3.1.5.1. Scattering

As with optical remote sensing, microwave interactions with vegetation are more complex than those relating to soil or water alone, due to the complex architecture of canopy structures and soil background effects. Each of these components has different dielectric and roughness

properties which thus affect the backscatter response. Scattering from vegetation is usually represented by volume scattering as there is no distinct air-canopy boundary (Ulaby *et al.*, 1982a) and in some situations this can include a ground contribution if the canopy is sparse (Figure 3.1.5). The scattering mechanisms contributing to total backscatter come from:

- direct scattering from the soil
- direct scattering from vegetation canopy elements (stems, branches and leaves)
- double-bounce reflections between the soil surface and the canopy
- multiple scattering from vegetation layers
- multiple scattering from soil, vegetation interactions

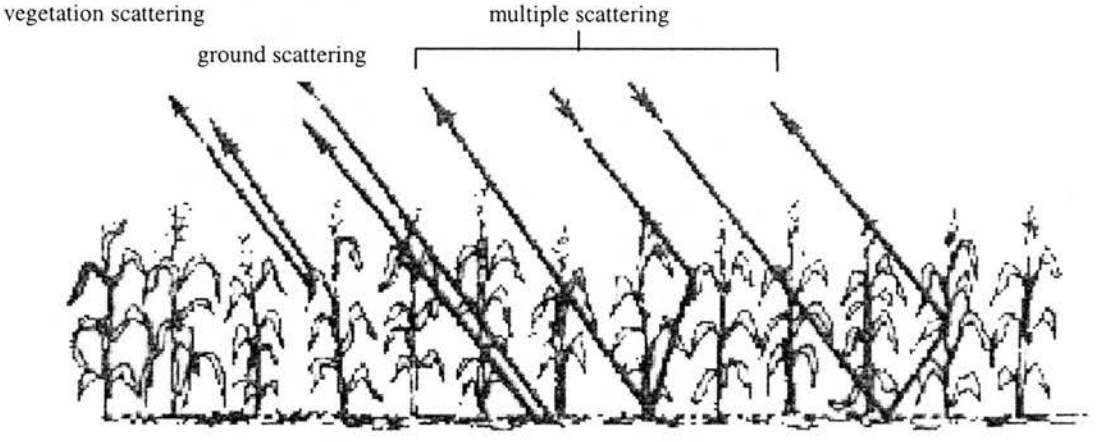

Figure 3.1.5. Some backscatter interactions relating to soil and vegetation. Adapted from Ulaby et al., 1986.

Typically, vegetation backscatter is greater from vegetation than from soil. This is mainly due to variations in roughness. A vegetation canopy tends to produce more diffuse or incoherent scattering than a bare soil surface, even a very rough one (Burke and Schmugge, 1982) although these differences are not absolute and can only be considered in relation to canopy geometry, incidence angle and frequency. The radar cross-section of a canopy over a surface can be approximated by (Ulaby *et al.*, 1986):

$$\sigma_{can}(\theta) = \sigma_v(\theta) + \frac{\sigma_s(\theta)}{l^2(\theta)} \qquad 1.3.8$$

where the volume scattering cross-section ($\sigma_v(\theta)$), depends on the number of scattering elements per unit volume, and the cross-section of each scattering element, which is dependent on dielectric constant. $\sigma_s(\theta)$ is the surface cross-section which depends on surface roughness and dielectric constant. $l(\theta)$ is the attenuation through the canopy which is exponential depending on an extinction factor, and the extinction factor depends on the moisture content of the scattering elements and frequency (with higher frequencies penetrating further into the canopy). $l(\theta)$ becomes $l^2(\theta)$ to take account of the two-way travel through the canopy (Ulaby *et al.*, 1986).

3.1.5.2. Effects of frequency

It has been observed that as frequency increases, backscatter values from vegetation increase exponentially at incidence angles greater than 20° (Ulaby *et al.*, 1982a). At higher microwave frequencies, backscatter is dominated by leaves (Tan and Chuah, 1992; Le Vine and Karam, 1996). For example, for a deep and dense vegetation canopy with many randomly orientated leaves that are large in relation to wavelength, it is difficult for the wavelengths to penetrate the vegetation canopy. In this case the majority of scattering comes directly from interactions within the canopy layer (volume scattering), and therefore the backscatter response is high. Conversely at longer wavelengths and where the leaves are small in relation to wavelength, the radiation is able to penetrate the canopy further - there is less attenuation by leaf elements and backscatter tends to be dominated by thick stems and scattering from the soil surface. The same soil background will also appear smoother than at shorter wavelengths. Thus producing lower backscatter values as a result of increased forward scattering. There are exceptions to this, for example in the case of the double bounce, and these interactions are clearly dependent on canopy architecture and density, as well as incidence angle and sensor type.

3.1.5.3. Effects of incidence angle

In general transmissivity of a vegetation canopy decreases with increasing incidence angle (Ulaby *et al.*, 1986). This is because at greater incidence angles the path length through the

canopy increases and backscatter from the soil layer is less likely, even for relatively sparse canopies. Canopy structure is also important in relation to incidence angle. For vertically orientated canopies the contribution from ground reflectance with incidence angles closer to the nadir, is significant (Mo *et al.*, 1984; Touré *et al.*, 1994) and backscatter tends to be greater than for dense horizontally orientated canopies, due to contributions from the soil background. At greater incidence angles, volume scattering is dominant for vertically orientated canopies (Mo *et al.*, 1984) (Figure 3.1.6). However, for dense randomly orientated canopies volume scattering is less incidence-angle dependent. For a pure volume scatterer, backscatter is proportional to the projected area on the ground which increases in proportion to the cosine of θ (Figure 3.1.7).

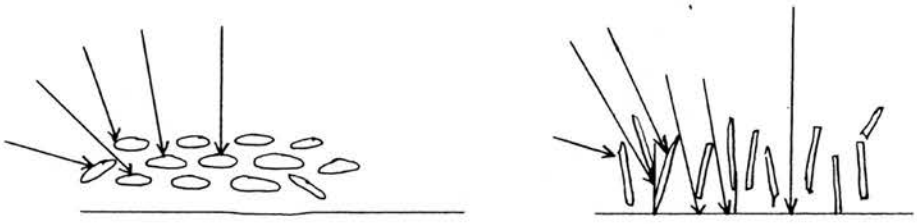

Figure 3.1.6 Effect of scatterer size and orientation in relation to canopy penetration depth at increasing incidence angles. The arrows represent incoming microwaves at varying inclination angles.

Frequency is a further important factor affecting the influence of incidence angle on backscatter. Ulaby *et al.* (1986) show that for a soybean canopy at longer wavelengths (1.1 GHz) the variation in backscatter with incidence angle is much greater than for shorter wavelengths (4.6, 8.6 and 17 GHz). This is also shown to be true for modelled wheat canopies (Touré *et al.*, 1994) with L-band backscatter showing greater variation than C-band backscatter. This is due to variations in canopy penetration depth. As microwaves penetrate further into a given canopy there are a greater number of possible scattering outcomes: (i) they may reach the soil surface and be scattered in any direction depending on soil roughness and water content, (ii) equally, they could be scattered from a vegetation element back towards the sensor or, (iii) they may be attenuated by the vegetation on their return and be further scattered.

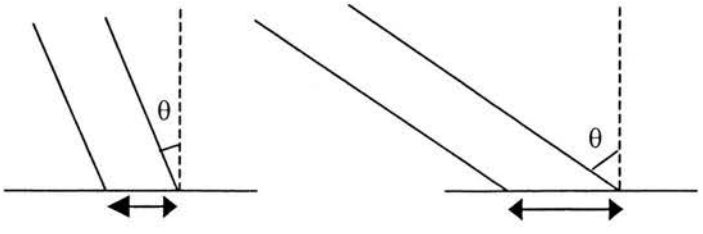

Figure 3.1.7. Diagram showing the effects of incidence angle on the projected ground area of an incoming beam

As incidence angle varies across the swath width adjustments may be applied to side-looking radar sensor systems to account for this variation. There may also be angle dependent variations between different radar looks or passes, for further information on this refer to Ban and Howarth (1997) and Saich (1999).

3.1.5.4. Canopy architecture

The vegetation structure and thus transmissivity of a vegetation layer are dependent on the shape, orientation and size of the layer's scattering elements relative to wavelength (Ulaby *et al.*, 1986). Skriver *et al.*, (1999) show backscatter variations with incidence angle for spring and winter barley, winter wheat and oil seed rape. They demonstrate a high volume scattering response from oil seed rape compared with the vertically aligned cereal vegetation canopies. The structure of an oil seed rape canopy is many small leaves orientated in random directions. Results show that there is little change in backscatter values for oil seed rape with increasing incidence angle as randomly orientated leaves appear 'rougher' to radar systems than more homogeneous canopy orientations (for example a cereal canopy), resulting in increased backscatter. Conversely, with increasing incidence angle (from 40 to 60 degrees) there is increasing backscatter from the vertically orientated canopies. Canopies with vertically orientated leaves and stems are more 'transparent' to microwaves than horizontally orientated canopies, regardless of incidence angle.

3.1.5.5. Dielectric constant of vegetation

By their nature the dielectric properties of canopies have a high degree of complexity due to large variations in the dielectric properties of different vegetation elements (leaves, stems, fruits, flowers), heterogeneity between the different elements and heterogeneity within individual elements. Vegetation canopies are inhomogeneous, anisotropic layers that both scatter, and absorb radiation and the interface between elements is complex, making the canopy dielectric constant difficult to estimate. However, we can make comments on the relationship between canopy water content and dielectric constant. Research on wheat heads (Nelson and Stetson, 1976) shows that as moisture content increases so does the permittivity (ε') and loss factor (ε''). Similar results are shown for wheat stalks and leaves (Ulaby and Jedlicka, 1984) with increasing

volumetric moisture content resulting in a greater dielectric constant. Another study showed that water droplets on winter wheat canopies increased direct backscatter by 3 dB (Ulaby *et al.*, 1986,). Thus, it is possible to determine information regarding canopy water content from microwave remote sensing due to the link between dielectric constant and water content, with canopies that contain more water having greater backscatter values than drier canopies. This is demonstrated by Steven *et al.* (1999), who modelled the response of sugar beet canopies to wilting, with results suggesting a drop of 3dB for wilted canopies at all incident angles.

3.1.6. Influence of variations in soil moisture content.

Ulaby *et al.*, (1975) showed that for incidence angles less than 30°, increasing soil moisture resulted in increasingly high backscatter values for corn. Similarly, Chauhan *et al.* (1994) suggested that for corn canopies measured using L-band at a 40.3° incidence angle, and as soil moisture increases, the relative contribution from leaves and stalks changes so that with increased soil moisture the contribution from stalks increases for both horizontally and vertically polarised waves. This is due to an increase in the reflection coefficient at the soil surface and results in greater backscatter values. Ulaby *et al.*, (1982b) demonstrated that for soil at 50% field capacity or less (where 100% field capacity represents a fully saturated soil) and at frequencies around 4.5 GHz with incidence angles of 0-10°, the contribution from a given vegetation canopy limits the radar's ability to detect soil moisture (this is proportional to the density of the overlying vegetation). However, between 50 and 150% field capacity (where 150% represents a state beyond field capacity and becomes surface ponding), backscatter is dominated by soil and water contributions which increase with increasing moisture content (Figure 3.1.8). These studies have implications for this work because they suggest that it may be possible to detect recently occurring leaks that manifested themselves as wet soil surfaces in addition to surface standing water behind vegetation. It may be possible to extrapolate these results to include greater incidence angles, particularly where vegetation density is sparse.

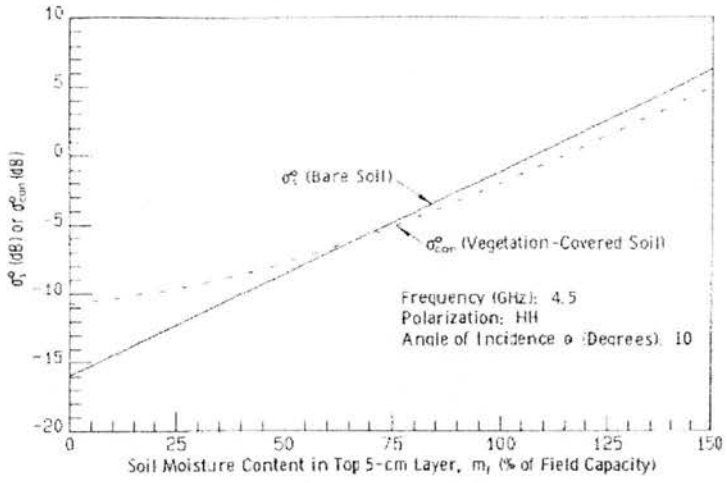

Figure 3.1.8. The influence of soil moisture on soil and vegetated soil backscatter responses(Ulaby et al., 1982a).

Therefore, in summary soil moisture is inherently related to vegetation water content and as canopy water content increases, backscatter from the vegetation components increases, and canopy penetration is reduced (Jackson and O'Neill, 1990; Jackson and Schmugge, 1991; Le Vine and Karam, 1996). However, total backscatter is also dependent on canopy geometry (Le Vine and Karam, 1996), and soil moisture content, as demonstrated by Ulaby *et al.* (1982b).

3.1.7 Effects of polarisation

Polarimetry will not be explored in great detail as it is beyond the scope of the thesis. It is therefore sufficient to define some basic terminology and provide some generalised explanations of the polarisations used. Polarisation describes the oscillation direction of transverse electromagnetic waves. Convention defines the direction of polarisation to be that of the electrical field vector rather than the magnetic field vector (Woodhouse, 2003). Polarisation is determined by the plane of vibration of the electrical field of a transverse wave (van der Sanden, 1997). A detailed understanding of polarimetry requires knowledge of both the amplitude and phase of an electromagnetic wave. Amplitude (A) describes the total power of the wave and may be defined as the height of the wave crest. Phase is measured in radians as an angle (θ) which

can be described as a pointer within a circle where the radius is equal to the amplitude of the wave, it ranges between 0 and 2π (Figure 3.1.9) (Woodhouse, 2003).

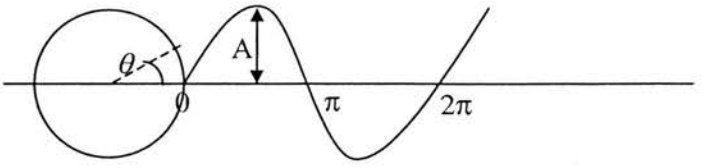

Figure 3.1.9 Diagramatic representation of phase (θ) and amplitude (A), where θ radians is equal to angle in degrees, multiplied by 2 π/ 360.

The technical specifications of each radar system determines the wavelength, polarisation, amplitude and phase of the transmitted waves. Return waves may have a different polarisation, phase and/or amplitude to the outgoing signal due to interactions between the waves and surface objects. Traditional active radar systems have antenna arrays that are aligned either vertically or horizontally, thus transmitted waves are either horizontally (H) or vertically (V) polarised, the radar system then records the amplitude of the received H- and/or V-component. More recently, polarimetric radar systems were designed to transmit horizontal and vertically polarised waves simultaneously and record the amplitude and phase of the H- and V-components. The terms HH and VV refer to the transmitted and received polarisation of the microwave. HH polarisation responses refer to waves that are both transmitted and received horizontally. VV polarisation responses refer to waves that are transmitted and received vertically. Cross polarisation responses refers to waves that are transmitted vertically and received horizontally (VH) and those transmitted horizontally and received vertically (HV). Changes to polarisation, phase and amplitude are often object specific thus resulting in particular response patterns for different surface objects which facilitates interpretation of microwave imagery. For example, with surface scattering VV responses produce greater backscatter values than HH responses. VV responses are greater then HH responses when interacting with vertically aligned dipoles, and HH responses are greater than VV responses when interacting with horizontally aligned dipoles, however, this is also dependent on the dimensions of the object relative to wavelength (Woodhouse, 2003). HV and VH responses are higher where the object is neither aligned to the horizontal or the vertical axis. HH and VV responses give the most similar responses to each

other when interacting with random components, for example, vegetation canopies. At zero degrees incidence angle V and H polarised waves appear the same to a sensor due to laws of symmetry (Woodhouse, 2003).

3.1.8 Influence of standing water on vegetation backscatter

For this section much of the research comes from investigations of microwave backscatter from rice crops which are seasonally flooded as part of their annual growth cycle (Le Toan *et al.*, 1989, 1997; Ribbes and Le Toan, 1998; Durden *et al.*, 1995). These studies are convenient in that they provide us with an agricultural crop that is comparable to a grass canopy in a leak. However, other studies include backscatter from flooded and nonflooded forest (Wang, *et al.*, 1995), work by Pope *et al.* (1997) focuses on flooding of marshes in Mexico. Backscatter from wetlands have also been studies (Krohn *et al.*, 1983; Ormsby *et al.*, 1985). Engheta and Elachi (1982), presented a simple mathematical model to describe backscatter from emergent vegetation against a water background.

Typically the presence of water beneath a vegetation canopy can have three responses depending on frequency, canopy height and structure. It can cause: (i) an increase in backscatter for tall and sparse vegetation canopies due to double bounce effects, (ii) a decrease in backscatter for shorter and/or more sparse vegetation due to forward scattering from the water surface or, (iii) no effects from presence of water where vegetation is both tall and dense and the water is masked by the vegetation layer, here backscatter increases due to volume scattering. These interpretations of backscatter responses relate to incidence angles greater than 20 °. Double bounce effects are only significant for large vertical scattering objects such as tree trunks, or objects that are large in relation to wavelength.

It is suggested that longer wavelengths (for example, L-band) are likely to be most appropriate for studies where canopies are taller and more dense, as they are able to penetrate the canopy further and thus maximise the contribution from the surface layer (Wang *et al.*, 1995). However, C-band is likely to be more effective for smaller, sparser canopies (Pope *et al*, 1997). Therefore, frequency is important in relation to canopy height and density in order to maximise the surface

contribution in the microwave context, as it is the presence or absence of water that is of primary concern in this study. Information on polarimetry is also useful to these studies due to the different responses of H and V polarised waves in relation to vegetation canopy penetration, interactions with smooth surfaces and their individual responses to different canopy geometries. In studies by Pope *et al.* (1997), C-band VV and L-band HH at approximately 26 degrees incidence angle provided the best polarisations for detecting flooding in marshes. Other studies have found that HH polarisations at all frequencies were better than VV for detecting water under forest canopies. (Wang *et al.,* 1995; Ribbes and Le Toan, 1998)

3.1.9 Microwave modelling

There have been many measurements of radar backscatter from crops over the last 30 years or so, and interpretation of these has led to the development of many different models to explain the observed scattering from vegetation. One of the earliest of these was the water cloud model (Attema and Ulaby, 1978). It was based on models developed for scattering from atmospheric clouds. This model assumes that vegetation canopies, like atmospheric clouds, contains scattering objects of identical size and shape with strong dielectric properties, randomly and sparsely distributed and separated by an unknown spatial component (of much lower dielectric constant). In the vegetation version of the model, soil background effects are taken into account with coefficients for surface roughness and sensitivity to soil moisture. Plant height, soil moisture and canopy water content are required input parameters and a volume extinction coefficient is applied to describe the relationship between canopy water content and number of scatterers per unit volume. A canopy loss factor is also applied to the model to account for absorption relative to incidence angle. One problem with the model is that it does not account for the geometry of the scatterers.

Since the water cloud model there has been a great deal of research into radiative transfer models for microwaves to improve understanding of the relationship between vegetation canopies and microwave backscatter. These include:

- MIMICS – a first order model (Ulaby *et al.*, 1990)
- Matrix doubling solution models - Ferrazzoli *et al.*, 1991.
- First and second order vector radiative transfer theory solutions - Tsang and Ding, 1991
- Santa Barbara model – first order model (Wang *et al.*, 1993)
- Branching model for vegetation using distorted Born approximation – Yueh *et al.*, 1992
- Discreet scatter model, using distorted Born approximation – Lang and Sidhu, 1993
- Discreet scatter model using distorted Born approximation for corn canopies – Chauhan *et al.*, 1994
- Discreet scatter model using distorted Born approximation for grass canopies - Saatchi *et al.*, 1994
- Adaptation of the MIMICS model for wheat and canola canopies at HH and VV polarisation – Touré *et al.*, 1994
- Fully polarimetric multiple scattering model for crops – Bracaglia *et al.*, 1995
- Second order RT2 model – Saich, 1995
- First order spatial model – Sun and Ranson, 1995

Many of the first radiative transfer models were developed for forest applications, but have since been adapted and applied to agricultural crops. Radiative transfer models are considered to approximate well, where the separation between individual scatterers is more than a few wavelengths (Saich, 1999). The models are, however, limited due to intrinsic assumptions about the behaviour of electromagnetic radiation, as well as the assumptions that are made about the relationships between dielectric constant and water. For example, many canopy reflectance models assume a linear relationship between water content and dielectric constant. This is a good approximation, but it remains an over simplification. Similarly, radiative transfer models are limited as the complex geometry of a true vegetation canopy cannot be fully represented in the models; the fact that leaves are attached to stems and branches ise not accounted for. With better understanding and greater computational power, more accurate representations have developed into coherent scattering models (Lin and Sarabandi, 1995) and stochastic models, for example the AMAP model for modelling backscatter from Austrian pine trees (Castel *et al.*, 2001). However, for this study the use of radiative transfer models are sufficient as we are considering gross differences between the backscatter of vegetation, soil and water.

References

Attema, E. P. W and Ulaby, F. T. 1978. Vegetation modeled as a water cloud. Radio Scince, **13**, 357-364.

Ban, Y. and Howarth, P.J. 1997. Multispectral spaceborne SAR data for crop classification: a sequential-masking approach. Proceedings of the Geomatics in the era of RADARSAT Symposium, Ottawa, May 1997. Canadian Geomatics CD-ROM. Paper number 156.

Borgeaud, M., Attema, E., Salgado-Gispert, G. Bellini, A. and Noll, J. 1995. Analysis of bare soil surface roughness parameters with ERS-1 data. In: Symposium Extraction of Bio and Geophysical Parameters from SAR Data for Land Applications. ESA.

Bracaglia, M., Ferrazzoli, P. and Guerriero, L. 1995. A fully polarimetric multiple scattering model for crops. Remote Sensing of Environment, **54**, 170 - 179.

Burke, H. K and Schmugge, T. J. 1982. Effects of varying soil moisture contents and vegetation canopies on microwave emissions. IEEE Transactions on Geoscience and Remote Sensing, **GE20**, 268-274.

Castel, T., Beaudoin, A., Floury, N. Le Toan, T., Caraglio, Y. and Barczi, J. F. 2001. Deriving forest canopy parameters for backscatter models using the AMAP architectural plant model. IEEE Transactions on Geoscience and Remote Sensing, **39(3)**, 571-583.

Chauhan, N. S., Le Vine, D. M. and Lang, R. H. 1994. Discrete scatter model for microwave radar and radiometer response to corn: comparison of theory and data. IEEE Transactions on Geoscience and Remote Sensing, **32**, 416-426.

Davidson, M. W. J., Le Toan, T., Mattia, F., Satalino, G., Manninen, T. and Borgeaud, M. 2000. On the characterization of agricultural soil roughness for radar remote sensing studies. IEEE Transactions on Geoscience and Remote Sensing, **38**(2), 630-640.

Dobson, M. C., Ulaby, F. T., Hallikainen, M., and El-Rayes, M. 1985. Microwave dielectric behaviour of wet soil – part II: dielectric mixing models. IEEE Transactions on Geoscience and Remote Sensing, **GE23**, 35-46.

Durden, S. L., Morrissey, L. A. and Livingston, G. P. 1995. Microwave backscatter and attenuation dependence on leaf area index for flooded rice fields. IEEE Transactions on Geoscience and Remote Sensing, **33**, 807-810.

Engheta, N. and Elachi, C. 1982. Radar scattering from a diffuse vegetation layer over a smooth surface. IEEE Transactions on Geoscience and Remote Sensing, **20**, 212-216.

Ferrazzoli, P., Guerriero, L. and Solimini, D. 1991. Numerical model of microwave backscattering and emission from terrain covered with vegetation. Applied computing and Electromagnetics Society Journal, **6**, 175-191.

Henderson, F. M. 1985. Confusion errors among urban land-cover types on SAR imagery. International Journal of Remote Sensing, **6 (10)**, 1607-1622.

Hallikainen, M., Ulaby, F. T., Dobson, M. C., El-Rayes, M. and Wu, L. K. 1985. Microwave dielectric behaviour of wet soil – part I: empirical models and experimental observations. IEEE Transactions on Geoscience and Remote Sensing, **GE23**, 25-34.

Jackson, T. J. and O'Neill, P. E. 1990. Attenuation of soil microwave emissivity by corn and soybeans at 1.4 and 5 GHz. IEEE Transactions on Geoscience and Remote Sensing, **28**, 978-990.

Jackson, T. J. and Schmugge, T. J. 1991. Vegetation effects on the microwave emission of soils. Remote Sensing of Environment, **36**, 203 - 212.

Krohn, M. D., Milton, N. M. and Segal, D. B. 1983. Seasat synthetic aperture radar (SAR) response to lowland vegetation types in eastern Maryland and Virginia. Journal of Geophysical Research, **88**, 1937-1952.

Lang, R. H. and Sidhu, J. S. 1993. Electromagnetic backcattering from a layer of vegetation: a discrete approach. IEEE Transactions on Geoscience and Remote Sensing, **GE21**, 62-71.

Le Toan, T., Laur, H., Mougin, E. and Lopes, A. 1989. Multitemporal and dual-polarization observations of agricultural vegetation covers by X-band SAR images. IEEE Transactions on Geoscience and Remote Sensing, **27**, 709-717.

Le Toan, T., Ribbes, F., Wang, L., Floury, N., Ding, K., Kong, J. A. Fujita, M. and Kurosu, T. 1997. Rice crop mapping and monitoring using ERS-1 data based on experiment and modeling results. IEEE Transactions on Geoscience and Remote Sensing, **35**, 41-54.

Le Vine, D. M. and Karam, M. A. 1996. Dependence of attenuation in a vegetation canopy on frequency and plant water content. Transactions on Geoscience and Remote Sensing, **34**, 1090-1096.

Lin. Y. –C. and Sarabandi, K. A 1995. Monte Carlo coherent scattering model for forest canopies using fractal-generated trees. IEEE Transactions on Geoscience and Remote Sensing, **39**, 440-451.

Mo, T., Schmugge, T. J., and Jackson, T. J. 1984. Calculations of radar backscattering coefficient of vegetation-covered soils. Remote Sensing of Environment, **15**, 119 - 133.

Nelson, S. O. and Stetson, L. E. 1976. Frequency and moisture dependence of the dielectric properties of hard red winter wheat. Journal of Agricultural Engineering Research, **21**, 181-192.

Ormsby, J. P., Blanchard, B. J. and Blanchard, A. J. 1985. Detection of lowland flooding using active microwave systems. Photogrammetric Engineering and Remote Sensing, **51**, 317-328.

Pope, K. O., Rejmankova, E., Paris, J. F. and Woodruff, R. 1997. Detecting seasonal flooding cycles in marshes of the Yucatan Peninsula with SIR-C polarimetric radar imagery. Remote Sensing of Environment, **59**, 157 - 166.

Ribbes, F. and Le Toan, T. 1998. Mapping and monitoring rice crop with RADARSAT. IEEE Geoscience and Remote Sensing Symposium Proceedings. IGARSS '98, **5,** 6-10 Jul 1998, 2749 –2751.

Saatchi, S. S., Le Vine, D. M. and Lang, R. H. 1994. Microwave backscatter and emission for grass canopies. IEEE Transactions on Geoscience and Remote Sensing, **32**, 177-186.

Saich, P. 1995. Backscatter software user guide. BSATC document, RET-4-MRC-027 (issue 1.1). ESA contact 10644/93/NL/NB, ref. Y/218/3383.

Saich, P. 1999. Monitoring vegetation dynamics using SAR, ESTEC Working Paper, no. 2048. ESA.

Schaber, G. G. and Breed, C. S. 1999. The importance of SAR wavelength in penetrating blow sand in northern Arizona. Remote sensing of Environment, **69**, 87-104.

Skriver, H., Svendsen, M. T. and Thomsen, A G. 1999. Multitemporal C- and L-band polarimetric signatures of crops. IEEE Transactions on Geoscience and Remote Sensing, **37**, 2413-2429.

Steven, M. D., Cookmartin, G., Jaggard, K. W. and Gill, G. 1999. Monitoring wilting in sugar beet with SAR. 25th Annual Conference of the Remote Sensing Society, Cardiff, UK

Sun. G. and Ranson, K. J. 1995. A three-dimensional radar backscatter model of forest canopies. IEEE Transactions on Geoscience and Remote Sensing, **33**, 372-382.

Tan, H. S. and Chuah, H. T. 1992. Dielectric properties and electromagnetic scattering from foliage and vegetation. IEEE Proceedings from the 1992 Asia-pacific Microwave Conference, Adelaide, Australia., 575-582.

Tsang, L. and Ding, K. 1991. Polarimetric signatures of a layer of random nonspherical discrete scatterers overlying a homogenous half-space based on first- and second-order vector radiative transfer theory. IEEE Transactions on Geoscience and Remote Sensing, **29**, 242-253.

Touré, A. Thomson, K. P. B., Edwards, G., Brown, R. J and Brisco, B. G. 1994. Adaptation of the MIMICS backscattering model to the agricultural context – wheat and canola at L and C bands. IEEE Transactions on Geoscience and Remote Sensing, **32**, 47-61.

Ulaby, F. T., Bush, T. F. and Batlivala, P.P. 1975. Radar response to vegetation II: 8-18 GHz band. IEEE Transactions on Antennas and Propagation, **AP23**, 608-618.

Ulaby, F. T., Moore, R. K. and Fung, A. K. 1982a. Microwave Remote Sensing: active and passive, Volume II, Radar remote sensing and surface scattering and emission theory. Edited by F. T. Ulaby, published by Artech House, MA.

Ulaby, F. T., Aslam, A. and Dobson, M. C. 1982b. Effects of vegetation cover on the radar sensitivity to soil moisture. IEEE Transactions on Geoscience and Remote Sensing, **GE20**, 476-481.

Ulaby, F. T. and Jedlicka, R. P. 1984. Microwave dielctric properties of plant materials. IEEE Transactions on Geosciences and Remote Sensing, **GE-22**, 406-414.

Ulaby, F. T., Moore, R. K. and Fung, A. K. 1986. Microwave Remote Sensing: active and passive, Volume III, From theory to applications. Edited by F. T. Ulaby, published by Artech House, MA.

Ulaby, F. T., Sarabandi, K., McDonald, K., Whitt, M. and Dobson, M. 1990. Michigan microwave canopy scattering model (MIMICS). International Journal of Remote Sensing, **11**, 1223-1253

van der Sanden, J. J. 1997. Radar remote sensing to support tropical forest management. Unpublished PhD Thesis, University of Wageningen.

van Oevelen, P. J. 2000. Estimation of areal soil water content through microwave remote sensing. Unpublished PhD Thesis, The University of Wageningen.

Wang, J. R. 1980. The dielectric properties of soil-water mixtures at microwave frequencies. Radio Science, **15**, 977-985.

Wang, Y., Day, J. L. and Sun, G. 1983. Santa Barbara microwave backscatter canopy model for woodlands. International Journal of Remote Sensing, **14**, 1477-1493.

Wang, Y. Hess, L. L., Filoso, S. and Melack, J. M. 1995. Understanding the radar backscatter from flooded and nonflooded amazonian forests: results from canopy backscatter modeling. Remote Sensing of Environment, **54**, 324-332.

Woodhouse, I. H. 2003. Introduction to microwave remote sensing. In press.

Yueh, S. H., Kong, J. A., Jao, J. K., Shin, R. T. and Le Toan, T. 1992. Branching model for vegetation. IEEE Transactions on Geoscience and Remote Sensing, **30**, 390-402.

3.2 E-SAR Field Methods and Results

3.2.1 Introduction

The ESAR ground campaign took place in less than perfect conditions on June 3rd 2000. It was raining heavily and the soil was saturated making leak identification difficult (refer to section 1.4.2). However, the weather did not affect the field techniques applied and similar measurements were performed for the ESAR flight line as those for the HYMAP campaign. These are fully described in Chapter 2.3. This section will outline the measurements made (Table 3.2.1), but only describe in detail the measurements made in addition to those made during the HYMAP data collection. The results of the in-situ measurements are also presented (Tables 3.2.2 and 3.2.3).

Table 3.2.1 Summary of in situ field measurements taken during the ESAR camplaign.

Topographic measurements:	**Soil measurements:**
• Slope description • Slope direction • Proximity to boundaries	• Wet weight • Dry weight • Percentage moisture • Soil roughness • Surface roughness (correlation length)
Atmospheric measurements:	**Vegetation measurements:**
• Horizontal line of site • Air temperature • Cloud cover • Cloud type • Wind speed • Wind direction	• Canopy height • Biomass • Dry weight • Freshweight • Percentage moisture • Leaf area • Leaf density

3.2.1.1 Soil roughness

Soil roughness measurements were determined using a needle board. Measurements were only taken outside the leaks as the leak water surface was considered to be flat and microwaves are unable to penetrate water. Six separate needle board measurements were taken at each site and in two different perpendicular directions. The needle board had 40 needles and height variations were measured in cm. Each needle was 1.5cm apart. The results were then plotted to create a surface profile.

3.2.1.2 Correlation length

Correlation length is perhaps most commonly used to provide a reference for estimating the statistical independence of two surface points (Ulaby *et al,* 1986). In this case it is more specifically used as an indication of soil surface roughness as a function of soil height variations over distance. It was calculated from the needle board measurements made in the field. Firstly the normalised autocorrelation function is calculated for a given spatial displacement $\rho(x')$:

$$\rho(x') = \frac{\sum_{i=1}^{N+1-j} Z_i Z_{j+i-1}}{\sum_{i=1}^{N} Z_i^2} \qquad 3.2.1$$

where: N is the number of samples, j is the interval between samples, Z is height and i is the distance along the x axis.

Surface correlation length (l) is then defined as the displacement x' for which $\rho(x')$ is equal to 1/e:

$$\rho(l) = \frac{1}{e} \qquad 3.2.2$$

In cases where the surface is perfectly smooth (specular), correlation length l is infinity. This was the value assumed for leak surface water. The correlation lengths at all of the Cheshire leak sites are given in Table 3.2.2.

3.2.1.3 Stone content

For radar remote sensing studies of soil it is common to count the percentage of stones per volume and record stone size to provide us with more information on soil texture. This is usually achieved by counting the number of stones per unit volume and measuring maximum stone diameter in one dimension. However, the presence of stones was considered to be of little relevance to this particular study. The land had been well tilled and given the wavelengths used in this study (L-band), the resolution of the image data (9m) and the presence of vegetation in all cases, it was unlikely that stones would have a significant effect on backscatter.

References

Ulaby, F. T., Moore, R. K. and Fung, A. K. 1986. Microwave Remote Sensing: active and passive, Volume III, From theory to applications. Edited by F. T. Ulaby, published by Artech House, MA.

Table 3.2.2. Non leak surrounding area vegetation biophysical parameters.

Site	Crop	Canopy height (cm)	Percentage cover	Dry weight (g/625cm^2)	% moisture content	Leaf area (cm^2)	Leaf density/m^2	LAI	Non leak % soil moisture	Correlation length
C1	Wheat	59.2	85	18.3	78.57	79.04	8876	3.1	31.1	0.614
C2	Grass	9.05	85	25.6	83.31	2.13	12820	2.7	44.8	0.609
C3	Grass	3	70	6.6	78.91	0.71	4082	1.2	34.7	0.619
C5	Grass	12	99	9.7	87.89	2.83	10616	3	27.7	0.615
C6	Grass	5.87	100	14.5	86.78	1.38	7328	3.4	70.0	0.606

Table 3.2.3. Inside Leak Vegetation biophysical characteristics.

Site	Crop	Canopy height (cm)	Percentage cover	Dry weight (g/625cm^2)	% moisture content	Leaf area (cm^2)	Leaf density/m^2	LAI	Leak dimensions (m^2)
C1	Low vegetation	5.65	15	6.8	75.09	2.47	396	2.2	20.8 x 18
C2	Grass	10.3	60	25.6	83.31	2.13	12449	2.7	13 x 5
C3	Grass	5	65	6.2	86.31	1.18	16977	0.5	7.5 x 5.5
C5	Grass	12	95	9.7	87.89	2.83	10616	3	2.5 x 2.5
C6	Grass	25.65	95	22.3	85.75	6.24	24705	4.6	15.6 x 10.3

3.3 Radar backscatter modelling methods

3.3.1 Introduction

Radiative transfer theory has become an increasingly well-developed approach to modelling microwave backscatter from vegetation over the last 20 years. The model selected for the microwave modelling section of this project was RT2 - a radiative transfer model specifically designed for simulating vegetation canopies, developed by Saich (1995). Using RT2, each canopy type may be represented by up to 3 different layers with a maximum of 5 scatterer types in each layer. The scatterer types are uniformly positioned groups of discs, elongated discs and cylinders which are used to represent flowers, leaves and stems, respectively. Extinction and phase matrices describing how the energy in each vegetation layer is attenuated and scattered, are calculated based on the different structures of the modelled canopies. These matrices are then used to calculate direct backscatter (σ^0). RT2 is a second order model which means that it is not only able to calculate ground - layer interactions (first order model capability), it can also calculate interactions between layers.

3.3.2 Modelling strategy

The purpose of the modelling was to identify optimal microwave wavelengths for leak identification and predict backscatter characteristics for a range of vegetation types at different growth stages, under varying leak conditions. A similar strategy was adopted for the radar, as for the optical modelling (chapter 2.4) such that comparisons could be made between the two sets of results. The only differences were between certain model input parameters. For RT2 the input parameters were kept the same or as close as possible to the optical model input parameters and the same range of crop types and growth stages were used. As a reminder the simulated crops were:

Cereal	growth stage 1	-Young,
	growth stage 2	-Mid growth
	growth stage 3	-Ripe crop
	growth stage 4	-Stubble, after cutting
Row crop	growth stage 1	-Young
	growth stage 2	-Mid growth
	growth stage 3	-Fully grown
Canopy crop	growth stage 1	-Young
	growth stage 2	-Mid growth stage
	growth stage 3	-Flowering
	growth stage 4	-Desiccating
Grass	growth stage 1	-5 cm high
	growth stage 2	-10 cm high
	growth stage 3	-20 cm high
	growth stage 4	-30 cm high

and the leak scenarios were:

- *Dry soil* – used as a comparison for the following four wet scenarios
- *Wet soil* - a leak in its immediate expression, which has had no time to have any influence on the overlying canopy. As all other values are constant, this is a similar scenario to the leaks simulated in the field.
- *Ponding* - a recent leak where there has been no time for the presence of excess water to have an influence on the overlying canopy.
- *Puddling* - a leak of more prolonged duration but which has led to a positive response from the vegetation in the form of increased growth (LAI). This scenario is similar to that encountered at site C6 in Cheshire.
- *Water logging* - a very prolonged leak which has had a negative effect on the vegetation leading to a reduction in LAI and discolouring of the canopy.

3.3.3 Parameterising the model

The RT2 model takes up to 30 different input parameters depending on the complexity of the vegetation structure to be modelled. The scope of the model is broad enough to include a wide range of different vegetation canopy structures. As for the optical modelling, the choice of input parameters was heavily dependent on measurements taken in the field.

The 11 basic input parameters for RT2 are:

- Wavenumber ($k = 2\pi/\lambda$)
- Incidence angle (in degrees)
- Option to select levels of interaction between ground and layer, first, second and third order interactions are available
- Ground scatterer model option – choice of 6 models
- Ground susceptibility model option
- Height of vegetation layer
- Scatterer type – 4 options
- Number of scatterers per cubic metre
- Vegetation susceptibility model – choice of 3
- Scatterer inclination angle distribution – 8 options
- Axial angle distribution

Several inputs are used to determine how the direct, layer-ground and layer-layer backscatter interactions are calculated. The standard input uses Monte Carlo algorithms where it is possible to manually set the number of iterations. In deciding the number of iterations it is important to consider how precise the data needed to be. Here the model output was to be compared with airborne E-SAR data and therefore to make the model output values much more precise than the radiometric resolution of the imagery (3dB), would be of little value. In this case the default values were appropriate (for option 0: tolerance 1.0e-5, and number of loops 7.0e3). For leak scenarios, where the vegetation was standing in water, a Fresnel reflection coefficient was used for the ground-layer interaction. This parameter option assumes that the background surface is smooth and the scattering is specular. It was therefore considered to be suitably representative of surface water.

RT2 incorporates a ground scattering component and provides a variety of theoretical and empirical ground scattering models to choose from. The choice of model is largely determined by surface roughness, wavelength and incidence angle. To establish the most appropriate model it was necessary to consider the ground scattering model validity conditions, which are summarised in Table 3.3.1:

Table 3.3.1 Validity conditions for a range of ground scattering models.

Model	Validity conditions
Small Perturbation Model	$k\sigma < 0.3$
Kirchhoff Physical Optics	$m < 0.25,\ kl > 6,\ l^2 > 2.76\sigma\lambda$
Kirchhoff Geometric Optics	$(2\ k\sigma\ \cos\theta_{inc})^2 > 10,\ kl > 6,\ l^2 > 2.76\sigma\lambda$
Oh, Sarabandi & Ulaby (1992)	$k\sigma < 0.1,\ kl > 2.6,\ \theta_{inc} > 30°$ $k\sigma < 6,\ kl < 19.7,\ \theta_{inc} > 50°$ $kl > 2.5,\ \theta_{inc} \geq 30°$
Dubois et al (1995)	$k\sigma \leq 2.5,\ kl < 20,\ \theta_{inc} < 65°$

where:

k = wavenumber *m = surface slope (inset equation)*
σ = RMS height variation *l = correlation length*
λ = wavelength

Measurements taken in the field were compared with the above validity conditions to establish which would be the most appropriate model to use (Table 3.3.2). The purpose of matching the field measurements and model input parameters was to see how closely the model reproduced the remotely sensed E-SAR data.

Correlation length, which is a required input for the theoretical models, may be described as "a reference for estimating the statistical independence of two points on a surface" (Ulaby et al., 1982 p825). This statistic provides a means of relating the variance between surface height variations with their separation distance. The intrinsic hypothesis, in terms of spatial variation, is that points that are closer together are more similar than points further away. Thus, in this case, beyond a given length, variations in soil height may be considered statistically independent. The rougher the surface, the lower the correlation length value. A smooth surface is characterised by a correlation of $l = \infty$. Correlation lengths were calculated for all field sites and taken as input variables in the calculation of the theoretical ground scattering models. The empirical models assume specular forward scattering from a smooth surface, but the model would not accept a surface roughness value of zero for the Fresnel option, which is the value expected from a specular surface. To circumnavigate this problem the minimum allowable surface roughness value (characterized by RMS height) was established for each of the ground scattering models through trial and error, by incrementally decreasing the standard deviation. The result was a value of 4 mm.

Table 3.3.2. Validity conditions met by field data for each ground scattering model at each of the Cheshire leak sites.

	Site 1	Site 2	Site 3	Site 5	Site 6
Small Perturbation Model	✓	×	✓	✓	×
Kirchhoff Physical Optics	✓	✓	✓	✓	✓
Kirchhoff Geometric Optics	×	×	×	×	×
Oh, Sarabandi & Ulaby (1992)	✓	✓	✓	✓	✓
Dubois et al (1995)	✓	✓	✓	✓	✓

The results in table 3.3.2 show that the most appropriate ground scattering model for use in the dry model scenarios was the Kirchoff Physical Optics model. The Oh model was selected for leak scenarios because it did not require correlation length and it assumed specular forward scattering. Out of all the available models the Oh model accepted an RMS height value closest to zero, which best represented a water surface.

The default (and only available) ground susceptibilty model was used. It uses a model developed by Hallikainen *et al.* (1985) which considers soil type by taking parameters for fractional sand, clay and volumetric soil moisture. Soil samples were taken in the field and texture analysis performed using the well-documented Soil Survey texture analysis method (see methods chapter). Mid-range values were taken for each classified soil type as only the broad classification was known (and not exact fractions of sand silt and clay). Volumetric moisture contents were estimated by drying field samples in the laboratory.

The last six basic input parameters deal with the canopy architecture to be simulated. It is possible to have up to 3 different layers, for example stems and ears may be modelled separately. Each layer may have up to 5 different scatterer types, such as leaves, stems, flowers, and lateral branches. The scatterer types used in the simulations for each layer depended on the growth stage modelled and the vegetation type. The most complicated vegetation types were the cereal and canopy crops which each included stems, leaves and ears/flowers. The scatterer types used were all geometrical shapes and therefore calculated in the standard way. The most commonly used were flat elliptical disks (leaves), and cylinders (stems and ears). The widths, lengths and thicknesses of each object were defined based on field measurements. The input file also took the number density of each scatterer type and the angle distibution. The default random angle distribution value was used here for simplicity. A description of the available leaf inclination definitions follows (Goel and Strebel, 1984):

- Planophile – horizontal leaves most frequent
- Erectophile – vertical leaves most frequent
- Plagiophile – oblique leaves most frequent
- Extremophile - oblique leaves least frequent
- Uniform – same proportion of leaves at any angle
- Spherical – leaf angle same as for surface elements of a sphere

RT2 also contains an option for selecting a vegetation susceptibility model. The 'leafy' selected model is a dual dispersion model for leaves (Ulaby & El-Rayes, 1987) which required parameters for temperature (measured in the field) and gravimetric moisture (estimated from fresh and dry weight vegetation measurements). The RT2 input parameter tables are too large to include in the text. Therefore, they have been placed in Appendix 4.

Figure 3.3.1 provides a visual interpretation of how the model regards each of the crop types used in the study.

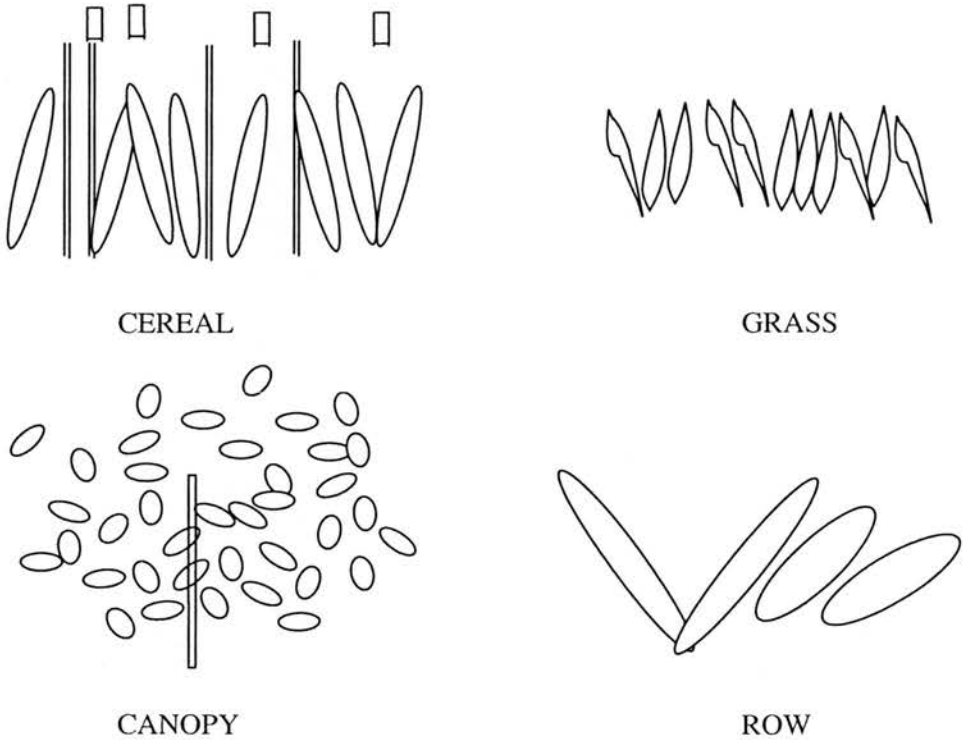

Figure 3.3.1. Visual representation of how RT2 regards a cereal, grass, canopy and row crop. The drawings are not to scale.

3.3.4 Model validation

Preliminary results from the RT2 model are outlined in Figure 3.3.2, and compared with E-SAR image data. These data demonstrate the model's ability to predict changes in backscatter between leaks and surrounding vegetation. Data with which to compare the model results were limited due to adverse conditions at the time of data acquisition (refer to chapter 3.2). Table 3.3.3 shows the absolute difference in dB between the modelled and image data. This table shows that on average the dry differences are smaller than the wet differences for the HH polarization, but the wet differences are smaller than the dry differences for the VV and cross polarizations. The results presented in Figure 3.3.2 show that the model tends to produce lower backscatter values than the image data. The modelled leak results are considered to fit the leak data well while the 'dry' image data are considered to fit the dry modelled data poorl, this is mainly due to the shape of the graphs and the position of the HH polaration values relative to the VV polarization values. These results are as expected considering the adverse conditions at the time of acquisition (Table 3.3.3 and Figure 3.3.2).

N. B. Other studies have indicated the model's ability to accurately predict backscatter for a range of wheat canopies at a variety of growth stages, particularly at L and C-bands (Saich, 2002).

Table 3.3.3.Differences in dB values between model and image data for all Cheshire sites at HH, VV and cross polarization channels. The minus indicates where the model values were lower than the image data values.

WET differences (dB)

	Site C1	Site C2	Site C3	Site C5	Site C6
HH	-2.94	-8.61	-9.14	-5.13	-2.07
VV	1.10	-4.65	-1.67	-4.21	-5.03
X-POL	-2.05	-7.03	-6.27	-7.78	-5.20

DRY differences (dB)

	Site C1	Site C2	Site C3	Site C5	Site C6
HH	7.50	-2.13	-7.73	-0.57	4.54
VV	-3.06	-7.13	-13.35	-11.02	1.53
X-POL	8.18	-19.43	-14.59	-5.50	-8.67

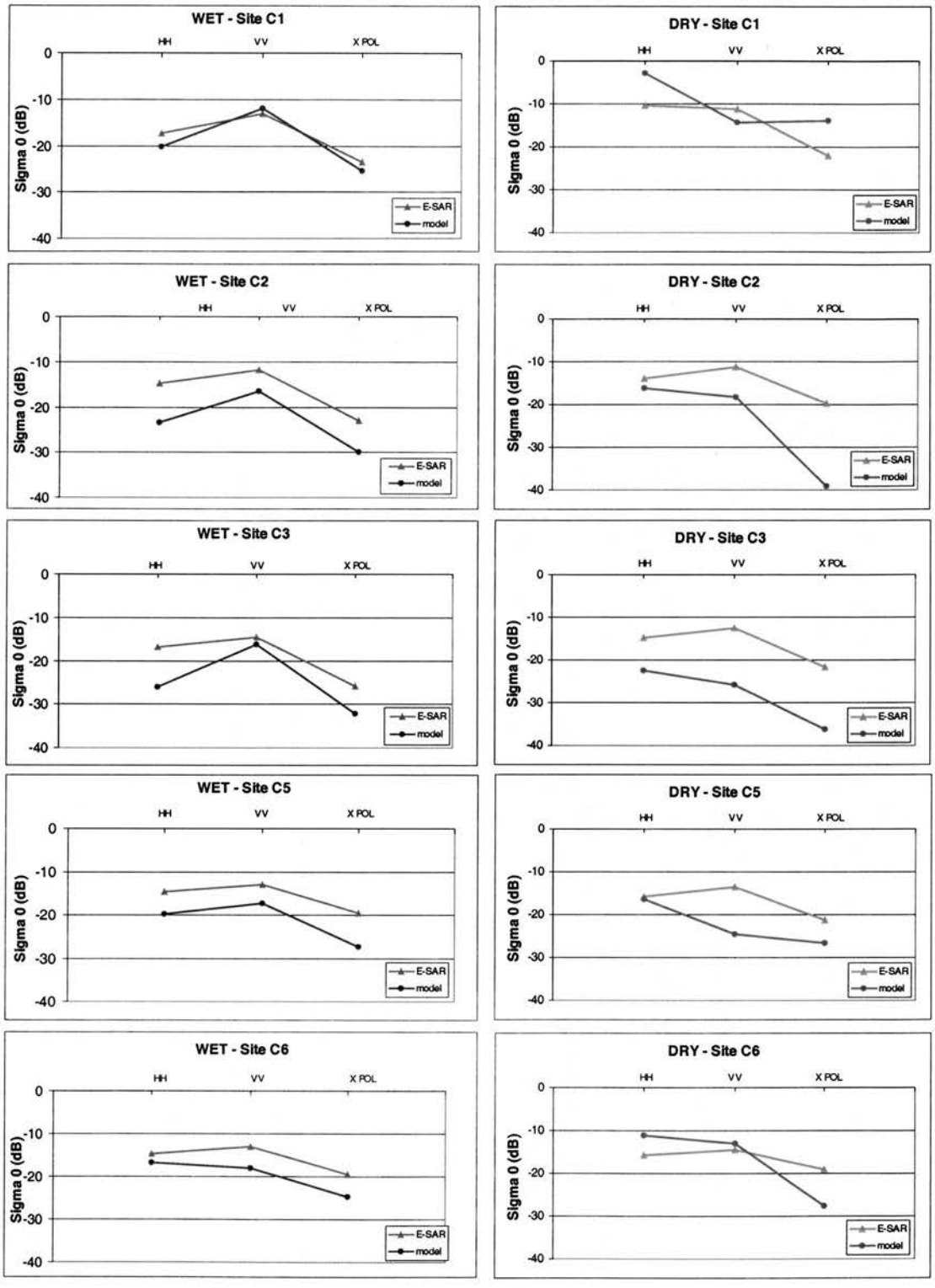

Figure 3.3.2. Comparison of the RT2 model's ability to reproduce backscatter values with E-SAR observations (where graphs on left show leak backscatter; right, show 'dry' surrounding vegetation backscatter).

References

Dubois, P. C., van Zyl, J. J. and Engman, E. T. 1995. Measuring soil moisture with imaging radars. IEEE Transactions on Geoscience and Remote Sensing, **33**, 915-926. Corrections in: **33**, 1340, November 1995.

Goel, N. S and Strebel, D. E. 1984. Simple beta distribution representation of leaf orientation in vegetation canopies. Agronomy Journal, **76**, 800-802.

Hallikainen, M., Ulaby, F. T., Dobson, M. C., El-Rayes, M. and Wu, L. K. 1985. Microwave dielectric behaviour of wet soil – part I: empirical models and experimental observations. IEEE Transactions on Geoscience and Remote Sensing, **GE23**, 25-34.

Oh, Y., Sarabandi, K. and Ulaby, F. T. 1992. An empirical model and an inversion technique for radar sattering from bare soil surfaces. IEEE Transactions on Geoscience and Remote Sensing, **30**, 370-381.

Saich, P. 1995. Backscatter software user guide. BSATC document, RET-4-MRC-027 (issue 1.1). ESA contact 10644/93/NL/NB, ref. Y/218/3383.

Saich, P. 2002. Comparison of microwave model with observational data. Report on workpackage 41, ESA contract 14940, ref. 14940/UCL/PS/.

Ulaby, F. T. and El-Rayes, M.A. 1987. Microwave dielectric spectrum of vegetation part II: dual dispersion model. IEEE Transactions on Geoscience and Remote Sensing, **25**, 550-557

Ulaby, F. T., Moore, R. K. and Fung, A. K. 1982. Microwave Remote Sensing: active and passive, Volume II, Radar remote sensing and surface scattering and emission theory. Edited by F. T. Ulaby, published by Artech House, MA.

3.4 Radar modelling results

3.4.1 Introduction

The results presented here are from the radar modelling study which used RT2, the fully polarimetric second order radiative transfer model, to reproduce backscatter measurements for a variety of vegetation and leak scenarios over a range of wavelengths. In most cases the same modelling approach that was used for the optical modelling was applied here (chapter 2.3), that is; four different canopies at a variety of different growth stages and under five wetness scenarios. The microwave modelling approach is outlined in chapter 3.3. The radar modelling forms the backbone of the radar work carried out in this thesis. It is particularly important because there are no supporting ground based measurements like those provided by the spectroradiometer in the optical study, and also because the conditions under which the E-SAR imagery were acquired were unfavorable making leak identification difficult.

The aim of this chapter is to present the responses of three different microwave wavelengths to the various modelled vegetation and leak scenarios. Figures 3.4.1 – 3.4.3 display C-, L-, and P-band RT2 model outputs for each modelled crop at all growth stages and for the five different leak scenarios. Each graph shows direct backscatter (σ^0 in dB) for each polarisation (HH, VV and HV). In the following graphs a cut-off value was selected for the y axis because beyond approximately –40 to -50 dB (depending on instrument sensitivity) noise levels for an operational radar system are such that the signal is indistinguishable from noise. So, while these values may be used to compare model output, from an operational perspective they are unlikely to be of use for interpretation of microwave data, therefore values lower than -50 dB have been omitted.

The main emphasis of the results is the HH and VV polarisations. In addition to oriented scatterers, cross polarisation responses can also be associated with multiple scattering interactions. RT2 estimates layer-layer interactions but it does not estimate the multiple interactions between scattering elements resulting in an underestimation of cross polarisation scattering (Woodhouse and Hoekman, 2000). To accurately calculate multiple scattering interactions is computationally intensive. For convenience, in the following discussion HH polarisation responses are commonly described in relation to VV responses, as it was found that VV backscatter varies less with growth stage and changing surface water conditions than HH backscatter responses. In general, for surfaces the VV is greater than the HH response. As the HH response increases, up to a situation where HH responses are equal to VV responses, it implies double bounce or more facet scattering from objects such as leaves. When HH values are greater than VV values it is likely that scattering is from horizontal dipole interactions or strong double bounce.

3.4.2 C-band

3.4.2.1 Canopy crop results

The C-band modelled crop results (Figure 3.4.3) showed that for all dry, wet and ponding scenarios the HH response is greater than the VV response at all growth stages. For the puddling scenarios the HH and VV values were more similar to each other, particularly at the later growth stages (i.e. 2-4). The HH and VV responses varied relatively little over different leak scenarios except the waterlogged scenario. For the waterlogged scenario VV responses were characteristically lower than for other leak scenarios. At the earliest and latest growth stages the HH waterlogged responses were lower than from growth stage 2-3a, the HH response was also lower than the VV response at growth stages 1 and 4.

3.4.2.2 Cereal crop results

Overall backscatter values for the C-band modelled cereal crop were lower than the C-band modelled canopy crop due to variations in canopy structure. The first three growth stages

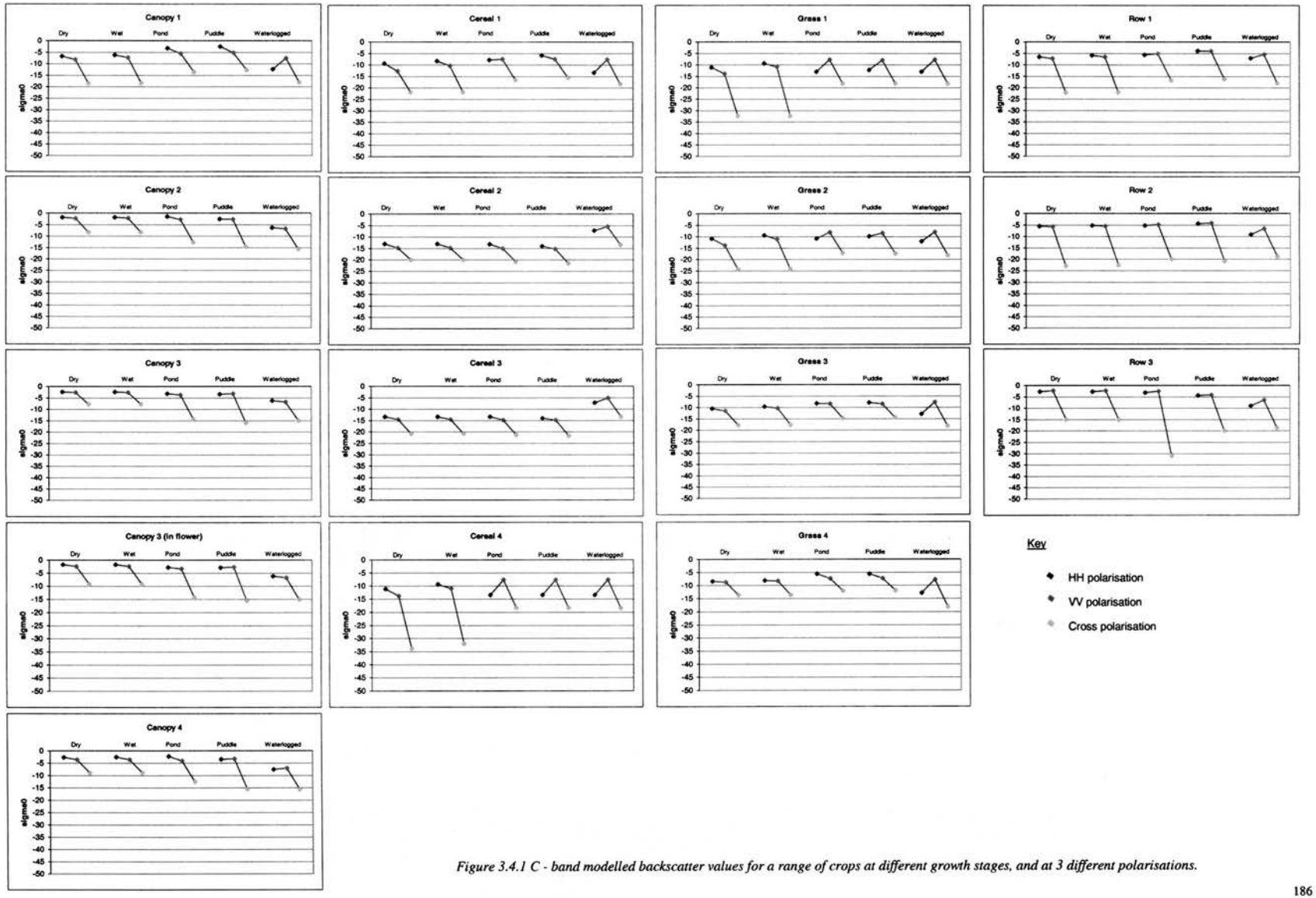

Figure 3.4.1 C - band modelled backscatter values for a range of crops at different growth stages, and at 3 different polarisations.

produced similar responses to each other across all leak scenarios, where HH responses were greater than, or equal to the VV responses for the first 4 leak scenarios. The waterlogged response produced a result where the HH response was lower than the VV response. For growth stages 2 and 3 the HH and VV values were greater than for the other leak scenarios at each growth stage. At growth stage 4 the surface water leak scenarios showed greater VV responses and lower HH responses than for those at other C-band cereal growth stages.

3.4.2.3 Grass crop results

At early growth stages and for the waterlogged scenario at all growth stages the HH response for the surface water leak scenarios were lower than the VV responses. For the dry and wet scenarios at these growth stages the reverse was the case. The later growth stages showed results similar to those for cereal crops at growth stage 3 where there was little difference between HH and VV values for the first 4 leak scenarios and lower HH values with the waterlogged scenario.

3.4.2.4 Row crop results

The C-band modelled row crop results showed that there was very little variation between the relative HH and VV responses across leak scenarios 1-4 and at all growth stages. The waterlogged scenario differed in that the HH response was consistently lower than the VV response at all growth stages.

3.4.3 Discussion of C-band measurements

The C-band results (Figure 3.4.1) showed that shorter microwave wavelengths were not good for distinguishing between leak and surrounding vegetation where vegetation canopies were dense. With the canopy crop, the only distinguishable leak scenario was the waterlogged scenario at growth stage 1. For all other scenarios and growth stages there was little difference between leak and surrounding vegetation.

Against the cereal crop it was possible to identify variations between leak and surrounding vegetation for the waterlogged scenarios at all growth stages due to the characteristic lower HH (and cross polarisation) response in relation to the VV response. The pond and puddle scenarios only produced results where the HH response was lower than the VV response, at growth stage four (modelled stubble). The strong backscatter response for the waterlogged scenario at the maximum growth stages may be due to double bounce effects as a result of sparse vertically orientated stems, wavelength size and the flat water surface.

The grass crop is the canopy type that performs best at C-band with regard to characterising differences between leak and surrounding vegetation. It is possible to distinguish between dry and the standing water scenarios (pond, puddle and waterlogged) at growth stages one and two. However, only the waterlogged scenario could be identified at growth stages three and four.

With the row crop there was very little difference between the HH and VV responses across the first four leak scenarios due to canopy scattering and the horizontal orientation of the row crop canopy. Only for the waterlogged scenario was the HH response lower than the VV response, creating a contrast between leak and non leak at all of the growth stages.

3.4.4 L-band

3.4.4.1 Canopy crop results

Backscatter responses for the modelled canopy crop, shown in Figure 3.4.2, can be separated in response to leak type. The wet and dry scenarios produced similar responses to each other, where HH polarisation responses were greater than VV responses for all growth stages. The ponding and puddling scenarios have similar backscatter responses to each other, but total backscatter varied with crop growth stage. At the earliest growth stage, the HH responses were lower than the VV responses, and at later growth stages HH responses were typically 2 – 5 dB greater than the VV responses (except the ponding scenario for growth stage 4). The waterlogged scenario produced a response where the HH backscatter was lower than the VV responses and typically lower than for the other leak scenarios. For all growth stages and leak

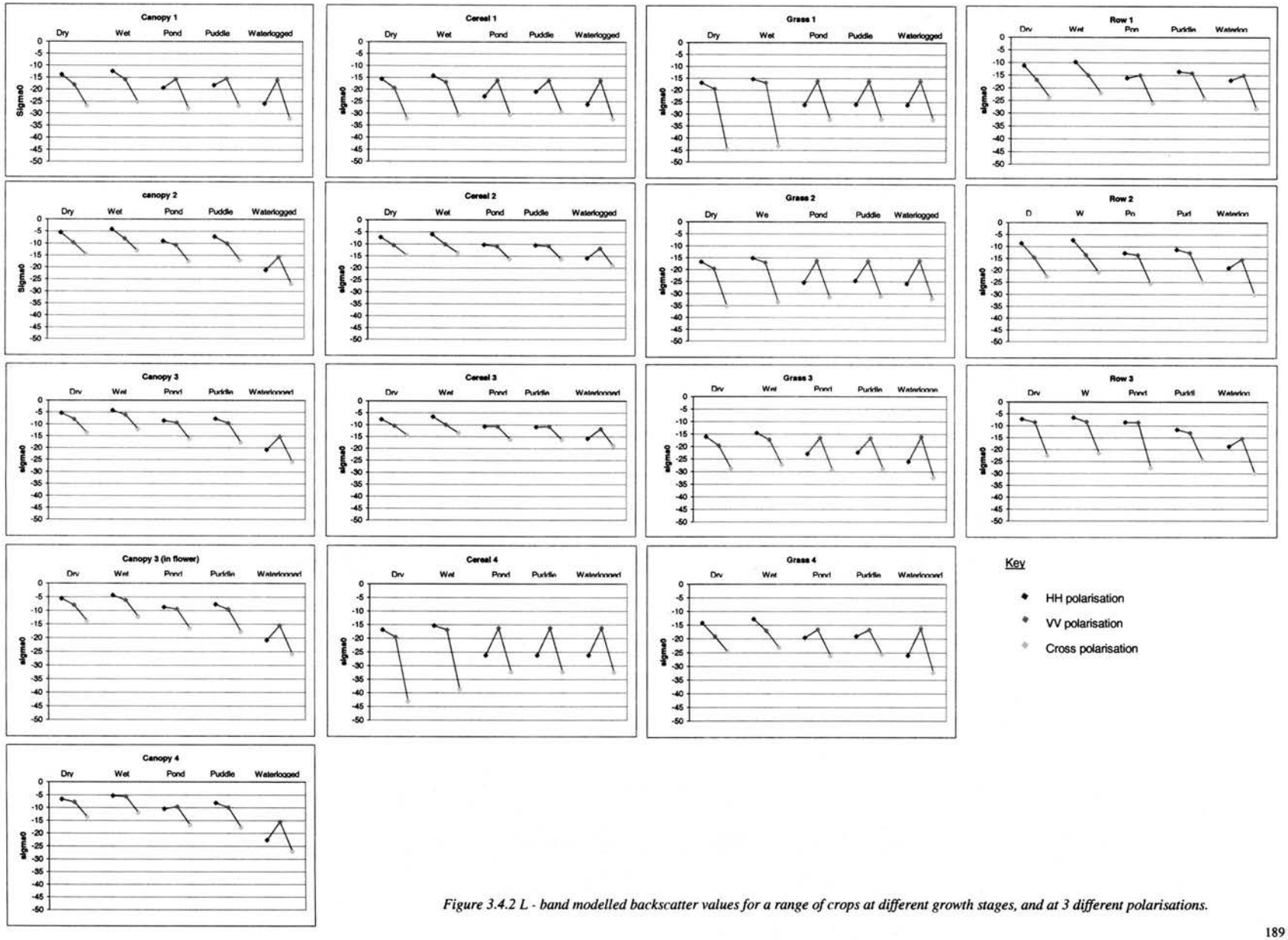

Figure 3.4.2 L - band modelled backscatter values for a range of crops at different growth stages, and at 3 different polarisations.

types, the cross polarisation response was lower than either the HH or VV responses, as expected because it is always lower. VV responses for growth stages 2-4 were greater for the dry and wet scenarios than they were for the ponding and puddling scenarios, and of all the VV responses the ones for the waterlogged scenarios produced the lowest responses across all growth stages.

3.4.4.1 Cereal crop results

The modelled cereal crop backscatter responses are shown in Figure 3.4.1. The cereal crop produces a similar L-band pattern in terms of the leak scenarios to the canopy crop. The wet and dry scenarios produce backscatter responses where the HH polarisation response is greater than the VV response. For leak scenarios where there is surface water present (ponding, puddling and waterlogged), the HH responses are lower than the VV responses for growth stages 1 and 4, and at all growth stages for the waterlogged scenario. The ponding and puddling scenarios demonstrate similar HH and VV responses at growth stages 2 and 3. At the maximum growth stages (i.e. two and three for the cereal crop) the variation in HH response is less than at growth stages 1 and 4 (stubble) and the HH and VV values for the first four leak scenarios are similar.

3.4.4.3 Grass crop results

The L-band backscatter responses for grass at a variety of different canopy heights and under a variety of leak conditions produced clear results (Figure 3.4.3). For dry and wet scenarios the HH response was greater than the VV. For leak scenarios where surface water was present the HH responses were lower than the VV responses. There was little variation in the VV backscatter response values, with changing leak conditions or with increasing biomass. The direct backscatter values for grass were typically less than that of the other canopies. This is due to the structure of the grass canopy which has thinner finer leaves, and has a much less complex vegetation structure with fewer volume scattering components than the other canopies. The canopy is only made-up of leaves which means fewer layer interactions and a lower backscatter response.

3.4.4.4 Row crop results

The wet and dry responses were similar to the other L-band modelled crops; the HH responses were greater than the VV responses, and the waterlogged HH responses were lower than the waterlogged VV responses for all growth stages. However, backscatter values for the ponding and puddling scenarios were more varied than for other modelled crops. For growth stages 1 and 3 the ponding scenario had lower HH responses than the VV, while the puddling scenario had greater HH values than VV. At growth stage 2 the ponding and puddling scenarios both had slightly higher HH than VV responses.

Differences between HH and VV responses were small for all leak scenarios (except the waterlogged scenario at growth stage 3) in comparison to results for other crops. The row crop is the only modelled canopy to have leaves close to the horizontal plane. The other canopies are near vertical, or spherical (in the case of the canopy crop). The more horizontal leaf orientation resulted in greater interactions between the canopy and H polarised waves which led to an overall increase in HH backscatter response for the leak scenarios mentioned above. The HH canopy interactions increased with leaf area which reached a maximum at growth stage 3, explaining why the HH and VV responses are more similar, particularly for the puddling scenario.

3.4.5 Discussion of L-band measurements

The first key point to note from these results is that as vegetation biomass, density or height increases (with increasing growth stage) total backscatter across all polarisations increases. The second point is that where vegetation density is low the VV backscatter values vary little, but as biomass increases there is more variation across the leak scenarios in the VV values due to increased scattering from canopy elements. The third point is that for the leak scenarios where there is surface water present (i.e. ponding, puddling and waterlogged) there is a clear reduction in the HH responses relative to those for the dry and wet scenarios. The final point is that HH varies much more with changing water content than the VV polarisation. This is because characteristically H polarised waves are better able to penetrate vegetation canopies (particularly

more vertical canopy structures) than V polarised waves (section 3.1.8), therefore more of the HH backscatter response comes from surface scattering than canopy scattering, which results in lower HH backscatter values (Figure 3.1.3).

Despite canopy and cereal crops both representing relatively tall, dense vegetation types the overall backscatter values were lower for the cereal crop across all growth stages and for all leak scenarios, than for the canopy crop. Also the HH responses were lower in relation to the VV responses in relation for the cereal crop than for the canopy crop. As vegetation becomes more similar to a dense random volume, HH responses become progressively more similar to VV responses. Variations in backscatter response between cereal and canopy crops may be explained by vegetation geometry. The cereal crop has a more vertical orientated canopy compared with the spherical leaf distribution represented in the model for the canopy crop. H polarised waves are able to penetrate the vegetation canopy further, and interact less with vertically aligned vegetation, thus the signal response is lower. This also makes the H polarised waves more likely to interact with the water beneath the vegetation canopy than V polarised waves. A flat, water surface creates forward scattering resulting in lower backscatter values. This explains why the presence of water results in a decrease in backscatter for H polarised waves in these modelled scenarios. These effects, however, appear to be wavelength dependent (Ulaby *et al.*, 1982; Dobson *et al.*, 1985).

The lack of variation between HH and VV responses at the maximum growth stages for the modelled crops with tall dense canopies promoted a more detailed exploration of backscatter components for cereal 3 (a ripe cereal canopy). HH and VV responses from each of the scattering components making-up total backscatter are plotted in Figure 3.4.3. The graphs show the individual backscatter contributions from ground, layer 1(leaves), layer 2 (stems) and layer 3 (ears), compared with the total backscatter response for 2 of the leak scenarios. The dry and ponding scenarios are used as they represent examples of vegetation over a relatively rough surface (dry), and vegetation over a flat surface water (ponding).

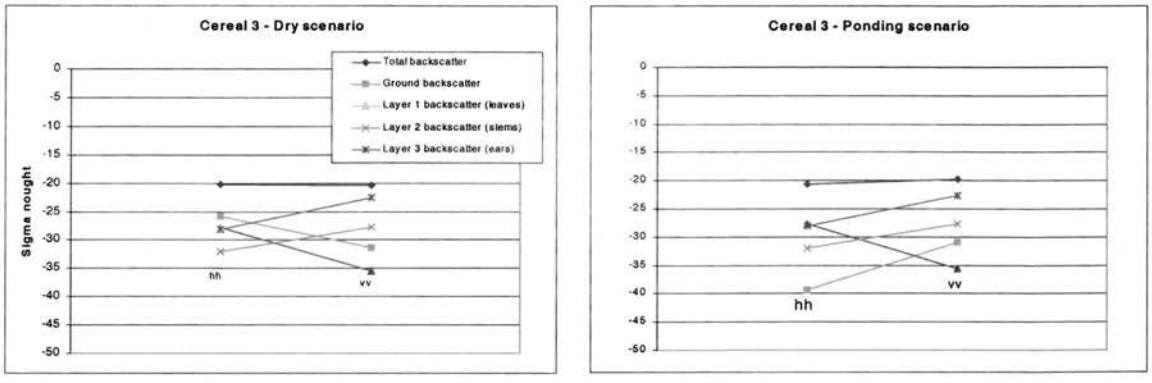

Figure 3.4.3. Graphs showing a break-down of scattering components in relation to HH and VV responses for a modelled cereal crop at growth stage 3 for a dry (left) and ponding (right) scenario.

The results show there are differences between the scattering responses of H and V polarised waves with changing surface characteristics and that the greatest variation between the two scenarios presented in Figure 3.4.3 comes from the ground scattering component. For the cereal crop at growth stage 3 under the dry scenario the ground scattering contribution is greater from H than from V polarised waves. For the ponding scenario the reverse is the case; the HH response is lower than the VV response. A further observation is that the VV ground scattering is greater for the ponding scenario than for the dry scenario, and that the HH backscatter for the ponding scenario is lower than the HH backscatter for the dry scenario.

The different contributions making-up the total HH and VV backscatter responses effectively combine to produce similar total backscatter values but the relative contributions differ. The VV responses show that there is greater scattering from the top of the canopy (i.e. ears) and less scattering from ground and leaf contributions for both the dry and ponding scenarios. However, the response from the ground is greater than the response from leaves for the ponding scenario. With the HH responses for the dry scenario most of the scattering is coming from the ground in relation to the rest of the canopy which suggests that the canopy is relatively transparent to the L-band microwaves. For the ponding scenario the majority of the scattering is coming from the vegetation elements and the HH ground scattering contribution is low which may be explained by the specular properties of a flat water surface resulting in a high level of forward scattering. In this situation separating the relative contributions is useful for interpretation of results.

3.4.6 P-band

3.4.6.1 Canopy crop results

The water logged scenario for growth stage 1 is not plotted as the backscatter values are lower than –50 dB across all polarisations. Results for the P-band modelled canopy crop (Figure 3.4.2) showed that for all growth stages the HH response was greater than the VV response for the dry and wet scenarios. For the leak scenarios where surface water was present (ponding, puddling, waterlogged), the HH response was lower than the VV response in most cases, the difference between HH and VV responses was most marked at growth stage 1. The cross polarisation response was lower than both the HH and VV responses at all growth stages and for all leak scenarios.

There were marked changes in the VV responses between the wet and dry scenarios, and the surface water scenarios at the earliest growth stage, however, at later growth stages the VV responses varied less. For the puddling scenario there were greater HH and VV responses (in relation to the wet, dry and pond scenarios) at all growth stages except 1. The HH and VV responses for the waterlogged scenario were lower relative to the dry, wet and pond scenarios at growth stages 2-4.

3.4.6.2 Cereal crop results

The cereal results are affected by having low σ^0 values where vegetation density is low (i.e growth stages 1 and 4 and the waterlogged leak scenarios). At growth stage 4 only the HH and VV responses for the dry and wet scenarios are plotted. The cross polarisation response for all leak scenarios at the stubble stage (growth stage 4) are off the bottom of the scale.

The P-band cereal crop results showed little variation between backscatter responses for H and V polarised waves at growth stages 2 and 3 for all leak scenarios except the waterlogged scenario. For the waterlogged scenarios at growth stages 2 and 3, the HH and VV responses were lower than for the other leak scenarios, and the HH response was lower than the VV response. At low crop densities (i.e. growth stages 1 and 4) the backscatter responses for dry and wet scenarios were significantly higher than for the surface water leak scenarios. For growth stage 1, the

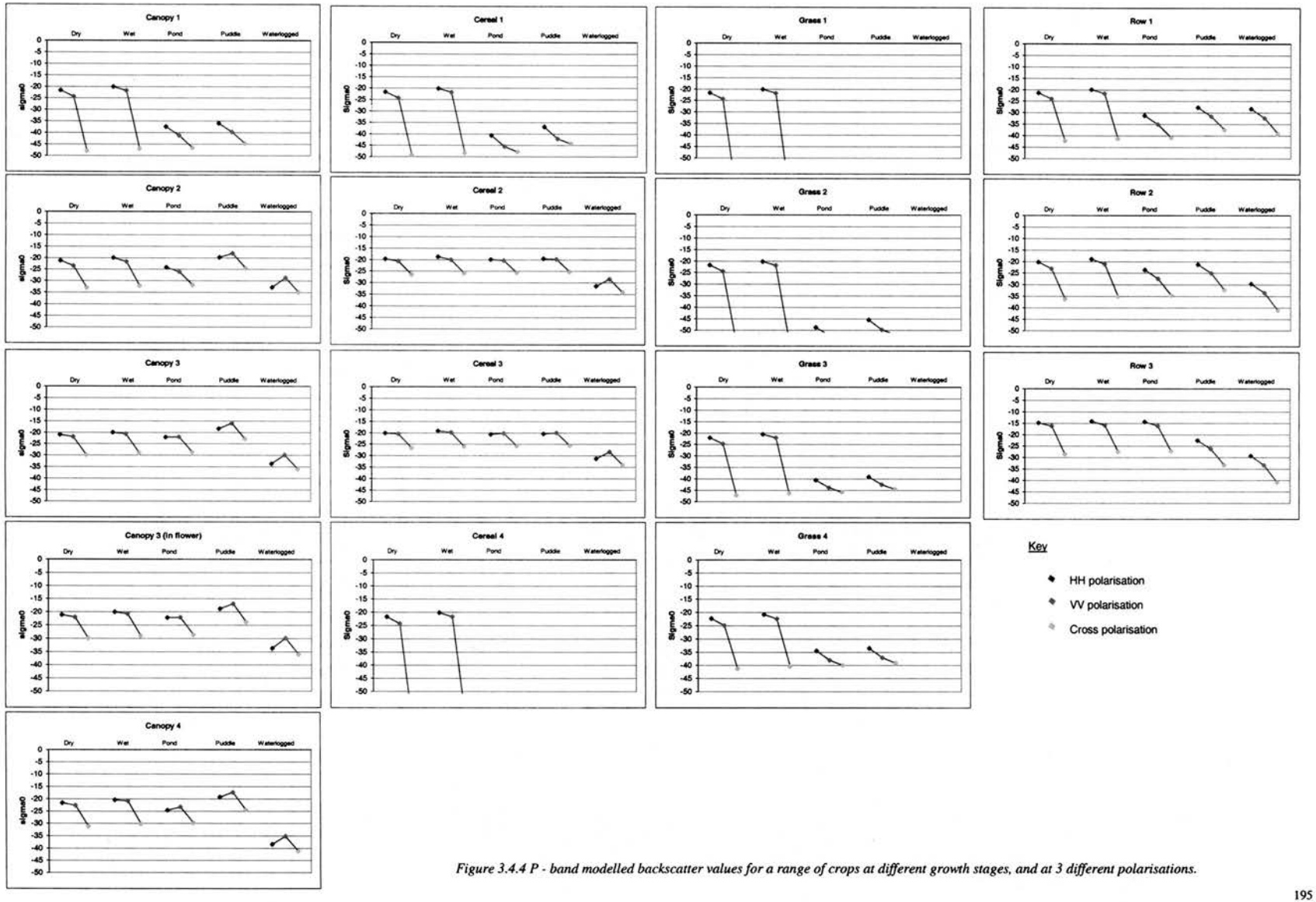

Figure 3.4.4 P - band modelled backscatter values for a range of crops at different growth stages, and at 3 different polarisations.

surface water leak scenarios produced greater HH backscatter relative to VV backscatter, rather than the more typical lower HH values found at growth stage 4. The results suggest that there are differences in scattering between the dry and wet scenarios and the ponding, puddling and waterlogged scenarios at growth stages 1 and 4.

3.4.6.3 Grass crop results

There was a clear distinction between results from the dry and wet scenarios, and the surface water scenarios at all growth stages. For the earliest growth stage the surface water leak scenarios are off the bottom of the scale, and the waterlogged scenario at all growth stages has σ^0 values lower than –50 they therefore, do not appear on the graphs. The HH and VV responses for the surface water leak scenarios had backscatter values -18 to -30 dB lower than for the HH and VV responses at the dry and wet scenarios. The combination of P-band and modelled grass crop produced the greatest difference in backscatter between HH and VV responses at different leak scenarios than any other crop or wavelength, particularly at early growth stages. The only other crop producing similar results is the P-band modelled stubble (growth stage 4 of the cereal crop) – however, from a microwave modelling perspective the appearance of stubble and a grass canopy are not dissimilar which explains the similarity on backscatter response. The VV response for the puddling scenario was –2 to -3 dB greater than for the pond and waterlogged scenario at growth stages 3 and 4. For all the plotted P-band grass (and row crop results) the HH response was always greater than the VV response, this differs from most of the other wavelength measurements (L- and C-band), particularly in relation to the surface water scenarios.

3.4.6.4 Row crop results

The P-band row crop results show that the HH and VV responses were relatively similar to each other across all leak types. There were decreases in the HH and VV responses with the surface water leak scenarios, particularly at growth stage 1. The HH response was greater than the VV response for all leak scenarios which appears to be a feature more characteristic of P-band freqencies than L-band frequencies. The puddling and waterlogged scenarios showed a reduction in backscatter values across all polarisations at growth stage 3.

3.4.7 Discussion of P-band measurements

The omission of the lower σ^0 values only affected the P-band results. The early growth stages of the grass crop, and the waterlogged scenario where canopy density was low (i.e. canopy 1, cereal 1 and 4, and grass at all growth stages) were affected. The reason is that where vegetation density is low, the longer P-band wavelengths do not 'see' the vegetation and the surface appears to be smoother (in relation to C- and L-band wavelengths). Therefore, there is greater forward scattering resulting in lower σ^0 values.

The overall backscatter values for the P-band results were lower than for the L- and C-band results due to the greater canopy penetration depth of longer wavelengths and vegetation interactions being influenced by the size of vegetation scatterers in relation to wavelength. Differences between leak and surrounding vegetation were greatest where vegetation canopy density was low, for example, the cereal crop at growth stage 4 and for waterlogged leak scenarios.

HH and VV responses were similar across the first three leak scenarios (dry, wet and ponding) where vegetation density was high. Between these leak scenarios there was no change in vegetation height or density; the results suggest that despite the longer wavelength and greater penetration depth, the P-band microwaves were still unable to penetrate the dense canopy crop. Therefore, the backscatter response was coming from canopy scattering. For the puddle scenario where vegetation height and density were increased, the VV backscatter was greater than for other leak scenarios, again due to increased canopy scattering. P-band appeared to be the only wavelength sensitive to backscatter response for the canopy crop puddling scenarios.

Where vegetation density was low and canopy structure was relatively simple the presence of standing water resulted in a decrease in backscatter values across the HH, VV and cross polarisation channels. The lower HH response in relation to the VV response which was characteristic of the waterlogged leak scenarios for most of the L- and C-band results, were not as apparent in the P-band results. It only appeared when crop density was high. The effect of the longer wavelength may make the vegetation appear semi transparent at the early growth stages which would explain the reduction in backscatter values across all polarisations rather than just

the HH. V polarised waves tend to interact more with vegetation elements than H polarised waves. However, if the vegetation scattering components are small in relation to wavelength then the VV interaction with vegetation will be minimal which means there will not be the contrast between the HH and VV.

3.4.8 Summary

The results have shown that the presence of surface water has a significant effect on microwave backscatter, particularly where vegetation height and density are low. Generally it is the decrease in HH backscatter relative to the VV response that appears to provide the most information with regard to the presence of water, particularly at C- and L-bands. VV backscatter responses tended to increase with vegetation biomass and decrease with wavelength. Overall, the waterlogged scenario produced the greatest contrast between leak and surrounding vegetation for all crop types, and at all frequencies. With dense cover types (for example canopy 2 and 3) the model results showed that differences between leak and surrounding vegetation were greatest under waterlogged scenarios where the vegetation in the leak is very depleted. Vegetation canopy structure can effect the polarised response of microwaves. More vertically orientated vegetation canopies produced greater scattering from V polarised waves than H polarised waves (for example the cereal crop). Similarly, H polarised waves tended to interact more with horizontally orientated canopies (for example the row crop). Thus, typically the VV response from vertically aligned vegetation was stronger than for canopies with other leaf orientations (e.g. the canopy crop), and there was a stronger HH response from horizontally aligned vegetation relative to other canopy orientations. The wet scenario was indistinguishable from the dry scenario at all frequencies, for all crop types, at all growth stages.

Overall, the total C-band backscatter responses were greater than for the same L-band or P-band modelled crop. At shorter wavelengths more of the scattering is from canopy scattering resulting in greater backscatter values across all polarisations. The microwave/canopy interactions meant that little of the return signal came from surface scattering. Thus the contrast between leak and surrounding vegetation was less at shorter wavelengths, making leak identification more difficult, except at the earliest grass growth stages and for the waterlogged scenario.

L-band appears to be effective at identifying differences between leak and surrounding vegetation where vegetation density is low and/or canopy structure is simple, and under conditions where the presence of water has had a negative effect on vegetation (i.e. the waterlogged scenario). Differences between leak and surrounding vegetation can be identified for leak scenarios where there is surface water present (ponding, puddling and waterlogged scenarios) by lower HH responses than VV responses, and/or where HH and VV values are similar, yet lower compared to the dry and wet scenarios. L-band is comparatively poor where vegetation density is high, except in the case of the waterlogged scenario. However, by exploring the individual scattering components that make up total backscatter (i.e. ground and layer scattering) it was demonstrated that for a cereal canopy at growth stage 3 it was possible to distinguish between dry and ponding scenarios by considering ground scattering for H and V polarised waves. L-band showed greater sensitivity to changes in leak scenario for denser canopy types than P-band results through the changing value of the HH response relative to the VV. Overall L-band modelled results provided more consistent responses to a range of leak scenarios over a variety of vegetation types than P- or C-band results.

P-band results showed that longer wavelengths are effective at distinguishing between leak and surrounding vegetation at early growth stages or where vegetation density is low (for example the modelled cereal crop growth stage 4), and for simple canopy structures (e.g. grass). However, while these leak scenarios and growth stages showed pronounced variations in backscatter between leak scenarios many of the values were outside the range of meaningful values for operational imaging radar. P-band was the only waveband affected by values lower than -50 dB, making it less suitable than L-band for leakage detection, particularly where vegetaiton density is low. Results showed that P-band was sensitive to small changes in vegetation biomass where vegetation density was high. Unlike L- and C-band results, however, lower HH values relative to VV values were not always observable for the waterlogged scenario. A further problem with P-band is that implementation of an operational P-band imaging radar is still some years away as P-band wavelengths are unable to penetrate the ionosphere.

3.4.9 Implications for leak detection

The results presented in this chapter suggest that L-band, HH and VV polarisations may usefully be employed for leakage detection from an imaging radar. C-band does not appear to be able to penetrate the given canopies modelled and P-band encounters difficulties relating to noise, it appears to 'see' too little of the vegetation and P-band microwaves are unable to penetrate the ionosphere. The criterion for deciding whether leaks are distinguishable in modeled radar data appears to be where HH responses are lower than VV responses.

References

Dobson, M. C., Ulaby, F. T., Hallikainen, M. T. and El-Rayes, M. A. 1985. Microwave dielectric behaviour of wet soil: Part II. Dielectric mixing models. IEEE Transactions on Geoscience and Remote Sensing, **GE-23**, 35-46.

Ulaby, F. T., Aslam, A. and Dobson, M. A. 1982. Effects on Vegetation cover on the radar sensitivity to soil moisture. IEEE Transactions on Geoscience and Remote Sensing, **GE-20**, 476-481.

Woodhouse, I. H. and Hoekman, D. H. 2000. A model-based determination of soil moisture trend in Spain with the ERS scatterometer. IEEE Transactions on Geoscience and Remote Sensing, **38(1)**, 126-140.

3.5 E-SAR image results

The results presented here are taken from the E-SAR image data, acquired in the rain on 3rd June 2000, after it had been geocoded, speckle reduced and converted to σ^0 - this degraded the image resolution to approximately 9m. The same method of pixel sampling that was applied to the HYMAP reflectance measurements presented in section 2.5 is applied to these data. Between 5 and 8 pixels were sampled from the surrounding 'dry' areas and 2-3 pixels were sampled from inside each leak. Due to the decrease in the image resolution arising from the image processing, the number of available 'leak' pixels was limited to just a few with which to compare the dry measurements. It is also likely that due to the increased pixel size, each of the selected leak pixels contained leak backscatter signals from the surrounding vegetation, thereby giving a mixed target response and making leak identification more difficult. It should also be mentioned that the areas occupied by the leaks were much larger during the ESAR data acquisition campaign than at the time of the optical data collection due to the prolonged period of rain prior to, and during the ESAR flight.

The results of the E-SAR image analysis are presented in Figure 3.5.1. While site C1 was an atypical leak at the time of the HYMAP acquisition as there was no leak, during the E-SAR campaign it provided one of the best examples as it was one of the largest leaks in terms of area and it had been present long enough for much of the vegetation in the leak to die back. As a result, there was contrast between the vigorous wheat canopy and the low level and sparse vegetation present in the leak. In graph 3.6.1a something that resembles the type of backscatter response typical of a vegetated surface and a sparsely vegetated water surface, can be observed i.e. a leak and non leak scenario, and in this example it is possible to distinguish leak, from surrounding vegetation. The characteristic VV spike is observable for the leak response, where the VV is higher than both the HH and cross polarisation channel, giving an indication of water.

For the non-leak measurements there is a greater VV response compared to the leak, typical of increased volume scattering from vegetation canopies. In this case it is possible that the backscatter response may be disproportionally high due to the presence of water droplets on the vegetation at the time of acquisition, this increases the dielectric constant, and therefore backscatter (Ulaby *et al.*, 1986). The reasons for differences in polarimetric response under changing wetness conditions and vegetation physiology are considered in more detail in the next chapter.

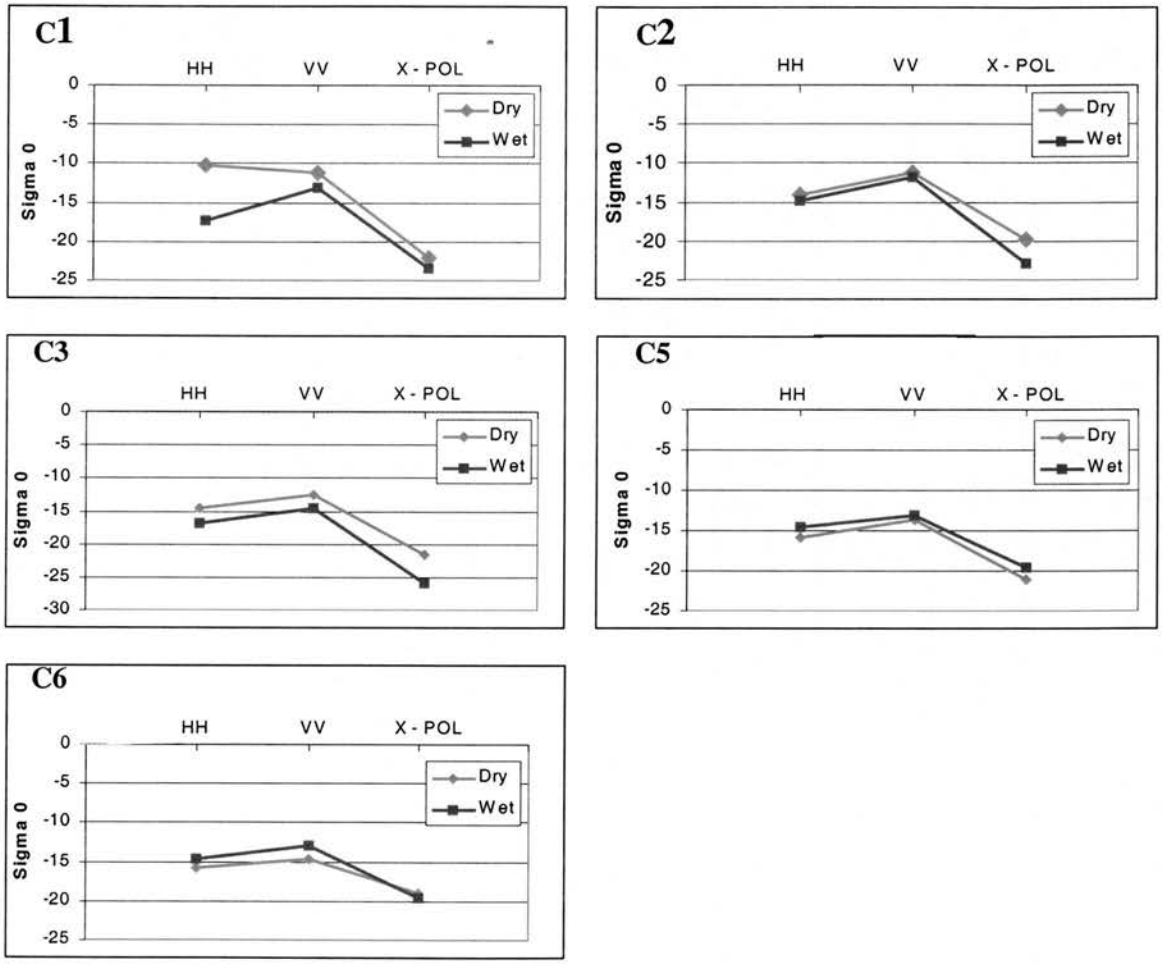

Figure 3.5.1. Polarimetric response of leak (blue line) and non leak (pink line) for each of the Cheshire sites. Values are taken from the ESAR image data.

It can be seen from the other graphs (b-e), that there is little difference between the wet and dry measurements, due to all ground surfaces being saturated at the time of acquisition. All the backscatter measurements are characteristic of leak (or wet) conditions with the VV spike. At sites C2 and C3 the 'dry' measurements at least have a greater backscatter response than the wet measurements which is expected due to differences in dielectric properties. However, this is not enough to successfully identify the leak. For sites C5 and C6 the dry measurements are lower than the wet measurements. With site C5 this is likely to be due to pixel heterogeneity. The leak at C5 was simulated rather unsuccessfully in that there was little difference between where the hose pipe was left running and anywhere else in the field, such was the volume of water. Therefore any site that was chosen in the field was as likely to be as wet as any other part of the field and the differences were sample point specific. At site C6 it is suggested that the wet backscatter measurements were greater than the dry measurements because the vegetation in the leak was more vigorous than the surrounding vegetation increasing volume scattering. So, despite the presence of water, the increased biomass effectively cancels-out the water effect, or masks the presence of water beneath the vegetation canopy.

References

Ulaby, F. T., Moore, R. K. and Fung, A. K. 1986. Microwave Remote Sensing: active and passive, Volume III, From theory to applications. Edited by F. T. Ulaby, published by Artech House, MA.

3.6 Radar analysis

3.6.1 Radar leak index

Due to the adverse weather conditions and soil saturation problems at the time of the radar image acquisition the calculation of microwave leak indices were limited to the modelled output. The modelled radar leak indices generated a great deal less output than the optical modelling, limiting the need for complex comparative surfaces. A simple ratio of leak (waterlogged scenario) against non leak (dry surrounding vegetation) was calculated. Only the HH and VV polarisations were used in this analysis as they were considered to be the most appropriate for identifying presence of water. The direct backscatter values (σ^0) calculated by the model for each polarisation (HH and VV) are measured in decibels which operate on a log scale. Therefore, the ratio can be calculated by simply considering the difference between the two values. The graphs presented in this chapter show the HH:VV ratios of dry (orange columns) and wet (blue columns) calculated for each modelled crop at all growth stages.

The advantage of using a model was that it allowed the extension of the range of measurements, and provided an opportunity to consider the impact of different wavelengths for leak identification. The model was run, and the ratios estimated for a range of microwave wavelengths in order to determine which might be the most appropriate for identifying leaks. Results for L-band, C-band and P-band ratios are presented in this chapter. The leak scenarios used were the ponding and waterlogged scenarios as these were the most frequently encountered in the field. They represent the most extreme leak scenario (waterlogged) and also an example of a recent leak (ponding scenario). While the ponding scenario was not the least extreme leak scenario (the wet soil scenario was), the results in chapter 3.4 indicated that for the wet scenario,

differences between leak and surrounding vegetation were indistinguishable from the dry scenario for all crops and at nearly all growth stages.

3.6.2 C-band

3.6.2.1 Waterlogged scenario

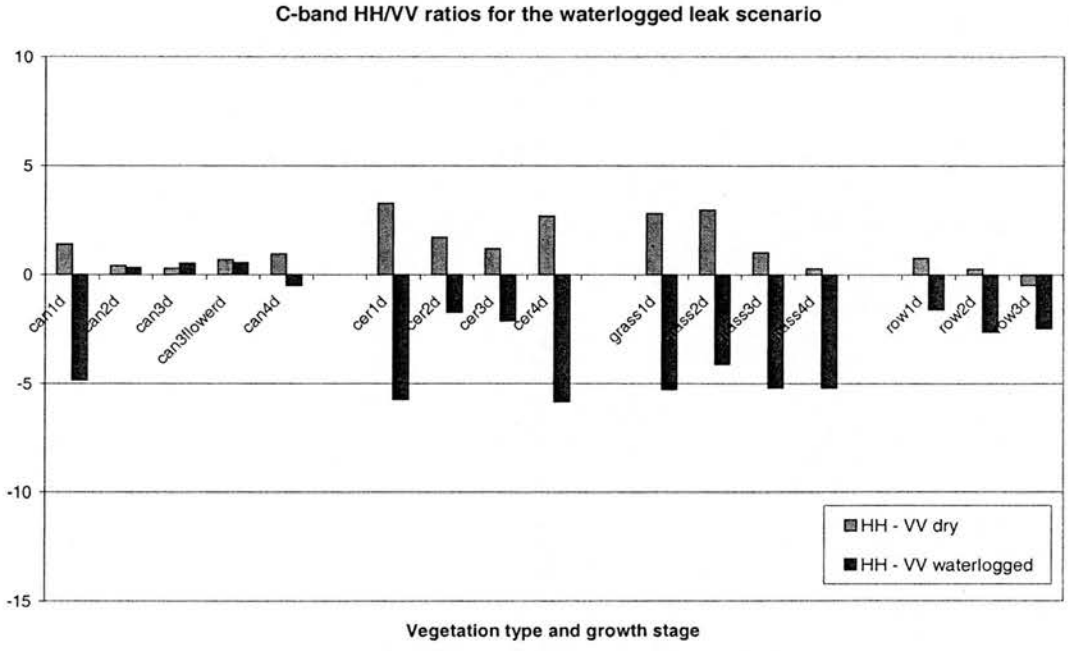

Figure 3.6.1. Comparison of C-band polarisation ratios for a variety of crop types at different growth stages using dry and waterlogged values.

With C-band responses it is possible distinguish the dry from waterlogged scenarios using HH:VV ratios, except those for the canopy crop at the growth stages 2 – 4 (Figure 3.6.1). Despite the waterlogged vegetation being depleted, it is suggested that the vegetation is still sufficiently dense to prevent the shorter wavelengths in this band from penetrating the waterlogged vegetation canopies. Generally, C-band responses are lower in overall magnitude than L-band responses by approximately 7dB, on average.

3.6.2.2 Ponding scenario

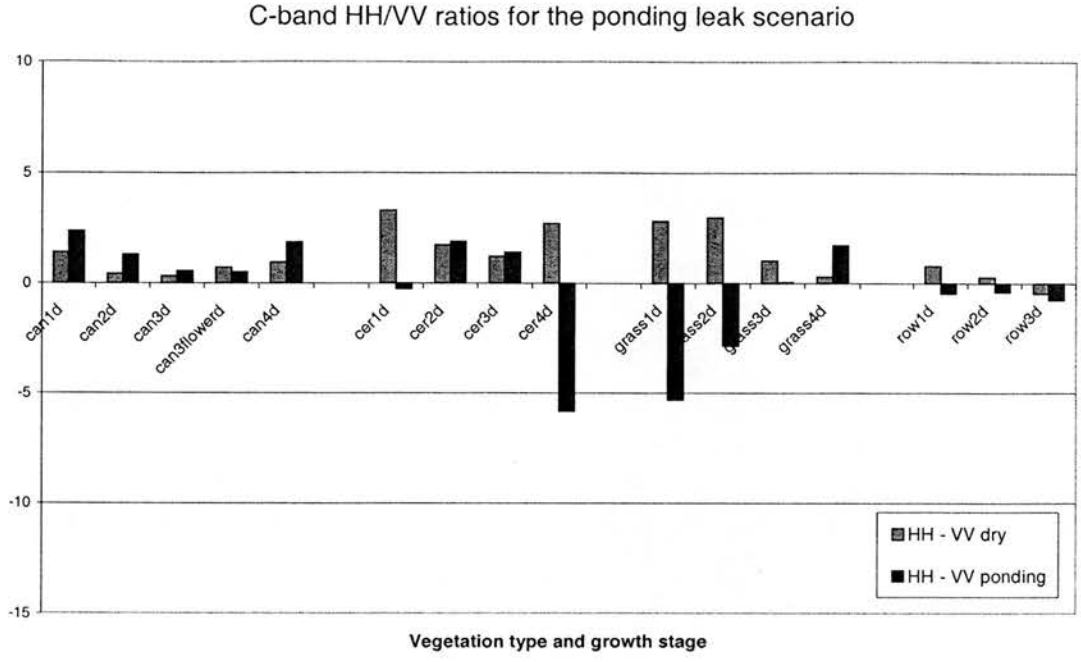

Figure 3.6.2.. C-band polarisation ratios for a variety of crop types at different growth stages using dry and ponding values.

At shorter wavelengths the microwaves are less able to penetrate the vegetation layers except for the more vertically orientated vegetation at the earliest growth stages and for the modelled row crop. In the ponding scenario (Figure 3.6.2) where there is no negative effect on vegetation the responses for all canopy types and growth stages are typical of volume scattering from vegetation. The standing water is effectively 'hidden' beneath the vegetation.

3.6.3 L-band

3.6.3.1 Waterlogged scenario

Figure 3.6.3 shows that for the modelled L-band ratios, comparing waterlogged and dry scenarios, it would be possible to identify leaks at all growth stages – with the waterlogged ratios characterised by negative values, while the dry ratios are positive for all measurements.

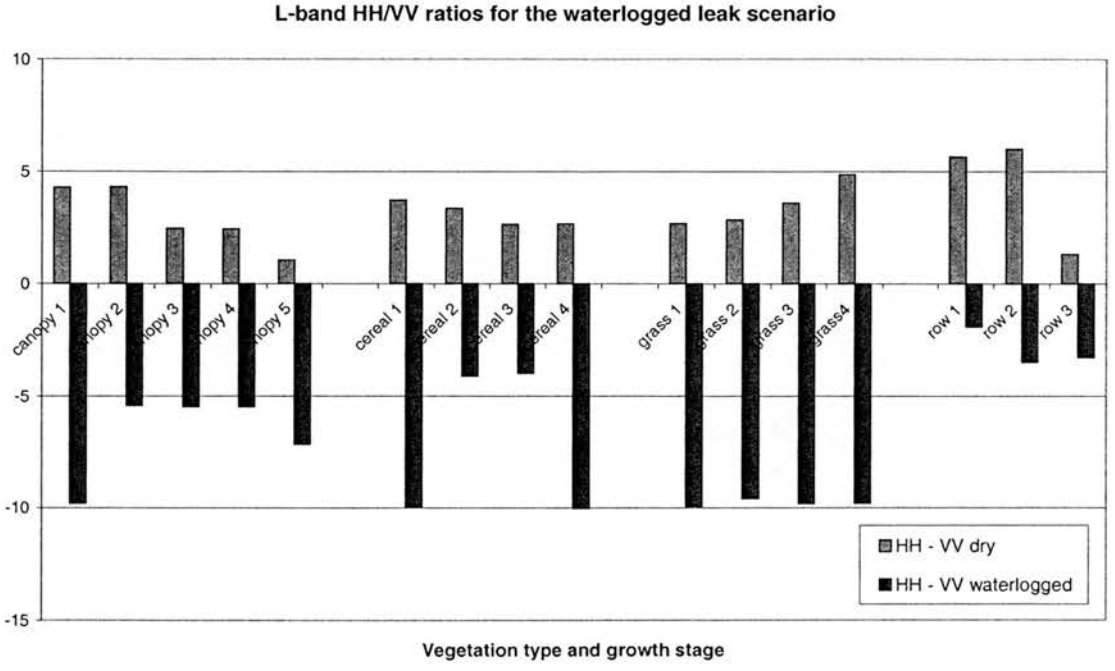

Figure 3.6.3 L-band polarisation ratios for a variety of crop types at different growth stages using dry and waterlogged values.

3.6.3.2 Ponding scenario

With regard to the ponding measurements (Figure 3.6.4) – it would be possible to identify leaks at the majority of growth stages. However, the identification index is not successful for tall, dense canopies i.e. canopy crop at later growth stages (excluding growth stage 5), and the cereal crop at growth stages 2 and 3, or canopies with large, more horizontally orientated leaves e.g. the modelled row crop at the maximum growth stages. It may be possible to identify the presence of standing water behind vegetation at later growth stages where the HH and VV produce similar responses.

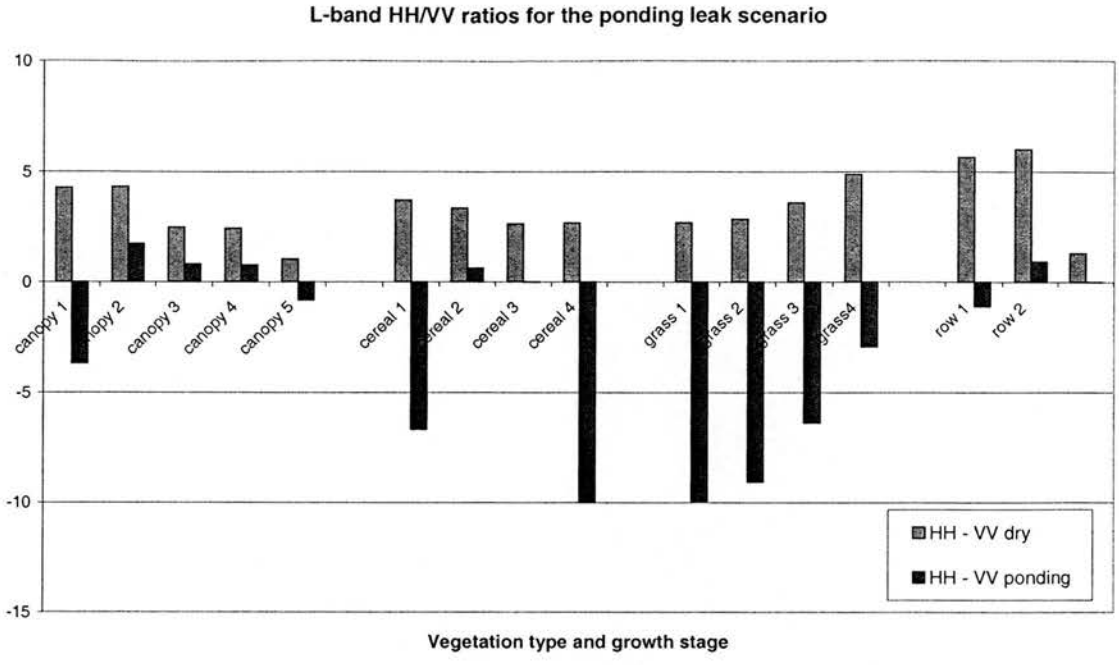

Figure 3.6.4. A comparison of L-band polarisation ratios for a variety of crop types at different growth stages using dry and ponding values.

3.6.4 P-band

The P-band HH and VV polarisation responses lower than 50 σ^0 that were omitted from the P-band results (section 3.4.6) have not been analysed here as they were outside the meaningful microwave backscatter range for imaging radars. The omissions mainly relate to the waterlogged scenario, and where vegetation density was low for the ponding scenario, in these cases the crop and growth stages are shown on the graphs but the values are not plotted.

3.6.4.1 Waterlogged scenario

For the P-band ratios in figure 3.6.5 it is only possible to distinguish the waterlogged scenario (in terms of negative values) where there is a distinct contrast between dense vegetation (i.e. canopy and cereal crops at later growth stages), and the depleted in-leak vegetation. At the early growth stages of these modelled crops and for the lower level and less dense canopies (grass and

row crops) the ratio values for the waterlogged scenario are greater than the dry values. It is suggested that the longer P-band wavelengths are better able to penetrate the lower level and less dense canopies, thus minimising the vegetation effect and reducing the contrast between wet and dry conditions. The P-band responses were overall lower in magnitude than L-band and C-band responses.

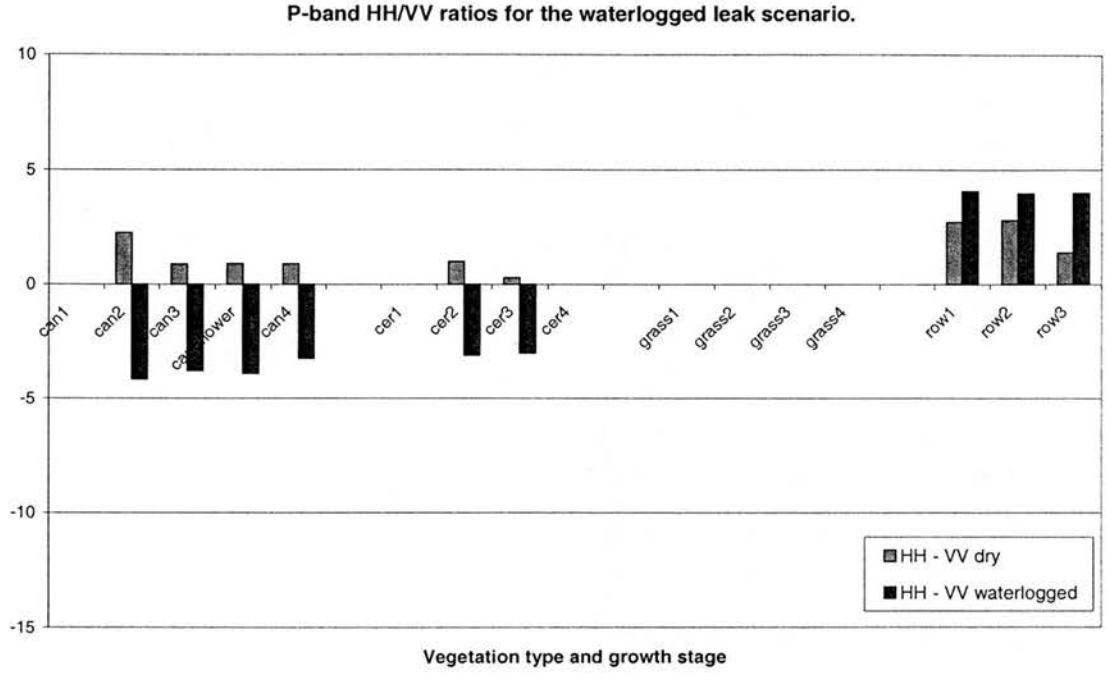

Figure 3.6.5. P-band polarisation ratios for a variety of crop types at different growth stages using dry and waterlogged values.

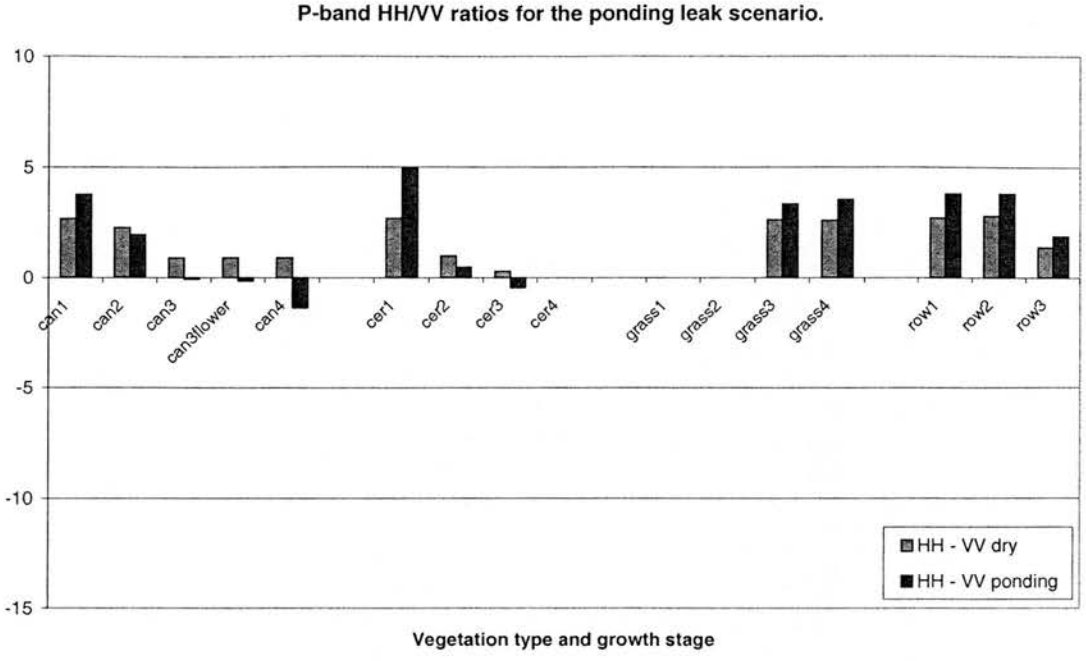

Figure 3.6.6.. P-band polarisation ratios for a variety of crop types at different growth stages using dry and ponding values.

3.6.4.2 Ponding scenario

With the ratios in figure 3.6.6 there is less contrast between wet (ponding) and dry scenarios compared with the waterlogged scenarios, except at the later canopy and cereal crop growth stages. Here there are some interactions between the microwaves and the vegetation resulting in greater volume scattering and thus more contrast between wet and dry. However the ratio values are lower than for the waterlogged scenarios. At the earlier growth stages the vegetation is transparent to the P-band wavelengths.

3.6.5 Implications for leak detection

These results suggest that leaks can be distinguished from surrounding vegetation for modelled radar data where the ratio of wet HH responses to VV responses are less than zero and dry HH to VV responses are greater than zero.

3.6.6 Summary

- Of the two scenarios the waterlogged scenario is effective at identifying leaks under a wider variety of wavelengths, crops and growth stages than the ponding scenario.
- L-band provides the optimal wavelength for identifying water leaks under both ponding and waterlogged leak scenarios.
- Within the L-band modelling, the waterlogged scenario provides the best opportunity for identifying leaks however, with the ponding scenario it is possible to identify leaks in nine out of sixteen cases – generally when vegetation density and/or height is low.
- P-band is the least successful wavelength for identifying water beneath a range of vegetation types and growth stages. There is too little contrast between surrounding vegetation and leak to enable successful identification, except at the maximum growth stages of cereal and canopy crops. This is due to low signal to noise problems, increased penetration depths at longer wavelengths and reductions in canopy interactions.
- For the waterlogged scenario C-band is successful at identifying leaks at all but the most dense vegetation growth stages. It is also possible to identify leaks in seven out of sixteen cases for the ponding scenario, typically where vegetation height and/or density is low. However C-band is not as successful as L-band at identifying leaks given the same conditions.
- Leak detection would appear possible where wet HH/VV ratios are less than zero, and dry HH/VV ratios for surrounding vegetation are greater than zero.

3.7 Part three summary

At the beginning of part three the properties of backscatter were described in relation to surface objects with particular reference to soil, water and vegetation. Backscatter responses of microwave polarisations were discussed, with particular attention to interactions with vegetation. A brief summary of microwave vegetation radiative transfer models was also provided.

A suit of ground-based measurements were made around Cheshire on 3rd June 2000 in support of the E-SAR image data acquisition. They were the same as for the optical acquisition, but with two extra sets of measurements which were related to surface roughness. These were stone content and surface correlation length. There were no supporting ground-based microwave data as we had from the spectroradiometer for the optical part of this study. Therefore, there were no Edinburgh-based measurements for the microwave part of the study.

The modelling methodology introduced RT2, a second order radiative transfer model. To allow for comparison of optical and modelled radar the same modelling strategy was used, and where possible the same input values were used. The parametisation of the model was described. Input parameters were based on all acquired field measurements, including Edinburgh field measurements of simulated leaks under oil seed rape and barley canopies at different growth stages.

From the microwave modelling study, polarisation responses for P-, L-, and C-band wavelengths were used to identify differences between leak and surrounding vegetation for a variety of crops at a variety of growth stages. There were various problems associated with the P-band results relating to noise and C-band was unable to penetrate the modelled vegetation canopies sufficiently to identify differences between leak types, except where vegetation density was low

and where waterlogging had had a negative effect on vegetation growth. L-band therefore, appeared to be the most appropriate wavelength for identifying differences between leak types and vegetation.

Due to environmental conditions at the time of microwave image acquisition here was little difference in backscatter between leak and surrounding vegetation. Non-leak backscatter responses were slightly higher than leak responses, but the polarisation responses for leak and non-leak followed a similar pattern where the VV response was greater than both the HH and cross-polarised responses.

The radar analysis highlighted the optimal wavelength and polarisations for identifying different types of leak against a variety of vegetation types and growth stages through calculation of a ratio-based index. The analysis found that L-band proved to be the most appropriate wavelength for identifying leaks, and an HH/VV ratio was the most useful from a leak identification point of view.

4.1 Discussion

4.1.1 Introduction

The aim of this chapter is to consider the original research questions in relation to the work that has been outlined in this thesis to assess the extent to which new understanding on the remote sensing of leaks has been gained. To this end this chapter is divided into four distinct sections. The first section of this chapter discusses the key findings from the optical and microwave field and modelling studies.

In the second section the individual utility and complementarity of multi-wavelength approaches are discussed in relation to optical and microwave modelled output. First, the results from the optical and microwave modelling studies are outlined. This is followed by a comparison of optical and microwave modelled results and a discussion of the relative merits of each for leak identification.

The third section quantifies the differences between leaks and non-leaks that were identified through the optical and microwave leak indices. These indices were used to identify the gross differences between non-leak and a range of leak scenarios, whilst attempting to ignore variations in canopy height and different canopy architectures. Using the optimal wavelength ratios identified from the analyses, this section demonstrates how variations in spectral reflectance and backscatter can be used to highlight leaks on the airborne image data.

The final section explores the implications of this work with regard to optimal times of year and environmental conditions for leak identification. The optimal sensor characteristics for an

operational leak detection system are then addressed. This chapter concludes with a discussion of further work.

4.1.2 Summary of key findings

A considerable body of field work has been completed which involved investigating a combination of real and simulated leaks at nine different sites in England and Scotland. Investigation of the physical characteristics of leaks indicates that they can affect vegetation growth, either through positive or negative growth responses depending on the vegetation type, the size of the leak and how long it has been present. Real leaks provided examples where the presence of water had had both negative and positive effects on vegetation growth. However, for all real leaks the vegetation inside the leak was less dense (although leaf area may have been larger) than the surrounding vegetation. Simulating a leak by wetting the underlying soil did not have any effect on vegetation on the times scales that were used in this study (20 minutes – 12 hours). Results showed that simulating leaks beneath dense canopies had less influence on reflectance and backscatter than simulating leaks beneath vegetation with short and simple canopy structures.

Analysis of the ground-based spectral data, obtained with the GER 3700 spectroradiometer showed that for all reflectance data from real and simulated leaks, the leak reflectance curves were lower than the non-leak reflectance curves. Spectroradiometer spectral comparison maps indicated that there was no adequate single index for identifying water leaks due to the variety of spectral responses between sites, leak types, vegetation types and growth stages. Therefore presence of water was not enough to successfully identify a water leak. There were no ground-based microwave measurements equivalent to those obtained with the spectroradiometer to support the optical data. One possible mechanism by which backscatter responses of wet and dry situations may be systematically and physically explored would be to use the GB-SAR facility at the University of Sheffield.

Results from the optical and microwave modelling studies suggest that optimal conditions for identifying leaks occur when vegetation density is low. This is the case for all types of leak.

Other conditions where leaks are easy to identify are when the leak has been present for long enough to have a negative effect on vegetation, so the vegetation in the leak has died and the surrounding vegetation remains vigorous. One of the most difficult scenarios for locating a leak is where the leak had a positive effect on vegetation growth and the canopy is large and vigorous. This situation relates to the puddle scenario where for later vegetation growth stages, the reflectance and backscatter properties were similar in some cases to the dry scenario. Fortunately this situation rarely occurs in the field as a positive growth response for non-wetland plants to water inundation is limited to a small number of species (Kozlowski, 1984). Another leak that was difficult to identify from the results presented in this thesis, particularly in the microwave domain and where vegetation is dense, is the wet soil scenario. This scenario represents a small and/or recent leak, that may occur over a well drained soil. The leak is manifested as a patch of wet soil.

The leak index analysis for the modelled microwave backscatter highlighted that L-band HH-VV ratios were the most appropriate for identifying leaks in the widest variety of leak types, vegetation types and growth stages. Surface water leak scenarios could be distinguished from the surrounding vegetation where the HH backscatter response changed from being greater than or equal to the VV response, to being markedly lower than the VV response. Results from analysis of the optimal optical leak indices were more varied as they included spectroradiometer, modelled and image results. However, overall an optimal normalised index across the data types and for the widest variety of leaks, vegetation types and growth stages was a visible and middle infrared wavelength combination.

Initial results showed that leaks may be distinguished from surrounding vegetation where:

- vegetation density is high and there is a significant contrast between the vegetation in the leak and the surrounding vegetation. This may occur where a leak has been present for a long time and has had a detrimental effect on vegetation growth.
- vegetation density is low or not present and the leak is easily visible as standing water. This may be when the leak is relatively recent and there has been no change to any vegetation.

Leaks were unidentifiable where:

- When vegetation density is high and a leak develops underneath the canopy. In this situation there is no effect on vegetation and the density of the canopy masks the leak.
- When the presence of water has had a positive effect on vegetation growth such that the vegetation in the leak is greater than that of the surrounding vegetation.

From the point of view of water companies the ability to identify a leak once it has already been present for long enough to have a negative effect on vegetation (from weeks to months) is not ideal. The longer the leak is present, the more of their resource they are losing. The challenge therefore, lies in the ability to identify the more subtle leaks, i.e. those that have occurred more recently and result in saturated soil or standing water beneath a vegetation canopy, and before there has been a negative effect on vegetation, for example, in the ponding scenario. Perhaps some of the most important analyses in this thesis relate to the ponding scenario results as they represent a relatively recent leak where there is no negative effect on vegetation. However, they present challenges to leak identification, particularly where vegetation canopies are dense. But, identification of leaks for this type of scenario would be more useful to the water industry than perhaps a leak index developed from the waterlogged scenario due to the reasons mentioned above. Results from the modelling studies and the optical measurements taken in and around Edinburgh with the spectroradiometer suggest that it is possible to identify recent leaks which are manifest as standing water, but generally only when vegetation density is low. The examples where identification was more difficult related to the crops at maximum growth stages. Leak identification was also difficult where there were large, more horizontally orientated leaves, for example, in the sugar beet canopy. The optical reflectance and microwave backscatter from the canopy layers and scattering elements were large enough to significantly obscure reflections from the ground surface layer. For optical wavelengths it has been demonstrated that with increased leaf area index the contribution from soil effects and the ground surface decreases to zero (Baret, 1991), and that leaf inclination angle has a significant effect on reflectance with increased reflectance from more horizontally orientated canopies (Kimes, 1984).

It would appear therefore, that the dedicated leak index that would best suit the water companies has certain limitations in relation to identification capabilities where vegetation is dense. Results in this study suggest that the problem cannot be solved using multiwavelength approaches. The

resolution of this problem points towards identification of optimal times of year for locating leaks (this is discussed further in section 4.1.5).

4.1.3 Comparing optical and microwave modelled data

The temporal separation and the extreme differences in ground conditions made direct comparison of the two image data sets difficult. Comparison of the optical and microwave data analysis is therefore, limited to the modelled data. The results complement each other and both provide opportunities for identifying water leaks against a variety of land cover types at different growth stages. Table 4.1.1 compares the differences between the optical and radar modelled output. Where possible the same input parameters were used for the optical and microwave modelling studies.

Table 4.1.1. Comparison of microwave and optical modelled data for identifying leaks. The ticks indicate where leaks can be clearly identified using the leak indices developed in chapters 2.7 and 3.6. The crosses represent situations where it has not been possible to identify the leaks from the modelled output. Question marks represent where leak identification may be possible but the leak index values are low.

	MICROWAVE				OPTICAL			
	Wet	Pond	Puddle	Water-logged	Wet	Pond	Puddle	Water-logged
Canopy 1	×	✓	✓	✓	✓	✓	✓	✓
Canopy 2	×	×	×	✓	×	✓	×	✓
Canopy 3	×	×	×	✓	×	×	×	✓
Canopy 4	×	×	×	✓	-	-	-	-
Canopy 5	?	✓	×	✓	×	✓	×	✓
Cereal 1	×	✓	✓	✓	✓	✓	✓	✓
Cereal 2	×	?	?	✓	?	✓	✓	✓

Cereal 3	×	?	?	✓	?	✓	✓	✓
Cereal 4	×	✓	✓	✓	✓	✓	✓	✓
Grass 1	×	✓	✓	✓	✓	✓	✓	✓
Grass 2	×	✓	✓	✓	✓	✓	✓	✓
Grass 3	×	✓	✓	✓	×	×	×	✓
Grass 4	×	✓	✓	✓	×	×	×	✓
Row 1	×	✓	×	✓	✓	✓	✓	✓
Row 2	×	×	×	✓	×	×	×	✓
Row 3	×	?	×	✓	×	✓	×	✓

The results of the modelling suggest that in the first instance optical wavelengths are better suited to leak identification than microwave wavelengths. The optical index performs better where vegetation canopies were vertically orientated. This may be due to effects of incidence angle as the optical model assumes a nadir view and incidence angle has been shown to affect reflectance (Norman *et al.*, 1985). The index performs least well for a dense canopy crop at later growth stages, with more horizontally orientated leaves. The microwave modelling that produced the greatest variation between leak and surrounding vegetation was the grass canopy. There were a greater number of positive leak index values for the dry scenarios, and negative leak index values for the leak scenarios than for other crops making leak identification easier (refer to chapter 3.6). This suggests that the microwave wavelength polarisation ratios used in this study are suited to identifying leaks behind vertically orientated canopies with simple structures. A sensitivity analysis of microwaves to soil moisture beneath grass canopies by Wang *et al.* (1989) supports these results by showing that retrieval of soil moisture information is more accurate for wet soils against burned grass canopies (i.e. shorter canopies), than unburned grass.

RT2 performs less well for the canopy crop for similar reasons of canopy structure and density as those applying to the optical model.

The greatest difference between the optical and microwave model results was for the wet soil scenario – despite its sensitivity to changes in dielectric constant, the RT2 model was unable to distinguish between the wet soil and the dry scenario for any crop at any growth stage. The combined SAIL and PROSPECT model was able to identify the wet soil scenario at the earliest growth stages for all crop types and for all cereal crop growth stages. This was supported by field measurements taken with the spectroradiometer around Edinburgh where leaks were simulated to achieve soil saturation. Differences between simulated leak and non-leak were evident in the measured reflectances. Optical wavelengths have also been shown to be effective at identifying contributions from the soil layer beneath vegetation canopies using simple spectral analysis in studies performed by Tucker and Miller (1977); Richardson and Wiegland (1977).

The radar analysis performed in this study is simple, using a ratio comparison between the HH and VV polarisations. While this is sufficient to identify a range of different leaks against a variety of crop types at different growth stages, more comprehensive analysis of polarimetric coherence data or polarimetric decomposition techniques would better highlight the changes in dielectric constant between wet and dry soil scenarios. This has been demonstrated by Cloude and Pottier, 1996; Cloude and Papathanassiou, 1998, and Papathanassio *et al.*, 1999. Development and use of such techniques are still relatively recent and are beyond the scope of this study.

Both the optical and microwave models failed to identify leaks behind tall, dense canopies, for example a modelled continuous canopy crop at maximum growth stages. Longer wavelengths may provide the answer to this problem by being better able to penetrate vegetation canopies, particularly in the microwave domain. However, P-band modelled results for dense canopies appeared to suffer from the same problem as L-band modelled results in that the total backscatter measurements were made-up of different scattering contributions between dry and surface water scenarios. Therefore, from only considering total backscatter it was not possible to identify leaks in a dense canopy. A further problem with P-band is that overall backscatter is low compared to

shorter microwave wavelengths; at backscatter values below –50 dB, the signal to noise ratio is low enough to render any signal uninterpretable. P-band wavelengths are unable to penetrate the ionosphere so a spaceborne imaging radar operating in P-band is unlikely.

In this study the optical sensors had certain advantages over the microwave sensor in relation to spatial resolution and there were fewer problems associated with noise. With the microwave data spatial resolution was lost through speckle reduction and noise interfered with P-band modelled results. However, microwave remote sensing enables data capture under a wider range of atmospheric conditions (not always advantageously) than optical remote sensing and with its sensitivity to variations in dielectric properties modelled results have shown the potential for leak detection using microwave remote sensing.

4.1.4 Interpretation of results

This general discussion now aims to explore the remaining three objectives of this thesis by putting the theoretical modelling and empirical remote sensing into the wider context of leak identification from the acquired imagery. Leak indices were used to identify the gross differences between non-leak and different leak scenarios, whilst attempting to ignore variations in canopy height and different canopy architectures. Through quantifying these differences, the identified optimal indices for the optical and microwave domains have been applied to highlight variations in spectral reflectance, and backscatter on the airborne image data, where the size of each leak was limited to a few pixels in an entire image containing much more detailed information.

4.1.4.1 Optical data analysis

Using pixel sampling for leak and non-leak regions of the image data to create spectral reflectance graphs, resulted in positive identification of all leaks (section 2.7.5). However, some were more easily identified than others, for example leak C6 was more difficult to detect than the others, due to the positive effect of the leak on vegetation growth. The vegetation in leak C6 was more vigorous and dense than the surrounding vegetation. The optimal wavebands for leak

identification for all sites on the image data, apart from C1 were a combination of visible and middle infrared wavelengths and also NIR. The optimal wavelengths for identifying the leak at site C1 was a near and middle infrared wavelength combination, but this was an atypical leak. Had there been water present at the site at the time of acquisition it would probably have been the most prominent leak as it was possible to locate the leak on the image, even without there being water present. There was significant contrast between the tall wheat canopy and the low vegetation and bare soil where the leak had been. The easiest leak to identify was at site C2, where there was maximum contrast between leak and surrounding vegetation. The surrounding vegetation was short grass and the leak was large with little vegetation inside the leak. From the results presented in chapter 2.7 it is shown that where the variances between leak and non-leak are great, the leak is easily identifiable (e.g. sites C2 and C3). However where the variances are small e.g. leak C5 the leaks become almost impossible to identify.

By considering the problem of leak identification from a different perspective, and considering whether it is possible to establish and identify leaks along a pipeline in the context of an entire image data set, a step is taken closer towards an operational leak detection tool. Rather than selecting known leak and non leak pixels and comparing them as we have done up to now, the information gained from the analysis of the spectral surfaces and ratios, was applied to the image data to see whether leaks are distinguishable from the surrounding vegetation in the context of the whole image. These results are presented in Figure 4.1.1.

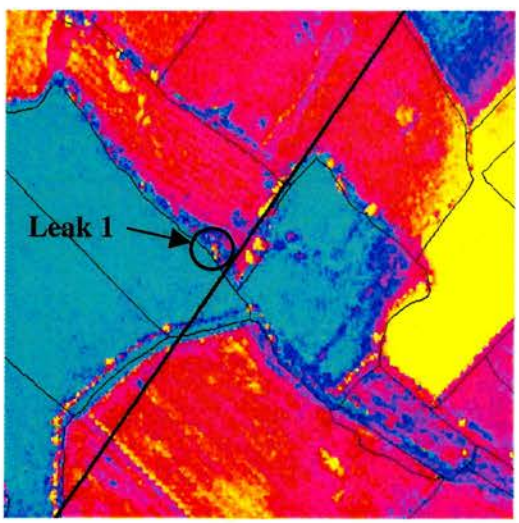

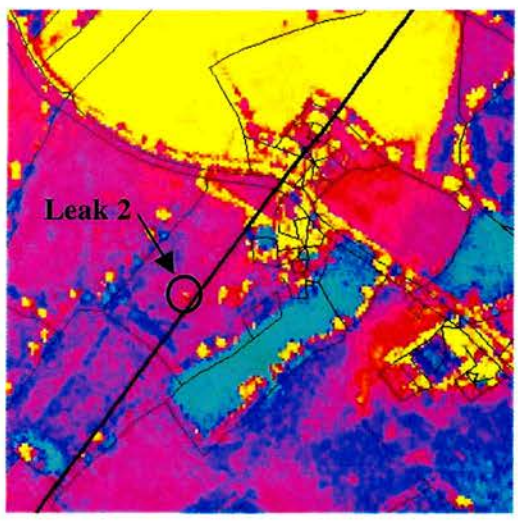

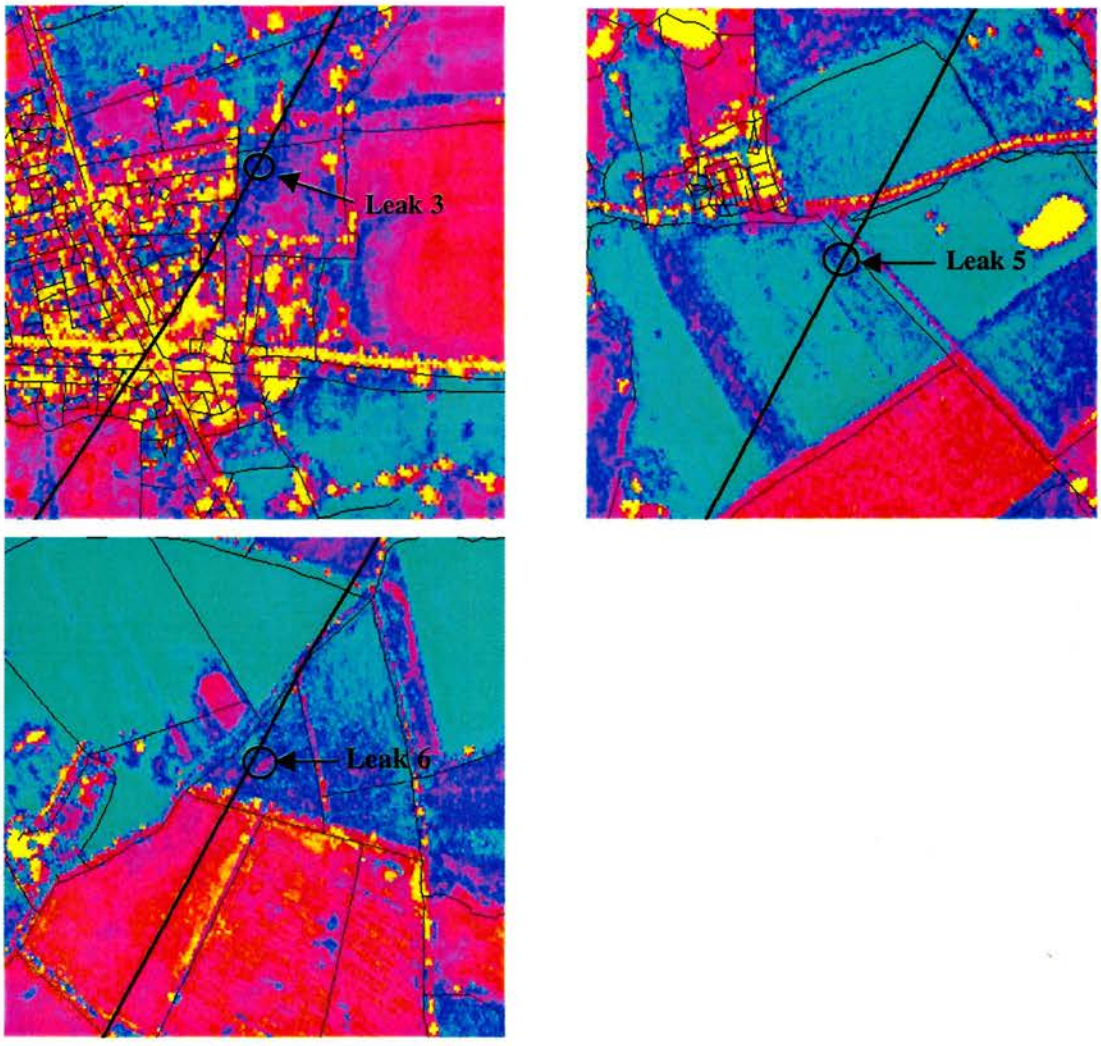

Figure 4.1.1. Images of leak sites viewed using a normalised difference leak index of 676 and 2206 nm (thin black lines are field boundaries, the thick black line is the path of the aqueduct).

Using the red and middle infrared wavelength combination shown in Figure 4.1.1 it is possible to clearly identify leaks C1, and C2. It was not possible to identify leak 5 due to the nature of the simulated leak – surface ponding through leak simulation was not achieved as the soil was too well-drained. The leak at site 3 was identifiable but it was more difficult to observe than expected given that it was a large and distinct leak in the field. However, the optimal wavelengths identified in the spectral comparison map (Figure 2.7.11) taken from the HYMAP imagery for this leak produced a red and a shorter infra red wavelength combination (around 1160 nm). It is suggested that leak 6 was difficult to identify due to the small differences in

reflectance between the leak and surrounding vegetation. These results suggest that there is no single leak index that could be used to identify all the Cheshire leaks from the imagery that was obtained. However, the available data are limited to 4 real leaks, this is not a sufficient number on which to judge the technique. Modelling results are certainly more consistent across a range of vegetation types and they support a visible and middle infrared wavelength combination for optimal leak identification particularly where there has been negative effects on vegetation growth. Where vegetation has not been negatively affected the optical modeling results (section 2.7.4) suggest that a visible/near infrared or near and middle infrared wavelength combinations may also be applicable.

In the results presented above a new problem is encountered – one pertaining to heterogeneity. Agricultural crop fields are typically regarded as homogenous relative to other landcover types. However, Figure 4.1.1 shows there is significant variation across individual fields. When field heterogeneity is high, leak identification becomes more difficult. The worst case scenario applies to leak C6 where in-field heterogeneity is high and leak index is low. When leak indices are high, heterogeneity becomes less significant.

4.1.4.2 Identifying leaks using radar data analysis

It would appear that in order to identify leaks in the active microwave domain surface scattering from standing water beneath the vegetation canopy is required, compared with situations where there is no standing water beneath the vegetation canopy. This requires that canopy penetration depth is high relative to wavelength.

It was not possible to identify any of the leaks on the E-SAR imagery using the HH-VV ratio combination. Figure 4.1.2 shows two leak sites, they were chosen as examples because they were where the largest leaks at the time of the E-SAR acquisition were found. The reason for the lack of success at leak identification from the microwave imagery is likely to be due to the degradation of spatial resolution to 9m through speckle reduction, as well as the saturated conditions. However, for the sites where the vegetation inside the leak was less than the surrounding vegetation, backscatter values were lower. This is a typical result as forward

scattering results from microwave interactions with the water surface (Saich, 1999). However, this was not enough to distinguish between leaks and surrounding vegetation in this case.

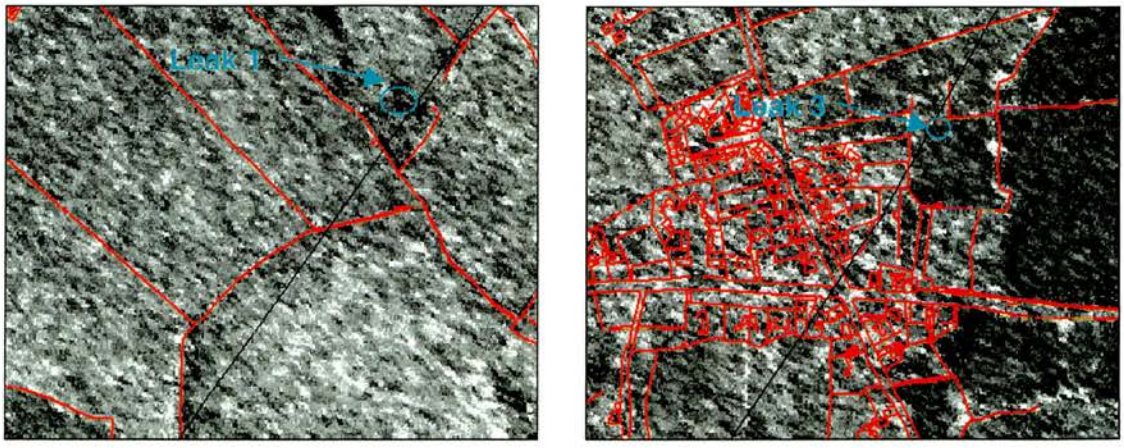

Figure 4.1.2. E-SAR image data - HH-VV ratio combination. The red lines are field boundaries and the black line shows the path of the aqueduct.

4.1.5 Optimal times of year for leak identification

The results from the modelling studies suggest that optimal conditions for identifying leaks are when vegetation density is low. It also highlights the fact that different vegetation canopy structures affect reflectance and backscatter, thus impacting on leak identification. These findings lead to implications in terms of identifying optimal times of the year in which to carry out leak surveys. The results would suggest that early in the growing season or post harvest/cutting would be the most appropriate times of the year to acquire remotely sensed data to identify water leaks from pipelines. This equates to the months of August to October, and January to March; however, these might not be most appropriate times of year from the point of view of cloud cover (where optical image acquisition is required).

Perhaps the most important factor in determining frequency of acquisition of suitable optical data for leak detection within the United Kingdom is the amount and persistence of cloud cover. Frequent cloud-free data over the areas of interest are required. Cloud cover in the UK is

Frequent cloud-free data over the areas of interest are required. Cloud cover in the UK is dominated by a procession of eastward moving depressions and orthogenic cloud with passing cycles measured in days (Slater et al. 1999).

One of the most extensive studies of the ability to acquire cloud-free imagery over Britain was that performed by Legg (1988, 1991) who investigated the ability to acquire cloud free Landsat MSS coverage over a number of target sites throughout the UK, using image data archived over an 11 year period (1976 – 1986). Generally the ability to acquire cloud free images varied considerably from year to year, largely dictated by the differences in weather year on year. Legg's studies showed that the best periods of image acquisition were mid April to the end of May, Early July and Mid August to Mid September. The December/January period represented the worst period. His study further highlighted the significant regional variation in clear view acquisition with cloud cover increasing the further north and west and over upland areas; southern lowland sites have the highest probability for cloud-free acquisition. Similar conclusions were drawn by Fuller *et al.* (1994) from their experience of acquiring seasonal Landsat TM images for the first Land Cover Map of Great Britain. Legg (1991) concluded that the chances of acquisition of data on an annual basis are good (with only about one Landsat pass in six resulting in cloud free data), but obtaining repetitive coverage over specific sites in any single year is difficult and variable. At the frequency of coverage of a single Landsat platform (18 days) he concluded that applications requiring frequent imagery within specific time intervals are impractical in the UK. However, using the case of both Landsat 4 and 5 platforms which operated simultaneously for two years, he further showed that when there are more sensors from which to select data the chances of acquiring cloud free imagery are significantly increased.

He concluded that a total of four Landsat-type sensors operating simultaneously would image most parts of the UK every two days. Coverage is also roughly doubled if land areas of interest are located in the overlap zone between adjacent satellite paths. Pointability - the capability of some sensors to be pointed off-nadir into neighbouring paths (e.g. SPOT, IKONOS) further increases the probability of clear data acquisition but only if they are controlled in real time and are programmed to preferentially image cloud free areas. Thus, to meet the requirements for leak

detection, a leak detection system may need to take advantage of a number of different sensors in order to increase the chance of acquisition of cloud free data over the area of interest.

There are also issues of optimal time of year with regard to soil saturation with prolonged periods of persistent rain inhibiting leak identification. An ideal scenario would be cloud free and after a period of a week with no rain. Soil moisture deficit data calculated from meteorological measurements may provide a useful tool for determining when it might be appropriate to acquire imagery (Pickerill and Malthus, 1998).

From the microwave perspective, while cloud cover is not a problem the same issues of soil saturation and time of year apply to the radar data as to the optical measurements. A further time of year to avoid may be during crop emergence – studies by Saich (1999) and van Leeuwen and Huete (1996) demonstrate that in-field heterogeneity has been found to be particularly high at these times. This is problematic in terms of detecting leaks from imagery and makes identification more difficult. Further work would need to be done before considering whether heterogeneity is offset by the more visible presence of water against a low vegetation canopy.

4.1.6 Towards satellite coverage

4.1.6.1 Optical sensors

There are a wide range of current and future optical satellite data available which largely can be separated into three main groups:

- Moderate to coarse resolution (~ 200 m to 1 km pixel resolution), high temporal frequency sensors used for global scale observations of land and oceans (e.g. AVHRR, ATSR-2, SeaWiFs, MODIS, MERIS, SPOT-4 VI)
- Moderate resolution sensors used for regional scale mapping of terrestrial and coastal processes (e.g. Landsat 7, SPOT-4)
- High spatial resolution sensors used for local scale observation (e.g. IKONOS, QuickBird2).

On the basis of the characteristics deemed desirable for a leak detection system only those which fall into the latter category could be regarded as suitable. Thus, there are only three instruments currently in space which may meet required characteristics in terms of spatial resolution. These are:

- IKONOS – 4 m spatial resolution multispectral in four bands, 1 m spatial resolution panchromatic.
- QuickBird2 – 2.6 m spatial resolution multispectral in four bands, 0.6 m spatial resolution panchromatic.
- EROS.1A – 1.8 m spatial resolution panchromatic.

A number of other sensors will also soon be available to expand this availability over the next few years. These are:

- OrbView3 - due for launch in 2002, 4 m resolution multispectral in four bands, 1 m resolution panchromatic.
- EROS.B1 - due for launch in late 2003, 0.82 m resolution panchromatic.
- Pan 2 on SPOT 5 - due for launch in April 2002, 2.5 and 5 m panchromatic

Of these present and future sensors it can be seen that of those offering multispectral capabilities, none have the capability to measure in the middle infrared. Of the panchromatic-only sensors, whilst offering very high spatial resolution, their utility for leak detection may be limited on the basis of only being able to detect a leak on the basis of broad differences in the brightness of a leak compared to its surrounding area.

Thus, spectral limitations in the middle infrared notwithstanding, it would appear that there are appropriate space-borne sensors worthy of further investigation for their capabilities to detect water leaks. If middle infrared wavelengths were to be required then the only space-borne sensors offering these are, or will be, at the order of 10s of metres spatial resolution.

The only other alternative to space-borne optical data is the continued use of airborne sensors, a number of which are currently available (e.g. CASI, HYDICE, HYMAP, AISA). Airborne

sensors carry a number of advantages over satellites in that spatial resolution can be tailored and is determined by the altitude of the aircraft, they are ideally suited to acquiring coverage of linear features such as aqueducts, and they can be deployed at relatively short notice to take advantage of favourable weather conditions. However, images from airborne sensors will likely be necessarily more expensive to acquire.

4.1.6.2 Radar sensors

The data supplied by existing spaceborne SAR imagers is limited for its use in leak detection by a number of factors. The most successful sensors to date, namely ERS-1/2 and RadarSat, can only detect in C band and in single polarization mode (VV and HH, respectively). Ground resolution is also poor with the best resolution available being 10 m on RadarSat. Temporal frequency is adequate given few limitations associated with the presence of clouds in the atmosphere.

Three future sensors are currently under development and offer promise for leakage detection these are RadarSat-2, offering 3 m resolution in fine beam mode albeit in C band single polarization only. ALOS-Palsar, due for launch in summer 2002 which will be L-band multipolarimetric potentially at 10 m resolution. TerraSAR, developed by ESA but not due for launch until 2005, which will also offer L band multipolarimetric data reportedly at a lowest achievable resolution of 1m. All will provide relatively high temporal frequency of potential coverage.

A number of Space Shuttle radar missions have been flown and it is the multi-waveband, multipolarimetric datasets (particularly the SIR-C datasets) that these have provided which has really led to the development of algorithms and for a wide range of applications, including the detection of soil moisture. However, Shuttle data are only of historical interest and no plans for any new Shuttle SAR missions are currently in development. A number of airborne SAR sensors are available, some of which are located in Europe (e.g. E-SAR, Do-SAR, EMISAR, Pharus). Similar to Shuttle missions, these instruments have largely been developed as prototypes for future satellite missions. As with airborne optical data, acquisition of airborne SAR data can be expensive compared to satellite products.

4.1.7 Further work

This work has identified a need for further testing using image data obtained at altitude (air or space-borne). It also recognises that there were few examples of real leaks and that greater coverage is required to obtain more experience with a range of leak types. It must also be acknowledged that the E-SAR data taken under less than ideal conditions. The microwave results ideally need to be tested with radar data obtained under conditions more favourable for leak detection.

In this study it has not been possible to answer the question 'how long does a leak have to be present before it has a negative effect on vegetation?' The literature gives an indication that standing water can have a negative impact on vegetation within minutes and lasting until the vegetation dies or is colonised by a new, more water tolerant species. However, studies on wheat showed that after 25 days of flooding there was an 83% decrease in leaf area (Trought and Drew, 1980), which is comparable to the waterlogged scenario. Jackson and Drew (1984) suggest that growth of tomato, potato and sunflower may be retarded within 2 days, and after 48 hours of flooding, the orientation of tomato plant leaves changes by 50° due to epinasty- giving the appearance of drooping. Much of the research that has been carried out in this field is approached from a biological perspective, in terms of physiological effects of inundation on vegetation. However it would be both interesting and feasible to conduct prolonged leak simulation experiments on a variety of vegetation types over time using remote sensing tools to monitor changes to vegetation.

Problems in finding enough real leaks to study is the nature of such research when leaks are sporadic, transitory and unpredictable. Ideally more leaks are required. Simulating leaks did not fully replicate those real leaks found making them of value, but of limited value. More extensive studies might locate a greater number of real leaks to investigate under a wider range of land cover conditions and seasons - and simulation might involve more extensive/longer periods of wetting (i.e. days), so more accurately simulating the actual leak conditions observed during this study.

A further analysis of wavelengths that would complete the suite of wavebands would include analysis of thermal imagery. Some leak surveys have already used thermal imagery for leak identification with some success (Barrett and Curtis, 1992). However, thermal imagery was not available for this study and analysis of thermal imaging results was beyond the scope of this study.

The work presented here is instrumental to the development of an automated leak detection system that could ultimately be available to water companies. This was always beyond the scope of the current project although, the work presented here provides a sound basis for the technique and is a vital step in the development towards such a tool.

This work shows the capability of optical and microwave data to locate water leaks against a variety of different vegetation types at various growth stages under certain conditions. There is overlap between the two techniques in where they perform well at identifying leaks however, there also appears to be situations where radar is better and those where optical wavelengths are better for leak identification. This presents a case for combining these data to provide a more comprehensive leak index in the future using synergistic techniques.

References

Baret, F. 1991. Vegetation canopy reflectance factors of variation and application for agriculture. In Remote Sensing and Geographical Information Systems for Resource Management in Developing Countries. Edited by A.S. Belward and C.R. Valenzuela. Published by Dordrecht ; London : Kluwer.

Barrett, E. C. and Curtis, L. F. 1992. Introduction to environmental remote sensing. Published by Chapman and Hall, London.

Bowers, S. S. and Hanks, R. J. 1965. Reflection of radiant energy from soils. *Soil Science*, **100**, 130-138.

Cloude, S. R. and Papathanassiou, K. P. 1998. Polarimetric SAR interferometry. IEEE Transactions on Geoscience and Remote Sensing, **36(5)**, 1551-1565.

Cloude, S.R. and Pottier, E. 1996. A review of target decomposition theorums in radar polarimetry. IEEE Transactions on Geoscience and Remote Sensing, **34(2)**, 498-518.

Fuller, R.M., Groom, G. B. and Wallis, S. M. 1994. The availability of LandsatTM images of Great Britain. International Journal of Remote Sensing, **15(6),** 1357-1362.

Jackson, M. B. and Drew, M. C. 1984. Effects of flooding on growth and metabolism of herbaceous plants. In Flooding and Plant Growth, 47-128. Edited by T. T. Kozlowski, Academic Press Inc. London.

Kimes, D. S. 1984. Modelling the directional reflectance from complete homogeneous vegetation canopies with various leaf-orientation distributions. Journal of the Optical Society of America, **1**, 725-737.

Kozlowski, T. T. 1984. Responses of woody plants to flooding. In Flooding and Plant Growth, 129-163. Edited by T. T. Kozlowski, Academic Press Inc. London.

Kriebel, K. T. 1976. On the variability of the reflected radiation field due to differing distributions of the irradiation. Remote Sensing of Environment, **4**, 257-264

Kriebel, K. T. 1978. Average variability of the radiation reflected by vegetated surfaces due to differeing irradiations. *Remote Sensing of Environment*, **7**, 81-83

Legg, A. C. 1991. A review of Landsat MSS image acquisition over the United Kingdom 1976 - 1988, and the implications for operational remote sensing. International Journal of Remote Sensing, **12**, 93 - 106.

Legg, A. C. 1988. Operational Remote Sensing in the United Kingdom: problems of image acquisition. IEEE Geoscience and Remote Sensing Symposium Proceedings. IGARSS'88, Edinburgh, **ESA SP-284**, 13 - 16th Sept 1988, 1457 - 1461.

Norman, J. M., Welles, J. M. and Walter, E. A. 1985. Contrasts among bidirectional reflectances of leaves, canopies and soils. IEEE Transactions on Geoscience and Remote Sensing, **GE-23**, 659-668.

Papathanassiou, K. P., Reigber, A. and Cloude, S. R. 1999. Vegetation and Ground Parameter Estimation using Polarimetric Interferometry, Part II: The Role of Polarisation. Proceedings of CEOS'99, Toulouse, 1999.

Pickerill, J. M. and Malthus, T. J. 1998. Leak detection from rural aqueducts using airborne remote sensing techniques, International Journal of Remote Sensing, **19**, 2427-2433.

Richardson, A. J. and Wiegland, C. L. 1977. Distinguishing vegetation from soil background. Photogrammetric Engineering and Remote Sensing, **43**, 1541-1552.

Saich, P. 1999. Monitoring vegetation dynamics using SAR, ESTEC Working Paper, no. 2048. ESA.

Slater, M. T., Sloggett, D. R., Rees, W. G. and Steel, A. 1999. Potential operational multi-satellite sensor mapping of snow cover in maritime sub-polar regions. International Journal of Remote Sensing, **20**, 3019-3030.

Trought, M. C. T and Drew, M. C. 1980. The development of waterlogging damage in wheat seedlings (*Triticum aestivum* L.). Shoot and root growth in relation to changes in the concentrations of dissolved gases and solutes in the soil solution. Plant Soil, **56**, 77-94.

Tucker C. J. and Miller, L. D. 1977. Contribution to the soil spectra to grass canopy spectral reflectance. Photogrammetric Engineering and Remote Sensing, **43**, 721-726.

van Leeuwen, W. J. D. and Huete, A. R. 1996. Effects of standing litter on biophysical interpretation of plant canopies with spectral indices. Remote Sensing of Environment, **55**, 123-138.

Wang, J. R., Shiue, J. C., Schmugge, T. J. and Engman, E. T. 1989. Mapping surface moisture with L-band radiometric measurements. Remote Sensing of Environment, **27**, 305-312

4.2 Conclusions

4.2.1 Effects of water on vegetation growth

- Leaks can have an effect on vegetation growth, positive effects on vegetation growth or negative effects on vegetation growth depending on the vegetation type, the size of the leak and how long it has been present for.

4.2.2 Identifying leaks - optical domain

- Typically, wet backgrounds or presence of leaks results in a decrease in reflectance across all wavelengths but is particularly noticeable in the near and middle infrared wavelengths

4.2.3 Identifying leaks – microwave domain

- Generally it is the decrease in HH backscatter relative to the VV that provides us with the most information with regard to presence of water.
- For microwave data the presence of a water leak beneath a vegetation canopy is indicated clearly with a spike, where the HH and cross polarisation channels are lower than the VV polarisation under waterlogged conditions and during early vegetation growth stages.
- L - band is the most appropriate microwave wavelength for identifying water leaks.

4.2.4 Optimal vegetation structures for identifying leaks

- Optimal conditions for identifying leaks occur when vegetation density is low. This is the case for all types of leak.

- It is easier to detect water beneath Vertical canopy structures for both optical and microwave wavelengths than horizontal and spherical canopy structures although this is dependent on canopy density.
- It is easiest to identify leaks on imagery where crops homogeneity is at a maximum – in-field heterogeneity makes leak identification difficult.

4.2.5 Leak scenarios

- Other conditions where leaks are easy to identify are when the leak has been present for long enough to have a negative effect on vegetation, so the vegetation in the leak has died and the surrounding vegetation is vigorous.
- The most difficult scenario for locating a leak is where the leak is very recent (there has been little effect on vegetation growth) and the canopy is large and vigorous. However, this occupies a small temporal window making it less likely to encounter in the field.

4.2.6 Leak indices

- For the HYMAP image spectral comparison maps the optimal index is a visible and near infra red wavelength combination.
- For the spectroradiometer spectral comparison maps the optimal index is visible and near infra red.
- For the modelled output, the predicted optimal wavelengths are visible and middle infrared.
- For the E-SAR data no leaks were successfully identified from the image data due to spatial resolution issues and adverse weather conditions
- An HH-VV ratio was the optimal index for identifying leaks amongst the modelled microwave results

4.2.7 Optimal time of year

- Under UK conditions, optimal times of the year for identifying leaks would be winter/early spring and late summer/autumn when vegetation density is low. However, these times may not be the best for acquiring remotely sensed imagery due to cloud cover for the optical data, and due to potential problems of soil saturation.
- The best time of year to identify leaks from a remote sensing perspective is during cloud free periods for hyperspectral data. Further work needs to be done to establish when there are cloud-free windows in the year.
- It is may be advisable to avoid crop emergence months due increased field heterogeneity, although this may be offset by the increased visibility of water when vegetation is short.

4.2.8 Sensor characteristics

- Any sensor that has potential for leak detection would need: high spatial resolution; frequent coverage; appropriate spectral bands. Currently there are no optical sensors, and only TerraSAR radar imaging sensor due for launch in 2005.

Appendix 1a

Leak questionnaire

University of Edinburgh
Department of Geography
Remote Sensing of Leaks from Aqueducts - Survey of potential end users

As part of a project funded jointly by the Natural Environment Research Council and British National Space Centre (DTI), we are investigating the application of air- and space-borne remote sensing technologies for detecting leaks from aqueducts. Part of the project involves an evaluation of end user's requirements to assess their needs for information on leaks in their supply areas, and of their perceptions as to the benefits or otherwise of remote sensing approaches for managing the problems of leakage.

We would very much welcome your completion of this questionnaire and would value your contribution to allow us to assess the potential role that remote sensing technologies may play in the leakage problem. The information you supply will be treated anonymously and in the strictest confidence and will be used only in a generalised and non-attributable form. It will not be distributed to any third party. Please answer the questions as fully as possible.

We enclose a stamped addressed envelope in which to return the questionnaire to us.
With thanks in advance.

Dr T J Malthus (Senior Lecturer)
Ms F M Taylor (PhD student)

Background

1. What is the name of your company? (This will be treated confidentially)

Company Name: _____

2. What is your position within the company? (This will be treated confidentially)

Position: _____

Your company's problem with unaccounted for distribution losses

3. What approximate percentage of total water throughput would you estimate is currently unaccounted for in your company's UK water region?

Percentage of unaccounted for distribution losses: _____

4. Would you rate this amount as a serious or not a serious problem for your company?

☐ Serious problem ☐ not a serious problem

5. What proportion of these unaccounted for losses do you think is due to leaks from your pipelines?

Proportion: _____

6. Would you say the leakage problem in your company's water region has worsened or improved over the last five years?

☐ Is improving ☐ Is worsening ☐ Stayed the same

7. Is your company actively working to control its leakage problem?

☐ Yes ☐ No

8. What percentage of leakage compared to total throughput, would you perceive as acceptable in your company.

Acceptable level: _____

9. What proportion of leaks in your region do you consider occur in rural and urban areas?

Urban: _____ Rural: _____

10. What percentage of leaks in your region do you think manifest themselves at the ground surface (rather than draining away to ground water or 'disappearing' into fissures etc)?

Percentage: _____

11. What percentage of leakage do you consider remains undetected?

Percentage: _____

12. Where do leaks most often occur in your pipelines (e.g. at joints, etc.)?

Answer: _____

13. How old are the majority of your pipelines?

Age: _____

14. What would you consider to be the <u>main</u> cause of leakage in your supply area (e.g. joint failures, pipeline failures, pressure fluctuations, etc.)?

Answer: _____

_____

15. At what depth do the majority of your rural pipelines lie?

Depth: _____

16. What is the frequency with which bursts occur?

1 - 3 per year ❑

4 - 6 per year ❑

7 - 9 per year ❑

10 - 12 per year ❑

More than 12 per year (please specify): _____

17. Is the leakage problem more acute at any particular time of year?

A problem all year round ❑

More acute in Winter ❑

More acute in Spring ❑

More acute in Summer ❑

More acute in Autumn ❑

Your company's current practices to detect and control leaks

18. Generally, how much time passes before a leak is identified?

1 - 2 days ❑

1 week ❑

1 month ❑

> 1 month (please specify a time): _____

19. Generally how soon is a leak repaired after it has been detected?

Answer: _____

20. What factors make leaks difficult to detect?

Answer: _____

_____

21. How frequently do you undertake leak surveys?

Weekly ❑

Monthly ❑

Annually ❑

Biannually or greater ❑

22. What methods do you currently use for detecting leaks from aqueducts and pipelines? Tick as many as are applicable

Walking pipelines ❑

Closed Circuit Television (CCTV) ❑

Ultrasonic pipe thickness measurement ❑

Thermal surveys ❑

Radiographic inspection ❑

Leak noise correlation ❑

Human-entry surveys ❑

Others (please specify): _____

_____

23. How effective do you consider these methods?

1	**2**	**3**	**4**	**5**
not effective at all				very effective

24. When would you consider the best time of year to survey leaks?

Winter ❑

Spring ❑

Summer ❑

Autumn ❑

No particular best time ❑

25. How much would you say your company spends on its leak problem in any year?

Amount: _____

Ideally, how frequently do you think your company would require updated information on the location of new leaks?

Weekly ❑

Monthly ❑

Annually ❑

Biannually ❑

Longer (please specify): _____

The potential role for remote sensing technologies

27. Has your company attempted to use remote sensing technologies to detect leaks?

❑ Yes ❑ No ❑ Don't know

If you answered no (or don't know) to the above question, please go to question 30

28. If yes, what remote sensing technologies has your company used?

airborne thermal survey ❑

aerial photography ❑

optical multispectral scanner ❑

radar/microwave systems ❑

Other (please specify): _____

29. How successful do you consider these approaches were?

1	2	3	4	5
not successful at all				highly successful

30. How would you rate your (or your company's) knowledge or expertise in remote sensing?

1	2	3	4	5
no knowledge				expert knowledge

31. Would you say you had insufficient knowledge about remote sensing technologies?

☐ Yes ☐ No ☐ Don't know

32. Would your company consider using remote sensing technologies to help manage its leakage problem?

☐ Yes ☐ No

33. Would you consider paying for such a service?

☐ Yes ☐ No

34. Would you consider remote sensing to be an expensive option compared to other approaches?

☐ Yes ☐ No

35. What would you perceive to be the limitations of using remote sensing technologies for detecting leaks?

_____

_____

_____

_____

36. How would you rate the following possible remote sensing approaches. Rank in order with 1 being the lowest value.

airborne thermal survey ☐

aerial photography ☐

optical multispectral scanner ☐

radar/microwave systems ☐

Any other comments you would like to make:

Thank you very much for taking the time to complete this questionnaire. Please return it in the envelope provided.

Appendix 1b

Questionnaire survey results

Due to a sparcity of available information on the nature and frequency of leaks, a questionnaire was designed to get feedback directly from water companies. It also presented an opportunity to get useful information on their user requirements with regard to using remote sensing as a potential leak detection tool. A copy of the questionnaire can be found in Appendix 1.

Questionnaires were sent to 23 of the 25 water companies in England and Wales. There was a 57% response, with 13 replies and 1 refusal. The questionnaire was separated into 3 sections:

- Problems with unaccounted for distribution losses
- Current practise on detection and control
- Potential role of remote sensing for leak detection

Unaccounted for losses

The percentage of unaccounted for losses as a percentage of total throughput varied between companies from 9 to 20%. The spread is shown below.

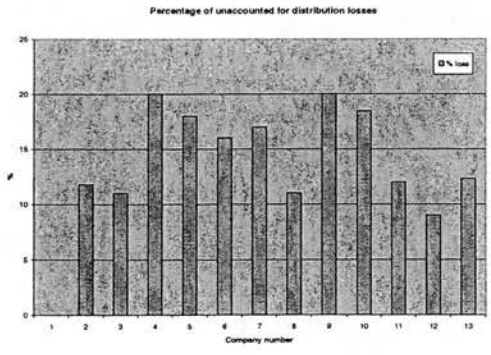

Figure A1. Percentage of unaccounted for losses as a percentage of total throughput

The majority of companies did not consider that their level of leakage was a serious problem and for most companies leakage has been reduced over the last 5 years. Only two companies differed

in their response saying that their leakage problem had stayed the same. All companies are actively seeking to control their leakage problems.

In terms of spatial distribution of leaks, from the questionnaire it would appear that more leakage occurs in rural areas than urban areas. However, this is dependent on catchment and percentage of pipelines in each company area. Some companies have predominantly urban pipelines, therefore losses from their system will occur in urban areas. However the distribution is as follows:

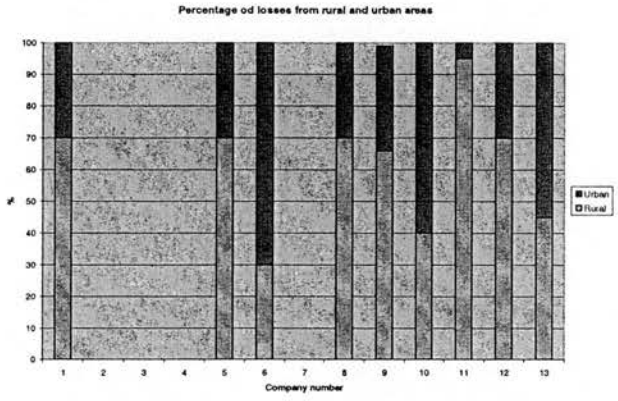

Figure A2. Distribution of urban and rural losses(%)

Most of the losses from pipelines occur at joints and fittings, with service and supply pipes being particularly susceptible. The main causes are thought to be corrosion or pipeline failure due to old age, corrosion by soil and constant pressure. It is hardly surprising that pipe age is a significant contributor to the leakage problem as all pipelines were considered to be at least 50 years old, with some as old as 120 years +. A further cause of pipeline failure is ground movement and weather extremes caused by freeze/thaw and wet/dry conditions.

A large number of leaks in rural areas manifest themselves at the surface. This is mainly because the pipelines are not buried deep; they range between 1.25 and 0.75 m and most are buried in soil. Water appears at the surface through soil capillary action or soil saturation. Approximately 20 % of leaks remain undetected, it is these leaks that are likely to drain away to ground water or 'disappear' into fissures. There is also a seasonal pattern for leak occurrence with all companies

saying that leakage is worse during the winter months – suggesting that extremes of weather contribute significantly to the leakage problem.

Leakage detection and control

Generally leaks are identified within 3 days and are fixed within 2 weeks according to results from the questionnaire. However, in some cases leaks can be left for years, as we discovered on returning to one particular leak site identified in Cheshire in 1995, to find it was still present in 2000. This is despite the fact that leak surveys are carried out at least annually with 6 companies performing weekly checks. However, there are a range of factors that make leaks difficult to detect. The most significant of these is the paucity of current detection methods. The most popular leak detection methods are walking the pipelines and noise correlation. For all but 3 companies these were their only detection methods. However a major flaw in the noise correlation method is that it is difficult to detect leaks from plastic pipes because they have poor sound transmission and there is also a problem with background noise. Ten companies identified this as one of the major problems associated with detecting leaks. Other problems include difficulty in accessing pipes and unfavourable ground conditions. Other technologies used for identifying leaks were ultrasonic pipe thickness measurements, radiographic inspection and ground microphones. Despite the problems with in identifying leaks, most companies were satisfied with their detection methods and considered them sufficient.

Potential for remote sensing technologies

About half of the water companies have tried remote sensing methods of leakage detection. The methods used were airborne thermal surveys, aerial photography and acoustic noise loggers. The response to these methods was mixed, of the 7 companies that had used remote sensing, 1 considered the technique to be successful while 2 responses were indifferent and 3 considered the techniques unsuccessful, 1 company is waiting for the data to be analysed. All companies except 2 said they would be prepared to try remote sensing to help manage their leakage control problem and would be prepared to pay for it, however, most considered that remote sensing would be an expensive option compared to other technologies.

Appendix 2

Optical data fieldwork sheet

Site number		**Date**		**Location (NGR)**	
Local topography				**Leak dimensions**	
Slope description			**Slope direction**		

CLIMATIC MEASUREMENTS

Time		**Horizontal line of sight (km)**			**Air temperature (°C)**		
Cloud cover	◐	**Cloud type**		**Wind speed**		**Wind direction**	
FURTHER COMMENTS eg proximity to boundaries							

VEGETATION

Landuse		IN LEAK	OUTSIDE LEAK	
Vegetation type				
Leaf angle				
Canopy heights (cm)				
Quadrat 1 - %age cover		Photo no.	Photo no.	
Quadrat 2 - %age cover		Photo no.	Photo no.	
No. stems sampled/quadrat ($25cm^2$)				
Vegetation colour				
FURTHER COMMENTS				

SOIL

	IN LEAK	OUTSIDE LEAK	
Soil samples taken	☐	☐	
Theta probe (mineral)			
Theta probe (organic)			
FURTHER COMMENTS			

Microwave data fieldwork sheet

Site number		**Date**		**Location (NGR)**	
Local topography				**Leak dimensions**	
Slope description			**Slope direction**		

CLIMATIC MEASUREMENTS

Time		**Horizontal line of sight (km)**				**Air temperature (°C)**	
Cloud cover	◐	**Cloud type**		**Wind speed**		**Wind direction**	
FURTHER COMMENTS eg proximity to boundaries							

VEGETATION

Landuse		IN LEAK	OUTSIDE LEAK	
Vegetation type				
Canopy heights (cm)				
Quadrat 1 - %age cover		Photo no.	Photo no.	
Quadrat 2 - %age cover		Photo no.	Photo no.	
No. stems sampled/quadrat ($25cm^2$)				
Vegetation colour				
Canopy roughness		Photo no.	Photo no.	
FURTHER COMMENTS				

SOIL

	IN LEAK	OUTSIDE LEAK	
Soil samples taken (2 per site)	☐	☐	
Soil texture			
Theta probe (mineral)			
Theta probe (organic)			
Soil colour			
Soil type			
Underlying geology			
Rock/stone content per unit area			
Max rock/stone size			
FURTHER COMMENTS			

SOIL ROUGHNESS - NAIL BOARD RECORDING SHEET

Site number	Alignment...	Alignment...	Alignment...	Alignment...	Alignment...	Alignment...
Nail number	Relative height	Relative height	Relative height	Relative height	Relative height	Relative height
1.						
2.						
3.						
4.						
5.						
6.						
7.						
8.						
9.						
10.						
11.						
12.						
13.						
14.						
15.						
16.						
17.						
18.						
19.						
20.						
21.						
22.						
23.						
24.						
25.						
26.						
27.						
28.						
29.						
30.						
31.						
32.						
33.						
34.						
35.						
36.						
37.						
38.						
39.						

Appendix 3

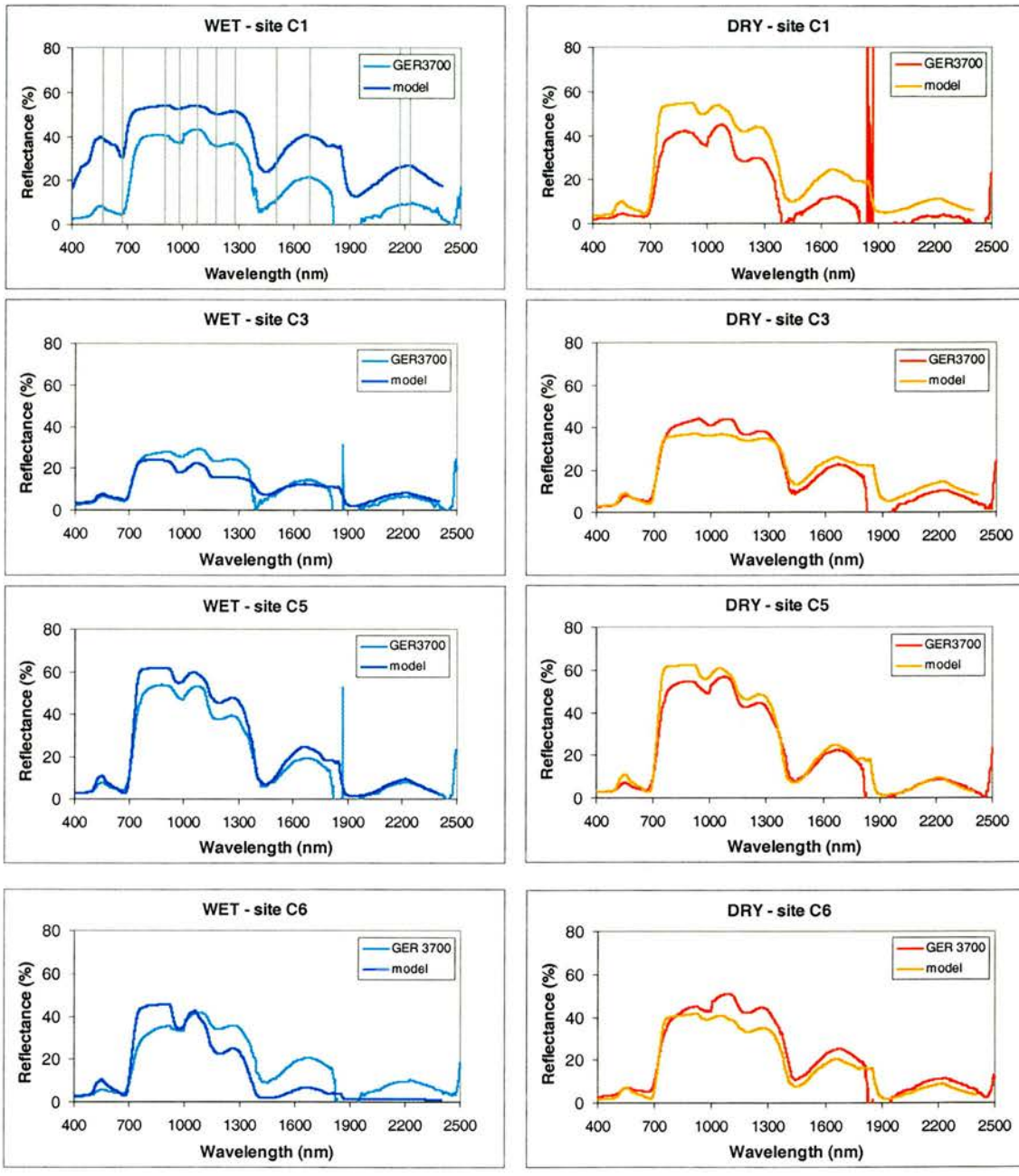

Figure A3. Comparison of the combined PROSPECT+SAIL model's ability to reproduce spectral reflectances with spectroradiometer observations for sites C1. C2, C5 and C6 (where the graphs on left show a comparison between modeled, and measured spectroradiometer reflectances for leaks. The graphs on the right show a comparison between modelled, and measured spectroradiometer reflectances for surrounding vegetation). The lines on the left hand graph for C1 (wet) show selected wavelengths used for a more detailed comparison of modelled and spectroradiometer data, shown in Table A3.

Table A3. Reflectance comparison between modelled and spectroradiometer data for wet and dry measurements respectively, over a range of 11 wavelengths from 569 nm to 2224 nm. The tables below show calculation for sites C1, C3, C5 and C6. Columns 4 and 7 show the percentage difference between the GER3700 and the model. The relative positions of these selected wavelengths are shown in FigureA3.

Site C1

Wavelength	WET 3700	WET MODEL	% difference	DRY 3700	DRY MODEL	% difference
569	7.78	38.70	-79.88	4.30	8.78	-51.06
676	4.62	30.20	-84.71	3.11	4.76	-34.57
905	40.39	53.80	-24.93	41.50	54.70	-24.12
984	37.17	52.60	-29.34	35.72	49.70	-28.13
1078	43.17	53.80	-19.76	44.71	52.50	-14.84
1181	35.67	50.10	-28.80	28.20	41.60	-32.20
1281	36.60	51.30	-28.66	29.43	43.60	-32.50
1503	10.93	27.80	-60.68	4.99	12.60	-60.42
1685	21.10	40.10	-47.38	11.84	23.90	-50.46
2172	9.00	25.90	-65.27	3.25	10.60	-69.31
2224	9.35	26.80	-65.10	3.29	11.40	-71.15

Site C3

Wavelength	WET 3700	WET MODEL	% difference	DRY 3700	DRY MODEL	% difference
569	6.43	7.04	-8.62	7.61	7.82	-2.74
676	4.30	4.92	-12.53	5.34	4.00	25.12
905	27.86	23.70	14.92	43.24	37.00	14.43
984	25.66	18.10	29.46	41.22	36.20	12.18
1078	29.22	22.40	23.33	44.00	36.50	17.04
1181	23.65	15.50	34.46	36.62	33.50	8.52
1281	24.29	15.70	35.37	38.03	34.70	8.75
1503	7.52	8.79	-14.40	11.96	16.20	-26.18
1685	14.40	12.40	13.90	22.19	25.20	-11.94
2172	6.26	7.77	-19.45	9.61	13.40	-28.29
2224	6.47	8.22	-21.33	10.15	14.40	-29.53

Site C5

Wavelength	WET 3700	WET MODEL	% difference	DRY 3700	DRY MODEL	% difference
569	7.15	9.25	-22.73	6.39	9.27	-31.10
676	4.31	2.76	36.00	3.82	2.78	27.16
905	53.49	61.60	-13.16	54.48	62.30	-12.55
984	47.03	54.80	-14.18	49.15	55.90	-12.07
1078	53.19	58.90	-9.69	56.79	59.70	-4.87
1181	37.50	45.60	-17.77	42.55	46.40	-8.30
1281	38.80	47.40	-18.14	44.03	48.40	-9.92
1503	8.79	10.10	-12.95	10.39	10.30	0.85
1685	19.16	24.10	-20.49	22.24	24.40	-8.86
2172	7.21	8.31	-13.26	8.19	8.44	-2.94
2224	7.70	9.40	-18.06	8.78	9.53	-7.89

Site C6

Wavelength	WET 3700	WET MODEL	% difference	DRY 3700	DRY MODEL	% difference
569	5.50	8.80	-37.51	6.85	5.98	12.73
676	4.19	2.91	30.55	5.26	2.08	60.47
905	35.28	45.60	-22.62	44.77	41.50	7.31
984	33.35	34.20	-2.48	42.86	39.00	9.02
1078	41.75	40.10	3.96	50.84	39.90	21.52
1181	33.84	22.50	33.50	42.01	33.10	21.21
1281	35.43	24.60	30.56	44.20	35.00	20.82
1503	11.38	2.22	80.50	13.73	10.30	24.96
1685	20.43	6.56	67.90	25.08	19.90	20.65
2172	9.60	1.50	84.38	10.66	7.99	25.03
2224	10.10	1.59	84.25	11.41	8.87	22.29

Appendix 4

Crop	CEREAL							
Scenario	Dry soil				Wet soil			
Growth stage	1	2	3	4	1	2	3	4
Surface roughness (correlation length m)	0.6094	0.6094	0.6094	0.6094	0.6094	0.6094	0.6094	0.6094
Ground volumetric moisture %)	22	22	22	22	45	45	45	45
Soil sand content (%)	65	65	65	65	65	65	65	65
Soil clay content (%)	25	25	25	25	25	25	25	25
Layer 1 height (m)	0.22	0.7	0.65	0.09	0.22	0.7	0.65	0.09
Scatterer type	elongated disc	elongated disc	elongated disc	cylinder	elongated disc	elongated disc	elongated disc	cylinder
Scatterer type half length (m)	0.00027	0.0005	0.0004	0.045	0.00027	0.0005	0.0004	0.045
Radius a (m)	0.11	0.35	0.352	0.002	0.11	0.35	0.352	0.002
Radius b (m)	0.006	0.0085	0.0085	na	0.006	0.0085	0.0085	na
Number density of scatterer type (per m2)	482	374.5	461	235	482	374.5	461	235
Vegetation inclination angle distributions	erectophile	erectophile	erectophile	erectophile	erectophile	erectophile	erectophile	erectophile
Vegetation moisture content (%)	0.735	0.846	0.805	0.5	0.735	0.846	0.805	0.6
Layer 2 height (m)		0.75	0.7			0.75	0.7	
Scatterer type		cylinder	cylinder			cylinder	cylinder	
Scatterer type half length (m)		0.375	0.35			0.375	0.35	
Radius (m)		0.003	0.003			0.003	0.003	
Number density of scatterer type (per m2)		188	230			188	230	
Vegetation inclination angle distributions		erectophile	erectophile			erectophile	erectophile	
Vegetation moisture content (%)		0.846	0.805			0.846	0.805	
Layer 3 height (m)		0.81	0.76			0.81	0.76	
Scatterer type		cylinder	cylinder			cylinder	cylinder	
Scatterer type half length (m)		0.03	0.035			0.03	0.035	
Radius (m)		0.007	0.007			0.007	0.007	
Number density of scatterer type (per m2)		188	230			188	230	
Vegetation inclination angle distributions		erectophile	erectophile			erectophile	erectophile	
Vegetation moisture content (%)		0.846	0.805			0.846	0.805	

Constants

Temperature = 17
Wavenumber =111 (C-band), 27.3 (L - band), and 9.3 (P-band)
Incidence angle = 40
Ground scattering model = hallik
Axial = uniform

Crop	CEREAL							
Scenario	Pond				Puddle			
Growth stage	1	2	3	4	1	2	3	4
Surface roughness (correlation length m)	0.004	0.004	0.004	0.004	0.004	0.004	0.004	0.004
Ground volumetric moisture %)	100	100	100	100	100	100	100	100
Soil sand content (%)	65	65	65	65	65	65	65	65
Soil clay content (%)	25	25	25	25	25	25	25	25
Layer 1 height (m)	0.22	0.7	0.65	0.09	0.274	0.75	0.7	0.09
Scatterer type	elongated disc	elongated disc	elongated disc	cylinder	elongated disc	elongated disc	elongated disc	cylinder
Scatterer type half length (m)	0.00027	0.0005	0.0004	0.045	0.00027	0.0005	0.0004	0.045
Radius a (m)	0.11	0.35	0.352	0.002	0.137	0.375	0.35	0.002
Radius b (m)	0.006	0.0085	0.0085	na	0.00675	0.00865	0.0087	na
Number density of scatterer type (per m2)	482	374.5	461	24	482	374.5	461	24
Vegetation inclination angle distributions	erectophile	erectophile	erectophile	erectophile	erectophile	erectophile	erectophile	erectophile
Vegetation moisture content (%)	0.735	0.846	0.805	0.6	0.740083507	0.84725537	0.80794702	0.6
Layer 2 height (m)		0.75	0.7			0.8	0.75	
Scatterer type		cylinder	cylinder			cylinder	cylinder	
Scatterer type half length (m)		0.375	0.35			0.4	0.375	
Radius (m)		0.003	0.003			0.003	0.003	
Number density of scatterer type (per m2)		188	230			188	230	
Vegetation inclination angle distributions		erectophile	erectophile			erectophile	erectophile	
Vegetation moisture content (%)		0.846	0.805			0.84725537	0.80794702	
Layer 3 height (m)		0.81	0.76			0.87	0.83	
Scatterer type		cylinder	cylinder			cylinder	cylinder	
Scatterer type half length (m)		0.03	0.035			0.035	0.035	
Radius (m)		0.007	0.007			0.007	0.007	
Number density of scatterer type (per m2)		188	230			188	230	
Vegetation inclination angle distributions		erectophile	erectophile			erectophile	erectophile	
Vegetation moisture content (%)		0.846	0.805			0.84725537	0.80794702	

Constants

Temperature = 17
Wavenumber =111 (C-band), 27.3 (L - band), and 9.3 (P-band)
Incidence angle = 40
Ground scattering model = hallik
Axial = uniform

Crop	CEREAL				CANOPY				
Scenario	Water logged				Dry soil				
Growth stage	1	2	3	4	1	2	3	4	5
Surface roughness (correlation length m)	0.004	0.004	0.004	0.004	0.6094	0.6094	0.6094	0.6094	0.6094
Ground volumetric moisture %)	100	100	100	100	22	22	22	22	22
Soil sand content (%)	65	65	65	65	65	65	65	65	65
Soil clay content (%)	25	25	25	25	25	25	25	25	25
Layer 1 height (m)	0.12	0.5	0.5	0.09	0.284	0.681	1.34	1.34	1.28
Scatterer type	elongated disc	elongated disc	elongated disc	cylinder	elongated disc	elongated disc	elongated disc	elongated disc	elongated disc
Scatterer type half length (m)	0.00027	0.0005	0.0004	0.045	0.0004	0.0004	0.0004	0.0004	0.0004
Radius a (m)	0.06	0.15	0.2	0.001	0.03	0.05	0.05	0.05	0.04
Radius b (m)	0.003	0.005	0.005	na	0.015	0.02	0.02	0.02	0.015
Number density of scatterer type (per m2)	48.22876992	37.44822135	46.09011859	24	707.36	1591.55	1591.55	1591.55	1856.81
Vegetation inclination angle distributions	erectophile	erectophile	erectophile	erectophile	extremophile	extremophile	extremophile	extremophile	extremophile
Vegetation moisture content (%)	0.740083507	0.84725537	0.80794702	0.6	0.871	0.7959	0.7841	0.7841	0.7573
Layer 2 height (m)		0.5	0.5			0.57	1.23	1.23	1.17
Scatterer type		cylinder	cylinder			cylinder	cylinder	cylinder	cylinder
Scatterer type half length (m)		0.25	0.25			0.285	0.615	0.615	0.585
Radius (m)		0.003	0.003			0.0055	0.0055	0.0055	0.0055
Number density of scatterer type (per m2)		37.44822135	46.09011859			3	3	3	3
Vegetation inclination angle distributions		erectophile	erectophile			erectophile	erectophile	erectophile	erectophile
Vegetation moisture content (%)		0.84725537	0.80794702			0.7959	0.7841	0.7841	0.7573
Layer 3 height (m)		0.56	0.56					1.34	
Scatterer type		cylinder	cylinder					disc	
Scatterer type half length (m)		0.03	0.03					0.0015	
Radius (m)		0.006	0.006					0.006	
Number density of scatterer type (per m2)		37.44822135	46.09011859					2000	
Vegetation inclination angle distributions		erectophile	erectophile					planophile	
Vegetation moisture content (%)		0.84725537	0.80794702					0.7841	

Constants

Temperature = 17
Wavenumber =111 (C-band), 27.3 (L - band), and 9.3 (P-band)
Incidence angle = 40
Ground scattering model = hallik
Axial = uniform

Crop	CANOPY					CANOPY				
Scenario	Wet soil					Pond				
Growth stage	1	2	3	4	5	1	2	3	4	5
Surface roughness (correlation length m)	0.6094	0.6094	0.6094	0.6094	0.6094	0.004	0.004	0.004	0.004	0.004
Ground volumetric moisture %)	45	45	45	45	45	100	100	100	100	100
Soil sand content (%)	65	65	65	65	65	65	65	65	65	65
Soil clay content (%)	25	25	25	25	25	25	25	25	25	25
Layer 1 height (m)	0.284	0.631	1.34	1.34	1.28	0.284	0.681	1.34	1.34	1.28
Scatterer type	elongated disc	elongated disc	elongated disc	elongated disc	elongated disc	elongated disc	elongated disc	elongated disc	elongated disc	elongated disc
Scatterer type half length (m)	0.0004	0.0004	0.0004	0.0004	0.0004	0.0004	0.0004	0.0004	0.0004	0.0004
Radius a (m)	0.03	0.05	0.05	0.05	0.04	0.03	0.05	0.05	0.05	0.04
Radius b (m)	0.015	0.02	0.02	0.02	0.015	0.015	0.02	0.02	0.02	0.015
Number density of scatterer type (per m2)	707.36	1591.55	1591.55	1591.55	1856.81	707.36	1591.55	1591.55	1591.55	1856.81
Vegetation inclination angle distributions	extremophile	extremophile	extremophile	extremophile	extremophile	extremophile	extremophile	extremophile	extremophile	extremophile
Vegetation moisture content (%)	0.871	0.7959	0.7841	0.7841	0.7573	0.871	0.7959	0.7841	0.7841	0.7573
Layer 2 height (m)		0.57	1.23	1.23	1.17		0.57	1.23	1.23	1.17
Scatterer type		cylinder	cylinder	cylinder	cylinder		cylinder	cylinder	cylinder	cylinder
Scatterer type half length (m)		0.285	0.615	0.615	0.585		0.285	0.615	0.615	0.585
Radius (m)		0.0055	0.0055	0.0055	0.0055		0.0055	0.0055	0.0055	0.0055
Number density of scatterer type (per m2)		3	3	3	3		3	3	3	3
Vegetation inclination angle distributions		erectophile	erectophile	erectophile	erectophile		erectophile	erectophile	erectophile	erectophile
Vegetation moisture content (%)		0.7959	0.7841	0.7841	0.7573		0.7959	0.7841	0.7841	0.7573
Layer 3 height (m)				1.34					1.34	
Scatterer type				disc					disc	
Scatterer type half length (m)				0.0015					0.0015	
Radius (m)				0.006					0.006	
Number density of scatterer type (per m2)				2000					2000	
Vegetation inclination angle distributions				planophile					planophile	
Vegetation moisture content (%)				0.7841					0.7841	

Constants

Temperature = 17
Wavenumber =111 (C-band), 27.3 (L - band), and 9.3 (P-band)
Incidence angle = 40
Ground scattering model = hallik
Axial = uniform

Crop	CANOPY								
Scenario	Puddle					Waterlogged			
Growth stage	1	2	3	4	5	1	2	3	4
Surface roughness (correlation length m)	0.004	0.004	0.004	0.004	0.004	0.004	0.004	0.004	0.004
Ground volumetric moisture %)	100	100	100	100	100	100	100	100	100
Soil sand content (%)	65	65	65	65	65	65	65	65	65
Soil clay content (%)	25	25	25	25	25	25	25	25	25
Layer 1 height (m)	0.31	0.71	1.38	1.38	1.31	0.15	0.5	0.6	0.6
Scatterer type	elongated disc	elongated disc	elongated disc	elongated disc	elongated disc	elongated disc	elongated disc	elongated disc	elongated disc
Scatterer type half length (m)	0.0004	0.0004	0.0004	0.0004	0.0004	0.0004	0.0004	0.0004	0.0004
Radius a (m)	0.0335	0.06	0.0625	0.0625	0.064	0.025	0.035	0.0375	0.0325
Radius b (m)	0.015	0.025	0.0265	0.0265	0.025	0.01	0.015	0.0125	0.01
Number density of scatterer type (per m2)	707.36	1591.55	1591.55	1591.55	1856.81	70.74	159.15	159.15	185.68
Vegetation inclination angle distributions	extremophile	extremophile	extremophile	extremophile	extremophile	extremophile	extremophile	extremophile	extremophile
Vegetation moisture content (%)	0.871	0.7959	0.7841	0.7841	0.7573	0.871	0.7959	0.7841	0.7573
Layer 2 height (m)		0.57	1.23	1.23	1.17		0.57	1.23	1.17
Scatterer type		cylinder	cylinder	cylinder	cylinder		cylinder	cylinder	cylinder
Scatterer type half length (m)		0.285	0.615	0.615	0.585		0.035	0.0375	0.0325
Radius (m)		0.0055	0.0055	0.0055	0.0055		0.015	0.0125	0.01
Number density of scatterer type (per m2)		3	3	3	3		3	3	3
Vegetation inclination angle distributions		erectophile	erectophile	erectophile	erectophile		erectophile	erectophile	erectophile
Vegetation moisture content (%)		0.797141819	0.785054868	0.785054868	0.759		0.797141819	0.785054868	0.759
Layer 3 height (m)				1.38					
Scatterer type				disc					
Scatterer type half length (m)				0.0015					
Radius (m)				0.006					
Number density of scatterer type (per m2)				2000					
Vegetation inclination angle distributions				planophile					
Vegetation moisture content (%)				0.785054868					

Constants

Temperature = 17
Wavenumber =111 (C-band), 27.3 (L - band), and 9.3 (P-band)
Incidence angle = 40
Ground scattering model = hallik
Axial = uniform

Crop	GRASS							
Scenario	Dry soil				Wet soil			
Growth stage								
Surface roughness (correlation length)	0.6094	0.6094	0.6094	0.6094	0.6094	0.6094	0.6094	0.6094
Ground volumetric moisture %)	22	22	22	22	45	45	45	45
Soil sand content (%)	65	65	65	65	65	65	65	65
Soil clay content (%)	25	25	25	25	25	25	25	25
Layer 1 height (m)	0.06	0.1	0.2	0.3	0.06	0.1	0.2	0.3
Scatterer type	elongated disc	elongated disc	elongated disc	elongated disc	elongated disc	elongated disc	elongated disc	elongated disc
Scatterer type half length (m)	0.00027	0.00027	0.00027	0.00027	0.00027	0.00027	0.00027	0.00027
Radius a (m)	0.03	0.05	0.1	0.15	0.03	0.05	0.1	0.15
Radius b (m)	0.001	0.0015	0.0015	0.0025	0.001	0.0015	0.0015	0.0025
Number density of scatterer type (per m2)	21220	16976	10610	5092	21220	16976	10610	5092
Vegetation inclination angle distributions	erectophile	erectophile	erectophile	erectophile	erectophile	erectophile	erectophile	erectophile
Vegetation moisture content (%)	66.25	72.73	82.25	83.25	66.25	72.73	82.25	83.25

Crop	GRASS							
Scenario	Pond				Puddle			
Growth stage								
Surface roughness (correlation length)	0.004	0.004	0.004	0.004	0.004	0.004	0.004	0.004
Ground volumetric moisture %)	100	100	100	100	100	100	100	100
Soil sand content (%)	65	65	65	65	65	65	65	65
Soil clay content (%)	25	25	25	25	25	25	25	25
Layer 1 height (m)	0.06	0.1	0.2	0.3	0.09	0.13	0.23	0.33
Scatterer type	elongated disc	elongated disc	elongated disc	elongated disc	elongated disc	elongated disc	elongated disc	elongated disc
Scatterer type half length (m)	0.00027	0.00027	0.00027	0.00027	0.00027	0.00027	0.00027	0.00027
Radius a (m)	0.03	0.05	0.1	0.15	0.0375	0.06	0.11	0.1625
Radius b (m)	0.001	0.0015	0.0015	0.0025	0.001	0.0014	0.0015	0.0025
Number density of scatterer type (per m2)	21220	16976	10610	5092	21220	16976	10610	5092
Vegetation inclination angle distributions	erectophile	erectophile	erectophile	erectophile	erectophile	erectophile	erectophile	erectophile
Vegetation moisture content (%)	70.8108108	73.9130435	82.665424	83.5820896	70.8108108	73.9130435	82.665424	83.5820896

Constants

Temperature = 17

Wavenumber =111 (C-band), 27.3 (L - band), and 9.3 (P-band)

Incidence angle = 40

Ground scattering model = hallik

Axial = uniform

Crop	GRASS				ROW		
Scenario	Water logged				Dry soil		
Growth stage							
Surface roughness (correlation length)	0.004	0.004	0.004	0.004	0.6094	0.6094	0.6094
Ground volumetric moisture %)	100	100	100	100	22	22	22
Soil sand content (%)	65	65	65	65	65	65	65
Soil clay content (%)	25	25	25	25	25	25	25
Layer 1 height (m)	0.5	0.9	0.18	0.25	0.1	0.2	0.2
Scatterer type	elongated disc	elongated disc	elongated disc	elongated disc	elongated disc	elongated disc	elongated disc
Scatterer type half length (m)	0.00027	0.00027	0.00027	0.00027	0.0004	0.0004	0.0004
Radius a (m)	0.025	0.045	0.09	0.125	0.075	0.125	0.11
Radius b (m)	0.001	0.001	0.001	0.001	0.035	0.06	0.55
Number density of scatterer type (per m2)	2122.065877	1697.652701	1061.032938	509.2958104	182	212	210
Vegetation inclination angle distributions	erectophile	erectophile	erectophile	erectophile	spherical	spherical	spherical
Vegetation moisture content (%)	70.8108108	73.9130435	82.665424	83.5820896	83.18	53.52	55.11

Crop	ROW					
Scenario	Wet soil			Pond		
Growth stage						
Surface roughness (correlation length)	0.6094	0.6094	0.6094	0.004	0.004	0.004
Ground volumetric moisture %)	45	45	45	100	100	100
Soil sand content (%)	65	65	65	65	65	65
Soil clay content (%)	25	25	25	25	25	25
Layer 1 height (m)	0.1	0.2	0.2	0.1	0.2	0.2
Scatterer type	elongated disc	elongated disc	elongated disc	elongated disc	elongated disc	elongated disc
Scatterer type half length (m)	0.0004	0.0004	0.0004	0.0004	0.0004	0.0004
Radius a (m)	0.075	0.125	0.11	0.0875	0.135	0.125
Radius b (m)	0.035	0.06	0.55	0.04	0.0675	0.06
Number density of scatterer type (per m2)	182	212	210	182	212	210
Vegetation inclination angle distributions	spherical	spherical	spherical	spherical	spherical	spherical
Vegetation moisture content (%)	83.18	53.52	55.11	83.9070568	55.2282769	56.8074228

Constants

Temperature = 17

Wavenumber =111 (C-band), 27.3 (L - band), and 9.3 (P-band)

Incidence angle = 40

Ground scattering model = hallik

Axial = uniform

Crop						
Scenario	Puddle			Water logged		
Growth stage						
Surface roughness (correlation length)	0.004	0.004	0.004	0.004	0.004	0.004
Ground volumetric moisture %)	100	100	100	100	100	100
Soil sand content (%)	65	65	65	65	65	65
Soil clay content (%)	25	25	25	25	25	25
Layer 1 height (m)	0.12	0.23	0.23	0.1	0.15	0.15
Scatterer type	elongated disc	elongated disc	elongated disc	elongated disc	elongated disc	elongated disc
Scatterer type half length (m)	0.0004	0.0004	0.0004	0.0004	0.0004	0.0004
Radius a (m)	0.05	0.06	0.06	0.075	0.125	0.11
Radius b (m)	0.25	0.25	0.25	0.035	0.06	0.55
Number density of scatterer type (per m2)	182	212	210	18.19	21.22	21.05
Vegetation inclination angle distributions	spherical	spherical	spherical	spherical	spherical	spherical
Vegetation moisture content (%)	83.9070568	55.2282769	56.8074228	83.9070568	55.2282769	56.8074228

Constants

Temperature = 17

Wavenumber =111 (C-band), 27.3 (L - band), and 9.3 (P-band)

Incidence angle = 40

Ground scattering model = hallik

Axial = uniform

Crop					
Scenario	site1_d	site2_d	site3_d	site5_d	site6_d
Growth stage					
Surface roughness (correlation length)	0.614019519	0.609399328	0.618890114	0.614767558	0.605745481
Ground volumetric moisture %)	27	28	22	19	50
Soil sand content (%)	65	82	82	82	10
Soil clay content (%)	25	18	18	18	34
Layer 1 height (m)	0.592	0.09	0.03	0.12	0.06
Scatterer type	edisc_rg	edisc_rg	edisc_rg	edisc_rg	edisc_rg
Scatterer type half length (m)	0.0006	0.00027	0.00027	0.00027	0.00027
Radius a (m)	0.3	0.03	0.05	0.1	0.15
Radius b (m)	0.0085	0.001	0.0015	0.0015	0.0025
Number density of scatterer type (per m2)	640	21220	21220	21220	21220
Vegetation inclination angle distributions	erectophile	erectophile	erectophile	erectophile	erectophile
Vegetation moisture content (%)	81.63	66.01	66.25	82.25	70.16

Crop					
Scenario	site1_w	site2_w	site3_w	site5_w	site6_w
Growth stage					
Surface roughness (correlation length)	0.004	0.004	0.004	0.004	0.004
Ground volumetric moisture %)	32	56	56	19	63
Soil sand content (%)	65	82	82	82	10
Soil clay content (%)	25	18	18	18	34
Layer 1 height (m)	0.0565	0.103	0.05	0.193	0.256
Scatterer type	edisc_rg	edisc_rg	edisc_rg	edisc_rg	edisc_rg
Scatterer type half length (m)	0.0006	0.00027	0.00027	0.00027	0.00027
Radius a (m)	0.0283	0.0515	0.025	0.0965	0.128
Radius b (m)	0.006	0.002	0.0015	0.002	0.0025
Number density of scatterer type (per m2)	640	21220	21220	21220	21220
Vegetation inclination angle distributions	extremophile	erectophile	erectophile	erectophile	erectophile
Vegetation moisture content (%)	83.14	87.74	75.14	81.95	79.91

Constants

Temperature = 17

Wavenumber =111 (C-band), 27.3 (L - band), and 9.3 (P-band)

Incidence angle = 40

Ground scattering model = hallik

Axial = uniform

SUPERVISOR
INTER-LIBRARY LOANS
ROBINSON LIBRARY
NEWCASTLE UNIVERSITY
NEWCASTLE UPON TYNE

14 NOV 2007

Dear SUPERVISOR,

RE: Request RG06952
RESTRICTED ACCESS ITEM: RENEWAL REMINDER

The following item is due for return on the 15 NOV 2007, but a renewal is possible. Please renew if necessary.

PHD THESIS
TAYLOR, F
REMOTE SENSING OF WATER LEAKS FROM RURAL AQUEDUCTS
2003 EDINBURGH UNIVERSITY
ISBN/ISSN:

Yours sincerely,
SUPERVISOR

INTER-LIBRARY LOANS
ROBINSON LIBRARY
NEWCASTLE UNIVERSITY
NEWCASTLE UPON TYNE
NE2 4HQ

Tel : +44 (0)191 222 7601
Email: web-ill@newcastle.ac.uk
RECEIPT FOR RESTRICTED ACCESS MATERIAL RG06952 Due: 15 NOV 2007

Requested by SUPERVISOR

I acknowledge receipt of: PHD THESIS
TAYLOR, F
REMOTE SENSING OF WATER LEAKS FROM RURAL AQUEDUCTS
2003 EDINBURGH UNIVERSITY

ISBN/ISSN:

I understand that this item MUST NOT BE REMOVED FROM THE LIBRARY and must be returned by me personally to an assistant at the ILL DESK on the day of